Engineered Emulsions, Polymer Structured Oils and Responsive Polymer Nanoparticles *via* Polymer Design and Emulsion Templating

By Robert Thomas Woodward

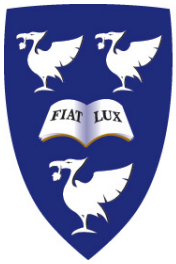

UNIVERSITY OF LIVERPOOL

Thesis submitted in accordance with the requirements of the University of Liverpool for the degree of Doctor in Philosophy by Robert Thomas Woodward

September 2012

ACKNOWLEDGEMENTS

Firstly, I would like to express my gratitude to The University of Liverpool for all of the opportunities offered to me over the last eight years.

I am forever grateful to my family for their continuous support, for never questioning my educational decisions and most importantly, for shouldering the burden of 8 years of chemistry. I am indebted to my wonderful girlfriend Emily, who, by putting up with me, has put almost as much effort into this PhD as I have.

I would like to thank all of my friends in the department over these last four years, in particular Jamie, Becca, Tamara, Mike, Rachel, Ben, Jaclyn, Fiona, Paul, Ste, Tom and Marco for their regular lunch and tea breaks, providing some stability and order to the working day.

I would like to thank Prof. Steve Rannard for offering me the opportunity to complete my PhD four years ago, and both Steve and Dr. Dave Adams for the continued support and guidance over the last four years, particularly in the absence of my supervisor. I am also grateful to Dr. Lin Chen for her continuous advice and also for the many, many discussions on just about anything, except materials science.

I would like to thank Erol Hasan and Cristina Olariu at the University of Liverpool for their contributions to Chapter 7 involving the synthesis and characterisation of Fe_3O_4. I am grateful to Michael Barrow at the University of Liverpool for mercury intrusion measurements included in Chapter 6 and also to Prof. Andrew deMello at the Swiss Federal Institute of Technology for the microfluidic analysis included in Chapter 4. I am grateful to Robert Bell at Imperial College London, who ran the Karl Fischer titrations in Chapter 4 and Nicolas Schaeffer, also as Imperial College London who ran the SEM images and ICP measurements in Chapter 6.

However, it is with a heavy heart that I wish to express my sincerest gratitude to Dr. Jonathan Weaver, my supervisor and great friend. Jon was truly gifted in the field of polymer chemistry, someone who I know I shall try to emulate throughout my career in science. I was never able to truly thank Jon for all of his support, guidance and advice, and would just like to add that this thesis is for him. I hope I have, and will continue, to make him proud.

ABSTRACT

The synthesis of branched copolymers with precise composition, specifically the ratio of methacrylic acid (MAA) to ethylene glycol (EG) has been demonstrated. These polymers were used to stabilise dodecane oil-in-water emulsion droplets. It was demonstrated in the literature that branched copolymers containing a 1:1 ratio of MAA:EG formed pH-responsive emulsions, capable of triggered inter-droplet hydrogen bonding to form engineered emulsions (EE). The effect of varying this ratio on the rate of engineered emulsion formation, and the resulting strength and stiffness of the emulsion droplet aggregates was investigated. This control over systems is exemplified by the demonstration of selective acid-triggered assembly of binary mixtures of droplets stabilised by polymer containing only EG functionality with droplets stabilised by polymers containing only MAA functionality.

EEs stabilised using a branched copolymer containing a 1:1 ratio of MAA:EG were produced and allowed to dehydrate, leading to the removal of water from droplet interstitial sites. The resulting single-phase materials are known as polymer-structured oils (PSOs), held structurally by the inter-droplet polymer-polymer interactions. These polymer boundaries provide enough of a barrier between droplets to prevent coalescence upon the removal of water, allowing reversible hydration of PSOs to reform EEs.

The production of large volume, well-defined EEs produced via the hydrolysis of glucono-δ-lactone (GδL) to gluconic acid in an emulsion's water phase was investigated. This process provides a homogeneous pH trigger for the formation of EEs, eliminating the slow diffusion of HCl. A homogeneous pH trigger also allows the formation of EEs to be studied *in situ* using rheology. A comparison between GδL and a conventional HCl trigger is presented.

Branched copolymer-stabilised ethyl acetate o/w emulsions were used as templates in the production of both pH-responsive, surface-functionalised poly(methyl methacrylate) (PMMA) colloidal nanoparticles and non-responsive PMMA particles via an emulsion-solvent-evaporation technique. Lowering of the solution pH can trigger the reversible aggregation of these highly dispersed pH-responsive colloids into 3D structures with internal macroporosities dictated by the method of dehydration employed. The colloids can also co-encapsulate various hydrophobic molecules without any effect on particle stability and pH-responsiveness.

The production of multi-responsive emulsion droplets via the encapsulation of oleophilic, magnetic Fe_3O_4 nanoparticles within a stable, surface-functionalised dodecane o/w emulsion was investigated. Droplet surface functionality allowed the formation of EE on lowering the pH, and encapsulated nanoparticles gave both the free-flowing and aggregated emulsions magnetic-responsiveness. The rate of aggregation and gel strength of multi-responsive EEs is compared to that of a standard pH-responsive emulsion.

PRIMARY PUBLICATIONS ARISING FROM THIS THESIS

1. **"Controlling responsive emulsion properties via polymer design"**, R. T. Woodward, R. A. Slater, S. Higgins, S. P. Rannard, A. I. Cooper, B. J. L. Royles, P. H. Findlay, J. V. M. Weaver, *Chemical Communications*, 2009, *24*, 3554-3556.

2. **"Fabrication of large volume, macroscopically defined and responsive engineered emulsions using a homogeneous pH-trigger"**, R. T. Woodward, L. Chen, D. J. Adams, J. V. M. Weaver, *Journal of Materials Chemistry*, 2010, *25*, 5228-5234.

3. **"The role of responsive branched copolymer composition in controlling pH-triggered aggregation of "engineered" emulsion droplets: towards selective droplet assembly"**, R. T. Woodward, J. V. M. Weaver, *Polymer Chemistry*, 2011, *2*, 403-410.

4. **"Multi-responsive polymer-stabilized magnetic engineered emulsions as liquid-based switchable magneto-responsive actuators"**, R. T. Woodward, C. I. Olariu, E. A. Hasan, H. H. P. Yiu, M. J. Rosseinsky, J. V. M. Weaver, *Soft Matter*, 2011, *7*, 4335-4340.

5. **"Reversible aggregation of responsive polymer-stabilized colloids and the pH dependent formation of porous scaffolds"**, R. T. Woodward, C. Hight, U. Yildiz, N. Schaeffer, E. M. Valliant, J. R. Jones, M. M. Stevens, J. V. M. Weaver, *Soft Matter*, 2011, *7*, 7560-7566.

6. **"Microfluidic production of monodisperse functional o/w droplets and study of their reversible pH-dependent aggregation behaviour"**, W. A. C. Bauer, J. Kotar, P. Cicuta, R. T. Woodward, J. V. M. Weaver, W. T. S. Huck, *Soft Matter*, 2011, *7*, 4214-4220.

7. **"Multiple, reversible transitions in polymer-stabilized responsive emulsions"**, R. T. Woodward, T. Gong, W. H. Briscoe, C. Sammon, A. DeMello, J. V. M. Weaver, *Manuscript in preparation*, 2012

CONTENTS

CHAPTER 1 - Introduction

CHAPTER 2 - Experimental

CHAPTER 5 - Large Volume, Macroscopically Defined, Responsive Engineered Emulsions Using a Homogeneous pH Trigger

CHAPTER 6 - Reversible Aggregation of Responsive Polymer-Stabilised Colloids and the pH-Dependent Formation of Porous Scaffolds

CHAPTER 7 Multi-Responsive Polymer-Stabilised Magnetic Emulsions in the Formation of Magnetic Engineered Emulsions

GLOSSARY

ATRP	atom transfer radical polymerisation
CRP	controlled radical polymerisation
C_t	chain transfer constant
CTA	chain transfer agent
CTR	chain transfer reaction
Φ_{oil}	volume fraction of oil
$D_{(4,3)}$	volume average diameter
DP_n	number average degree of polymerisation
EE	engineered emulsion
ESE	emulsion-solvent-evaporation
FRP	free radical polymerisation
FTIR	fourier transform infrared spectroscopy
G'	storage modulus
G"	loss modulus
ICP	inductively coupled plasma mass spectrometry
LVE	linear viscoelastic
MFM	monofunctional monomer
M_n	number average molecular weight
MvH	magnetisation hysteresis measurement
M_w	weight-average molecular weight
o/w	oil-in-water emulsion
PDI	polydispersity index (M_w/M_n)
PRBN	pH-responsive branched polymer nanoparticles
RAFT	radical addition-fragmentation chain transfer polymerisation
rpm	revolutions per minute
SCL	shell cross-linked
SCVP	self-condensing vinyl polymerisation
SEM	scanning electron microscopy
SQUID	superconducting quantum interface device
$t_{1/2}$	half life
TEM	transmission electron microscopy
TGA	thermogravimetric analysis
UV-Vis	ultraviolet-visible spectroscopy
w/o	water-in-oil emulsion

CHEMICAL GLOSSARY

AIBN	azoisobutyronitrile
DDT	1-dodecanethiol
DEAEMA	(2-diethylamino)ethyl methacrylate
DNA	deoxyribonucleic acid
EG	ethylene glycol
EGDMA	ethylene glycol dimethacrylate
EtOAc	ethyl acetate
GδL	glucono-δ-lactone
MAA	methacrylic acid
MPA	mercaptopropionic acid
P4VP	poly(4-vinyl pyridine)
PDEAEMA	poly(2-diethylamino)ethyl methacrylate
PEG	poly(ethylene glycol)
PEGDMA	poly(ethylene glycol) dimethacrylate
PEGMA	poly(ethylene glycol) methacrylate
PHPMA	poly(2-hydroxypropyl methacrylate)
PMAA	poly(methacrylic acid)
PMMA	poly(methyl methacrylate)
PVC	poly(vinyl chloride)
SDS	sodium dodecyl sulfate
TG	1-thioglycerol
THF	tetrahydrofuran
TMSDM	trimethylsilyl diazomethane

CHAPTER 1

Introduction

List of Figures

List of Schemes

List of Tables

1.1. Polymers

Since polymers were first produced, there have been many advances in this field of synthetic chemistry, resulting in polymers playing a major role in modern day life. The global demand for plastic materials had reached 245 million tonnes by 2009, with this number only expected to increase.[1] The idea of polymer chains was first introduced by Staudinger in 1920,[2] who later went on to win a Nobel prize in 1953 "*for his discoveries in the field of macromolecular chemistry*". His work on high molecular weight molecules, or macromolecules, paved the way for modern day polymer chemistry. A polymer is a macromolecule consisting of repeating subunits joined by covalent bonds. The name polymer is derived from the Greek words *poly* and *mer*, meaning "many" and "part", respectively. The 'parts' are monomers, which are relatively simple organic molecules that react to form polymers *via* polymerisation.

Carothers was the first to distinguish between polymers by the mechanism in which they were synthesised, i.e. by condensation or addition polymerisation.[3] Carothers thought that condensation polymers were made up from multifunctional monomers and proposed that small molecules are eliminated during polymerisation. This differed from addition polymers, in which the polymer's repeating unit has the same structure as individual monomer molecules with no small molecule elimination during polymerisation.

Addition and condensation polymerisations are now more commonly classed as chain-growth or step-growth polymerisations, respectively. This provides a more accurate insight into the mechanism of polymerisation, for example step-growth polymerisations often do not eliminate a small molecule, hence the change from "condensation" to "step-growth". The majority of polymers produced commercially are vinyl polymers, usually synthesised using 'free radical polymerisation'. However, in terms of controlled architectures and targeted structures, the ability to eliminate undesirable termination and transfer reactions is arguably one of the most important discoveries in polymer chemistry.

1.2. Step-Growth Polymerisation

Step-growth polymerisation occurs when two hypothetical functional groups, A and B, can react together to form C.[4] These two functional groups can exist in the same molecule, for example when a hydroxycarboxylic acid forms a polyester (Scheme 1.1(a)), or they can exist on two difunctional monomers, such as the formation of polyurethanes from diamine and bischloroformate (Scheme 1.1(b)).

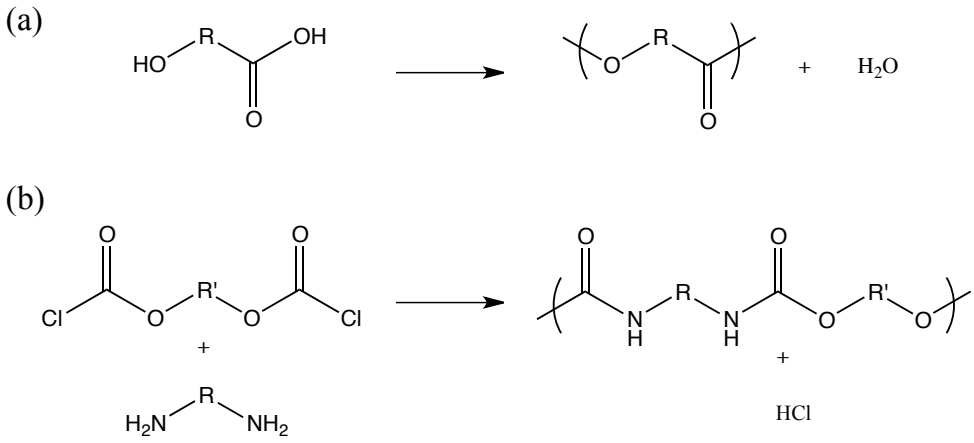

Scheme 1.1. Step-growth polymerisation of (a) a hydroxycarboxylic acid, which has both A and B functionality on one molecule and (b) a diamine and a bischloroformate, a system in which one monomer has difunctionality A, the other difunctional with respect to B.

Polymerisation of monomers containing both A and B on one molecule (as in Scheme 1.1(a)) results in polymer chains with active sites at both ends, with functional group A at one end and B at the other. However, when A-A and B-B monomers polymerise, either chain end may consist of A or B (Scheme 1.2).

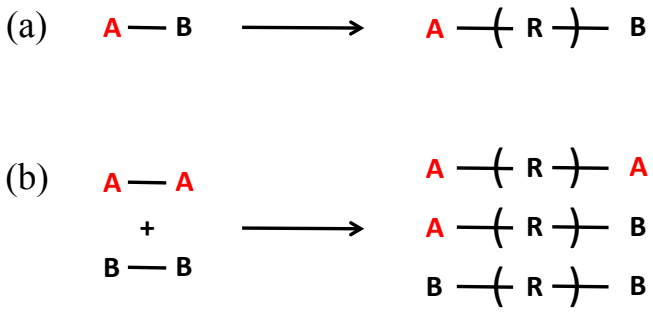

Scheme 1.2. Resulting chain end functionalities in the step-growth polymerisation of (a) an A-B monomer and (b) A-A and B-B monomers.

Step-growth polymerisation results in the consumption of monomer without initial large increases in molecular weight. Consider if all monomer had reacted to form small polymers, or oligomers, the increase in molecular weight would be relatively small. However, each polymer/oligomer formed still has two active sites, enabling further polymerisation between these small molecules. Therefore reaction rate will continue until the concentration of chain ends is sufficiently depleted. Step-growth polymerisation is represented schematically in Figure 1.1.

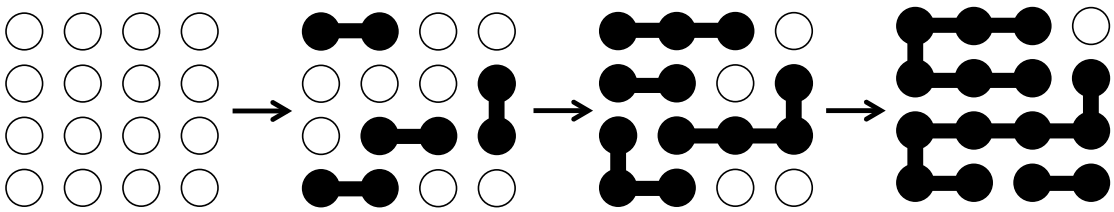

Figure 1.1. Schematic representation of step-growth polymerisation of an A-B monomer system. White dots represent monomer and black dots represent oligomer/polymer. (Figure from ref. 5).

1.3. Chain-Growth Polymerisation

Chain-growth polymerisation involves five distinct kinetic steps: decomposition; initiation; propagation; chain transfer and termination. These processes will be outlined in more detail in section 1.6. Initiators able to decompose, generating initiating species, are used to start the polymerisation, although the presence of an initiator to start the reaction is not always necessary.[4] Initiators come in many forms, for example, anions in anionic polymerisation and free radicals in radical polymerisation. In chain-growth polymerisation, propagation occurs at one end of the chain (active chain end) until termination reactions stop this process or until all monomer is consumed. In contrast to step-growth, chain lengths can increase rapidly even when large amounts of monomer remain unreacted. The most common form of chain-growth is free radical polymerisation of vinyl monomers: an example showing initiation (a) and propagation (b) of methacrylic acid is shown in Scheme 1.3.

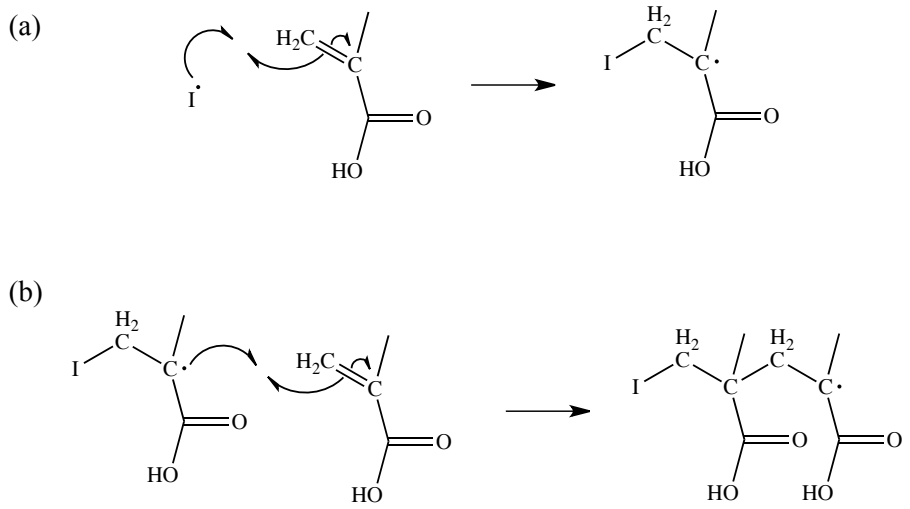

Scheme 1.3. Schematic of (a) initiation in the polymerisation of methacrylic acid and (b) the propagation process.

A representation of chain-growth polymerisation is shown in Figure 1.2. From this we can see that, although high chain lengths can be reached fairly rapidly, a lot of unreacted monomer is still present. However, in step-growth all monomer may be consumed rapidly, but molecular weights increase slowly.

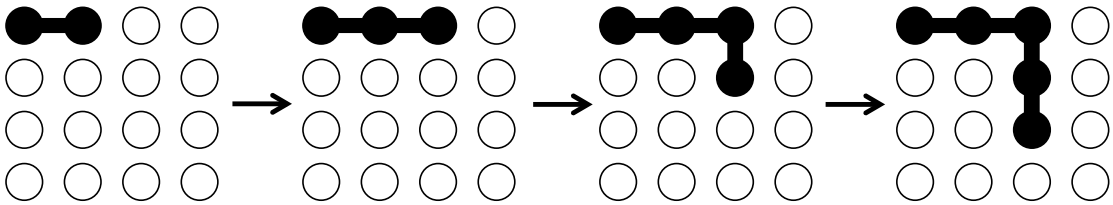

Figure 1.2. Schematic representation of chain-growth polymerisation. White dots represent monomer and black dots represent oligomer/polymer. (Figure from ref. 5).

All of the work presented in this thesis utilises chain-growth polymerisation. Chain growth allows chemists to design products, with the option to minimise termination reactions *via* so-called 'living' polymerisation.

1.4. 'Living' Polymerisation

A 'living' polymerisation is one in which termination does not occur on the timescale of polymerisation. Polymer chains propagate until all monomer present is consumed; however, polymers are described as 'living' because even after monomer

consumption, the ends of the chains remain active. This allows further polymerisation upon addition of more monomer. Although 'living' systems had been observed previously,[6] they were first defined as 'living' by Szwarc in 1956.[7] Due to the additional control 'living' polymerisation allows over the polymer composition, a number of different architectures are possible, including block copolymers, branched polymers (such as networks and ladders) and star polymers.[8]

This control comes from the ability to make polymer chains with pre-determined molecular weights, as the number-average degree of polymerisation (DP_n) is dependent on the initial monomer/initiator ratio, shown in eq (1). $\mathbf{[M]_o}$ and $\mathbf{[I]_o}$ represent the initial concentration of monomer and initiator respectively.

$$\textbf{Number average degree of polymerisation } (\mathbf{DP_n}) = \mathbf{[M]_o / [I]_o} \qquad (1)$$

Examples of 'living' polymerisation include both 'living' anionic and 'living' cationic polymerisation, ring opening metathesis polymerisation, and group transfer polymerisation. Another polymerisation method used to synthesise polymers with pre-determined DP_n is controlled radical polymerisation. This is sometimes known as 'living' radical polymerisation due to the precise macromolecular synthesis that is possible. However, as chain ends are in equilibrium between propagating radical chains and dormant species, these are not strictly 'living' systems. Controlled radical polymerisation (CRP) is discussed in more detail in section 1.5 below.

1.5. Controlled Radical Polymerisation

True 'living' polymerisations often require stringent reaction conditions, making the synthesis of these polymers difficult. One way to overcome this problem is *via* the use of transition metal catalysts in order to create an equilibrium between the polymer chain in both its active and dormant state. The lifetime of a propagating chain in its active state in a CRP process is comparable to the lifetime of a propagating chain in a conventional radical polymerisation; however, the equilibrium means that propagation is slowed. Propagation lifetimes can be extended from milliseconds to minutes or hours,[9] allowing a number of additional synthetic procedures, for example, chain-end functionalization or chain extension.[10] A number

of polymerisations employ this technique, two of the more widely used processes are known as atom transfer radical polymerisation (ATRP) and reversible addition-fragmentation chain transfer polymerisation (RAFT).

1.5.1. Atom Transfer Radical Polymerisation

The Sawamoto group and Wang and Matyjaszewski published work on this technique at a similar time, and both are now credited with its discovery.[11,12] Sawamoto and co-workers reported a controlled free radical polymerisation of methyl methacrylate catalysed by a ruthenium(II) complex, whereas Matyjaszewski and co-workers polymerised styrene using a copper catalyst. Both methods slow the rate of propagation, allowing individual polymer chains to grow at a similar rate, resulting in polydispersity indices <1.2. However, Matyjaszewski's method has become the more popular of the two, as the copper catalyst is more cost-effective than the ruthenium(II) catalyst used by the Sawamoto group. The mechanism of ATRP reported by Wang and Matyjaszewski is shown in Scheme 1.4.

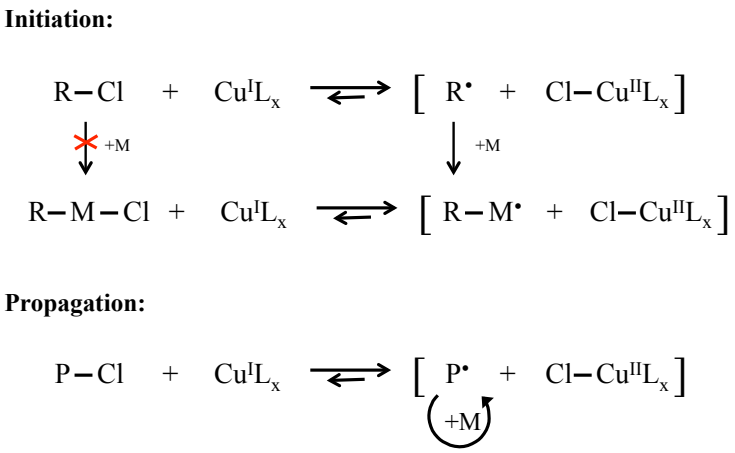

Scheme 1.4. Proposed mechanism of ATRP. The Cu catalyst removes the halogen (Cl) from the initiator (R-Cl), enabling addition of monomer (M). However, the removal of the halogen is reversible and addition of the Cl to the propagating chain (P) returns the polymer to its dormant state. (Scheme from ref. 12)

The initiator (R-Cl) contains a removable halogen atom, which is extracted by the Cu catalyst to form the oxidised species $Cu^{II}L_xCl$, generating a free radical species (R•). The free radical can then add to monomer (M) molecules initiating polymerisation. Slow propagation then occurs in the presence of this equilibrium. The equilibrium

must lie towards the formation of dormant chain ends in order to maintain a low concentration of polymer radicals, minimising termination reactions. Rapid exchange (activation and deactivation) enables controlled addition of monomer units, helping the propagating chains to grow at the same rate.

1.5.2. Reversible Addition-Fragmentation Chain Transfer Polymerisation

RAFT was first reported by Chiefari *et al.* in 1998.[13] RAFT is a radical polymerisation in the presence of an appropriate dithioester molecule (Z-C(=S)-S-R), which is known as a RAFT agent. The RAFT agent helps control polymerisation by consumption of the propagating radicals, however fragmentation releases another radical capable of reinitiating polymerisation. The resulting equilibrium between dormant and active polymer chains allows uniform chain growth.[14] The RAFT mechanism is outlined in Scheme 1.5.

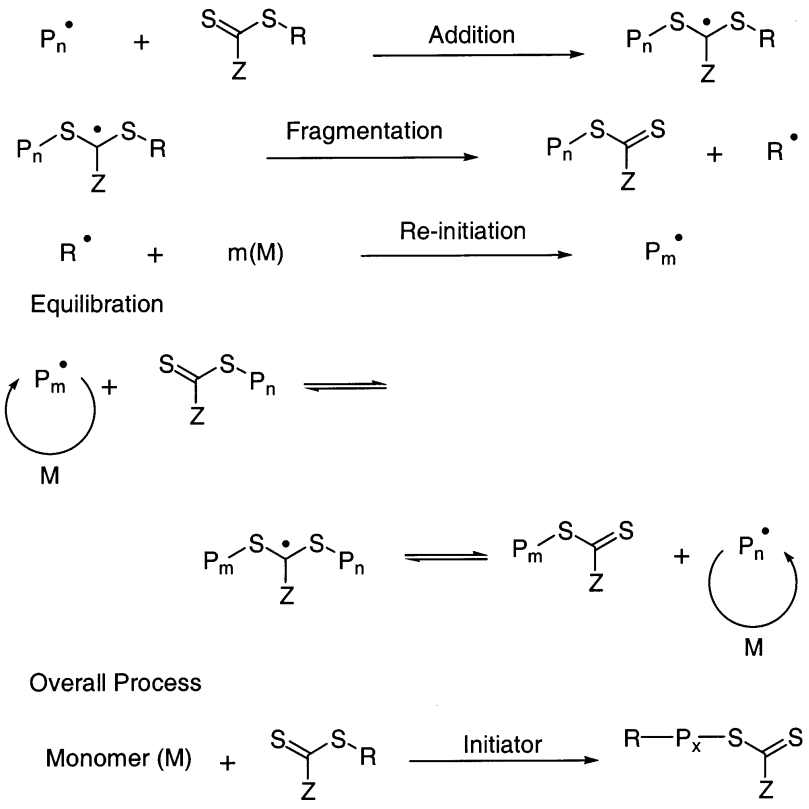

Scheme 1.5. Proposed mechanism of RAFT. P_n, P_m and P_x are polymer chains, M represents monomer and R is a radical capable of initiating polymerisation. (Scheme from ref. 14)

The nature of the Z and R groups is key to a successful polymerisation, the Z group should activate the C=S bond for radical addition, while the R group should be a stable leaving group that is also capable of re-initiating the polymerisation. Because of these criteria, RAFT agents have to be optimised for each monomer, and although RAFT can be used to polymerise a wide range of monomers,[14,15] the synthesis of copolymers can be difficult.

One method of polymerisation with less control is free radical polymerisation (FRP). However, FRP is a much more versatile approach to polymerisation due to its relatively non-specific nature. As free radical is the only form of polymerisation used in this thesis, it shall make up the bulk of the polymer discussion of this introduction.

1.6. Free Radical Polymerisation

Free radical polymerisation is a chain-growth process, with the polymer being formed *via* the successive addition of monomer building blocks to the growing chain end. Vinyl polymers are the most commercially important polymers as they have a vast number of commercial applications, including usage in packaging, insulation, clothing, construction and cosmetics. Structures such as polystyrene, polyethylene, poly(acrylic acid) and poly(vinyl chloride) (PVC) are just a few notable examples. Unlike other methods of polymerisation, such as ionic, free radical polymerisation can be applied to a wide range of monomers. The process is quite robust, showing more tolerance to impurities and monomer functionality, as well as being relatively cheap. For these reasons, vinyl polymers are predominantly produced commercially using free radical processes.

As mentioned in 1.3, chain-growth polymerisation involves five main steps, each of which is important to consider when designing a polymerisation.

1.6.1. Decomposition and Initiation

Free radical initiation involves the production of primary radicals *via* decomposition, followed by the addition of these radicals to the vinyl monomer, both shown in Scheme 1.6.

Decomposition:

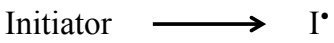

Initiation:

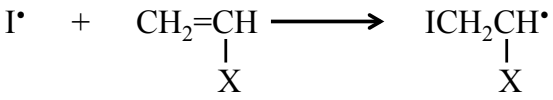

Scheme 1.6. Schematic of decomposition and initiation. I• is a radical capable of initiating polymerisation of monomer CH_2=CHX.

Some monomers, notably styrene,[16] often only require heating and do not need added free radical initiators in order to undergo polymerisation. However, in the majority of systems the addition of an initiator is required. Compounds providing the triggerable production of radicals can be used as initiators. The majority of initiators can be grouped into four categories. These are azo compounds,[17] peroxides (ROOR) and hydroperoxides (ROOH),[18] redox initiators and photoinitiators. Ionising radiation, for example α- and β-particles or γ- and x-rays, can also be used to generate radicals by random destruction, although this is much less common and only used in special cases.[19]

Thermal decomposition to form free radicals is the most common method of initiation, with peroxides, hydroperoxides and azo compounds all falling under this category. One of the most widely used peroxides is benzoyl peroxide, the decomposition of which is shown in Scheme 1.7. Peroxides are the most widely used initiators in industrial processes, as the large structural variation provides a wide range of decomposition temperatures. The differences in decomposition rates of initiators can be expressed in term of the initiator half-life ($t_{1/2}$), which is the time it takes for the concentration of the initiator to decrease to half of its original value. Variation in $t_{1/2}$ between initiators is due to differences in chemical structure, and the stabilities of the radicals produced on decomposition.[20] The more stable the initiator, the higher the $t_{1/2}$. Likewise, the more stable the resulting free radical, the lower the $t_{1/2}$. Initiators are commonly compared by quoting the temperature at which $t_{1/2}$ = 10 hours or 1 hour.

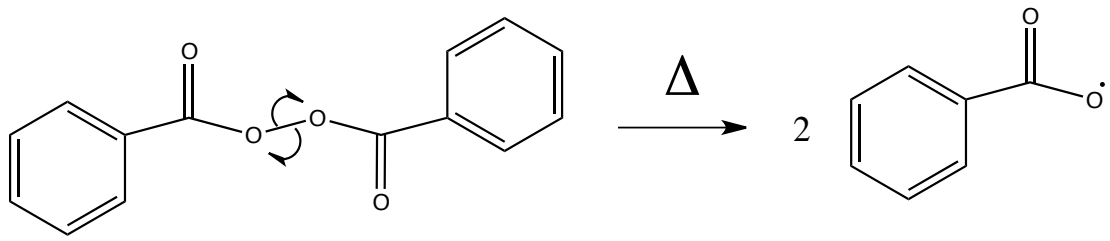

Scheme 1.7. Thermal homolysis of benzoyl peroxide to yield two benzoyloxy radicals.

Higher temperatures coupled with the release of N_2 drive the decomposition of azo compounds in radical formation. A common azo initiator, used throughout this piece of work, is azobisisobutyronitrile (AIBN), shown in Scheme 1.8. AIBN is usually decomposed at around 70 ^{o}C, where it has a half life of 4.8 hours.[20]

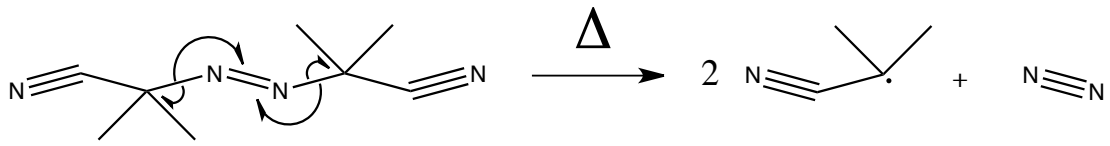

Scheme 1.8. Thermal decomposition of AIBN to give free radicals, driven by the formation of N_2.

1.6.2. Kinetics of Decomposition and Initiation

As initiation occurs in two steps, two rate constants are needed, one representing decomposition (2) and one for initial monomer addition (3).

$$\text{Initiator} \xrightarrow{k_{dec}} \text{I}\bullet \qquad (2)$$

$$\text{I}\bullet + \text{M} \xrightarrow{k_{add}} \text{P} \qquad (3)$$

$$R_i = \frac{d[I\bullet]}{dt} = 2 f k_{dec} [I] \qquad (4)$$

As (2) is a slow process in comparison to (3), this becomes the rate-determining step. Therefore in the rate equation, (4), $\mathbf{R_i}$ is the rate of initiation, **I•** is the initiating radical, and **f** is the initiator efficiency.

1.6.3. Propagation and Chain Transfer Reactions

Propagation occurs relatively quickly upon initiation, due to the inherent reactivity of the radicals formed. Addition of a monomer radical to another monomer molecule is the first step of propagation (Scheme 1.9(a)). Monomer molecules then continue to add to the end of the chain (hence chain-growth) (Scheme 1.9(b)), until all monomer is consumed or termination occurs.

Propagation:

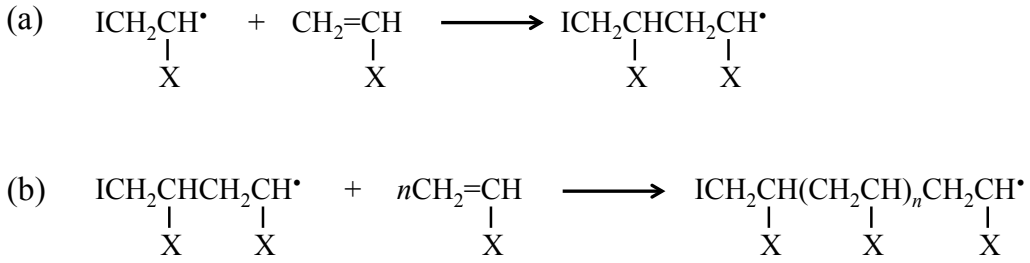

Scheme 1.9. (a) First step of propagation of monomer CH_2=CHX after initiation by I, (b) chain-growth of CH_2=CHX

Propagation usually results in head-to-tail addition (as in Scheme 1.9(a)) due to both steric and electronic effects, although cases have been reported in which head-to-head addition may occur to some extent.[21-23] A number of reactions, known as chain transfer reactions (CTR), can take place in this system when the propagating radical does not show high regioselectivity towards the monomer vinyl bond. CTRs involve radical transfer from the end of the growing polymer chain to another species. This can lead to shorter chain lengths and polymers with branched architecture, resulting in lower molecular weights and broader molecular weight distributions. For this reason, CTRs can be purposefully utilised to regulate the mean chain length by the addition of chain transfer agents (CTA), something discussed in greater detail in section 1.7. A number of examples of CTRs are shown in Scheme 1.10 for polyethylene. Both Scheme 1.10(b) and (c) lead to polymers with branched architecture, while (a) leads to shorter chain lengths.

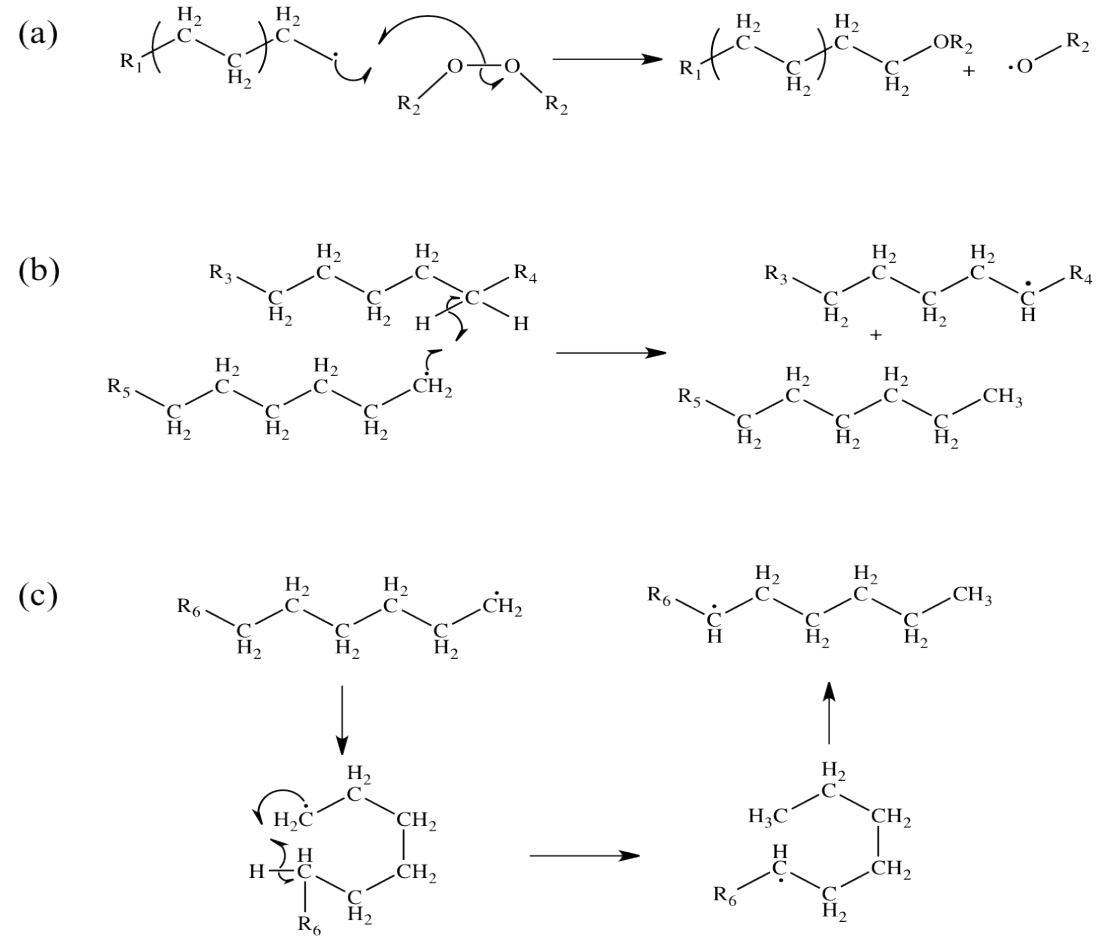

Scheme 1.10. Schematic showing undesirable chain transfer reaction such as, (a) with initiator molecules, (b) hydrogen abstraction from another polymer chain, and (c) backbiting, again hydrogen abstraction but this time from the propagating chain itself.

1.6.4. Kinetics of Propagation

The propagation step can be defined kinetically as:

$$P_n\bullet + M \xrightarrow{k_p} P_{n+1}\bullet \qquad (5)$$

$$R_p = \frac{-d[M]}{dt} = k_p[M][P\bullet] \qquad (6)$$

So in the rate equation, (6), $\mathbf{R_p}$ is the rate of propagation, **M** is monomer, and **P•** is the polymer radical. The rate of polymerisation is essentially dependent on the rate of propagation.

1.6.5. Termination

Termination is the cessation of propagation and occurs in all radical polymerisations. There are two standard types of termination, known as combination and disproportionation. Combination involves the coupling of two radicals to form a new covalent bond. This can involve two propagating chains (Scheme 1.11(a)), or combination of a propagating chain with an initiator fragment (Scheme 1.11(b)), both of which result in the linear polymer having an initiator group at each end of the chain.

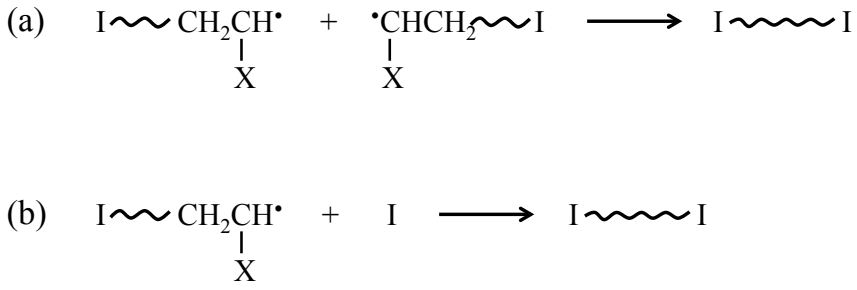

Scheme 1.11. The combination of two radicals, or coupling, to form a new covalent bond (a) two propagating chains and (b) a propagating chain with an initiator fragment.

Disproportionation involves the transfer of one atom from one polymer radical to another, similar to hydrogen abstraction in CTR but without generation of another free radical species (Scheme 1.12). Which termination mechanism prevails depends on the monomer type and the reaction conditions,[24] but it is usually assumed that both processes are occurring.[4] Disproportionation results in only one initiator group per chain, but forms a vinyl group in one of the chains that can then polymerise.

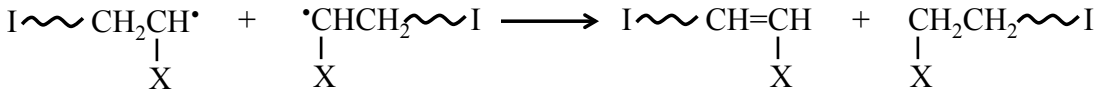

Scheme 1.12. Disproportionation between two chains by hydrogen abstraction.

1.6.6. Kinetics of Termination

As there are two possible types of termination, see (7) & (8) overleaf, the kinetics need to account for this.

$$P_n\bullet + P_m\bullet \xrightarrow{k_{ta}} P_{n+m} \quad (7)$$

$$P_n\bullet + P_m\bullet \xrightarrow{k_{tb}} P_n + P_m \quad (8)$$

Therefore termination can be defined as:

$$R_t = \frac{-d\,[P\bullet]}{dt} = 2\,k_t\,[P\bullet]^2 \quad (9)$$

In (9) $\mathbf{R_t}$ represents the rate of termination and $\boldsymbol{k_t} = k_{ta} + k_{tb}$, the overall rate of termination for both disproportionation and coupling.

1.6.7. Average Kinetic Chain Length

The average kinetic chain length, v, is defined as the average number of monomer units polymerised per chain initiated, which is equal to the rate of polymerisation (essentially the rate of propagation, R_p) divided by the rate of initiation, R_i.[4] Kinetic studies of free radical polymerisation tend to assume that the rate of initiation and termination are identical shortly after the reaction has begun. This is known as the 'steady-state' assumption, which allows us to assume that the concentration of polymer radicals, $[P_n\bullet]$, remains constant. From this it can be deduced:

$$v = \frac{R_p}{R_t} \quad (10)$$

Substituting R_p and R_t from equations (6) and (9) respectively:

$$v = \frac{k_p\,[M]}{2\,k_t\,[P\bullet]} \quad (11)$$

1.6.8. Kinetics of Chain Transfer Reactions

Deviations from predicted kinetic behaviour can arise from CTRs. As they play a key role as CTAs in the polymer synthesis conducted in this thesis, it is necessary to adjust the kinetic chain length, v, to account for these changes. Therefore the kinetic chain length, v_{tr}, shall be defined as the ratio of propagation rate to the combined rates of termination and transfer, hence

$$v_{tr} = \frac{R_p}{R_t + R_{tr}} \quad (12)$$

Where $\mathbf{R_{tr}}$ is the rate of transfer reactions. As transfer reactions are second order, if **T** is the transfer agent then R_{tr} can be expressed as:

$$R_{tr} = k_{tr}[P\bullet][T] \quad (13)$$

Therefore the expression for v_{tr} taking into account all possible transfer reactions is:

$$v_{tr} = \frac{k_p[M][P\bullet]}{2k_t[P\bullet]^2 + \Sigma k_{tr}[P\bullet][T]} = \frac{k_p[M]}{2k_t[P\bullet] + \Sigma k_{tr}[T]} \quad (14)$$

Remembering equation (11), the reciprocal of (14) is:

$$\frac{1}{v_{tr}} = \frac{1}{v} + \frac{\Sigma k_{tr}[T]}{k_p[M]} \quad (15)$$

The ratio of the transfer rate constant to the rate constant for propagation is known as the chain transfer constant, C_t:

$$C_t = \frac{k_{tr}}{k_p} \quad (16)$$

Substituting (16) into (15), we arrive at:

$$\frac{1}{v_{tr}} = \frac{1}{v} + \frac{\Sigma C_t[T]}{[M]} \quad (17)$$

From (17) it can clearly be seen that, as the rate of transfer and the concentration of the CTA are increased, the kinetic chain length becomes smaller, resulting in lower molecular weight polymers. By using different CTAs, the chain transfer constant, C_t, can be varied.

1.7. Chain Transfer Agents

Thiols, or mercaptans are probably the most common group of CTAs in radical polymerisation.[25] Thiols undergo reaction with radicals *via* the transfer of a hydrogen atom, forming a saturated chain end and generating a thiyl radical (Scheme 1.13).[25] A chain transfer agent is added to give controlled chain transfer reactions, which allows some degree of manipulation over polymer end groups and molecular weight.

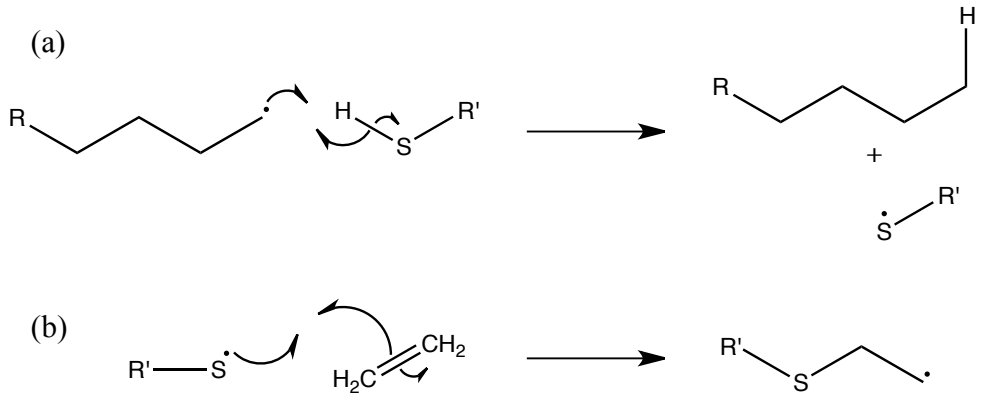

Scheme 1.13. A chain transfer process involving a thiol CTA, (a) abstraction of H and transfer of radical onto S group, (b) CTA behaving as an initiator and 'transferring' the radical to start a new polymer chain.

As mentioned in 1.6.8, the choice of CTA is important due to each species having a unique chain transfer constant (C_t). The C_t is essentially a measure of the reactivity of a CTA and therefore an insight on its effect on reducing a polymer's molecular weight.[26] It can be seen in equation (16) that $C_t = k_{tr}/k_p$. In a normal polymerisation, the rate constant of propagation is much larger than the rate constant of transfer ($k_p >> k_{tr}$), making C_t a small number. However, this effect is not detrimental to resulting chain lengths if the rate of reinitiation is rapid (case 1 in Table 1.1). C_t becomes large if the rate of transfer is much greater than the rate of polymerisation ($k_{tr} >> k_p$). If C_t becomes too large, telomers ($DP_n \approx 1 - 5$) are formed (case 2 in Table 1.1). The rate of reinitiation, k_a, displayed by the CTA should be comparable to that of the original propagating radical. If $k_p > k_a$, retardation of the polymerisation will occur as the CTA is a less efficient initiator (cases 3 and 4 in Table 1.1).

Table 1.1. Effect of chain transfer on R_p and DP_n. (Table from ref. 20)

Case	Relative Rates Constants for Transfer, Propagation and Reinitiation		Type of Effect	Effect on R_p	Effect on DP_n
1	$k_p >> k_{tr}$	$k_p \approx k_a$	Normal chain transfer	None	Decrease
2	$k_p << k_{tr}$	$k_p \approx k_a$	Telomerisation	None	Large decrease
3	$k_p >> k_{tr}$	$k_p > k_a$	Retardation	Decrease	Decrease
4	$k_p << k_{tr}$	$k_p > k_a$	Degradative chain transfer	Large decrease	Large decrease

As well as playing a crucial role in the synthesis of the polymer, chain transfer agents can also be used to impart functionality to the polymer chain ends. Many examples of this have been successful, including synthesis of epoxy-terminated polymers[27] and polymers capable of linking to biomolecules through their CTA.[28] CTAs are also used to increase hydrophilicity or hydrophobicity, sometimes contributing toward amphiphilicity, in order to create surface active-polymers.[29]

1.8. Branched Polymers

Polymers come in many different structural forms, both compositionally and architecturally. It is possible to describe polymers as linear, branched or a network, with a number of different structures already falling under the branched category. Some of the more common structures are shown in Figure 1.3.

Many forms of branched polymer have been reported in the literature, including dendrimers,[30,31] comb polymers,[32] star polymers[33] and hyperbranched polymers.[34,35] However, many of these materials are restricted to just a few structures as they may require multiple steps and/or difficult synthesis. The first report of hyperbranched polymers by the polycondensation of AB_2 monomers was by Kim and Webster in 1990.[36] Their work was further simplified by Fréchet and co-workers, who produced a more generic approach to hyperbranched polymers using self-condensing vinyl polymerisation (SCVP). Fréchet's method involved an AB monomer which provided a branching point every time a new monomer was added to the polymer chain. Fréchet and co-workers performed SCVP using many methods, such as controlled radical polymerisation, 'living' cationic polymerisation and group transfer.[37,38] Although these methods provided a number of different routes to highly

branched materials, the vinyl monomers that formed these polymers had been tailored to allow "self-condensation" (Scheme 1.14).

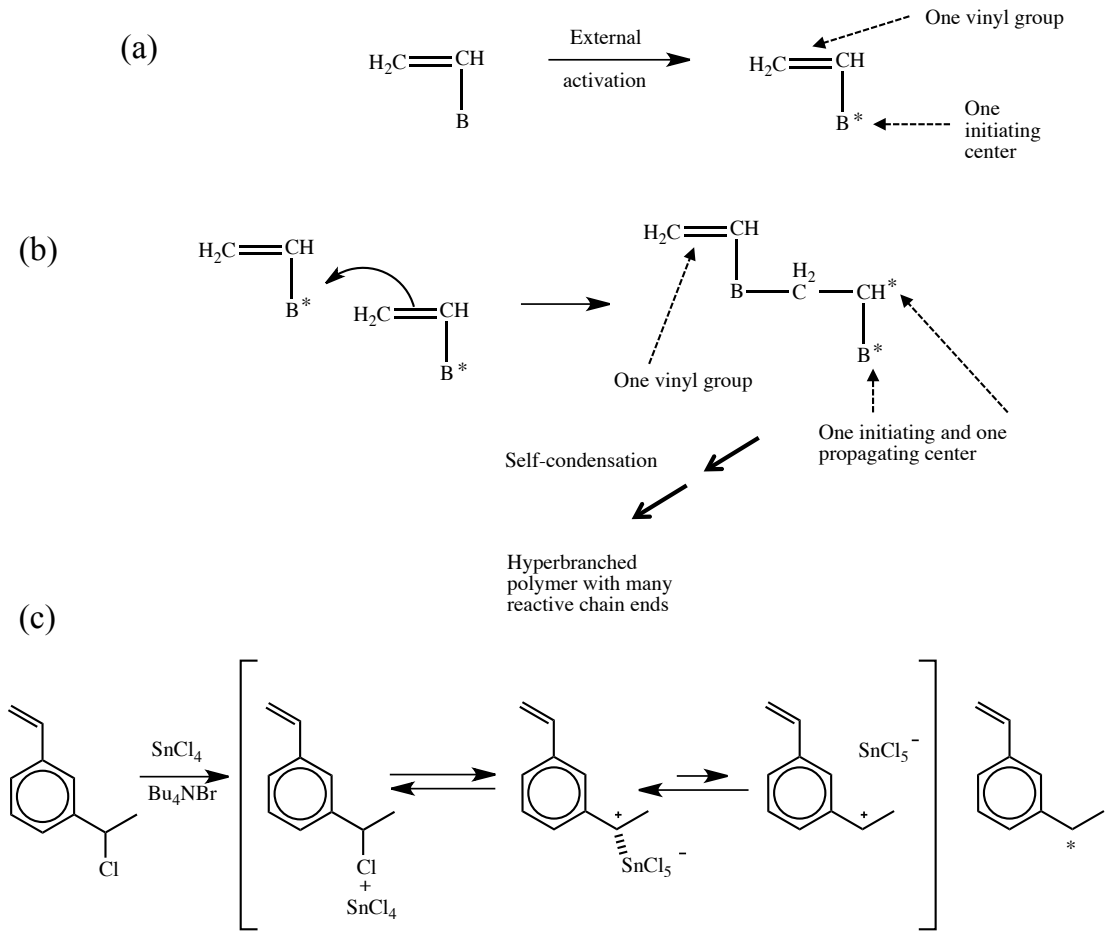

Scheme 1.14. (a) Basic concept of SCVP monomers with two active groups, (b) polymerisation is initiated at B*, resulting in a new initiating centre, a propagating centre and a vinyl group, which are all capable of polymerisation. (c) An example of an AB monomer used in SCVP, with tin(IV) chloride as an activator. (Scheme from ref. 38)

This then hinders the addition of added functionality to the resulting polymer, as it requires specific structural aspects in the monomer to allow branching. A number of other routes to branching by SCVP have been successful, such as using ATRP,[39] but none of these systems provide a general method for the simple branching of vinyl monomers, and generally require the use of specific, or specialised monomers.

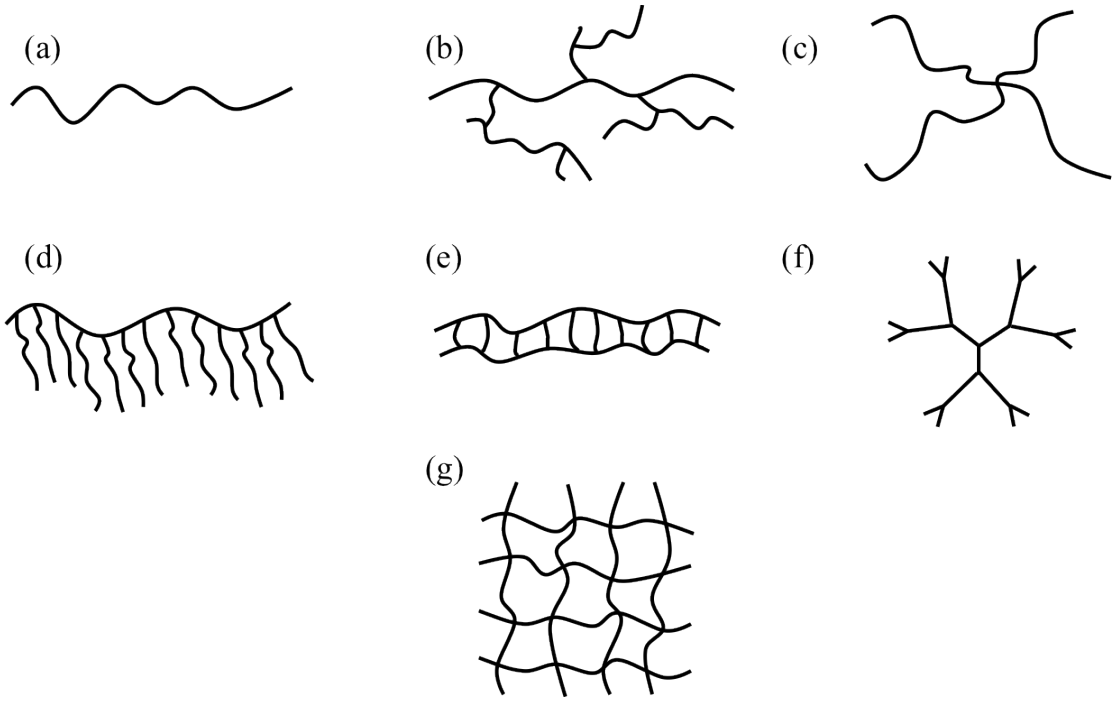

Figure 1.3. Representations of polymers with varied architecture. (a) Linear, (b) branched, (c) star, (d) graft or comb, (e) ladder, (f) dendrimer and (g) a network.

In 2000, Sherrington and co-workers produced a much more versatile and cost-effective route for the synthesis of branched vinyl polymers.[40] The methodology involved in the 'Strathclyde approach' is essentially free radical polymerisation with a branching agent (usually a bifunctional monomer) and a CTA. The addition of a CTA inhibits gelation by reducing the primary chain length. This prevents the formation of a network upon branching and allows the synthesis of soluble, branched vinyl polymers. In free radical polymerisation, the addition of only a very small amount of bifunctional monomer usually results in a cross-linked network.[41] An idealised representation of the 'Strathclyde approach' is shown in Figure 1.4 and compared to the same reaction in which the CTA is not present.

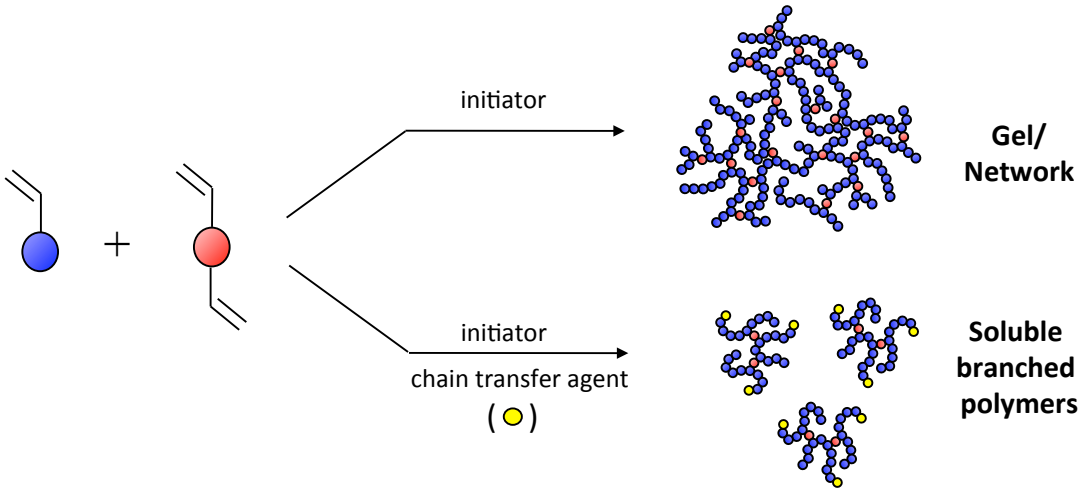

Figure 1.4. Schematic represent free radical polymerisation with bifunctional monomer (top) and the same system with an added chain transfer agent (bottom). CTA prevents gelation and produces soluble branched polymers.

As this method of polymerisation is relatively uncontrolled and branching is statistical, broad molecular weight distributions are achieved. However, Armes and co-workers have published examples of this branched polymer synthesis using controlled polymerisation techniques, allowing control over the primary chain length.[42,43] One particular report showed the synthesis of poly(2-hydroxypropyl methacrylate) (PHPMA) with a disulphide- based dimethacrylate branching agent, which could later be cleaved, resulting in polymers comparable to that of linear PHPMA.[44] This was a good demonstration of not only how successful branching was in these systems, but also how well the polymer backbone chain length could still be controlled using ATRP.

1.9. Copolymers

A copolymer is made up of two or more different monomeric units, whereas a homopolymer is a polymer that consists of a single monomer repeating unit. Copolymers can exist in a number of different architectures, including statistical copolymers,[45] alternating copolymers[46] and block copolymers.[47] A number of examples are shown in Figure 1.5, with A and B representing two structurally different monomers. Statistical copolymers are formed when the monomer units are statistically distributed, whereas alternating copolymers consist of alternating

monomers. Block copolymers are made up of 'blocks' of monomers and graft polymers[48] consist of one monomer branching from the backbone of another.

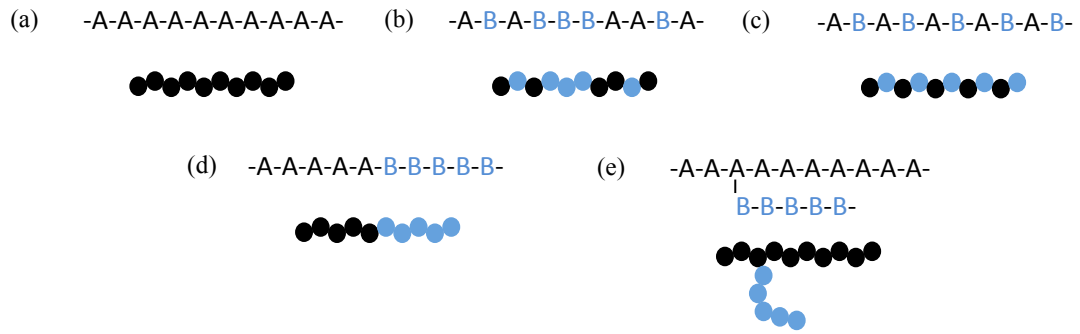

Figure 1.5. An array of copolymer compositions and architectures (with the exception of homopolymer (a), shown for ease of comparison). (b) Statistical copolymer, (c) alternating copolymer, (d) block copolymer and (e) graft copolymer.

Copolymerisation allows multi-functionality within one polymer molecule, which has led to many interesting properties in the literature, including surface functionality and micelle formation,[49-52] self-assembly,[53,54] encapsulation and drug delivery.[55,56] Many of these polymers are amphiphilic, that is both hydrophilic and hydrophobic in parts, which drives the self-assembly processes in aqueous solution involved in block copolymer application.

1.10. Responsive Polymers

Polymers found in nature, for example proteins and deoxyribonucleic acid (DNA), are capable of highly cooperative interactions, which are crucial in living organisms. The field of responsive polymers in synthetic chemistry is huge, with many different systems being designed to mimic only a fraction of biopolymers selectivity and functionality. Synthetic polymers have been designed to respond to many external stimuli, so-called 'smart' polymers.[57] Some of these include responsiveness to temperature,[58-61] pH,[62-64] glucose[65] and antigens.[66]

Weaver *et al.* used the 'Strathclyde approach' to create 'smart' pH-responsive branched polymer nanoparticles (PRBNs).[67] These nanoparticles consisted of poly(ethylene glycol) methacrylate (PEGMA) (M_n = 1,100 Da) and (2-diethylamino)ethyl methacrylate (DEAEMA) in a 5:95 molar ratio, roughly 1:1 when

considering the ratio of ethylene glycol (EG) repeat unit to DEAEMA comonomer. The brancher (ethylene glycol dimethacrylate (EGDMA)) and CTAs (1-dodecanethiol (DDT) and 1-thioglycerol (TG)) were varied throughout the series of copolymers in order to examine how varying the copolymer architecture influences the pH-responsiveness. In all cases, under acidic conditions, when the DEAEMA units are protonated, the cationic copolymers readily dissolved in water. Upon raising the pH, the PDEAEMA is deprotonated, (Scheme 1.15) and becomes hydrophobic. Light scattering confirmed that upon this switch to basic conditions, the hydrodynamic radius decreased significantly (from 45 nm to 25 nm) due to the formation of DEAEMA-based hydrophobic cores. Variation of chain-end hydrophobicity and degree of branching throughout these copolymers affected the apparent pK_a of the polymerised DEAEMA residues, providing the ability to tune pH-responsiveness of the nanoparticles.

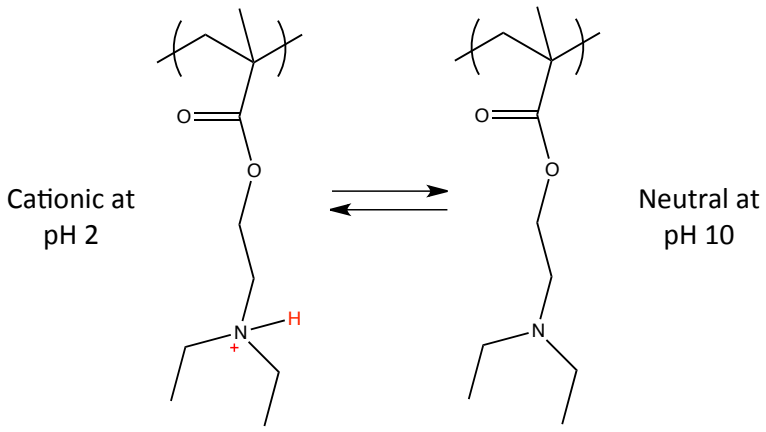

Scheme 1.15. Schematic showing pH responsiveness of PDEAEMA, switching from hydrophilic at low pH to hydrophobic at high pH.

1.11. Emulsions

Emulsions are metastable colloids consisting of two immiscible fluids, one being dispersed throughout the other, usually in the form of spherical droplets.[68] Emulsions are important materials in the formation of many products and formulations, and can be used as useful templates for the synthesis of complex materials.[69-74] Some of these examples involve the isolation of reaction solutions and the reproducible synthesis of nanocrystals and colloidal particles, which will be discussed further in Chapter 6.

Droplet diameters can range from <1 μm[75] (so called mini- or nano-emulsions) to >100 μm.[76,77] The immiscible fluids that make up emulsion systems are usually stabilised *via* the reduction of interfacial tension at the liquid-liquid interface. Interfacial tension arises due to the fact that molecules at a liquid-liquid interface are exposed to a different environment to the same molecules in the bulk of the liquid phase; a simplified schematic of this phenomenon is shown in Figure 1.6. This differs from surface tension, which is a measure of the energy at the interface of a gas and a liquid.

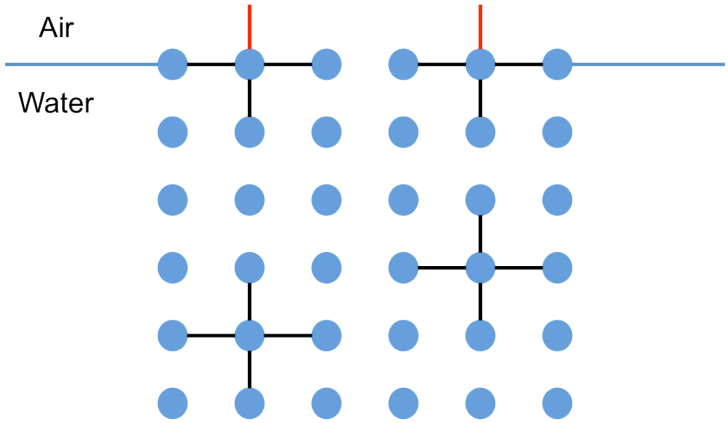

Figure 1.6. A simplified schematic of the cause of interfacial tension. Molecules in the bulk have four binding interactions (black), whereas at the surface they only have three. This imbalance caused by the lack of an interaction (red) results in a rise in energy at the air/water interface.

Molecules at the interface will exhibit a lower binding energy to molecules in the bulk, which manifests itself as interfacial tension, which may be defined as energy per unit of area of the interface at a fixed temperature and pressure. Surfactants reduce interfacial tension as they position themselves at the interface, reducing this imbalance of forces between the two liquid surfaces. A wide range of surface-active agents, or surfactants, are capable of this, for example small molecule surfactants (Figure 1.7(a)),[78,79] particulate surfactants[80,81] (Figure 1.7(b)) and polymeric surfactants (Figure 1.7(c)).[52,82] As most emulsions contain an aqueous phase, they are usually described as oil-in-water (o/w) or water-in-oil (w/o), denoting the dispersed phase and the continuous phase respectively.

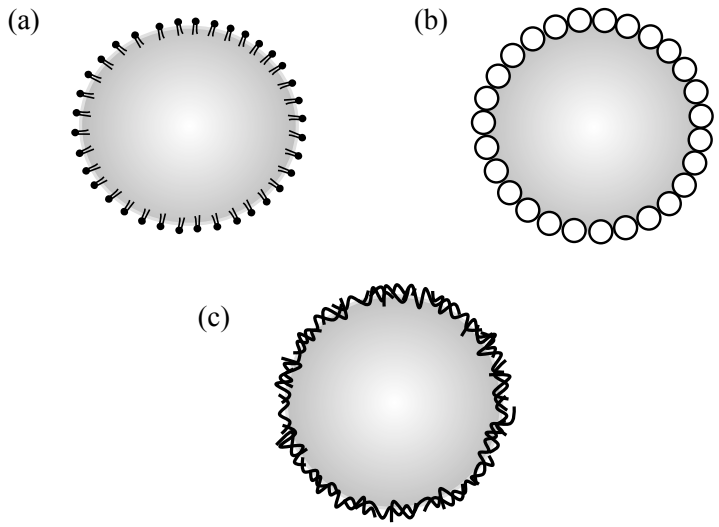

Figure 1.7. Schematic representations of emulsions stabilised using different materials, (a) small molecule surfactants, (b) particulate surfactants and (c) polymeric surfactants.

By reducing interfacial tension, surfactants can prevent droplets from coalescing, resulting in stable emulsions. With time, emulsions will destabilise in order to reduce surface tension because they are thermodynamically unstable.[83] Thermodynamic instability arises from the fact that coalescence increases entropy within the system meaning that, with time, coalescence is more favourable than the droplets remaining dispersed. Water molecules are ordered to minimise interactions with hydrophobic molecules, in this case the oil phase. As the contact area between the water and oil phases is greatly increased in an emulsion system, so is the ordering of the water molecules. Therefore, coalescence leads to a less ordered water phase, giving rise to an increase in entropy in the system. Instability is more common for small molecule surfactant-stabilised emulsions, as adsorption of molecules to the droplet surface is reversible, so interfacial tension cannot be reduced close to zero. Emulsions have four main potential instability mechanisms, some of which may occur simultaneously.[83] These include:

- Sedimentation or creaming (Figure 1.8(a))
- Coalescence (Figure 1.8(b))
- Flocculation (Figure 1.8(c))
- Ostwald ripening (Figure 1.8(d))

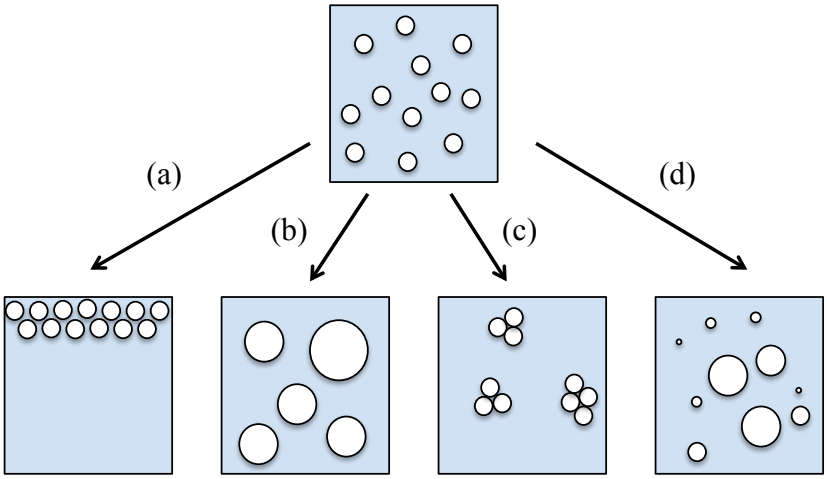

Figure 1.8. Different forms of emulsion instability, (a) creaming, (b) coalescence, (c) flocculation, (d) Ostwald ripening.

Creaming is the migration of an emulsion's dispersed phase due to differences in droplet density compared to the continuous phase. Coalescence is the combination of two or more dispersed droplets to form larger droplets. Flocculation is the clustering of droplets without coalescence; however, flocculation is the initial step in coalescence. Ostwald ripening involves the migration of the dispersed phase from the surface of small droplets to join larger ones and is more common in w/o emulsions. This can be brought about by the dispersed phase having a relatively low solubility in the continuous phase, permitting migration through the continuous phase. As a result of Ostwald ripening, a reduction in interfacial area is observed.

When creating an emulsion system with desired properties, the choice of surfactant not only dictates droplet size, but also plays a role in the resulting emulsion's stability.

1.11.1. Small Molecule Surfactants

The majority of industrial emulsions are typically stabilised using small molecule surfactants. Most of these surfactants are amphiphilic organic compounds, usually containing a hydrophilic 'head' and a hydrophobic 'tail'. In an emulsion, the hydrophilic component of the surfactant will preferentially reside in the water phase and the hydrophobic component in the oil phase. The resulting reduction in interfacial tension, allows an immiscible liquid to stay dispersed as droplets. These surfactants are usually classed as either ionic (such as anionic, cationic and amphoteric) or nonionic. Nonionics are surfactants that carry no charge in the

predominant working range of pH.[84] Most nonionics comprise alcohols, polyethers and esters. An example of a common nonionic surfactant is polysorbate 80 (or Tween 80), which is shown in Figure 1.9.

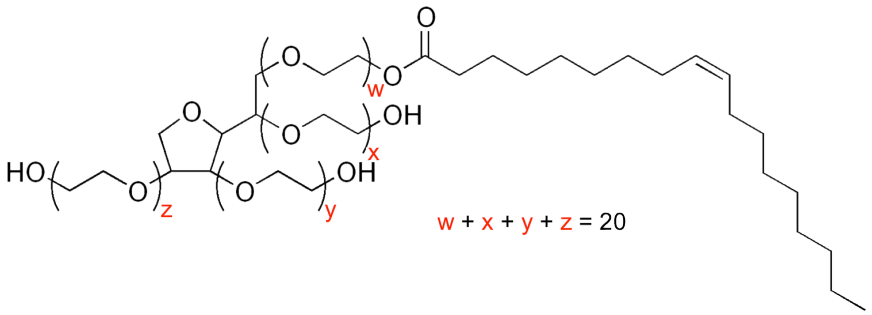

Figure 1.9. Structure of polysorbate 80, or Tween 80.

Of the ionic surfactants, anionic is commercially the most important. They are often named "detergents" and make up roughly 75 % of the world surfactant market, due to their applications in soaps.[84] They consist of an anionic hydrophilic head and a hydrophobic (usually a hydrocarbon chain) tail. A common example of an anionic surfactant is sodium dodecyl sulfate (SDS), shown in Figure 1.10.

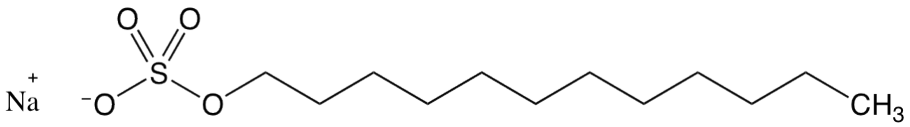

Figure 1.10. Structure of sodium dodecyl sulfate.

Small molecule surfactants do not adsorb strongly onto droplet surfaces. In contrast, particulate surfactants can have high interfacial energies of attachment and are able to form stable and reproducible emulsions.[81,85]

1.11.2. Particulate Surfactants

Particulate surfactants tend to give larger emulsion droplets as the particles are usually a few microns in diameter.[81] Studies have shown that larger particles leads to an increase in droplet size.[76] Control over the type (o/w or w/o) of emulsions and coalescence stability can also be determined by varying the inherent hydrophobicities of the particulate surfactants.[86] These emulsions are known as Pickering emulsions, named after S. U. Pickering, who first described emulsion droplets stabilised using

solid particles in 1907.[80] However, they were first recognised in 1903 by W. Ramsden.[87] Particles form emulsions *via* a reduction in interfacial tension, driving adsorption at the liquid-liquid interface. The type and stability of resulting liquid-liquid Pickering emulsions is determined by the particle contact angle, θ. If θ (with respect to the water phase) is $<90^{o}$ then the particles are deemed hydrophilic and stabilise an o/w emulsion, whereas if θ is $>90^{o}$, particles are more hydrophobic and stabilise a w/o emulsion. This allows good control over emulsion production by tuning the hydrophilicity of particle surfaces.[86] Particles used to form Pickering emulsions usually show partial hydrophilicity or hydrophobicity, not amphiphilicity. However, so-called Janus particles are able to exhibit amphiphilicity due to their surfaces having two or more physical properties in distinct areas.[88] These areas can exhibit different wettability, resulting in amphiphilic particles.[89] Figure 1.11 compares the adsorption of both particles with uniform wettability (a) and Janus particles (b). As particulate emulsifiers usually have large interfacial energies of attachment, large energies are required to desorb particles, thus Pickering emulsions tend to be much more stable than small molecule surfactant emulsions. Particles have been used to give droplet surfaces some functionality, and can lead to other structures, such as colloidosomes.[74]

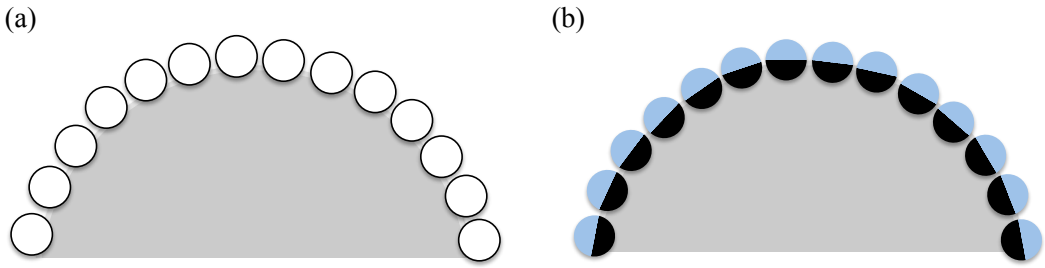

Figure 1.11. Schematic of Pickering emulsions stabilised by (a) particles with uniform wettability and (b) amphiphilic Janus particles with both a hydrophilic (blue) and a hydrophobic (black) component.

1.11.3. Polymeric Surfactants

Polymeric surfactants, although less well-defined than small molecule surfactants, probably offer greater opportunity in terms of diverse, functional materials.[52] Polymers can be surface-active due to their amphiphilic properties, like small molecule surfactants, and are widely used in the food and pharmaceutical industries.

Common examples of a polymeric surfactant are ethylene oxide and propylene oxide diblock and triblock systems.[90] These A-B and A-B-A block copolymers provide hydrophilic and hydrophobic blocks, represented as blue and black respectively in Figure 1.12(a) and (b).

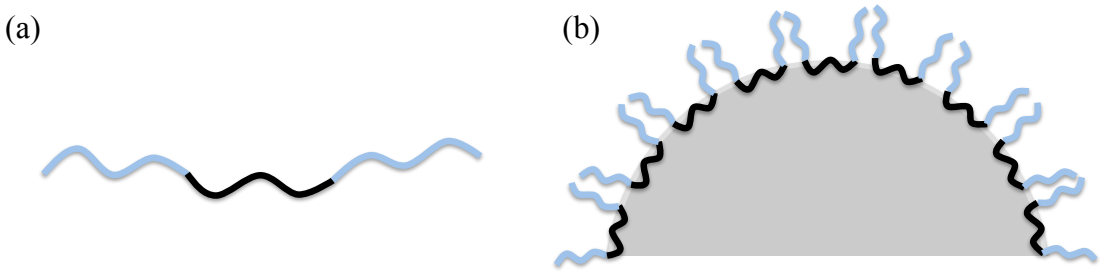

Figure 1.12. Schematic of (a) a triblock hydrophilic-hydrophobic-hydrophilic copolymer and (b) how this polymer may stabilise an o/w emulsion.

1.11.4. Responsive Surfactants

Responsive surfactants have received a lot of attention in recent years due to the fact that responsiveness can be transferred from a surfactant to the surface of an emulsion droplet. Responsiveness on emulsion surfaces comes in many forms, including surfactant sensitivity to pH,[91,92] temperature,[93] CO_2[94] and light.[95,96] In one of these examples, Armes and co-workers developed poly(4-vinylpyridine)/silica (P4VP/SiO_2) nanocomposite microgels *via* free radical polymerisation, which could be employed as pH-responsive particulate emulsifiers in a number of emulsions, including both o/w and w/o systems (Figure 1.13).[92]

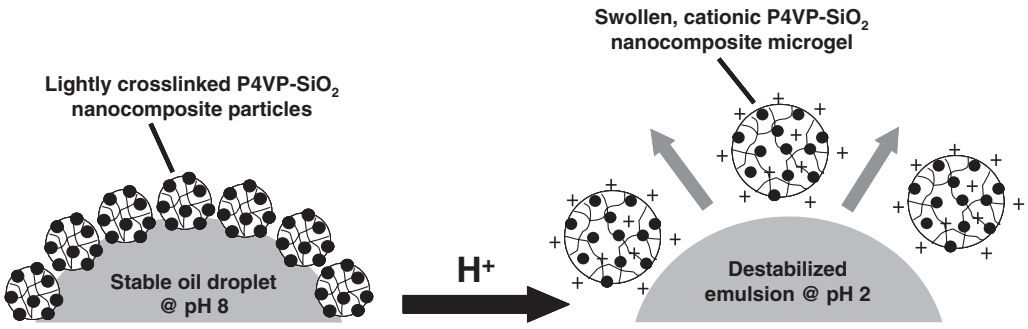

Figure 1.13. Schematic of pH triggered desorption of P4VP/SiO_2 microgels, leading to demulsification of an oil in water system. (Figure from ref. 92).

Protonation of the P4VP in the particles upon lowering the pH leads to cationic, swollen structures. The hydrophobic P4VP then becomes much more hydrophilic, and the particles more microgel-like, leading to demulsification due to desorption of the particles from the liquid-liquid interface. Further work was done by the Armes group on pH-responsive surfactants, this time using shell cross-linked (SCL) micelles.[91] This work drew inspiration from the pioneering work on SCL particles by Wooley and co-workers,[97-99] and once again achieved triggerable demulsification *via* a change in pH. The SCL micelle core was composed of hydrophobic DEAEMA blocks, which upon lowering the pH were protonated at the tertiary amine, allowing the core to become hydrophilic due to its cationic nature, triggering demulsification.

In 1998, Mathur *et al.* synthesised a pH-responsive graft (or comb) type polymer consisting of a poly(methacrylic acid) (PMAA) backbone with short grafts of poly(ethylene glycol) (PEG).[90] These units were selected as the literature reported a triggerable hydrogen-bonding capability between the repeating EG unit and the methacrylic acid (MAA) functional groups in solution.[100,101] The polymer Mathur *et al.* had developed was hydrophilic at high pH, but developed hydrophobic segments when the pH was lowered, due to hydrogen bonding between the methacrylic acid and the ethylene glycol repeat units (Figure 1.14).

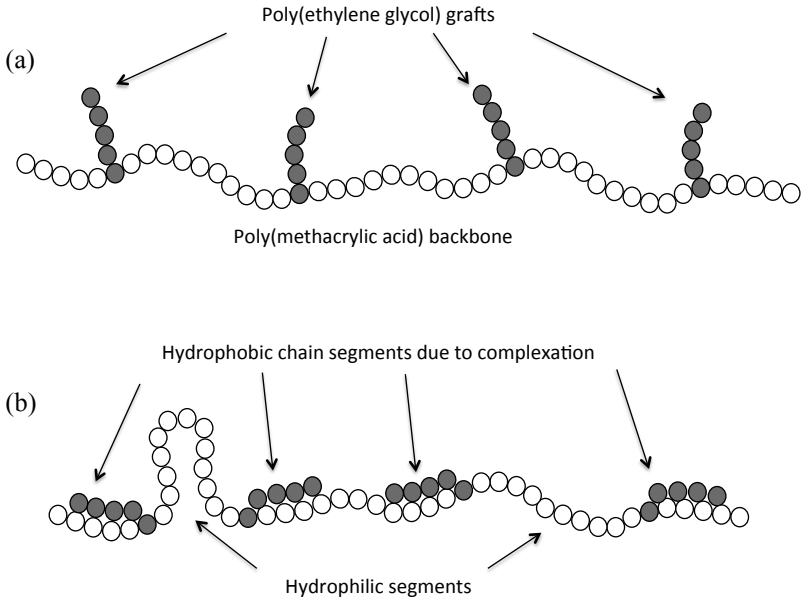

Figure 1.14. PEG-grafted PMAA polymer at (a) basic pH, no hydrogen bonding occurring so molecule remains completely hydrophilic and (b) acidic pH, complexation occurs resulting in both hydrophobic and hydrophilic segments. (Figure from ref. 90)

Due to its triggerable amphiphilicity, the polymer can be used as a responsive surfactant. At high pH, in its uncomplexed state, the polymer should completely dissolve in an aqueous phase. However, upon lowering the pH and forming hydrogen bonding complexes, sections of the polymer become hydrophobic, allowing interaction with an oil phase. The polymer in the amphiphilic state can then be used to stabilise acidic emulsions, with demulsification triggered by raising the pH and reversing the MAA-EG complex. Mathur *et al.* found that the ratio of MAA and EG repeat units had an effect on the stability of the resulting emulsion at varied pH, suggesting that "simple variations in molecular architecture may be used to tailor the pH range over which the emulsification capacities of the polymer change".[90]

In 2009, the Weaver group combined a number of these ideas and developed branched copolymer stabilised emulsion systems in which triggered hydrophilicity in polymerised DEAEMA units gives rise to demulsification.[29] However, in this case it was shown that subtle changes in the copolymer architecture and chain-end functionality could bring about significant changes in the resulting emulsion stabilities (Table 1.2). DEAEMA was copolymerised with PEGMA (M_n = 1,100 Da) to give six different copolymers and a 1:1 stoichiometric ratio was maintained throughout. The polymers varied only by the length of the branching monomer, or the chain transfer agent used. The target copolymer composition is denoted in Table 1.2 as a ratio of monofunctional monomers (MFM) PEGMA and DEAEMA and the molar percentage of both brancher and chain transfer added in comparison to total MFM. The total MFM always equalled 100, allowing easier determination of how much brancher and CTA is present in relation to the total MFM.

By varying the CTA used in the synthesis, the hydrophilicity of the linear chain ends can be changed. Looking at samples 1-3 in Table 1.2, only the chain transfer agent was changed, yet the percent demulsification, after 12 hours, varies greatly. When a copolymer prepared with a highly hydrophobic chain transfer agent (DDT) is used as a surfactant (sample 1), no demulsification occurs after 12 hours. When the non-ionic, hydrophilic TG is used as a CTA, 30 % demulsification occurs and when ionic, hydrophilic mercaptopropionic acid (MPA) is used, 50 % demulsification occurs. This suggests that the chain ends play a vital role in emulsion stabilisation. Three copolymers were prepared under identical conditions to samples 1-3, but using the longer branching unit poly(ethylene glycol) dimethacrylate (PEGDMA) which contained 14 EG repeat units compared to EGDMA's single

repeat unit. These are samples 4-6, which exhibit a similar trend in emulsion stability with increasing hydrophilicity at the chain ends. However, it is suggested that the subtle change in architecture enables more chain mobility, allowing the DEAEMA units to reorganise more efficiently, resulting in more effective dewetting of polymers from droplet surfaces in both TG and MPA systems.

Table 1.2. Characterisation data for branched copolymers and branched copolymer stabilised emulsions, all recorded at pH 10. (Table from ref. 29)

		Branched copolymer characterisation			Emulsion characterisation	
Sample	Target polymer composition	M_n[a] / g mol^{-1}	PDI[a]	MH-α[a]	$D_{(4,3)}$[b] / μm	% demulsification[c]
1	$PEGMA_5/DEAEMA_{95}$-$EGDMA_{15}$-DDT_{15}	7,400	2.8	0.31	8.7	0
2	$PEGMA_5/DEAEMA_{95}$-$EGDMA_{15}$-TG_{17}	20,500	2.8	0.30	10.6	30
3	$PEGMA_5/DEAEMA_{95}$-$EGDMA_{15}$-MPA_{15}	8,500	3.3	0.31	8.4	50
4	$PEGMA_5/DEAEMA_{95}$-$PEGDMA_{15}$-DDT_{15}	9000	4.5	0.39	11.6	<1
5	$PEGMA_5/DEAEMA_{95}$-$PEGDMA_{15}$-TG_{17}	25,800	7.9	0.44	12.5	>99
6	$PEGMA_5/DEAEMA_{95}$-$PEGDMA_{15}$-MPA_{15}	18,900	6.2	0.39	10.4	>99

[a] Measured by triple detection gel permeation chromatography in tetrahydrofuran. [b] Measured by laser diffraction at pH 10. [c] Quantified by measuring the oil volume separated 12 hours after addition of acid.

Regardless of the brancher used, polymers containing hydrophobic DDT chain ends did not demulsify, whereas all other samples showed signs of phase separation. This was a promising result, as it suggested that polymeric surfactants could be strongly anchored to oil droplets surfaces *via* their chain ends, even when the other components of the surfactants were hydrophilic. As branching allows the existence of more than one linear chain within each polymeric surfactant molecule, more chain ends are incorporated into each polymer. Therefore, if a hydrophobic CTA is used in the polymerisation, the polymer molecules should then contain a number of hydrophobic chain ends, rather than just one as in a linear polymer. Both architectures are shown in Figure 1.15 to illustrate this point. In the report by Weaver *et al.* branching provides multiple potential points of attachment per molecule to the droplet surface due to the increased number of hydrophobic DDT groups per chain.

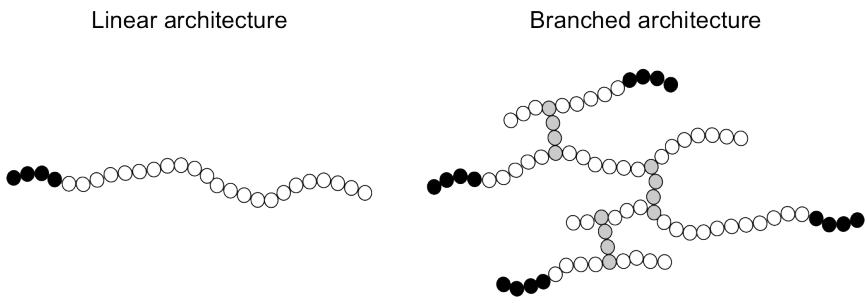

Figure 1.15. Schematic comparing both linear and branched architectures, demonstrating the multiple hydrophobic chain transfer molecules (black) that are present in the branched structure containing monofunctional monomer (white) and brancher (grey).

A lot of work has been published on responsive emulsions,[91-94] but responsiveness at droplet surfaces has been almost completely restricted to triggered demulsification.

Weaver *et al.* utilised this previous work in order to 'anchor' branched copolymers of similar composition to that of Mathur *et al.* discussed earlier, at both high and low pH, which was previously not possible.[102] This led to pH responsive polymeric surfactants with triggerable hydrogen bonding capabilities at an emulsion droplet surface. Weaver *et al.* found that this hydrogen bonding was not only limited to the surface of individual droplets (intra-droplet interactions), but interactions could also occur between droplets (inter-droplet interactions). This led to triggered droplet aggregation, giving rise to "engineered emulsions" (EEs). Figure 1.16(a) shows a schematic representation of the contra-functionality in one polymer molecule (red and blue) with hydrophobic chain ends (black). In Figure 1.16(b) a schematic shows how this polymer may interact with the surface of an oil droplet.

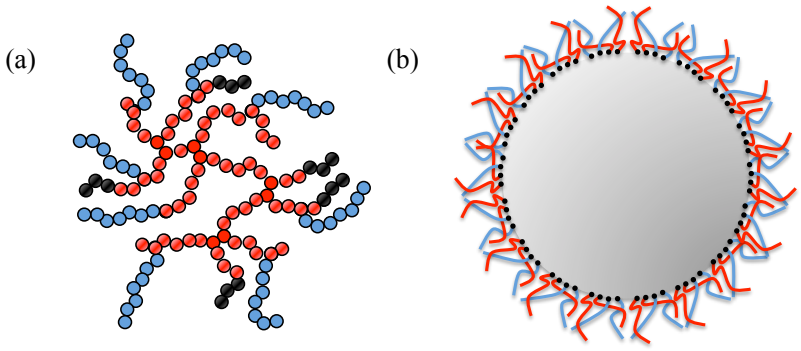

Figure 1.16. Schematics of (a) polymer containing contra-functionality (red and blue) with hydrophobic chain ends (black), (b) how (a) may interact with an oil droplet at the o/w interface.

1.11.5. Engineered Emulsions

The branched copolymer to form engineered emulsions consisted of monomers MAA and PEGMA, with the brancher EGDMA and CTA DDT both being added at 10 % of this total molar concentration. This polymer was denoted as $PEGMA_5/MAA_{95} – EGDMA_{10} – DDT_{10}$. The 5:95 ratio of PEGMA to MAA roughly represents a 1:1 ratio of EG to MAA as PEGMA contains 22 EG repeat units, with the total having been made 100 for ease of denoting the ratio of brancher and CTA present. Homogenisation of this polymer dissolved in a pH 10 aqueous phase with an equal amount of dodecane oil phase afforded highly stable droplets in the micrometre range. Droplets were highly stable at pH 10 due to the monomers providing both steric and electrostatic stabilisation. As PEGMA is hydrophilic, it sits in the water phase at the liquid-liquid interface and provides steric stabilisation. PEGMA has been used as a stabiliser at colloid surfaces previously and is known to provide a 'shielding effect'.[103] Electrostatic stabilisation is conferred by the MAA groups, which are deprotonated at high pH, resulting in droplets having anionic surfaces (Figure 1.17).

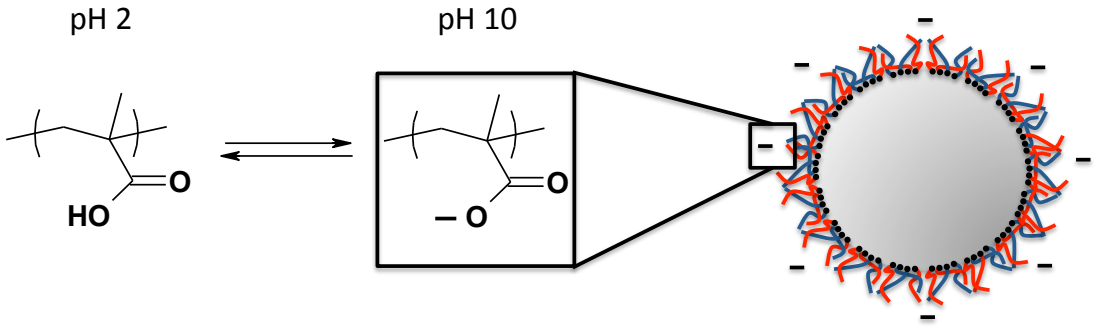

Figure 1.17. Schematic showing the pH responsiveness of the MAA monomer and how this results in electrostatically stabilised o/w droplets at high pH.

Upon lowering the pH, the MAA groups and the repeating EG units start to hydrogen bond.[90,101] This results in both intra-droplet and inter-droplet hydrogen bonding, and allows the droplets to aggregate without any sign of coalescence. This process is illustrated in Figure 1.18. This droplet 'trapping' is referred to as emulsion engineering, and allows emulsion droplets to undergo triggered aggregation, similar to concepts seen in colloid engineering.[104-106] Systems such as these mimic processes found in food science[107-109] and offer huge potential as responsive transport systems.

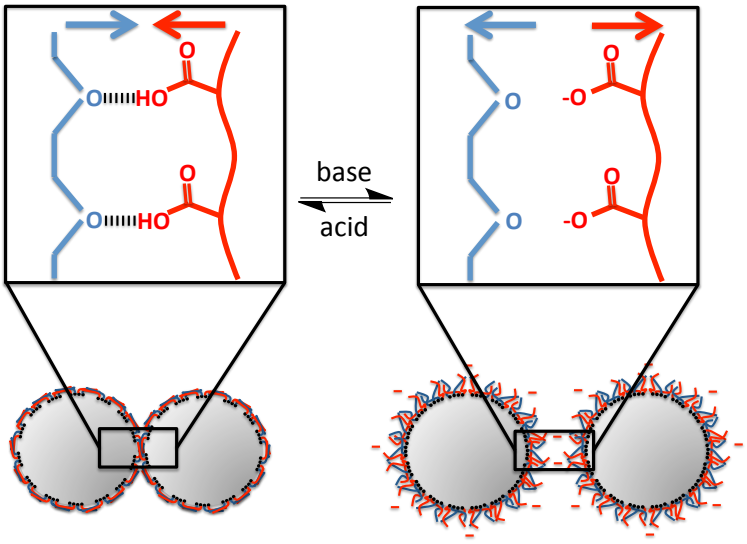

Figure 1.18. Triggerable inter-droplet hydrogen-bonding gives rise to engineered emulsions at low pH.

Lowering the pH of a concentrated o/w emulsion can create 3D emulsion droplet gel networks. When aggregated in a mould, self-supporting structures can be produced, supported only by droplet-droplet interactions (Figure 1.19). These interactions can be "turned off" *via* an increase in pH, resulting in the structure returning to a free-flowing emulsion sample. Figure 1.19 shows that a redispersed sample shows no sign of destabilisation and still consists of individual droplets.

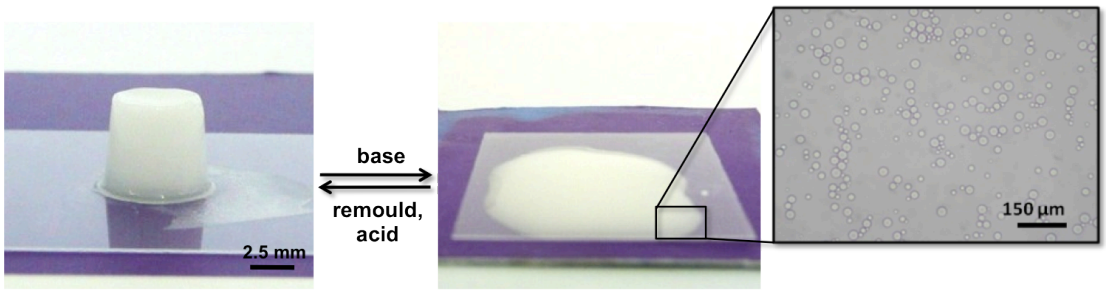

Figure 1.19. Engineered emulsion (left) which can be redispersed on the addition of base yielding discreet individual droplets (right). (Figure from ref. 102)

Strong adsorption of the surfactant at the oil-water interface means aggregation and redispersion can occur without any droplet destabilisation occurring.

Emulsion engineering allows individual droplets to be used to create hierarchical structures *via* intermolecular interactions. This process has been

achieved throughout a range of synthetic materials such as chiral molecules,[110] polymers,[111] colloidal particles,[74,105,112] and in the formation of metal-organic frameworks.[113]

1.12. Emulsions as Templates

Emulsions have been used as templates in a large range of applications due to their range in droplet sizes, and the ease of dispersed phase removal. These include the formation of porous materials,[73,114] latex particle assemblies,[115-117] polymer capsules,[118] and nanoparticles containing drugs.[117] In some cases an emulsion-solvent-evaporation (ESE) technique is employed to give polymer-stabilised nanoparticles.[69,119] ESE usually involves an emulsion comprising a dispersed volatile oil phase in an aqueous continuous phase. The removal of the volatile oil phase can then yield nanoparticles containing guest molecules by encapsulation of actives within oil droplets before removal of the volatile oil phase. Manoharan *et al.* reported the formation of clusters of cross-linked polystyrene microspheres with sulfate groups covalently bonded to the surface by the removal of toluene from an o/w emulsion.[69] The microspheres are initially dispersed in toluene, then water is added and the phases are mixed to yield an o/w emulsion. Particles are strongly bound to the interface, and upon removal of toluene, the microspheres pack together. This process is imaged in Figure 1.20.

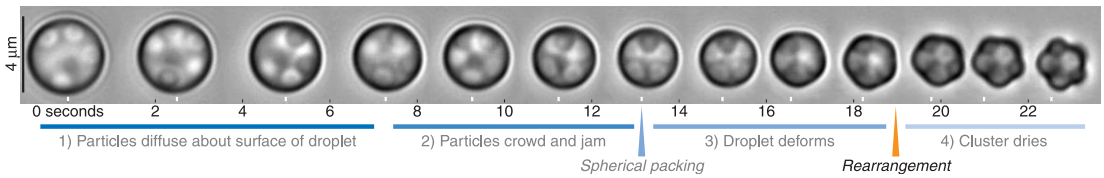

Figure 1.20. A time series of optical micrographs showing the removal of toluene and the subsequent packing of polystyrene microspheres to yield a cluster. (Figure from ref. 69)

ESE is a simple process that allows formation of well-characterised materials.[69,119] This process also enables the formation of hydrophobic-drug loaded polymer nanoparticles, which are dispersed in aqueous solution, so for this reason ESE has found a number of applications in pharmaceutical research. This includes the encapsulation of a number of drugs such as steroids,[120] doxorubicin,[121] bovine serum

albumin[122] and even the encapsulation and controlled release of local anaesthetics.[123] For these reasons emulsions have become important templates for the production of a wide range of materials in research.

1.13. Present Study

In the present work, the role of the branched copolymer surfactant's composition in the work presented by Weaver *et al.* on engineered emulsions[102] is investigated. The pH-responsive emulsions produced are then utilised in the production of a number of new pH-responsive, surface-functionalised materials.

In Chapter 3, the role that the ratio of MAA:PEGMA in a branched copolymer surfactant plays in triggerable inter-droplet hydrogen bonding is investigated. A series of these polymers are synthesised with polymers containing different MAA:PEGMA ratios. The effect of varying this ratio on the resulting dodecane o/w emulsion stability, kinetics of inter-droplet aggregation and resulting engineered emulsion gel strength is discussed. This triggerable hydrogen bonding interaction is then used in the development of a mechanism for selective droplet assembly.

Chapter 4 investigates the role of engineered emulsions in the production of copolymer-structured oils. Selective removal of water from droplet interstitial sites upon dehydration of an engineered emulsion gives rise to a structured oil comprising discreet individual droplets held together by polymer-polymer interactions. This polymer network provides enough of a barrier between droplets to allow rehydration of a structured oil to give an engineered emulsion.

In Chapter 5, the hydrolysis of glucono-δ-lactone as a homogeneous pH trigger is utilised in order to allow the kinetics of engineered emulsion formation to be monitored using rheology. This homogeneous pH trigger eliminates the diffusion process in HCl acidification and allows the production of engineered emulsions of much larger volumes than seen previously.

In Chapter 6, the synthesis of MAA/PEGMA surface-functionalised poly(methyl methacrylate) (PMMA) colloids from emulsions stabilised using the pH-responsive polymer reported by Weaver *et al.* is investigated. The reversible

aggregation of these responsive polymer-stabilised colloids and their formation of porous scaffolds is then discussed.

Lastly, Chapter 7 describes the production of multi-responsive emulsion droplets *via* the encapsulation of oleophilic polymer 'coated' Fe_3O_4 magnetic nanoparticles in a pH-responsive emulsion. The triggerable formation of magnetic-engineered emulsions results in the reversible formation of magneto-actuators.

1.14. References

(1) Andrady, A. L.; Neal, M. A. *Philos. T. Roy. Soc. B* **2009**, *364*, 1977.
(2) Staudinger, H. *Ber. Deut. Chem. Ges.* **1920**, *53*, 1073.
(3) Carothers, W. H. *J. Am. Chem. Soc.* **1929**, *51*, 2548.
(4) Stevens, M. P. *Polymer Chemistry: An Introduction*; Oxford University Press, New York, **1999**.
(5) Cowie, J. M. G. *Polymer: Chemistry and Physics of Modern Materials*; Taylor & Francis Group, Boca Raton, Fl, **2008**.
(6) Ziegler, K. *Angew. Chem. Int. Ed.* **1936**, *49*, 0499.
(7) Szwarc, M. *Nature* **1956**, *178*, 1168.
(8) Webster, O. W. *Science* **1991**, *251*, 887.
(9) Braunecker, W. A.; Matyjaszewski, K. *Prog. Polym. Sci.* **2007**, *32*, 93.
(10) Matyjaszewski, K. *Macromolecules* **1999**, *32*, 9051.
(11) Kato, M.; Kamigaito, M.; Sawamoto, M.; Higashimura, T. *Macromolecules* **1995**, *28*, 1721.
(12) Wang, J. S.; Matyjaszewski, K. *J. Am. Chem. Soc.* **1995**, *117*, 5614.
(13) Chiefari, J.; Chong, Y. K.; Ercole, F.; Krstina, J.; Jeffery, J.; Le, T. P. T.; Mayadunne, R. T. A.; Meijs, G. F.; Moad, C. L.; Moad, G.; Rizzardo, E.; Thang, S. H. *Macromolecules* **1998**, *31*, 5559.
(14) Mayadunne, R. T. A.; Jeffery, J.; Moad, G.; Rizzardo, E. *Macromolecules* **2003**, *36*, 1505.
(15) Lowe, A. B.; McCormick, C. L. *Prog. Polym. Sci.* **2007**, *32*, 283.
(16) Flory, P. J. *J. Am. Chem. Soc.* **1937**, *59*, 241.
(17) Engel, P. S. *Chem. Rev.* **1980**, *80*, 99.
(18) Mayo, F. R.; Gregg, R. A.; Matheson, M. S. *J. Am. Chem. Soc.* **1951**, *73*, 1691.
(19) Li, H.; Gao, D. Y. *Pigm. Resin. Technol.* **2011**, *40*, 24.
(20) Odian, G. *Principles of Polymerization*; John Wiley & Sons, New York, **2004**.
(21) Liu, B.; Yu, W. L.; Lai, Y. H.; Huang, W. *Macromolecules* **2000**, *33*, 8945.
(22) Van Cauter, K.; Van Speybroeck, V.; Waroquier, M. *ChemPhysChem* **2007**, *8*, 541.
(23) Xie, T. Y.; Hamielec, A. E.; Wood, P. E.; Woods, D. R. *Polymer* **1991**, *32*, 537.
(24) Buback, M.; Gunzler, F.; Russell, G. T.; Vana, P. *Macromolecules* **2009**, *42*, 652.
(25) Moad, G. *The Chemistry of Radical Polymerization*; Elselvier, Oxford, **2006**.

(26) Alger, M. *Polymer Science Dictionary*; Springer, London, **1997**.
(27) Murthy, K. S.; Kishore, K. *J. Polym. Sci. Pol. Chem.* **1996**, *34*, 1415.
(28) Takei, Y. G.; Aoki, T.; Sanui, K.; Ogata, N.; Okano, T.; Sakurai, Y. *Bioconjugate Chem.* **1993**, *4*, 42.
(29) Woodward, R. T.; Slater, R. A.; Higgins, S.; Rannard, S. P.; Cooper, A. I.; Royles, B. J.; Findlay, P. H.; Weaver, J. V. *Chem. Commun.* **2009**, *24*, 3554.
(30) Bosman, A. W.; Janssen, H. M.; Meijer, E. W. *Chem. Rev.* **1999**, *99*, 1665.
(31) Newkome, G. R.; He, E. F.; Moorefield, C. N. *Chem. Rev.* **1999**, *99*, 1689.
(32) Ikkala, O.; ten Brinke, G. *Science* **2002**, *295*, 2407.
(33) Hadjichristidis, N.; Pitsikalis, M.; Pispas, S.; Iatrou, H. *Chem. Rev.* **2001**, *101*, 3747.
(34) Gao, C.; Yan, D. *Progress in Polym. Sci.* **2004**, *29*, 183.
(35) Kim, Y. H. *J. Polym. Sci. Pol. Chem.* **1998**, *36*, 1685.
(36) Kim, Y. H.; Webster, O. W. *J. Am. Chem. Soc.* **1990**, *112*, 4592.
(37) Hawker, C. J.; Frechet, J. M. J.; Grubbs, R. B.; Dao, J. *J. Am. Chem. Soc.* **1995**, *117*, 10763.
(38) Frechet, J. M. J.; Henmi, M.; Gitsov, I.; Aoshima, S.; Leduc, M. R.; Grubbs, R. B. *Science* **1995**, *269*, 1080.
(39) Gaynor, S. G.; Edelman, S.; Matyjaszewski, K. *Macromolecules* **1996**, *29*, 1079.
(40) O'Brien, N.; McKee, A.; Sherrington, D. C.; Slark, A. T.; Titterton, A. *Polymer* **2000**, *41*, 6027.
(41) Degoulet, C.; Nicolai, T.; Durand, D.; Busnel, J. P. *Macromolecules* **1995**, *28*, 6819.
(42) Isaure, F.; Cormack, P. A. G.; Graham, S.; Sherrington, D. C.; Armes, S. P.; Butun, V. *Chem. Commun.* **2004**, *9*, 1138.
(43) Li, Y. T.; Armes, S. P. *Macromolecules* **2005**, *38*, 5002.
(44) Li, Y. T.; Armes, S. P. *Macromolecules* **2005**, *38*, 8155.
(45) Mansky, P.; Liu, Y.; Huang, E.; Russell, T. P.; Hawker, C. J. *Science* **1997**, *275*, 1458.
(46) Svensson, M.; Zhang, F. L.; Veenstra, S. C.; Verhees, W. J. H.; Hummelen, J. C.; Kroon, J. M.; Inganas, O.; Andersson, M. R. *Adv. Mater.* **2003**, *15*, 988.
(47) Matyjaszewski, K.; Xia, J. H. *Chem. Rev.* **2001**, *101*, 2921.
(48) Chen, G. H.; Hoffman, A. S. *Nature* **1995**, *373*, 49.
(49) Alexandridis, P.; Athanassiou, V.; Fukuda, S.; Hatton, T. A. *Langmuir* **1994**, *10*, 2604.
(50) Tuzar, Z.; Kratochvil, P. *Adv. Colloid Interface Sci.* **1976**, *6*, 201.
(51) Alexandridis, P.; Holzwarth, J. F.; Hatton, T. A. *Macromolecules* **1994**, *27*, 2414.
(52) Liu, S. Y.; Armes, S. P. *Curr. Opin Colloid Interface Sci.* **2001**, *6*, 249.
(53) O'Reilly, R. K.; Hawker, C. J.; Wooley, K. L. *Chem. Soc. Rev.* **2006**, *35*, 1068.
(54) Read, E. S.; Armes, S. P. *Chem. Commun.* **2007**, *29*, 3021.
(55) Bae, Y.; Fukushima, S.; Harada, A.; Kataoka, K. *Angew. Chem. Int. Ed.* **2003**, *42*, 4640.
(56) Kataoka, K.; Harada, A.; Nagasaki, Y. *Adv. Drug Deliv. Rev.* **2001**, *47*, 113.
(57) Galaev, I. Y.; Mattiasson, B. *Trends Biotechnol.* **1999**, *17*, 335.
(58) Fujishige, S.; Kubota, K.; Ando, I. *J. Phys. Chem.* **1989**, *93*, 3311.
(59) Aoyagi, T.; Ebara, M.; Sakai, K.; Sakurai, Y.; Okano, T. *J. Biomater. Sci.-Polym. Ed.* **2000**, *11*, 101.

(60) Bromberg, L. E.; Ron, E. S. *Adv. Drug Deliv. Rev.* **1998**, *31*, 197.
(61) Chambon, P.; Chen, L.; Furzeland, S.; Atkins, D.; Weaver, J. V. M.; Adams, D. J. *Polym. Chem.* **2011**, *2*, 941.
(62) Park, S. Y.; Bae, Y. H. *Macromol. Rapid Commun.* **1999**, *20*, 269.
(63) Philippova, O. E.; Hourdet, D.; Audebert, R.; Khokhlov, A. R. *Macromolecules* **1997**, *30*, 8278.
(64) Lee, A. S.; Butun, V.; Vamvakaki, M.; Armes, S. P.; Pople, J. A.; Gast, A. P. *Macromolecules* **2002**, *35*, 8540.
(65) You, L. C.; Lu, F. Z.; Li, Z. C.; Zhang, W.; Li, F. M. *Macromolecules* **2003**, *36*, 1.
(66) Miyata, T.; Asami, N.; Uragami, T. *Nature* **1999**, *399*, 766.
(67) Weaver, J. V. M.; Williams, R. T.; Royles, B. J. L.; Findlay, P. H.; Cooper, A. I.; Rannard, S. P. *Soft Matter* **2008**, *4*, 985.
(68) Bibette, J.; Calderon, F. L.; Poulin, P. *Rep. Prog. Phys.* **1999**, *62*, 969.
(69) Manoharan, V. N.; Elsesser, M. T.; Pine, D. J. *Science* **2003**, *301*, 483.
(70) Millman, J. R.; Bhatt, K. H.; Prevo, B. G.; Velev, O. D. *Nature Mater.* **2005**, *4*, 98.
(71) Miller, O. J.; Bernath, K.; Agresti, J. J.; Amitai, G.; Kelly, B. T.; Mastrobattista, E.; Taly, V.; Magdassi, S.; Tawfik, D. S.; Griffiths, A. D. *Nature Methods* **2006**, *3*, 561.
(72) Chan, E. M.; Alivisatos, A. P.; Mathies, R. A. *J. Am. Chem. Soc.* **2005**, *127*, 13854.
(73) Zhang, H.; Cooper, A. I. *Soft Matter* **2005**, *1*, 107.
(74) Dinsmore, A. D.; Hsu, M. F.; Nikolaides, M. G.; Marquez, M.; Bausch, A. R.; Weitz, D. A. *Science* **2002**, *298*, 1006.
(75) Tadros, T.; Izquierdo, R.; Esquena, J.; Solans, C. *Adv. Colloid Interface Sci.* **2004**, *108*, 303.
(76) Binks, B. P.; Lumsdon, S. O. *Langmuir* **2001**, *17*, 4540.
(77) Amalvy, J. I.; Unali, G. F.; Li, Y.; Granger-Bevan, S.; Armes, S. P.; Binks, B. P.; Rodrigues, J. A.; Whitby, C. P. *Langmuir* **2004**, *20*, 4345.
(78) Cochin, D.; Laschewsky, A.; Nallet, F. *Macromolecules* **1997**, *30*, 2278.
(79) Pichot, R.; Spyropoulos, F.; Norton, I. T. *J. Colloid Interface Sci.* **2010**, *352*, 128.
(80) Pickering, S. U. *J. Chem. Soc.* **1907**, *91*, 2001.
(81) Binks, B. P. *Curr. Opin. Colloid Interface Sci.* **2002**, *7*, 21.
(82) Liu, S. Y.; Armes, S. P. *Angew. Chem. Int. Ed.* **2002**, *41*, 1413.
(83) Petsev, D. N. *Emulsions: Structure, stability and interactions*; Elsevier, London, **2004**.
(84) Fainerman, V. B. *Surfactants: Chemistry, interfacial properties, applications*; Elsevier, Amsterdam, **2001**.
(85) Aveyard, R.; Binks, B. P.; Clint, J. H. *Adv. Colloid Interface Sci.* **2003**, *100-102*, 503.
(86) Binks, B. P.; Lumsdon, S. O. *Langmuir* **2000**, *16*, 8622.
(87) Ramsden, W. *P. Roy. Soc. Lond.* **1903**, *72*, 156.
(88) Glaser, N.; Adams, D. J.; Boker, A.; Krausch, G. *Langmuir* **2006**, *22*, 5227.
(89) Binks, B. P.; Fletcher, P. D. I. *Langmuir* **2001**, *17*, 4708.
(90) Mathur, A. M.; Drescher, B.; Scranton, A. B.; Klier, J. *Nature* **1998**, *392*, 367.
(91) Fujii, S.; Cai, Y. L.; Weaver, J. V. M.; Armes, S. P. *J. Am. Chem. Soc.* **2005**, *127*, 7304.

(92) Fujii, S.; Read, E. S.; Binks, B. P.; Armes, S. P. *Adv. Mater.* **2005**, *17*, 1014.
(93) Koh, A. Y. C.; Saunders, B. R. *Chem. Commun.* **2000**, 2461.
(94) Liu, Y. X.; Jessop, P. G.; Cunningham, M.; Eckert, C. A.; Liotta, C. L. *Science* **2006**, *313*, 958.
(95) Vesperinas, A.; Eastoe, J.; Wyatt, P.; Grillo, I.; Heenan, R. K.; Richards, J. M.; Bell, G. A. *J. Am. Chem. Soc.* **2006**, *128*, 1468.
(96) Khoukh, S.; Perrin, P.; de Berc, F. B.; Tribet, C. *ChemPhysChem* **2005**, *6*, 2009.
(97) Thurmond, K. B.; Kowalewski, T.; Wooley, K. L. *J. Am. Chem. Soc.* **1996**, *118*, 7239.
(98) Thurmond, K. B.; Kowalewski, T.; Wooley, K. L. *J. Am. Chem. Soc.* **1997**, *119*, 6656.
(99) Wooley, K. L. *J. Polym. Sci. Polym. Chem.* **2000**, *38*, 1397.
(100) Bekturov, E. A.; Bimendina, L. A. *Adv. Polym. Sci.* **1981**, *41*, 99.
(101) Kabanov, V. A.; Papisov, I. M. *Vysokomol Soed. A* **1979**, *21*, 243.
(102) Weaver, J. V. M.; Rannard, S. P.; Cooper, A. I. *Angew. Chem. Int. Ed.* **2009**, *48*, 2131.
(103) Dupin, D.; Armes, S. P.; Connan, C.; Reeve, P.; Baxter, S. M. *Langmuir* **2007**, *23*, 6903.
(104) Poon, W. C. K. *MRS Bull.* **2004**, *29*, 96.
(105) Leunissen, M. E.; Christova, C. G.; Hynninen, A. P.; Royall, C. P.; Campbell, A. I.; Imhof, A.; Dijkstra, M.; van Roij, R.; van Blaaderen, A. *Nature* **2005**, *437*, 235.
(106) Arsenault, A. C.; Puzzo, D. P.; Manners, I.; Ozin, G. A. *Nature Photon.* **2007**, *1*, 468.
(107) Donaldis, A. *Nature Mater.* **2004**, *3*, 579.
(108) Lucey, J. A.; Singh, H. *Food Res. Int.* **1997**, *30*, 529.
(109) Mezzenga, R.; Schurtenberger, P.; Burbidge, A.; Michel, M. *Nature Mater.* **2005**, *4*, 729.
(110) Prins, L. J.; De Jong, F.; Timmerman, P.; Reinhoudt, D. N. *Nature* **2000**, *408*, 181.
(111) Harada, A. *Science* **1999**, *283*, 65.
(112) Velev, O. D. *Science* **2000**, *287*, 2240.
(113) Li, H.; Eddaoudi, M.; O'Keeffe, M.; Yaghi, O. M. *Nature* **1999**, *402*, 276.
(114) Imhof, A.; Pine, D. J. *Nature* **1997**, *389*, 948.
(115) Velev, O. D.; Furusawa, K.; Nagayama, K. *Langmuir* **1996**, *12*, 2374.
(116) Velev, O. D.; Furusawa, K.; Nagayama, K. *Langmuir* **1996**, *12*, 2385.
(117) Lassalle, V.; Ferreira, M. L. *Macromolecular Bioscience* **2007**, *7*, 767.
(118) Harbron, R. L.; McDonald, T. O.; Rannard, S. P.; Findlay, P. H.; Weaver, J. V. *Chem. Commun.* **2012**, *48*, 1592.
(119) Chognot, D.; Leonard, M.; Six, J. L.; Dellacherie, E. *Colloids. Surface. B* **2006**, *51*, 86.
(120) Cavalier, M.; Benoit, J. P.; Thies, C. *J. Pharm. Pharmacol.* **1986**, *38*, 249.
(121) Juni, K.; Ogata, J.; Nakano, M.; Ichihara, T.; Mori, K.; Akagi, M. *Chem. Pharm. Bull.* **1985**, *33*, 313.
(122) Desai, M. P.; Labhasetwar, V.; Amidon, G. L.; Levy, R. J. *Pharm. Res.* **1996**, *13*, 1838.
(123) Wakiyama, N.; Juni, K.; Nakano, M. *Chem. Pharm. Bull.* **1982**, *30*, 2621.

CHAPTER 2

Experimental

List of Figures

2.1. Synthetic Processes Applicable to the Whole Thesis

2.1.1. Preparation of $PEGMA_x/MAA_y$ – $EGDMA_{10}$ – DDT_{10} Branched Copolymers

In order to make a branched copolymer with a 1:1 stoichiometric molar ratio of methacrylic acid groups to ethylene glycol repeat units (P5 in Chapter 3), a mixture of PEGMA (6.732 g, 6 mM), MAA (10.000 g, 116 mM), EGDMA, 2.302 g, 12 mM), and DDT (2.349 g, 12 mM) was degassed. Ethanol (190 mL) was degassed separately and added to the monomer mixture. After heating to 70 ^{o}C, the copolymerisation was initiated by addition of AIBN (190 mg) and was left stirring for 48 hours. Ethanol was then removed by distillation and the resulting copolymers were washed with cold diethyl ether and dried. In order to synthesise copolymers of varying composition, the initial molar ratios of PEGMA to MAA were adjusted, while the EGDMA and DDT molar ratios remained unchanged. ^{1}H NMR was used to confirm the various mean copolymer compositions. As the applications of P5 as a pH responsive copolymer surfactant makes up the bulk of this thesis, a demonstration of reproducibility is presented in 4.2.1. Three P5 copolymers were synthesised separately in order to assess the reproducibility of the free radical copolymerisation protocol.

2.1.2. Emulsion Preparation

An aqueous solution of branched copolymer (2.0 w/v %, 3 mL) at pH 10 was prepared and an equal volume of dodecane (3 mL) was added. This biphasic mixture was homogenised at 24,000 rpm for 2 minutes using a T25 digital Ultra-Turrax. Following homogenisation the emulsions were left to equilibrate for 24 hours before characterisation.

2.1.3. Emulsions with Guest Molecules Encapsulated

A number of emulsions were produced with guest molecules encapsulated within the oil droplets. These guest molecules include Oil Red, Oil Blue, poly(methyl methacrylate) (PMMA), 3,3'-dioctadecyloxacarbocyanine perchlorate (DiO), Lumogen® Rosa 285 and post-functionalised Fe_3O_2 nanoparticles. These were always dissolved in the oil phase before homogenisation. Dyes were always added at 0.1 wt. % unless stated otherwise, PMMA at 8 wt. % and Fe_3O_2 at 0.17 wt. %.

2.1.4. Engineered Emulsion (EE) Formation

A sample of a P5-stabilised, dodecane-in-water emulsion's creamed layer (150 μL, volume fraction of oil (Φ_{oil}) = 0.69-0.71) was pipetted into a template, and HCl (1 M, 100 μL) was added to the top of the sample. This system was then left for 2 hours to aggregate, after which time, any excess HCl was removed, and upon removal of the template, an EE was produced. Preparation techniques for EEs produced *via* glucono-δ-lactone hydrolysis are outlined in 2.5.2. Small spherical aggregates (or spheroids) were produced by dropping 10 μL aliquots of the emulsions creamed layer into a HCl (1 M) reservoir.

2.2. Characterisation Techniques

2.2.1. Light Scattering

All emulsion size distributions were assessed using laser diffraction with a Malvern Mastersizer 2000 equipped with a Hydro 2000 SM dispersion unit. For all emulsion droplet measurements, a 40 μL drop of emulsion was added to the dispersion unit

containing 80 mL water (pH adjusted to pH 10 using 1 M NaOH) with a stirring rate of 1,100 rpm. The volume-average droplet diameters ($D_{(4,3)}$) quoted were obtained from at least 3 repeat runs ($D_{(4,3)} = \Sigma D_i^4 N_i / \Sigma D_i^3 N_i$). The span is a measure of the width of the droplet size distribution and is expressed mathematically as (D(0.9) − D(0.1))/D(0.5), where D(0.9) is the diameter under which 90 % of the particles fall, D(0.5) is the diameter under which 50 % of the particles fall and D(0.1) is the diameter under which 10 % of the particles fall.

2.2.2. Gel Permeation Chromatography (GPC)

GPC measurements were used to determine the molar mass, molar mass distribution and Mark-Houwink values of branched copolymers. A triple-detection Viscotek, TDA-302 system equipped with refractive index, viscometry and dual-angle light scattering detectors was used. The eluent was tetrahydrofuran (THF) with a flow rate of 1 mL min^{-1}. Two Viscotek GMPWXL columns and an additional guard column were used with an oven temperature of 35 °C. All samples were prepared at 5 mg/mL.

2.2.3. Rheology

Rheological experiments were carried out on an Anton Parr Physica MCR101 rheometer, using either a sand-blasted parallel top plate or a standard parallel top plate with a diameter of 50 mm. A 1 mm gap distance was used in all experiments. Time sweeps measured the change in storage modulus (G') and loss modulus (G") over time under constant strain (γ = 1 %) and angular frequency (ω = 10 $rad.s^{-1}$). Amplitude sweeps measure the strain that an engineered emulsion can withstand without breaking down at a constant angular frequency (ω = 10 $rad.s^{-1}$).

2.2.4. Surface Tensiometry

All surface tension measurements were performed on a Kibron Delta-8 high-throughput tensiometer. Surface tension profiles of the branched copolymer solutions were performed as a function of copolymer concentration. A stock solution of each branched copolymer was prepared (8.0 w/v %) and this stock solution was diluted by 50 % 11 times and the surface tension of each dilution measured.

2.2.5. Optical Microscopy

Optical microscopy images of emulsion droplets and engineered emulsions were obtained using light microscopy on a calibrated Meiji MX9300 microscope equipped with a digital camera.

2.2.6. Confocal Microscopy

Confocal images showing emulsions loaded with 0.05 wt. % DIO (Invitrogen) were recorded by Rachel Harbron at Imperial College London using a Zeiss LSM710 microscope with a Leica TCS SP5 Spectral Confocal Microscope (40x magnification) with excitation from the 488 nm line of an argon ion laser and emission detected between 497 and 540 nm.

2.2.7. Thermogravimetric Analysis (TGA)

Gravimetric weight loss of water from both engineered emulsions and colloidal aggregates was measured using a TA Instruments TGA Q5000 with an automated vertical overhead thermobalance. Samples were kept at 25 ^{o}C and all measurements were recorded at 10 minute intervals.

2.2.8. Nuclear Magnetic Resonance

All ^{1}H NMR spectra were recorded in deuterated methanol (CD_3OD) using a Bruker DPX-400 spectrometer operating at 400 MHz. ^{1}H NMR was used to determine the chemical composition of the final copolymers.

2.2.9. Ultraviolet-Visible Spectroscopy

All transmittance and absorption spectra of samples were recorded at wavelengths between 200-800 nm, using a BioTek instrument and a 96-place well plate.

2.2.10. Karl Fischer Titration

Robert Bell at Imperial College, London collected Karl Fischer titration data. The precise water content of various emulsions was quantified using Karl Fischer titration on a Mettler Toledo, V20 Compact Volumetric Karl Fischer Titrator instrument.

2.2.11. Scanning Electron Microscopy of Colloidal Aggregates

Scanning electron microscope (SEM) images were recorded by Dr. Nicolas Schaeffer at Imperial College London on a Gemini 1525 FEGSEM, using an acceleration voltage of 5kV. Samples were mounted on carbon tabs and coated with carbon and copper (~5 nm thickness) prior to imaging to avoid charge build-up.

2.2.12. Mercury Intrusion Porosimetry Measurements

Intrusion volumes and macropore size distributions were recorded by Michael Barrow at the University of Liverpool using a Micromeritics Mutopore IV 9500 porosimeter. Colloidal aggregates were weighed accurately into a penetrometer. The penetrometer was then sealed and placed into the low-pressure port of the instrument where the sample and penetrometer were evacuated to 50 mmHg and then filled with mercury. A pressure cycle from 0.5 to 60,000 psi was then performed on the assembly in predefined steps.

2.2.13. Fourier Transform Infrared Spectroscopy

FT-IR measurements were recorded by Erol Hasan at the University of Liverpool using a Bruker Tensot 27 spectrometer. Samples were analysed as KBr discs for 16 scans with a resolution of 4 cm^{-1}. Spectra were recorded in reflection mode.

2.2.14. Superconducting Quantum Interference Device (SQUID)

Magnetisation measurements were performed by Cristina Olariu at the University of Liverpool using a Quantum Design MPMS SQUID magnetometer. Magnetisation curves (MvH) as a function of magnetic field were measured at 300 K for magnetic fields from -10 to 10 KOe.

2.2.15. Transmission Electron Microscopy

Transmission electron microscopy (TEM) images were recorded by Cristina Olariu at the University of Liverpool using a Tecnai G2 Spirit BioTWIN model, operating at an accelerating voltage of 100 kV.

2.3. Chapter 3

2.3.1. Materials

Poly(ethylene glycol) methacrylate (M_n = 1,100 g.mol^{-1}), methacrylic acid, ethylene glycol dimethacrylate 1-dodecanethiol, dodecane, trimethylsilyl diazomethane (TMSDM) (2 M in hexanes) and 1-dodecanol were all purchased from Aldrich and used as received. Ethanol, methanol and toluene were all standard laboratory grade. 2,2'-Azobis(isobutyronitrile) (AIBN) was purchased from BDH and recrystallised from methanol prior to use.

2.3.2. Esterification of Methacrylic Acid Containing Polymers

Polymer (50 mg) was placed in a glass vial, to which methanol (0.2 mL) was added. The resulting solution was then agitated by hand until a homogeneous solution was formed, after which toluene (0.2 mL) was added, and the vial was again agitated to obtain a homogeneous solution. TMSDM was then added dropwise, until a yellow colour was just apparent which did not become colourless upon agitation.[1] Resulting solutions were purified *via* evaporation, and left to dry in the vacuum oven for 24 hours. ^{1}H NMR was used to confirm the copolymer composition by comparing the methyl ester peak of PMMA to peaks corresponding to PEGMA residues. Full NMR spectra are shown for copolymers with varying EG:MAA molar ratios are shown in Figure 2.1.

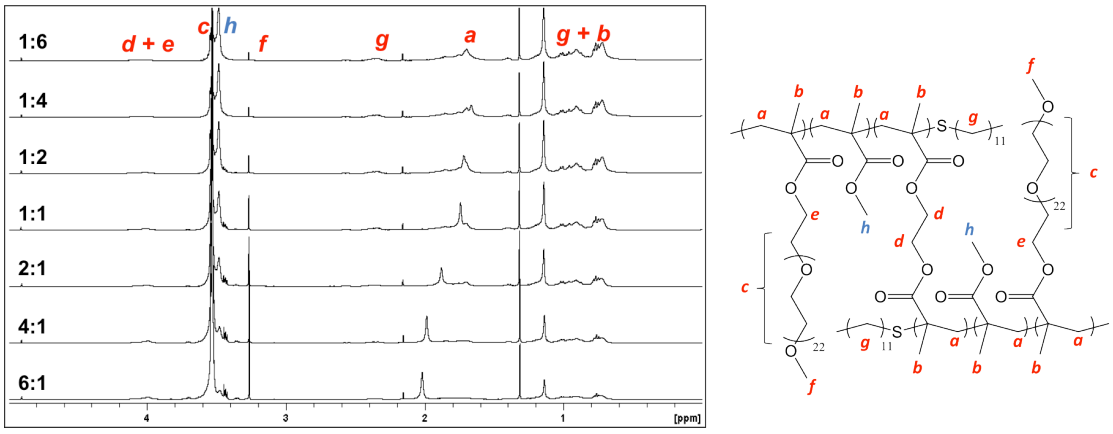

Figure 2.1. Stacked ^{1}H NMR spectra of branched copolymers containing methylated MAA groups with varied EG:MAA molar ratios, and their structural assignment.

2.3.3. Calculating Free Polymer in Emulsions by Surface Tension

In order to calculate the amount of unabsorbed polymer in the continuous water phase after homogenisation, the surface tension of the aqueous continuous phase of an emulsion was measured. Using a calibration curve comprising the surface tension values of pH 10 solutions containing known amounts of pH responsive polymer (Figure 2.2), the amount of free polymer in an emulsion system was calculated. Results between 0.03125 wt. % to 0.25 wt. % in Figure 2.2 were used to calculate a line equation as it gave a linear trend (Figure 2.3) in the surface tension range for the emulsion's continuous phase.

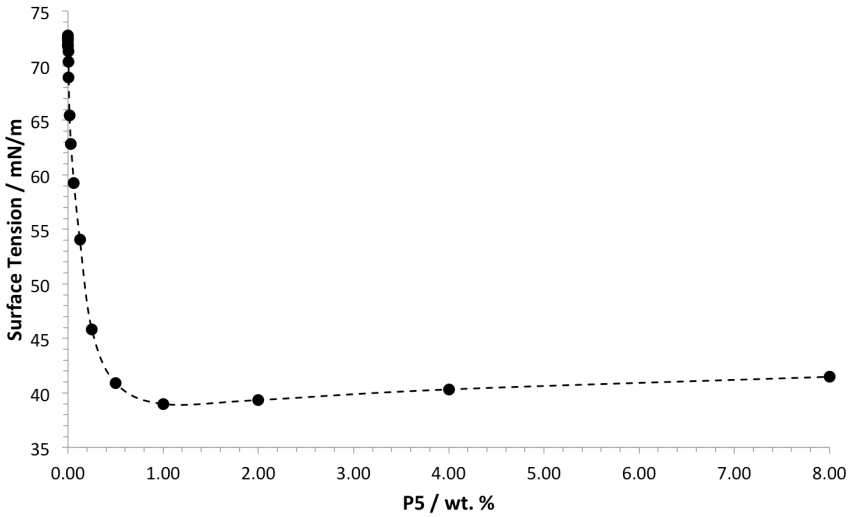

Figure 2.2. Surface tension of aqueous solutions containing increasing amounts of copolymer P5.

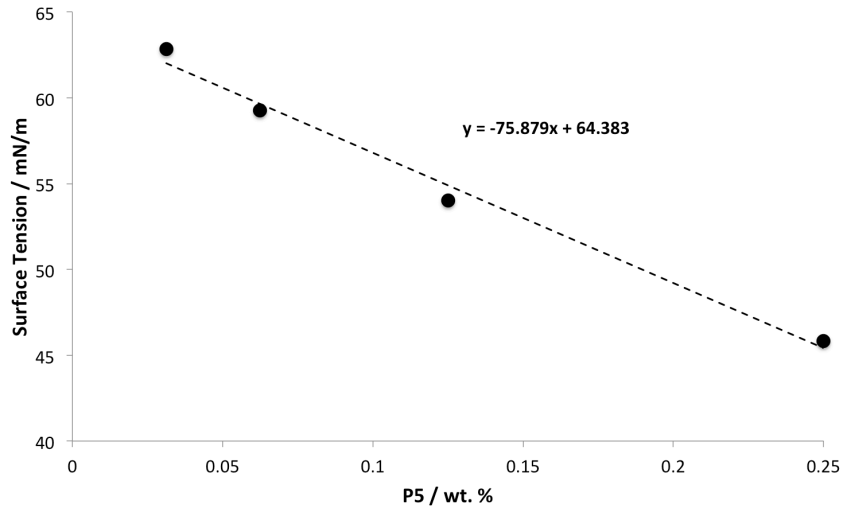

Figure 2.3. Linear range in the surface tension of P5 from which the amount of free copolymer was calculated.

Using the line equation in Figure 2.3, the results of the surface tension measurements (56.2, 56.7, 57.3 and 56.9 mN/m) were calculated and gave an average free copolymer concentration of 0.1 wt. %, or 5 % of the initial copolymer added.

2.3.4. Measuring Emulsion Droplet Aggregation Using Light Scattering

Aggregation of dilute dispersions of the emulsions on addition of acid was measured as a function of time using laser diffraction. All measurements were performed under the aforementioned conditions in 2.2.1, but with 20 repeat runs to provide sufficient time to ascertain the relative rates of droplet interaction. After four repeat measurements of the droplets dispersed at pH 10, HCl (1 M, 0.8 mL) was added to the dispersion unit to produce a pH 2 solution. The change in volume-average droplet diameter, $D_{(4,3)}$, was then measured as a function of time. For the binary mixture measurements by laser diffraction, the initial 40 μL was divided into 20 μL of each 100 % MAA and 100 % EG sample.

2.3.5. Rheological Measurements of Acidified Emulsions

2.5 mL of the creamed layer of each emulsion sample was acidified *in situ* and left to aggregate for 2 hours before measurement. After removal of any excess HCl, amplitude sweeps were then performed on each sample. The binary mixture consisted of 1.25 mL of 100 % MAA and 1.25 mL of 100 % PEGMA which was acidified *in situ* and left to aggregate for 2 hours, again excess HCl was removed before measurement.

2.3.6 Light Microscopy of Selective Droplet Assembly

Light microscope images of the binary mixtures of 100 % MAA/1-dodecanol and 100 % EG/dodecane emulsions were achieved by first imaging the isolated droplets at high and low pH. 1-Dodecanol emulsions were prepared using an identical procedure to the other emulsifications, but the temperature of all materials, glassware and equipment was maintained at around 40 °C. When homogenisation was complete, the resulting emulsion was immediately diluted in water (40 °C, 120 mL, pH 10) and stirred overnight, to prevent ‘jamming’ of the solidifying emulsion

droplets. In order to image the selective binary aggregated droplets, a sample of each emulsions creamed layers (20 μL each) were both added to a vial containing 0.5 mL of pH 10 water. The sample was gently mixed and then HCl (50 μL, 1M) was added to acidify the solution. The resulting solution was stirred gently and then imaged.

2.4. Chapter 4

2.4.1. Materials

Poly(ethylene glycol) methacrylate (M_n = 1,100 g.mol^{-1}), methacrylic acid, ethylene glycol dimethacrylate 1-dodecanethiol, dodecane, Oil Red and Oil Blue were purchased from Aldrich and used as received. DiO was purchased from Invitrogen and used as received. Lumogen® Rosa 285 was purchased from BASF and used as received. Ethanol was standard laboratory grade. 2,2'-Azobis(isobutyronitrile) was purchased from BDH and recrystallised from methanol prior to use.

2.4.2. UV-Visible Spectroscopy

Thin cross-sections (1.5 mm) of EEs were placed into well plates and their transmittance recorded; after 6 hours the change in transmittance with dehydration to form polymer structured oils (PSOs) was also recorded.

In order to measure the rate of release of a hydrophobic dye from EEs and PSOs, dodecane EE monoliths containing Oil Blue were prepared from 150 μL of creamed, dye-loaded emulsion. Following aggregation, the EEs were either kept hydrated by submersion in excess aqueous HCl solution, or allowed to dehydrate for 2 hours to form a PSO. Both the engineered emulsions and PSOs were then transferred into vials containing dodecane (12 mL) over gentle stirring. Samples of the dodecane (100 μL) were then taken at 15 minute intervals and the Oil Blue release was determined by the absorption of the sample at a wavelength of 600 nm.

Sequestration of Oil Blue from a surrounding dodecane reservoir into EEs and PSOs was also measured using UV-Vis spectroscopy. Stock solutions of Oil Blue dissolved in dodecane were prepared at a range of different concentrations (1.25 x 10^{-3} – 0.08 wt. %). Spheroids were produced and allowed to dehydrate for various times, and uptake of Oil Blue from solutions containing different concentrations was measured. All samples were left in Oil Blue solutions for 1 hour,

and upon removal were quickly washed twice with pure dodecane to remove any non-sequestered Oil Blue from the spheroid surface. Each spheroid was then dissolved in ethanol (100 μL) and transferred to a well plate for measurement on the UV-Vis. Oil Blue sequestration was determined by the adsorption of the sample at a wavelength of 600 nm.

2.4.3. Karl Fischer Titration Sample Preparation

EEs (150 μL) were prepared using the standard protocol and allowed to dehydrate at ambient temperature for various times before the water content was measured by Karl Fischer titration. Two repeats of each measurement were taken. Rehydrated samples were allowed to dehydrate for 6 hours before being submerged in HCl (1 M) for 30 minutes to allow sufficient rehydration.

2.4.4 Generation of Oil Droplets in Microfluidic Channels

Microfluidic devices were structured in polydimethylsiloxane (PDMS) using standard soft lithographic methods described elsewhere and bonded to a planar glass slide by exposure to an oxygen plasma for 30 seconds.[2] The microfluidic device consisted of a 14 cm long serpentine channel downstream of the T-junction, used to incubate droplets and ensure adequate contact of dodecane and the polymer solution (approximately 2 minutes). The smallest cross-sectional channel dimensions at the "T" junction are 100 μm height and 25 μm in width. The incubation channel was 100 μm high and a 200 μm wide along its entire length. The chip has two inlets where polymer solution (4 %) and dodecane were introduced respectively. Liquid was loaded into 1 mL syringes and mounted on a syringe pump (PHD 2000, Harvard Apparatus). To obtain 25 μm diameter dodecane droplets the flow rate was set to 4 μL/minute, and the flow rate of inlet "b" set to 1 μL/minute. Images were recorded using a high speed camera (Phantom, v5.1, Vision Research)

2.4.5. Rheological Measurements of EEs, PSOs and Free-Flowing Emulsions

2.5 mL of the creamed layer of a P5 dodecane emulsion (pH 10) was placed on the rheometer and was acidified *in situ* in the case of EE and PSO formation *via* the addition of HCl (0.5 mL). Both samples were then allowed to stand for 2 hours to

aggregate before any excess HCl was removed, after which time the measurement was either performed (in the case of the EE) or the sample was left for a further 4 hours to dehydrate, forming a PSO. After dehydration, an amplitude sweep was performed on the PSO. For a rehydrated PSO the same procedure was followed, but after dehydration, HCl (1 M, 1 mL) was added to the structure, and it was allowed to rehydrate for 1 hour before excess HCl was removed and the measurement was performed. To measure a free-flowing emulsion, after the pH 10 emulsion's creamed layer was transferred to the rheometer, the measurement was started immediately. The EE that was redispersed before measurement was allowed to form in the same way, but was redispersed using *via* the addition of NaOH (0.5 M, 2 mL) in a vial and allowed to cream overnight. After this time, the resulting creamed layer (2.5 mL) was transferred to the rheometer and measured. The binary mixture consisted of 1.25 mL of 100 % MAA and 1.25 mL of 100 % PEGMA which was acidified *in situ* and allowed to aggregate for 2 hours before measurement.

2.5. Chapter 5

2.5.1. Materials

Poly(ethylene glycol) methacrylate (M_n = 1,100 g.mol^{-1}), methacrylic acid, ethylene glycol dimethacrylate 1-dodecanethiol, dodecane, Oil Red, Oil Blue and Glucono-δ-lactone (GδL) was purchased from Aldrich and used as received. Ethanol was standard laboratory grade. 2,2'-Azobis(isobutyronitrile) was purchased from BDH and recrystallised from methanol prior to use.

2.5.2. GδL Engineered Emulsion Preparation and Characterisation

All EEs were created using the creamed layer of the standard P5-stabilised dodecane o/w emulsion (φ_{oil} = 0.69-0.71), to which GδL (2 wt. % based on the total emulsion volume) was added, stirred slowly, and left to stand for at least 2 hours. Formation of the EE rook was achieved by first transferring the creamed emulsion (5 mL) into a mould. GδL (100 mg, 2 wt. %) was added and gently stirred into the sample. The resulting mixture was left for 4 hours before the structure was removed from the mould. Disassembly was triggered by addition of NaOH (1 M, 3 mL). The large volume EE was formed by trapping 180 mL of the emulsion's cream layer within a

plastic beaker using the addition of GδL (2 wt. %) and allowing hydrolysis to occur overnight. Large volumes of emulsion were produced by adding dodecane (50 mL) to a pH 10 P5 aqueous solution (2 wt. %, 50 mL) and mixing the two using a more powerful homogeniser (Polytron PT2100, 28,000 rpm for 4 minutes, using a 20 mm diameter crown dispersion head rotor stator). The well-defined complex engineered emulsion was prepared using emulsion droplets in which the hydrophobic dyes Oil Blue and Oil Red (0.1 wt. %) were encapsulated. Sequential layers of each emulsion (30 mL) were added to a small mould immediately after GδL addition and allowed to aggregate. The HCl aggregated complex EE was formed by the addition of sequential layers of each emulsion. After each layer was added to the mould, HCl (1 M, 50 μL) was added and the sample was allowed 30 minutes to aggregate. After this time excess HCl was removed, the next layer was added and the process was repeated.

2.5.3. Rheology of emulsions

Rheological experiments in Chapter 5 were carried out using an Anton Parr Physica MCR101 rheometer, equipped with a sand-blasted parallel top plate with a diameter of 50 mm. 1 mm gap distance was used in all experiments and evaporation of water was minimised by coating the sides of the plate with a low viscosity mineral oil. Time sweeps required initially dispersed sample of a P5 dodecane emulsion (2.5 mL) while amplitude sweeps required fully aggregated engineered emulsion (2.5 mL), thus different sample preparations were employed which account for differences in the magnitude of the moduli observed. Samples for strain sweep measurements were prepared by gently mixing the creamed emulsion (2.5 mL) with GδL solution (2 wt. %, 0.66 mL). The sample was then left for 2 hours at room temperature to allow hydrolysis of the GδL (and aggregation of the emulsion) to occur. After this time the engineered emulsion (2.5 mL) was transferred to the rheometer and the experiment run according to the conditions provided above. No additional creaming was visible during the rheometry experiments although this cannot be completely discounted.

2.5.4. Monitoring pH change with hydrolysis of GδL

pH measurements on emulsion samples containing GδL (1 wt. % and 2 wt. %) were performed using a HANNA instruments pH meter HI8424 and a HANNA

instruments pH probe FC200B. The pH change for GδL solutions alone was measured using a HANNA instruments pH probe, HI1230. 1 mL of creamed emulsion was mixed gently with the desired concentration of GδL solution. Resulting solutions were placed in a fridge (4 ^{o}C) for 1 hour. On removal the separated water phase was removed before pH monitoring to provide a direct comparison with the rheometry data.

2.6. Chapter 6

2.6.1. Materials

Poly(ethylene glycol) methacrylate (M_n = 1,100 g.mol^{-1}), methacrylic acid, ethylene glycol dimethacrylate 1-dodecanethiol, Oil Red, Oil Blue, Toluidine Blue O and poly(methyl methacrylate) (M_w = 15,000 g.mol^{-1}) were all purchased from Aldrich and used as received. Ethanol and ethyl acetate were both standard laboratory grade. 2,2'-Azobis(isobutyronitrile) was purchased from BDH and recrystallised from methanol prior to use.

2.6.2. Colloid Preparation Via Emulsion-Solvent-Evaporation (ESE)

An aqueous P5 solution (2 wt. %, 3 mL) was homogenised with an equal volume of ethyl acetate containing PMMA (Mw = 15,000 g.mol^{-1}, 8 wt. %). Following emulsification, the ethyl acetate o/w system was diluted in distilled water (120 mL, pH 10) while stirring. The solution was gently purged with air using a submerged needle for 24 hours to remove the volatile ethyl acetate, yielding PMMA colloids. Unadsorbed branched copolymer surfactant was removed via centrifugation (14,000 rpm, 20 minutes x 3) and redispersion cycles using fresh water (pH 10), and the level of polymer surfactant desorption was quantified by both ICP analysis and surface tension measurements of the supernatants. Dye-loaded PMMA colloids were produced by initially dissolving hydrophobic dye (0.1 wt. %) in ethyl acetate before homogenisation. Dye-loaded PMMA colloids emulsions underwent the same purification process. Colloid sizes and polydispersities were recorded using laser diffraction.

2.6.3. Fabrication of Colloidal Aggregates

Aggregated colloid monoliths were prepared by acidifying colloid solutions in their dispersed state (pH 10) using HCl (1 M) to approximately pH 2. Colloidal aggregation could be observed within 1 minute by sedimentation. To form a monolithic aggregate, the mixture was centrifuged (4500 rpm, 20 minutes) and the supernatant removed. This process could then be repeated using different aggregated colloid mixtures (optionally loaded with hydrophobic dyes) to produce 'layered' monoliths.

2.6.4. Measuring Colloid Size at pH 10

All colloid size distributions were measured using laser diffraction. This technique allows measurement of the colloid particles in both their dispersed state (pH 10) and in the formation of micron-sized aggregates (pH 2). The general measurement protocol was as follows: 3 mL of the dilute colloid particle solution (the original 6 mL emulsion after dilution in 120 mL of pH 10 water, or 2.4 mg/mL total copolymer) was added to the dispersion unit containing 80 mL of distilled water (pH adjusted to 10 using 1 M NaOH). This solution was then pushed through the system as a stirring rate of 1,100 rpm. The resulting volume-average diameter, $D_{(4,3)}$, was obtained from at least 3 repeat runs.

2.6.5. Measuring Aggregation of Colloids

All colloidal aggregation was assessed using the same laser diffraction protocol described above. After at least three measurements of the colloids in their dispersed state at pH 10, the pH was lowered by addition of HCl (0.5 mL, 1 M), and the average size measured every minute. After seven measurements at pH 2, the pH was returned to pH 10 *via* the addition of NaOH (1 mL, 1 M). Repeated aggregation/redispersion processes were performed by changing the solution pH a number of times during the same measurement. This was done using successive HCl and NaOH additions and checking the resulting pH after every addition.

2.6.6. Washing Particles

In order to wash particles and remove any unadsorbed polymer, particle solutions were centrifuged (14,000 rpm, 20 minutes) and the resulting supernatant was

removed. The particles were redispersed in distilled water, the pH of which had been adjusted to pH 10 by the addition of NaOH (1 M). This process was then repeated twice more.

2.6.7. Qualitative Adsorption of Cationic Dye to Colloid Surfaces.

Aqueous solutions of washed PMMA colloids with three different branched copolymer stabilisers (EG:MAA 1:0, EG:MAA 1:1 and EG:MAA 1:2) were prepared at pH 10. Each solution was mixed with an aqueous solution of Toluidine Blue O (0.5 mM) at pH 10 for 1 hour. This suspension was then centrifuged (14,000 rpm, 20 minutes) to isolate the colloidal particles along with any dye that had been adsorbed onto the surface of the particles. The water phase was replaced with fresh water (pH 10) and the particles redispersed *via* stirring overnight (~16 hours). The resulting dispersions were then centrifuged once more to separate any remaining un-adsorbed dye and any desorbed dye. Particles were left to dry overnight at 35 ^{o}C and digital images were recorded to qualitatively show the levels of dye adsorbed on the colloid surfaces.

2.6.8. Calculating Free Polymer After Emulsion-Solvent-Evaporation

The amount of free copolymer in the nanoparticles solutions (2.4 mg/mL of total copolymer) before washing was calculated using both tensiometry and inductively coupled plasma mass spectrometry (ICP). Particles were sedimented *via* centrifugation (14,000 rpm, 20 minutes), after which a sample of the supernatant was removed and centrifuged twice more before analysis of the resulting supernatant. This was to ensure as many of the colloidal particles as possible were removed from the solution. In both cases, solutions containing known amounts of free copolymer P5 were measured in order to create a calibration curve. ICP was used to measure the sulfur content of samples and tensiometry measured the surface tension of samples. The sulfur content and surface tension of samples containing unknown amounts of P5 were then measured and the amount of free polymer was calculated.

2.6.9. Preparation of Air-Dried and Freeze-Dried Colloidal Aggregates

Two samples of the dilute colloid solution (15 mL, 2.4 mg/mL total copolymer) was acidified and centrifuged (4,500 rpm, 20 minutes) in order to form two colloidal aggregates. One of the aggregates was left at ambient temperature overnight to dehydrate; the other was frozen using liquid N_2 and freeze-dried overnight.

2.7. Chapter 7

2.7.1. Materials

Unfunctionalised superparamagnetic Fe_3O_4 magnetic nanoparticles (mNPs) were obtained as 20 – 30 nm nanopowders from Alfa Aesar. 3-Bromopropyl trimethoxysilane (Fluorochem), poly(ethylene glycol) methacrylate (M_n = 1,100 $g.mol^{-1}$), methacrylic acid, ethylene glycol dimethacrylate, 1-dodecanethiol, dodecane and 2-(diethylamino)ethyl methacrylate (PEAEMA) were all purchased from Aldrich and used as received (DEAEMA monomer was passed through an alumina column). The magnet used was a rare earth NdFeB magnet (MagnetSales) with 10 mm diameter, 5 mm thickness and 1.18 T strength. 2,2'-Azobis(isobutyronitrile) was purchased from BDH and recrystallised from methanol prior to use.

2.7.2. Synthesis of polyDEAEMA-Functionalised Fe_3O_4 Particles

In order to cover the surface of particles in ATRP initiator groups, iron oxide mNPs (1 g) were dispersed in toluene (50 mL) using ultrasonic agitation for 5 minutes. Excess 3-bromopropyl trimethoxysilane was then added dropwise and the mixture was sonicated for a further 5 minutes. The mixture was then refluxed overnight using mechanical stirring. The bromine-functionalised nanoparticles (Br-mNPs) were collected using a NdFeB permanent magnet, followed by repeated washing with acetone and drying under vacuum. Elemental analysis confirmed the degree of functionalisation. Based on the carbon content of the nanoparticles (C: 0.94 % and H: 0.39 %) and their surface area of 46.5 $m^2.g^{-1}$ (calculated using the 25 nm particle

size) a number of approximately 6,600 functional groups per nanoparticle was estimated.

Polymerisation from the surface of the mNPs was performed by dispersing Br-mNPs (50 mg) in isopropanol (10 mL) using ultrasonic agitation. DEAEMA (5 g) monomer was added to the magnetic dispersion and the mixture was degassed using N_2. Copper(I) bromide (0.1 g) and bipyridyl (0.33 g) were added to the degassed mixture. The sealed reaction system was then agitated by rolling at room temperature for 24 hours. polyDEAEMA (PDEAEMA) grafted mNPs remained discrete and successful grafting was confirmed by FTIR and elemental analysis.

2.7.3. Characterisation of PDEAEMA-Functionalised Fe_3O_4 Particles

SQUID samples were prepared by adding a small amount of PDEAEMA functionalised nanoparticles or magnetic EE (1.8 mg and 6.3 mg respectively) into a capsule filled with cotton. In order to prepare such a small EE, a spheroid was created using a magnetic P5-stabilised dodecane emulsion (15 μL), and roughly cut in half using a scalpel. TEM samples were dispersed in a few mL of ethanol and a drop of this dispersion was placed on a copper grid and allowed to dry in air.

2.7.4. Magnetic Engineered Emulsion Preparation

All EEs were created using the creamed layer of the emulsion (Φ_{oil} = 0.71) formed after equilibration. The creamed emulsion was pipetted into a tapered vial and HCl was added to trigger hydrogen bonding between the protonated MAA and EG residues on droplet surfaces. Removal of the vial left a monolithic emulsion assembly, which conformed to the dimensions of the vial template. In the case of the monolith which 'leans' toward the magnet, the structure was sculpted to half its original size using a scalpel, and it remained hydrated throughout the process *via* the addition of 1 M HCl. Magnetic EE spheroids were made by simply dripping aliquots of emulsion (10 μl) into aqueous acid using a micropipette. EEs containing site-isolated magnetic-engineered emulsion were made by firstly creating a monolithic emulsion assembly using the PDEAEMA-mNP containing emulsion. Upon vial removal, a larger vial was placed around the monolith and non-magnetic pH responsive emulsion was aggregated. After aggregation for 24 hours, the larger vial

was removed, and the resulting monolith was sliced horizontally to give 1-2 mm thick 'discs' of this 2-component EE with localised magnetic domains.

2.8. References

(1) Graham, S.; Cormack, P. A. G.; Sherrington, D. C. *Macromolecules* **2005**, *38*, 86.
(2) Xia, Y. N.; Whitesides, G. M. *Annu. Rev. Mater. Sci.* **1998**, *28*, 153.

CHAPTER 3

The Role of Branched Copolymer Composition in Controlling pH Triggered Aggregation of Emulsion Droplets

(Publication arising from this Chapter: **"The role of responsive branched copolymer composition in controlling pH-triggered aggregation of "engineered" emulsion droplets: towards selective droplet assembly"**, R. T. Woodward, J. V. M. Weaver, *Polym. Chem.*, 2011, *2*, 403-410.)

List of Figures

List of Tables

3.1. Introduction

Controlled and reversible assembly of functional materials *via* precise design is becoming increasingly popular in scientific literature. Much of the drive for these types of materials stems from similar processes in biological systems.[1,2] Synthetic materials with a number of different properties, such as self-assembly[3,4] and self-organisation[5] have also been used to create more complex polymer assemblies or 'supramolecular polymers'.[6,7] Non-covalent interactions can drive many of these assembly processes, for example, hydrogen bonding,[8] π–π stacking,[9,10] hydrophobic interactions[11] and electrostatic interactions.[12] Processes involving non-covalent interactions are more favourable due to greater adaptability of the products to a local environment, for example the varied strength of hydrogen bonding in proteins, dependent on environment.[13] Synthesis is also achieving similar targeted interactions, such as an enantiomerically pure hydrogen-bonded assembly[14] and selective assembly.[15] Similar to nature, these selective interactions are being utilised to create complex, ordered, hierarchical structures.[16-18] Some of these assembly mechanisms employ emulsion droplets as templates for the formation of hierarchical materials.[19-21]

Emulsion droplets have a number of key characteristics, which may aid the understanding of inter-particle interactions. Emulsions can be very stable, and can have functionalised surfaces *via* surfactant design.[22-26] In Chapter 1.11.5 the formation of engineered emulsions was discussed, permitted by oil droplets stabilised with branched copolymeric surfactants comprising mainly poly(ethylene glycol) (PEG) and poly(methacrylic acid) (PMAA).[24] In previous reports, the MAA and EG have been synthesised in polymers in a 1:1 stoichiometric ratio as EG:MAA hydrogen bonds occur following precise stoichiometry.[24,27]

In this Chapter, the role of the branched copolymer composition, specifically the EG:MAA ratio, in the formation of engineered emulsions is investigated. A change in the EG:MAA ratio may alter the rate of droplet assembly, potentially resulting in a change of the engineered emulsion's mechanical properties. This study also examines what role the design of the copolymer plays in selective inter-droplet hydrogen bonding, again exploiting the pH-triggered interaction of MAA and EG groups.

3.2. Results and Discussion

3.2.1. Synthesis of Branched Copolymer Surfactants

A library of branched copolymers was synthesised comprising poly(ethylene glycol) methacrylate (PEGMA) (M_n = 1,100 g.mol^{-1}) and MAA with 1-dodecanethiol (DDT) chain-ends and an ethylene glycol dimethacrylate (EGDMA) branching agent. In this study the molar ratio of EG:MAA in the polymers was varied around previously reported 1:1, as this was suggested as the theoretical maximum hydrogen bonding system.[27] An efficient, hydrophobic chain transfer agent was required in order to anchor the polymer to the oil droplet surface. DDT was selected as it has previously been shown to interact favourably with dodecane oil phases, allowing stable droplets.[22,24] EGDMA was present in all polymers, incorporated at 10 mol % relative to the total amount of monofunctional monomer. Theoretically, all copolymers have compositions of MFM_{100}–$EGDMA_{10}$–DDT_{10}, in which MFM can be MAA, PEGMA or various ratios of the two. All copolymers were produced in a one-pot synthesis at 70 ^{o}C in ethanol *via* the 'Strathclyde approach'. AIBN was used as an initiator, and all reactions were allowed to proceed for 48 hours. After this time, the ethanol was removed and the copolymers were then washed with cold diethyl ether and dried. Table 3.1 shows the target composition and actual calculated monomer ratio data for the branched copolymers.

Table 3.1. Target copolymer composition and comonomer molar ratio calculated using ^{1}H NMR. Target EG:MAA ratios are shown in the last column.

ID	Target Copolymer Composition	Calculated Monomer Ratio[a]	Theoretical EG:MA Molar Ratio
P1	MAA_{100}-$EGDMA_{10}$-DDT_{10}	MA_{100}	0:1
P2	$PEGMA_{0.83}/MA_{99.17}$-$EGDMA_{10}$-DDT_{10}	$PEGMA_{1.83}/MA_{98.2}$	1:6
P3	$PEGMA_{1.25}/MA_{98.75}$-$EGDMA_{10}$-DDT_{10}	$PEGMA_{2.5}/MA_{97.5}$	1:4
P4	$PEGMA_{2.5}/MA_{97.5}$-$EGDMA_{10}$-DDT_{10}	$PEGMA_{4.4}/MA_{95.6}$	1:2
P5	$PEGMA_{5}/MA_{95}$-$EGDMA_{10}$-DDT_{10}	$PEGMA_{7.7}/MA_{92.3}$	1:1
P6	$PEGMA_{10}/MA_{90}$-$EGDMA_{10}$-DDT_{10}	$PEGMA_{13.8}/MA_{86.2}$	2:1
P7	$PEGMA_{20}/MA_{80}$-$EGDMA_{10}$-DDT_{10}	$PEGMA_{24.5}/MA_{75.5}$	4:1
P8	$PEGMA_{30}/MA_{70}$-$EGDMA_{10}$-DDT_{10}	$PEGMA_{34.4}/MA_{65.6}$	6:1
P9	$PEGMA_{100}$-$EGDMA_{10}$-DDT_{10}	$PEGMA_{100}$	1:0

[a] Determined by ^{1}H NMR of esterified branched copolymers

The calculated comonomer ratios within the final copolymers were determined by ^{1}H NMR spectroscopy of the copolymers. The MAA groups of the copolymers were esterified using trimethylsilyl diazomethane (TMSDMA)[28] in order to render them soluble in THF for measurement by GPC. Esterification also allowed determination of EG:MAA ratio within each copolymer, due to an extra peak arising from the new terminal methyl group on the ester (in order to calculate this molar ratio, it was assumed all MAA groups were esterified). Changing EG:MAA ratios in some cases requires only a very subtle change of PEGMA and MAA monomer feed ratios and such small changes are within the error of the characterisation techniques employed. The copolymers, however, did display systematic variation throughout the series and gave the expected general trend in ratios. Stacked ^{1}H NMR spectra of esterified copolymers P2–P8 show this change in EG:MAA peaks (peaks c and h represent the EG and esterified MAA respectively), allowing calculation of the actual comonomer ratio (Figure 3.1). Full ^{1}H NMR spectra are shown in the experimental section in Chapter 2.3.2.

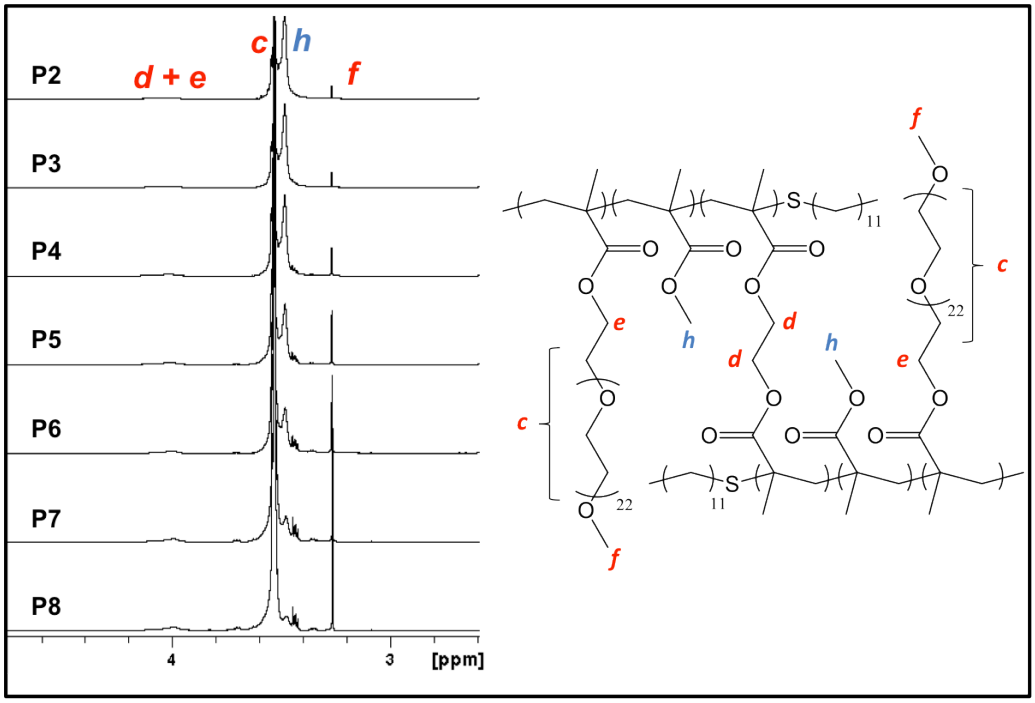

Figure 3.1 Figure showing partial ^{1}H NMR spectra in which the EG:MAA molar ratio is calculated *via* peaks representing esterified MAA (h) and the repeating EG group (c). Theoretical copolymer structure is shown for reference.

Triple-detection GPC analysis in a THF eluent of the copolymers, after esterification, was used to analyse all MAA-containing copolymers, the chromatograms of which are shown in Figure 3.2. Chromatograms of copolymers P1-P4 all appear similar in shape, with broad distributions indicative of branched copolymers. However, chromatograms for P5-P8 suggest that copolymers become less polydisperse with increasing PEGMA content/decreasing MAA content.

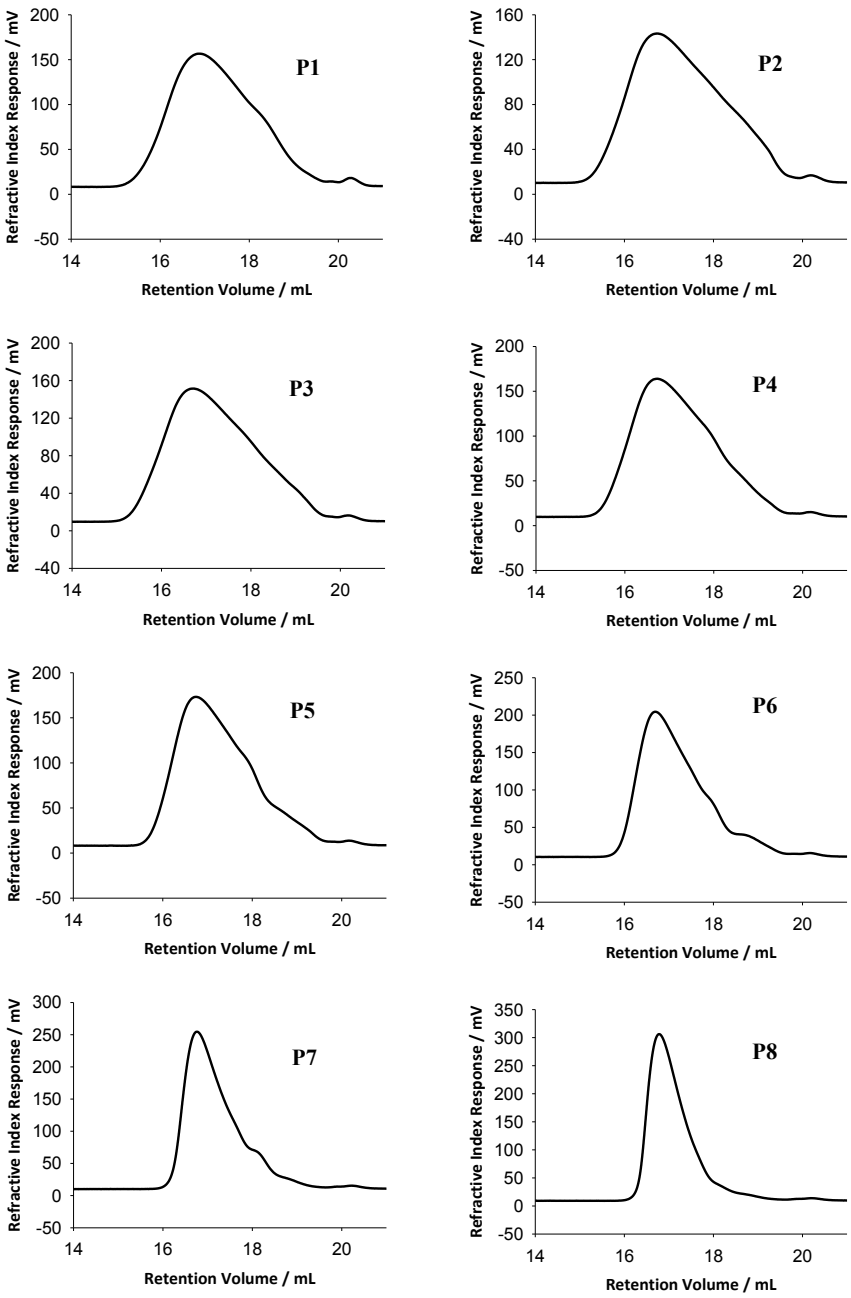

Figure 3.2. THF GPC chromatograms of copolymers P1-P8.

GPC results are shown in Table 3.2. These results were consistent with previous studies on similar systems,[26,29,30] suggesting that soluble copolymers with branched architectures were produced. GPC data could not be obtained for the $PEGMA_{100}$-$EGDMA_{10}$-DDT_{10} (P9) branched copolymer using this eluent. The GPC data in Table 3.2 recorded for these copolymers may not be absolute due to the complex architecture of the molecules.[22,29] Nevertheless, similar weight-average molecular weights (M_w) were obtained for all copolymers. The number-average molecular weights (M_n) increased with increasing PEGMA resulting in a reduction in M_w/M_n, known as the polydispersity index (PDI). As M_n is more sensitive to small molecules, this suggests that fewer short chains are being produced in polymerisations containing more PEGMA. However, the upper end of molecular weight remained roughly the same, most likely due to the large amount of chain transfer agent added. Systematic increase in M_n may be due to the polymerisation of larger monomers, as PEGMA is more than ten times the molecular weight of MAA. Only three PEGMA monomers need to polymerise to obtain a molecule with a molecular weight of 3,300 $g.mol^{-1}$, therefore, fewer copolymer chains with low molecular weights are produced.

Table 3.2. Summary of surface tension and GPC data of all copolymers (excluding P9 in GPC).

ID	EG:MAA	M_w / g mol^{-1}	M_n / g mol^{-1}	PDI	α [a]	Surface Tension / mN m^{-1} [b]
P1	0:1	17,700	3,700	4.7	0.29	42
P2	1:6	18,300	3,300	5.6	0.27	39
P3	1:4	19,700	3,400	5.9	0.26	41
P4	1:2	18,800	3,700	5.1	0.26	42
P5	1:1	17,100	4,100	4.1	0.23	39
P6	2:1	17,800	4,100	4.4	0.22	43
P7	4:1	16,900	6,900	2.4	0.21	37
P8	6:1	18,400	6,500	2.8	0.21	48
P9	1:0	-	-	-	-	49

[a] Mark-Houwink alpha values determined by GPC. [b] Measured using a Kibron Delta-8 parallel plate tensiometer and represents surface tension of 2 wt. % aqueous solutions at pH 10.

From both the GPC and ^1H NMR, we have high confidence that, within this series, the relative EG:MAA molar ratio follow a systematic trend. All Mark–Houwink α-

values are below 0.3 for the branched copolymers, indicating relatively compact conformations, which is expected of copolymers with branched architectures.[24,29,31] Linear analogues of both P5 and P6 were produced and analysed. The α-values of these linear analogues were measured by THF GPC as 0.79 for P5 and 0.51 for P6, more than doubling the values measured for the branched equivalents (0.23 and 0.22 respectively). The α-values for all branched copolymers vary systematically in Table 3.2, decreasing with increasing PEGMA content. This is expected, as PEGMA is itself a polymer, therefore the structure of the resulting copolymer backbones should become more comb-like. This results in both inter-backbone branching and the PEG grafts from the copolymer backbone contributing to increased branching in copolymers with increasing PEGMA:MAA molar ratio, resulting in lower α-values.

Table 3.2 also shows the surface tension of each copolymer in pH 10 solution at a mass percentage of 2 wt. %. All of these copolymers reduce the surface tension to between 37 and 49 mN/m^{-1}, meaning they are all surface-active. The surface tension of P1-P7 are in are good agreement with each other (between 37-42 mN/m^{-1}), but P8 and P9 solutions show slightly higher surface tensions (48 and 49 mN/m^{-1} respectively), suggesting that when a large excess of PEGMA is present, copolymers are not as surface-active. This may be due to increased amounts of the large PEGMA monomer hindering rearrangement of the copolymer, meaning hydrophobic chain ends may not be as readily available to anchor the copolymers at the air-water interface, leading to increased surface tension. The surface tension of copolymer solutions with increasing copolymer concentration are shown in Figure 3.3. It can be seen from these results that all copolymers show similar curves with increasing concentration, with the exception of P8 and P9.

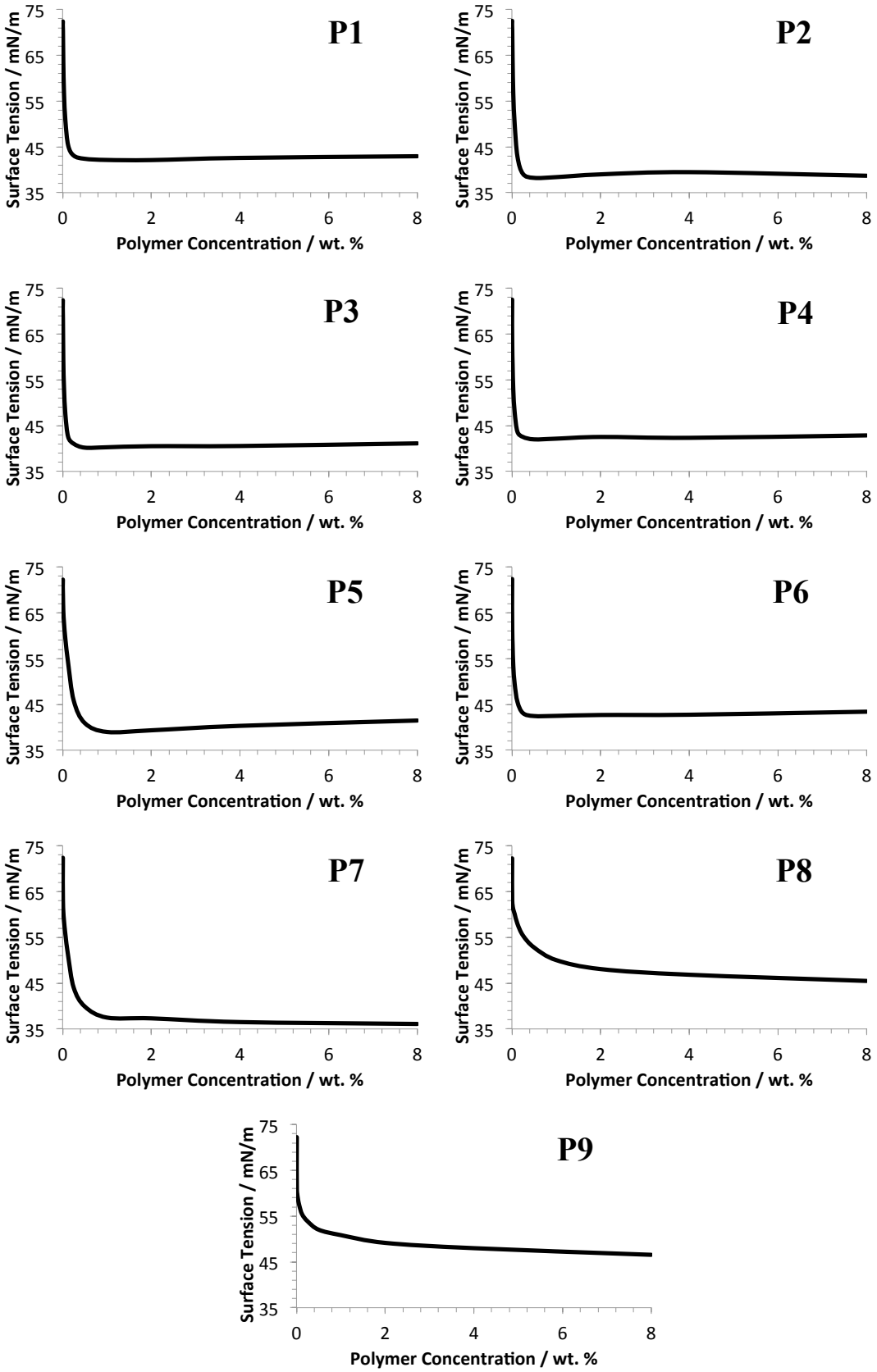

Figure 3.3. The surface tension of copolymers P1-P9 was measured at pH 10 with increasing concentration.

3.2.2. Efficiency of Branched Copolymers as Emulsifiers

To form the emulsions, aqueous solutions (3 mL) of each of the branched copolymers (2.0 wt. %, pH 10) were homogenised for 2 minutes (at 24,000 revolutions per minute (rpm)) with an equal volume of dodecane. The resulting emulsions were then left to equilibrate for 24 hours. All polymers resulted in a dodecane o/w emulsion, as demonstrated in Figure 3.4 by the addition of a P5 dodecane emulsion (100 μL) to both a water (5 mL) and a dodecane (5 mL) continuous phase. Upon addition of the emulsion to water, the sample dispersed across the surface of the sample, indicative of an o/w emulsion as it is diluted in the water phase. The emulsion did not disperse in dodecane, as expected for an o/w emulsion.

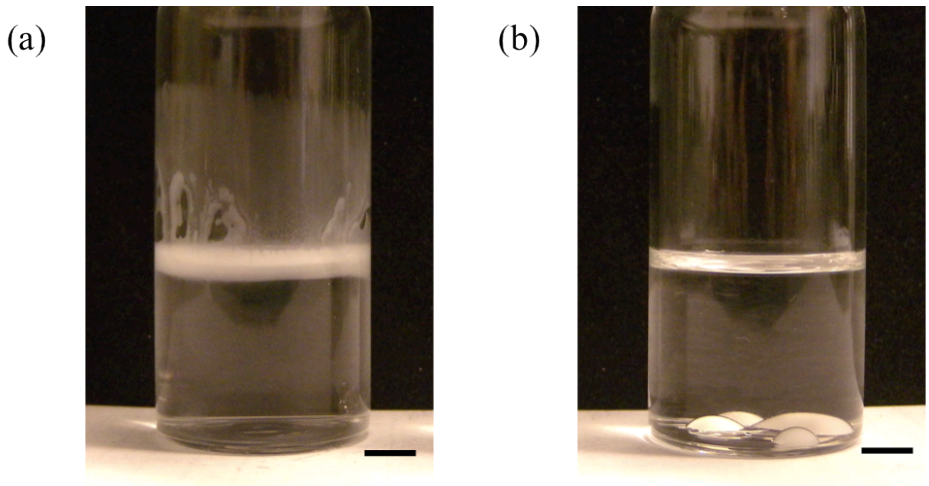

Figure 3.4. Digital images of a P5 dodecane emulsion after addition to (a) a continuous water phase and (b) a continuous dodecane phase. Scale bars represent 5 mm.

Dodecane o/w emulsions produced using linear equivalents of copolymers P5 and P6 coalesced over 3-4 weeks, presumably due to weak adhesion to droplet surfaces *via* a single hydrophobic chain end. In contrast for branched copolymer stabilised emulsions, no demulsification was observed in any of the 9 samples (P1-P9) over at least 6 months. During equilibration, the oil droplets creamed as expected, due to the dispersed dodecane being less dense (0.75 g cm^{-3}) than the continuous aqueous phase (1.0 g cm^{-3}). The volume fraction of oil (Φ_{oil}) in the creamed layer of each emulsion, shown in Table 3.3, was judged by measuring the volume of the creamed layer and the water below. Assuming all of the oil was in the creamed layer, as both water and dodecane were added in equal amounts, this ratio of creamed layer to remaining

water allowed for simple calculation of Φ_{oil}. The creamed layer could be redispersed by simple agitation if necessary. The volume-average droplet diameters ($D_{(4,3)}$) of each sample were measured by laser diffraction at pH 10 (Table 3.3), with E1 representing an emulsion stabilised by P1, E2 by P2 etc. $D_{(4,3)}$ ($D_{(4,3)} = \Sigma D_i^4 N_i / \Sigma D_i^3 N_i$) is used to provide average droplet diameters as its calculation does not require the amount of particles present, only the diameter of each particle measured. This is useful for laser diffraction measurements as the scattering angle of particles is measured to calculate droplet diameter, but the amount of particles in the system is not known.

Excess copolymer in the water phase was measured for a P5 stabilised dodecane o/w emulsion (E5) using surface tensiometry (see Chapter 2.3.3.) and was found to correlate to 5.0 % of the initial copolymer added (or 0.1 wt. %). A calibration curve was produced measuring the change in surface tension with decreasing concentration of P5 in an aqueous pH 10 solution. The amount of free polymer was then calculated using the surface tension measured for E5's water phase. From this result we can assume that the remaining 95 % of the polymeric surfactant is adsorbed at the o/w interface. $D_{(4,3)}$ of the droplets ranges between 5.7 and 10.9 μm at pH 10 in all samples, which is lower than for similar branched polymers.[26]

Table 3.3. Table of emulsions stabilised with copolymers from Table 3.1, showing span of droplets, oil fraction volume (ϕ_{oil}), volume-average diameter ($D_{(4,3)}$) at pH 10 and at pH 2 (after 10 min).

ID	EG:MAA	ϕ_{oil}[a]	$D_{(4,3)}$ at pH 10 / μm[b]	Span[b]	Increase in $D_{(4,3)}$ at pH 2 / μm[c]
E1	0:1	0.73	9.6	1.25	0.6
E2	1:6	0.71	10.9	1.01	3.7
E3	1:4	0.71	5.7	1.43	3.1
E4	1:2	0.71	6	1.23	23.7
E5	1:1	0.69	5.7	1.18	39.1
E6	2:1	0.69	7.1	1.18	0
E7	4:1	0.71	7.7	1.17	0
E8	6:1	0.71	7.9	1.10	0
E9	1:0	0.71	6.9	1.24	0

[a] Determined by phase volume on creaming. [b] Measured by laser diffraction. [c] Measured by laser diffraction 10 minutes after reducing pH to pH 2.

Table 3.3 also shows droplet spans and increase in $D_{(4,3)}$ when the solution pH is lowered to pH 2 during laser diffraction measurements. The span is a measure of the width of a particle size distribution. It is expressed mathematically as (D(0.9) – D(0.1))/D(0.5), where D(0.9) is the diameter under which 90 % of particles fall, D(0.5) is the diameter under which 50 % of particles fall and D(0.1) is the diameter under which 10 % of particles fall. The spans of E1-E9 samples ranged between 1.01 and 1.43 at pH 10. Size effects of droplets on the kinetics of aggregation are therefore minimised, as the droplets are all of a similar diameter.

The change in $D_{(4,3)}$ presented in Table 3.3 was measured after 10 minutes in the pH 2 solution, either showing a large change in average droplet diameter due to aggregation (e.g. E4 & E5), or minimal change in size as no inter-droplet hydrogen bonding occurs (e.g. E6-E9). The laser diffraction measurement for each emulsion sample at pH 10 is shown in Figure 3.5. All samples, with the exception of E2, gave bimodal distributions. However a large majority of droplets in all samples fall under a single peak. The existence of this bimodal droplet distribution could be due to slight variations in emulsion preparation such as homogenisation times and speeds as bimodal distributions are not always obtained upon emulsification. It is seen throughout the thesis that both unimodal and bimodal distributions are obtained, even when emulsion samples are produced using apparently the same conditions.

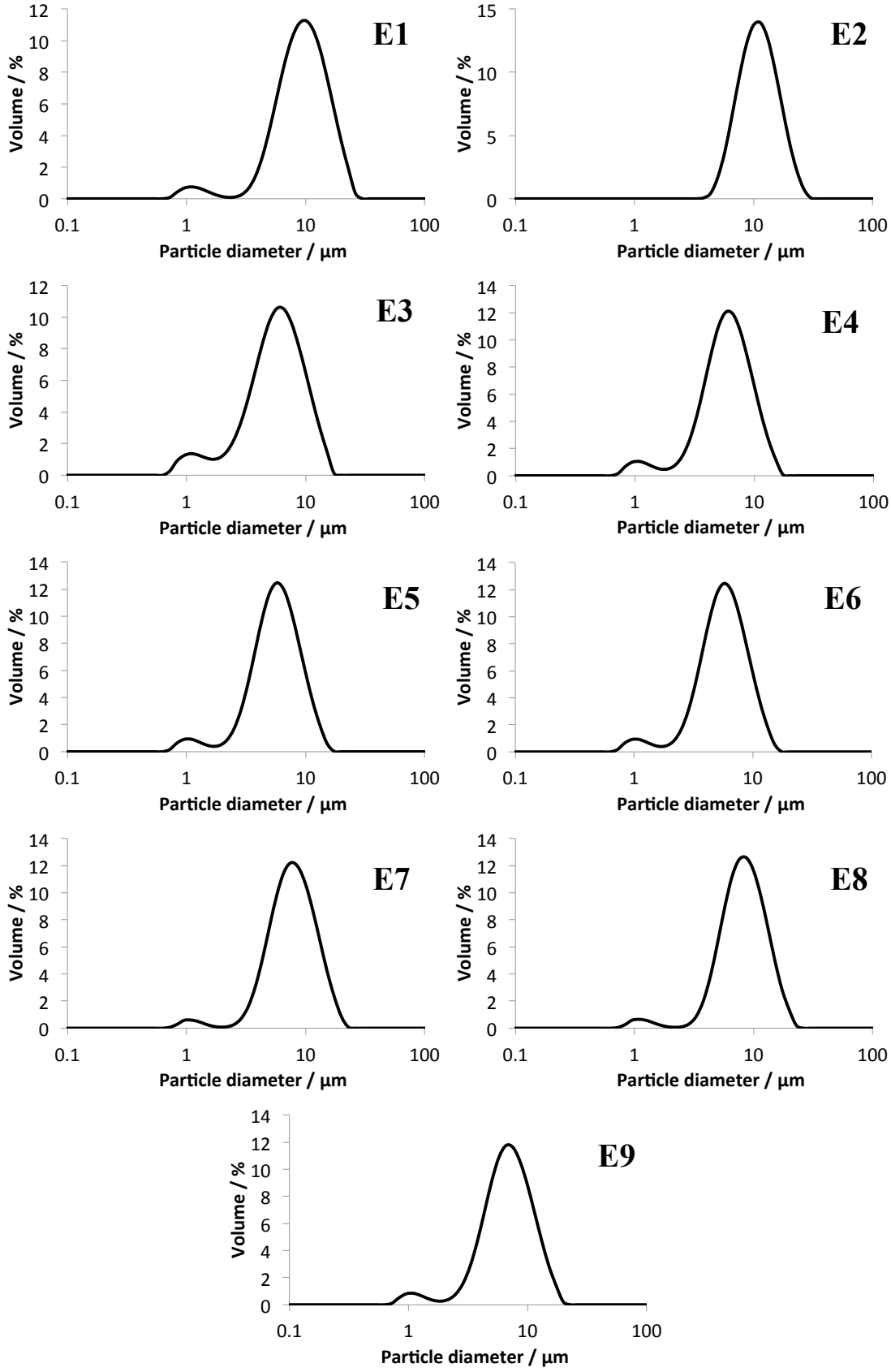

Figure 3.5. Laser diffraction droplet size distributions for all emulsions (E1-E9) (40 µL) diluted in pH 10 water (80 mL). All measurements were recorded at a stirring rate of 1,100 rpm.

3.2.3. Droplet Aggregation with Varying Polymer Composition

As it is now known that each of the branched copolymers gave stable droplets upon homogenisation at pH 10, the acid-triggered aggregation of each emulsion in the formation of engineered emulsions was investigated. Dilute aqueous solutions of each emulsion sample (40 μL of creamed emulsion in 80 mL water) at pH 10 were analysed by laser diffraction at one measurement per minute for around 3 minutes. This allowed the emulsion some equilibration time in the relatively large volume of pH 10 water. After this time the dilute emulsion systems were acidified by addition of hydrochloric acid (HCl) (1 M, 0.8 mL), and the $D_{(4,3)}$ was monitored as a function of time, again at one measurement per minute, for 10 minutes. Inter-droplet aggregation was then measured by any subsequent increase in $D_{(4,3)}$. Samples E6-E9, those stabilised with branched copolymers containing excess PEGMA, showed negligible change in $D_{(4,3)}$ suggesting that even in small excess relative to MAA, PEGMA provides an efficient steric barrier to prevent inter-droplet interactions, and therefore aggregation (Figure 3.6).

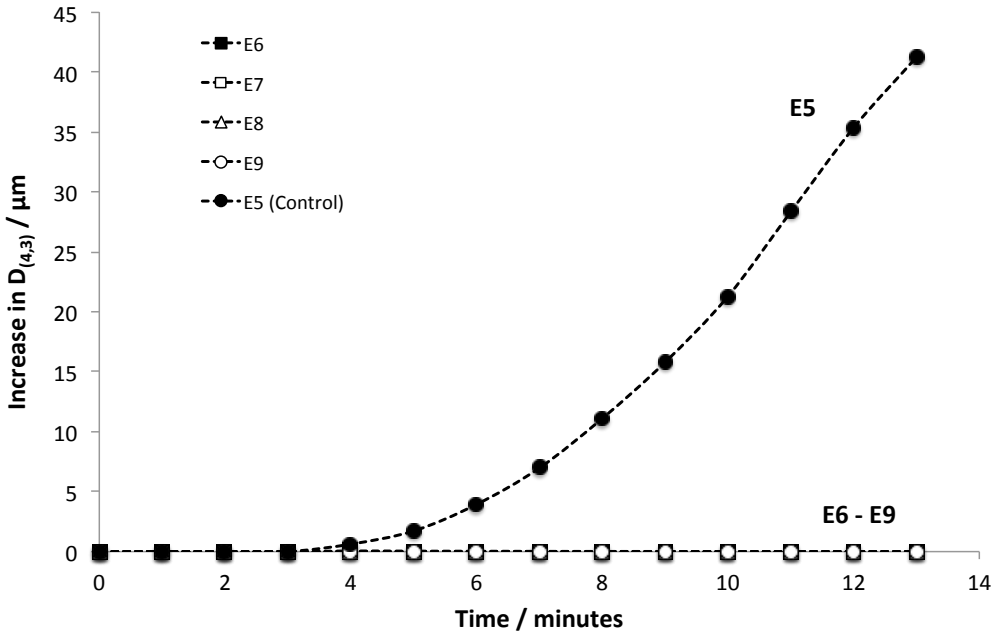

Figure 3.6. Change in $D_{(4,3)}$ as a function of time for samples with an increasing EG:MA ratio. Excess PEGMA inhibits aggregation as shown by no increase in $D_{(4,3)}$ for samples E6 – E9 upon a lowering of pH. Solution is switched from pH 10 to pH 2 at 3 minutes.

With the exception of P9 used to stabilise E9, MAA groups are still present in all the copolymeric surfactants, suggesting that some hydrogen bonding must still occur, yet

the excess EG residues at droplet surfaces effectively ‘‘switch off’’ inter-droplet aggregation. Droplets may only undergo intra-droplet hydrogen bonding in the presence of excess PEGMA, but consumption of all of the acid sites on droplets surfaces may result in the remaining non-hydrogen bonded PEGMA providing sufficient steric stabilisation for the droplet. This agrees with the literature on the efficiency of PEG in restricting both ionic[32] and covalent[33] cross-linking within localised micellar domains.

Samples E1-E4 droplets stabilised with branched copolymers containing excess MAA were acidified under the same conditions as the EG-rich droplets. All droplets showed some increase in $D_{(4,3)}$ over a 10 minute period (Figure 3.7), but only the E4 droplets showed signs of significant aggregation. This again suggests that intra-droplet hydrogen bonding may saturate all EG sites upon the addition of acid, meaning no PEGMA remains to allow inter-droplet hydrogen bonding. The E4 droplets gave an average diameter increase of 24 μm over 10 minutes, compared to 2.1 μm and 3.2 μm for E2 and E3 respectively. Both the E3 and E2 samples increase in size initially but reach a plateau after 1-2 minutes.

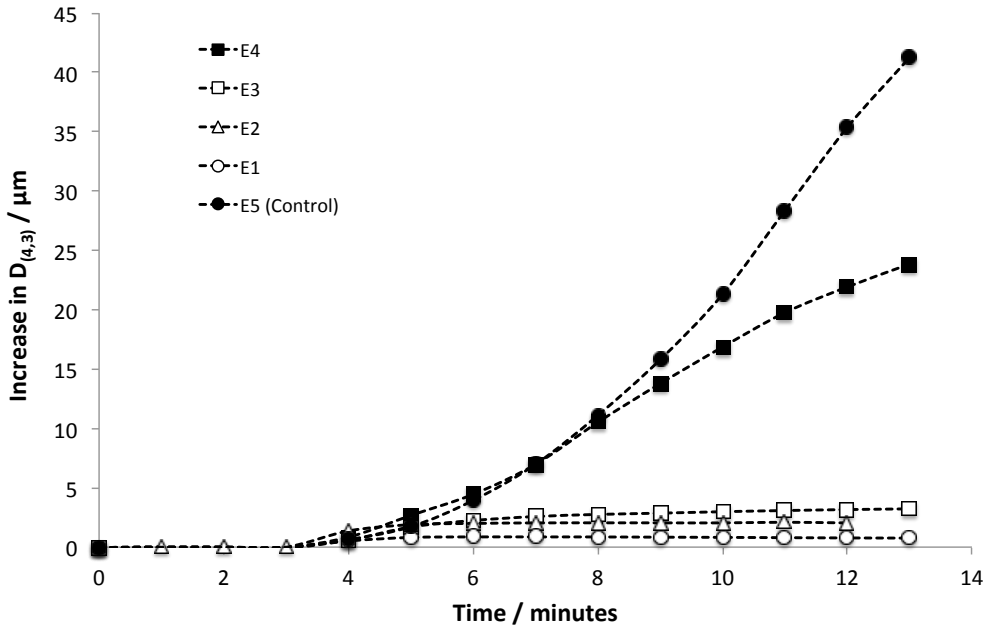

Figure 3.7. Change in $D_{(4,3)}$ as a function of time for samples with a decreasing EG:MAA ratio. Excess MAA slows aggregation, but does not stop it completely. Solution is switched from pH 10 to pH 2 at 3 minutes.

Unlike the EG-rich droplets, all droplets with excess surface MAA groups are able to aggregate to some extent when the solution is lowered to pH 2. Lower shear environments may actually allow continued aggregation, as when droplets are highly concentrated, as in the creamed layer, visible aggregation appears to occur upon lowering the pH. Continued aggregation with increasing concentration of MAA residues could be due to increased hydrophobicity caused by the protonation of MAA groups, leading to hydrophobic interactions. This process also removes the electrostatic stabilisation present at high pH. Aggregation may also be due to the formation of MAA dimers, giving rise to inter-droplet MAA-MAA interactions.[34-36]

Figure 3.8 shows the increase in $D_{(4,3)}$ after 10 minutes for all emulsion droplets displayed as a function of EG mole % content with respect to MAA. The maximum amount of aggregation occurs in sample E5, when EG and MAA are present in a 1:1 stoichiometric ratio. This is consistent with previous work,[24,27] and suggests that hydrogen bonding plays a crucial role in the inter-droplet aggregation process. However, unlike surfaces rich in EG, aggregation still occurs in MAA-rich droplets. This result implies that, in addition to EG–MAA hydrogen bonding, some hydrophobic interactions and MAA dimer hydrogen bonding may contribute towards aggregation in all systems with no excess PEGMA. This is an important result, as previously inter-droplet aggregation was attributed solely to hydrogen bonding.[24]

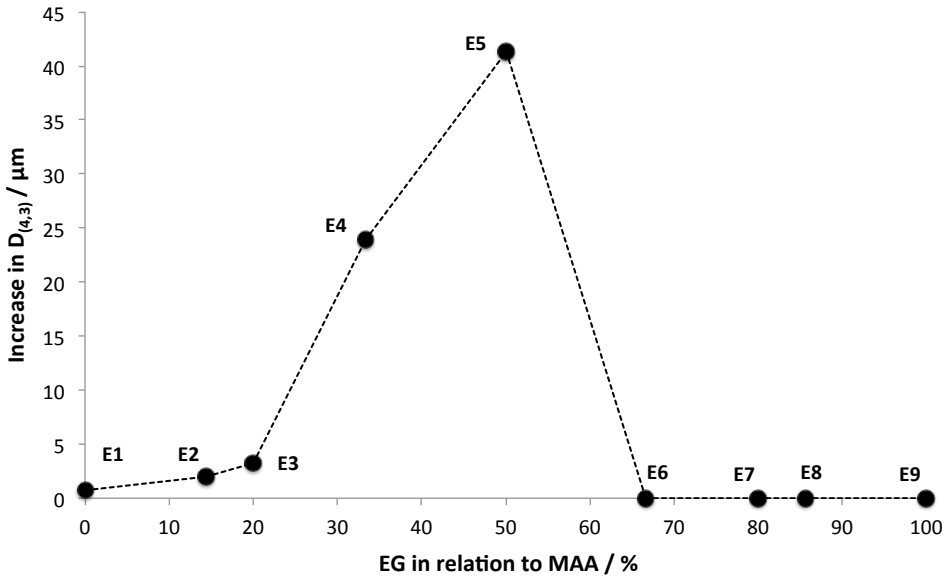

Figure 3.8. Increase in volume-average droplet diameter $D_{(4,3)}$ after 10 minutes at pH 2, as a function of EG % relative to MAA for emulsions E1-E9.

3.2.4. Rheology of Engineered Emulsions

Now that more was understood about the role that EG and MAA play in inter-droplet aggregation, their influence on the mechanical properties of the resulting EEs was investigated. Rheometry was used to measure the storage (G') and loss (G") moduli for the engineered emulsion samples at acidic pH (pH < 2). G' is a measure of deformation energy stored by the sample when undergoing strain, or a measure of a material's elastic behaviour. G" is a measure of the deformation energy lost by the sample undergoing strain, due to a change in structure, for example the breaking down of a structured material.[37] G" can be defined as a measure of the viscous behaviour of a material. Amplitude sweeps measure G' and G" of samples undergoing increasing strain while maintaining a constant angular frequency (ω = 10 rad.s^{-1}). These measurements were performed on all samples (E1-E9) and are shown in Figure 3.9.

When G' > G", a material is considered to be more solid-like than liquid-like (or more elastic than viscous), whereas when G" > G', the material displays more liquid-like behaviour.[38] Each emulsion's creamed layer (2.5 mL) was placed on the rheometer prior to measurement and acidified *in situ*. HCl (1 M, 0.5 mL) was added to each sample 2 hours prior to measurement, after which time amplitude sweeps were performed. Samples E1-E5 appeared to aggregate within 1-2 minutes of the addition of the HCl, but samples E6-E9 did not appear to shown any EE formation. Excess HCl solution was removed from both systems prior to measurement. Some creaming had occurred in samples E6-E9 due to the lack of aggregation, but the resulting water phase was easily removed by pipette.

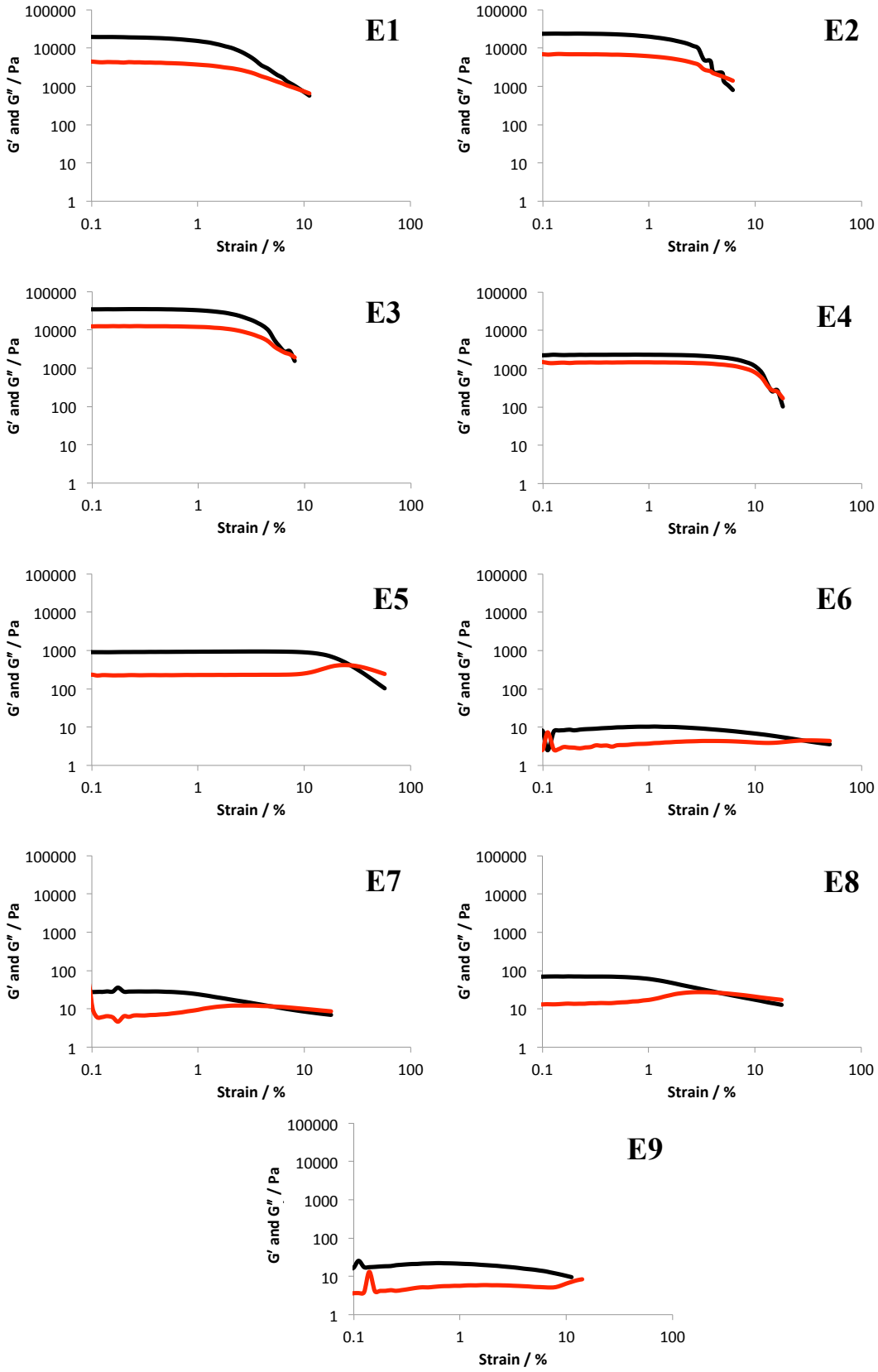

Figure 3.9. Amplitude sweeps for all emulsions showing both G' (black) and G" (red) for each sample.

From Figure 3.9 it is clear that, initially, all samples had G' > G", suggesting that all samples showed a greater elastic than viscous response. To compare the stiffness of each system, the G' of each sample at 0.5 % strain was plotted (Figure 3.10). This strain value was selected as it was in the linear viscoelastic (LVE) region for each sample, this is the region in which G' and G" are linear with increasing strain. As droplets containing excess PEGMA at their surfaces do not form aggregates, they remained as free-flowing emulsions after acidification, which resulted in low G' in the LVE. All MAA-rich emulsion droplets showed signs of aggregation on the addition of acid.

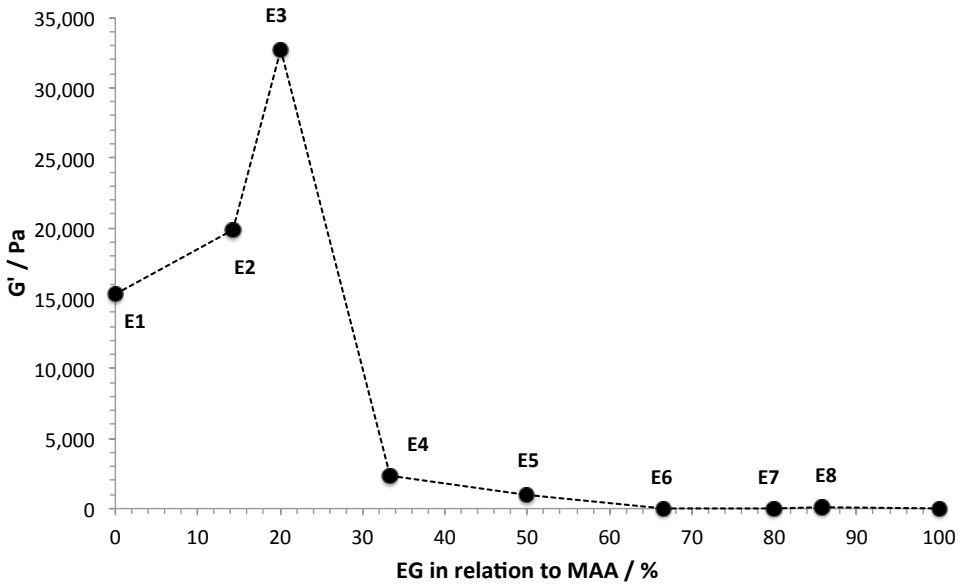

Figure 3.10. Storage modulus (G') at 1 % strain as a function of EG content (expressed as a % relative to MAA residues) at pH 2.

This result was in contrast to the aggregation data measured by laser diffraction. However, it is worth noting that laser diffraction data was recorded at high dilution, ($\Phi_{oil} \approx 4 \times 10^{-4}$) which may hinder droplet-droplet interaction. The droplet concentrations were much higher in rheometry measurements as the creamed emulsion layer was used (Φ_{oil} = 0.69–0.74). This large difference is due to differences in measurement techniques between instruments, as samples are dispersed in an aqueous reservoir for laser diffraction measurements. The rheology data of the concentrated emulsions confirmed that excess MAA induces greater engineered emulsion gel stiffness, with a peak in G' at around 80 mol % MAA with

respect to EG (E3). Above this amount of MAA the G' is reduced, but remains larger than that obtained for the 1:1 EG:MAA stabilised droplets (E5). As G' peaks at 80 mol % MAA, this suggests that some EG units are required for hydrogen bonding in order to achieve significant mechanical strength.

As these materials are subjected to higher strain, the G' starts to decrease as the structure begins to break down (as seen in Figure 3.9). As a measure of this, the strain at which G' becomes 90 % of its LVE region value can be quoted, in order to give an indication of the point at which materials begin to break down. This value for each emulsion (E1-E9) has been plotted against EG content relative to MAA in Figure 3.11. These data suggest that, although E5 does not yield the stiffest engineered emulsion, it does exhibit the maximum resilience to strain. E5 does not reach 90 % of its LVE region G' value until 14.2 % strain, whereas none of the other samples exceeded 4.5 % strain before the G' has fallen below this value.

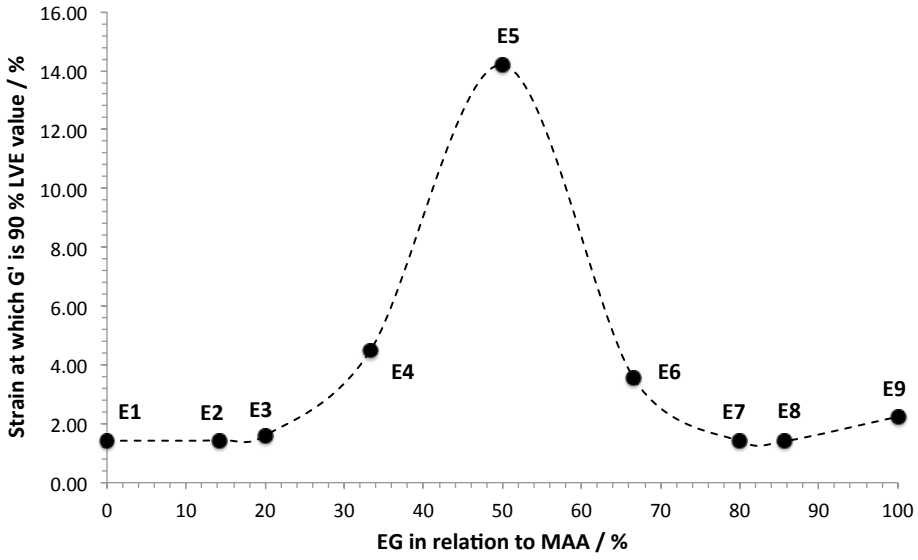

Figure 3.11. The strain at which G' is 90 % its LVE region value vs. EG content (expressed as a % relative to MAA units).

3.2.5. Selective Droplet Aggregation

As little or no aggregation was measured for 100 % MAA (E1) and 100 % EG (E9) emulsions by laser diffraction, we investigated whether binary mixtures of these droplets with complementary functionality could produce any inter-droplet aggregation. As both samples produced stable emulsions (no demulsification occurring for at least 6 months), each droplet should be stabilised with one half of

this triggered hydrogen bonding system. In theory, droplets should assemble selectively, EG droplets seeking out MAA and vice versa (Figure 3.12(a) and (b)).

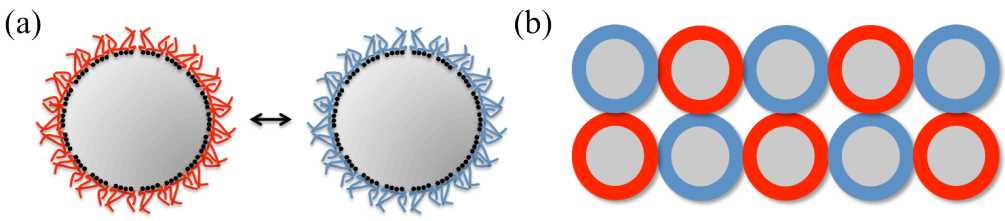

Figure 3.12. Schematic representation of (a) selective assembly between EG (blue) and MAA (red) droplets and (b) the theoretical composition of their resulting engineered emulsion assuming monodisperse emulsion droplets.

Acid-triggered aggregation of dilute dispersions containing both 100 % EG and 100 % MAA droplets was measured by laser diffraction as a function of time and compared to acid-triggered aggregation of the pure EG and MAA droplets in isolation (Figure 3.13). The binary mixture displays a significant and immediate increase in $D_{(4,3)}$ in comparison to little or no aggregation for the isolated samples. Selective aggregation of the contra-functional droplets provides additional confirmation that EG–MAA hydrogen-bonding plays a crucial role in the engineering of emulsions.

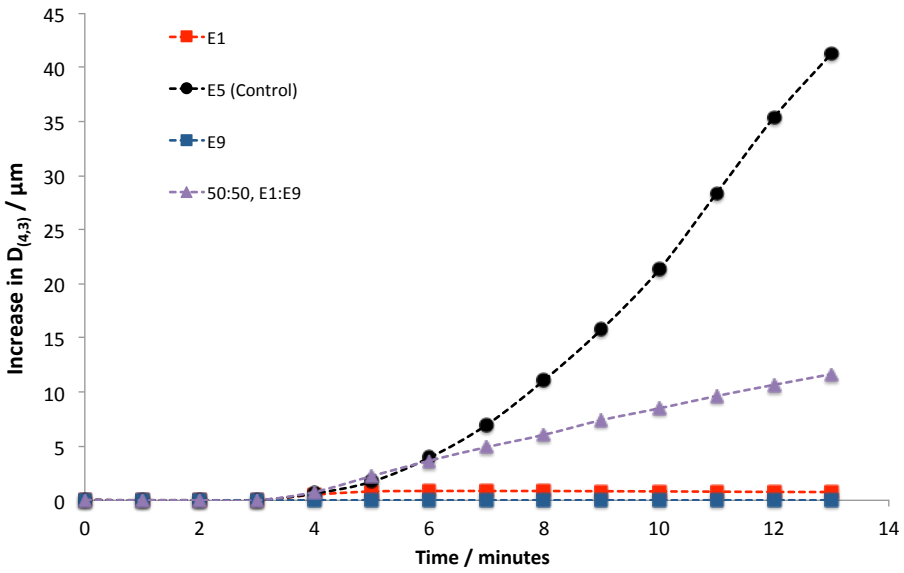

Figure 3.13. Change in volume-average droplet diameter ($D_{(4,3)}$) with time. pH = 10 for the first four measurements, and the solution is lowered to pH 2 after this point.

In comparison to the aggregation of E5 droplets, the change in $D_{(4,3)}$ at acidic conditions is slower. This was expected, as droplets stabilised using P5 are less selective as inter-droplet hydrogen bonding can occur between any two droplets in the system. However, as a 100 % EG droplet can only exhibit hydrogen bonding with a 100 % MAA droplet, half of the droplets in the system cannot interact with the EG droplets. This means that engineered emulsion formation should be slower compared to the P5 single-component system.

Binary mixtures were also assessed using rheometry (Figure 3.14). 1.25 mL of each sample was gently mixed together and acidified *in situ*: gel formation was visible after 1-2 minutes. An amplitude sweep was performed on the resulting 50:50, 100 % MAA (E1) : 100 % EG (E9) mixture. The amplitude sweeps of the 50:50 binary mixture gave a G' of 1,100 Pa in the LVE region. This is in close agreement with the P5 stabilised emulsion, which at the same strain, had a G' of 930 Pa. Similar G' values suggest that the binary mixture is able to achieve similar gel strengths to the P5 stabilised emulsion.

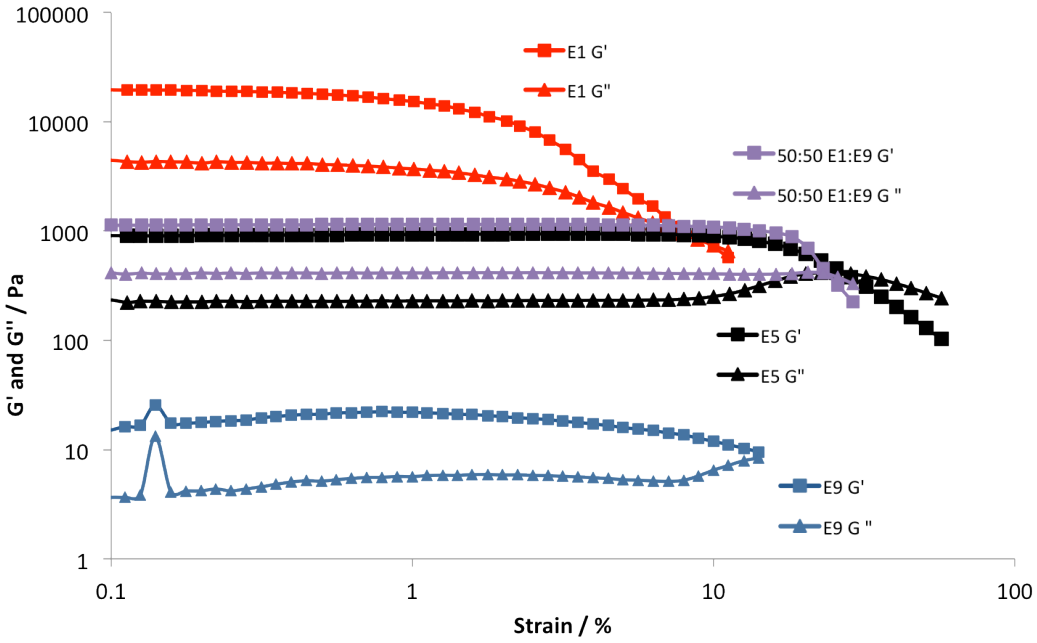

Figure 3.14. G' and G" for 100 % MAA (red), 100 % EG (blue), a 50:50 binary mixture of 100 % MAA and 100 % EG (purple) and 1:1 EG:MAA (or E5) is shown as a control (black). G' is shown as squares and G" is shown as triangles.

This result indicates that the bulk EG:MAA ratio is important. However, whether these groups share droplet surfaces or the two complementary functionalities are present on different droplets seems less important. The point at which the G' of the binary mixture reached 90 % of its LVE region value is 14.2 % strain, in very good agreement with that observed for the single-droplet system. Both of are higher than those of the 100 % EG droplets and 100 % MAA droplets as individual samples (2.24 % and 1.43 % respectively). The data shown in Figure 3.14 confirms that hydrogen bonding in the binary system has the same effect on the engineered emulsion mechanical properties as it does in the single droplet system. Selective interactions lead to hierarchical structure, something which is often desirable in throughout synthetic chemistry.[16,39]

Having determined that selective hydrogen bonding plays a role in the aggregation of mixtures of pure EG and pure MAA droplets, it was then investigated whether selective aggregation events between these contra-functional droplets could be observed using microscopy. 100 % MAA polymer-stabilised o/w emulsion droplets were prepared using 1-dodecanol as the oil phase. 1-Dodecanol is a solid at room temperature; therefore below its melting point (24 ^{o}C), droplets are non-spherical due to crystallisation of the oil phase. 1-Dodecanol emulsions were prepared using an identical procedure to the other emulsifications, but the temperature of all materials, glassware and equipment was maintained at around 40 °C. When homogenisation was complete, the resulting emulsion was immediately diluted in water (40 °C, 120 mL, pH 10) and stirred overnight at room temperature to prevent 'jamming' of the solidifying emulsion droplets. This process resulted in easily identifiable MAA droplets when in the presence of spherical dodecane droplets, which were functionalised with 100 % EG. Figure 3.15 (a) and (b) show optical microscope images taken at room temperature of both the 100 % EG/dodecane and 100 % MAA/1-dodecanol droplets at pH 10, respectively. Both samples appeared well dispersed and the MAA/1-dodecanol droplets were non-spherical as expected.

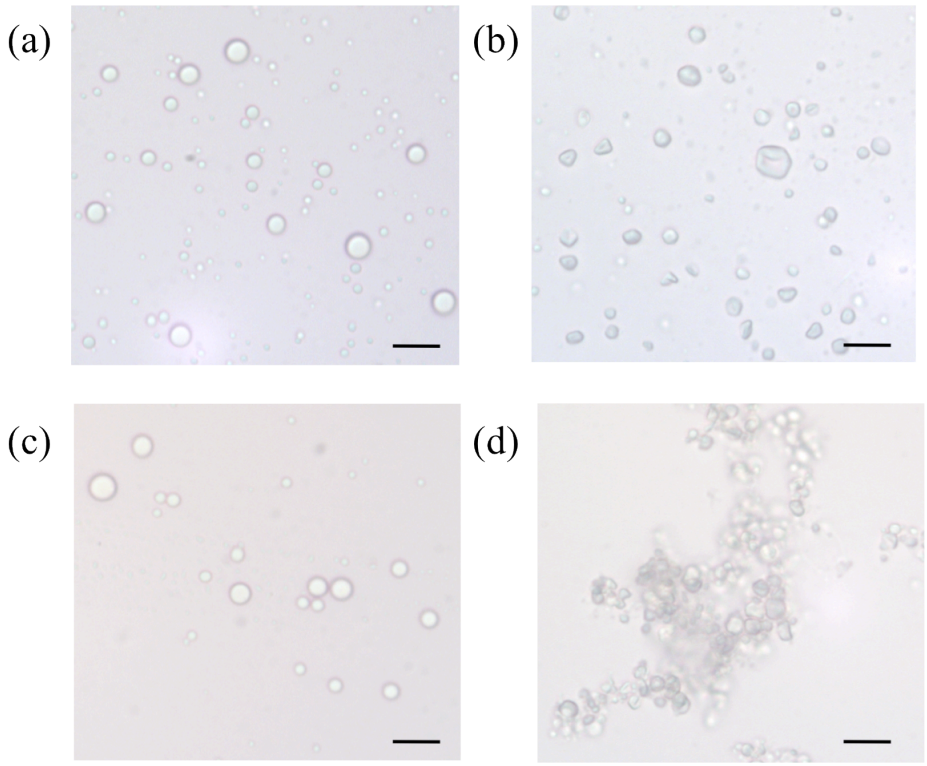

Figure 3.15. Optical microscopy images of, (a) 100 % EG/dodecane droplets at pH 10, (b) 100 % MAA/1-dodecanol droplets at pH 10, (c) 100 % EG/dodecane droplets at pH 2, (d) 100 % MAA/1-dodecanol droplets at pH 2. All images were taken at 20 ^{o}C. Scale bars represent 20 µm.

On lowering the solution pH to around pH 2, the 100 % EG/dodecane droplets remained completely dispersed (Figure 3.15(c)). The 100 % MAA/1-dodecanol droplets appeared to aggregate when concentrated (Figure 3.15(d)), in agreement with the rheological data of a concentrated, 100 % MAA-stabilised dodecane o/w emulsion (Figure 3.9).

The two samples were mixed in a dilute aqueous pH 10 solution before acidification to pH 2. Light microscopy revealed that a substantial portion of droplets had aggregated, although samples had purposefully been kept dilute to minimise any hydrophobic interactions between MAA/1-dodecanol droplets. Although there appeared to be some MAA-MAA droplet interactions, a number of aggregates consisted of MAA droplets selectively interacting with EG droplets (Figure 3.16 (a)-(c)). This provided direct evidence of selective aggregation as EG droplets alone at low pH remain dispersed, but in the binary systems EG droplets aggregated in the presence of the non-spherical MAA droplets.

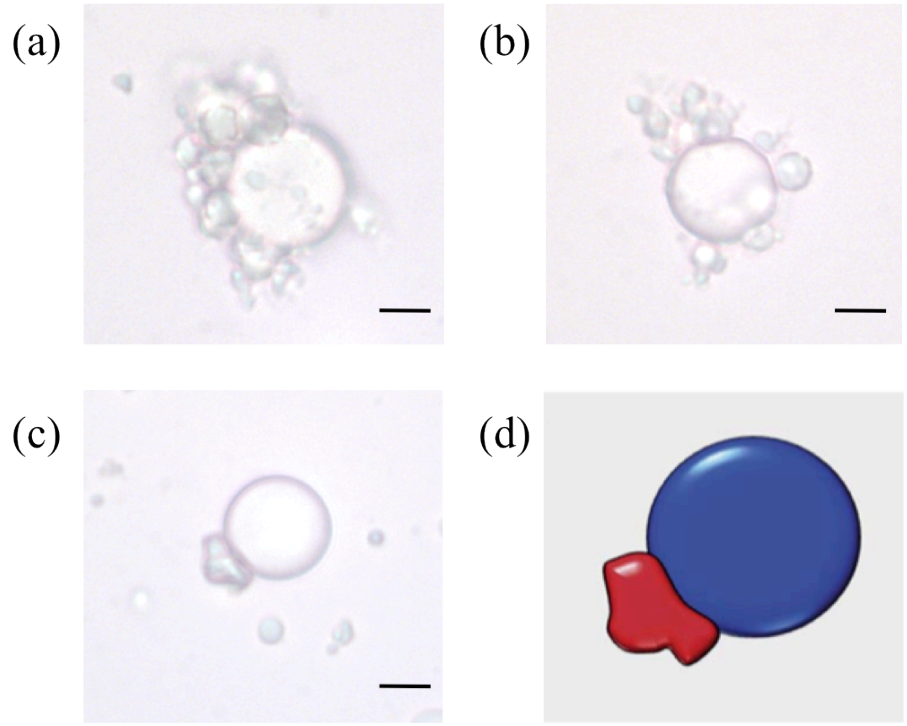

Figure 3.16. Optical microscopy images of (a)-(c) Contra-functional droplets at pH 2, showing selective interaction of 100 % EG/dodecane droplets (spherical) with 100 % MAA/1-dodecanol droplets (non-spherical) (d) Schematic of selective assembly in (c). Scale bars represent 10 µm.

3.3. Conclusions

This Chapter presents a one-pot polymerisation process that allows the production of branched vinyl copolymers with distinct compositions. The copolymers all showed surface activity and were used as highly efficient emulsifiers in the preparation of o/w emulsions at pH 10. From previous work,[24,27,40] it is known that MAA and EG units in a 1:1 ratio will hydrogen bond upon protonation of MAA, enabling inter-droplet hydrogen bonding in emulsion systems. Variation of this 1:1 molar ratio in the branched copolymers was assessed to see what effect this had on acid-triggered aggregation of droplets. From laser diffraction, it appeared that equimolar ratios of EG:MAA in the polymeric surfactant gave the fastest droplet aggregation, with excess MAA slowing aggregation and excess EG preventing it all together. The aggregation for MAA-rich surfaces suggests that some hydrophobic interactions and the formation of MAA-MAA dimers may contribute to the formation of EEs. Rheometry studies show that an increase in MAA units (relative to EG) on droplet surfaces yield ‘stiffer’ engineered emulsions, whereas samples containing 1:1

EG:MAA proved to be the most strain-resistant structures, breaking down at higher strains than other EEs.

It was shown that binary mixtures of contra-functionalised droplets (100 % MAA droplets and 100 % EG droplets) show selective hydrogen bonding in order to form an EE with strength comparable to that of a P5 stabilised emulsion.

This Chapter therefore demonstrates that emulsion droplets stabilised with architecturally similar branched copolymer surfactants can be used to control triggered inter-droplet interactions. By changing the composition of the polymers only very slightly, the functionality of the resulting o/w emulsion can vary drastically. Although some other interactions appear to contribute to inter-droplet aggregation, it is shown that hydrogen-bonding interactions are important in controlling the rate of inter-droplet aggregation and play a crucial role in the resulting strength of EEs.

3.4. References

(1) Tsai, C. J.; Ma, B. Y.; Kumar, S.; Wolfson, H.; Nussinov, R. *Crit. Rev. Biochem. Mol.* **2001**, *36*, 399.
(2) Klug, A. *Angew. Chem. Int. Ed.* **1983**, *22*, 565.
(3) Whitesides, G. M.; Grzybowski, B. *Science* **2002**, *295*, 2418.
(4) Elemans, J. A. A. W.; Rowan, A. E.; Nolte, R. J. M. *J. Mater. Chem.* **2003**, *13*, 2661.
(5) Lehn, J. M. *Science* **2002**, *295*, 2400.
(6) Fox, J. D.; Rowan, S. J. *Macromolecules* **2009**, *42*, 6823.
(7) Brunsveld, L.; Folmer, B. J. B.; Meijer, E. W.; Sijbesma, R. P. *Chem. Rev.* **2001**, *101*, 4071.
(8) Sherrington, D. C.; Taskinen, K. A. *Chem. Soc. Rev.* **2001**, *30*, 83.
(9) Adams, D. J. *Macromol Biosci.* **2011**, *11*, 160.
(10) Claessens, C. G.; Stoddart, J. F. *J. Phys. Org. Chem.* **1997**, *10*, 254.
(11) Dischер, D. E.; Eisenberg, A. *Science* **2002**, *297*, 967.
(12) Lvov, Y.; Ariga, K.; Ichinose, I.; Kunitake, T. *J. Am. Chem. Soc.* **1995**, *117*, 6117.
(13) Deechongkit, S.; Nguyen, H.; Powers, E. T.; Dawson, P. E.; Gruebele, M.; Kelly, J. W. *Nature* **2004**, *430*, 101.
(14) Prins, L. J.; De Jong, F.; Timmerman, P.; Reinhoudt, D. N. *Nature* **2000**, *408*, 181.
(15) Leunissen, M. E.; Christova, C. G.; Hynninen, A. P.; Royall, C. P.; Campbell, A. I.; Imhof, A.; Dijkstra, M.; van Roij, R.; van Blaaderen, A. *Nature* **2005**, *437*, 235.
(16) Velev, O. D. *Science* **2000**, *287*, 2240.
(17) Li, H.; Eddaoudi, M.; O'Keeffe, M.; Yaghi, O. M. *Nature* **1999**, *402*, 276.

(18) Park, S. Y.; Lytton-Jean, A. K.; Lee, B.; Weigand, S.; Schatz, G. C.; Mirkin, C. A. *Nature* **2008**, *451*, 553.
(19) Dinsmore, A. D.; Hsu, M. F.; Nikolaides, M. G.; Marquez, M.; Bausch, A. R.; Weitz, D. A. *Science* **2002**, *298*, 1006.
(20) Velev, O. D.; Furusawa, K.; Nagayama, K. *Langmuir* **1996**, *12*, 2374.
(21) Velev, O. D.; Furusawa, K.; Nagayama, K. *Langmuir* **1996**, *12*, 2385.
(22) Woodward, R. T.; Slater, R. A.; Higgins, S.; Rannard, S. P.; Cooper, A. I.; Royles, B. J.; Findlay, P. H.; Weaver, J. V. *Chem. Commun.* **2009**, *24*, 3554.
(23) Harbron, R. L.; McDonald, T. O.; Rannard, S. P.; Findlay, P. H.; Weaver, J. V. *Chem. Commun.* **2012**, *48*, 1592.
(24) Weaver, J. V. M.; Rannard, S. P.; Cooper, A. I. *Angew. Chem. Int. Ed.* **2009**, *48*, 2131.
(25) Fujii, S.; Read, E. S.; Binks, B. P.; Armes, S. P. *Adv. Mater.* **2005**, *17*, 1014.
(26) Fujii, S.; Cai, Y. L.; Weaver, J. V. M.; Armes, S. P. *J. Am. Chem. Soc.* **2005**, *127*, 7304.
(27) Mathur, A. M.; Drescher, B.; Scranton, A. B.; Klier, J. *Nature* **1998**, *392*, 367.
(28) Graham, S.; Cormack, P. A. G.; Sherrington, D. C. *Macromolecules* **2005**, *38*, 86.
(29) O'Brien, N.; McKee, A.; Sherrington, D. C.; Slark, A. T.; Titterton, A. *Polymer* **2000**, *41*, 6027.
(30) Chambon, P.; Chen, L.; Furzeland, S.; Atkins, D.; Weaver, J. V. M.; Adams, D. J. *Polym. Chem.* **2011**, *2*, 941.
(31) Costello, P. A.; Martin, I. K.; Slark, A. T.; Sherrington, D. C.; Titterton, A. *Polymer* **2002**, *43*, 245.
(32) Weaver, J. V. M.; Tang, Y.; Liu, S.; Iddon, P. D.; Grigg, R.; Billingham, N. C.; Armes, S. P.; Hunter, R.; Rannard, S. P. *Angew. Chem. Int. Ed.* **2004**, *43*, 1389.
(33) Liu, S. Y.; Weaver, J. V. M.; Tang, Y. Q.; Billingham, N. C.; Armes, S. P.; Tribe, K. *Macromolecules* **2002**, *35*, 6121.
(34) Hao, J.; Li, Z.; Cheng, H.; Wu, C.; Han, C. C. *Macromolecules* **2010**, *43*, 9534.
(35) Dong, J.; Ozaki, Y.; Nakashima, K. *Macromolecules* **1997**, *30*, 1111.
(36) Koenig, J. L.; Angood, A. C.; Semen, J.; Lando, J. B. *J. Am. Chem. Soc.* **1969**, *91*, 7250.
(37) Mezger, M. G. *The Rheology Handbook*; Vincentz, **2006**.
(38) Rao, M. A. *Rheology of Fluid and Semisolid Foods: Principles and Applications*; Springer, **2007**.
(39) Boal, A. K.; Ilhan, F.; DeRouchey, J. E.; Thurn-Albrecht, T.; Russell, T. P.; Rotello, V. M. *Nature* **2000**, *404*, 746.
(40) Kabanov, V. A.; Papisov, I. M. *Vysokomol. Soed. A* **1979**, *21*, 243.

CHAPTER 4

Reversible Phase-Transitions in Responsive Polymer Stabilised Emulsion Systems: Generation of Polymer Structured Oils

(Publication arising from this Chapter: **"Multiple, reversible transitions in polymer-stabilized responsive emulsions"**, R. T. Woodward, T. Gong, W. H. Briscoe, C. Sammon, A. deMello, J. V. M. Weaver, *Manuscript in preparation*, 2012)

List of Figures

List of Schemes

List of Tables

4.1. Introduction

Liquid emulsions are important biphasic materials both commercially and from an academic perspective. They are composed of one liquid dispersed throughout another immiscible phase in the form of spherical droplets.[1] Interfacial stabilisation is a key factor is producing stable emulsions and is achieved a number of ways, including using surface-active small-molecules,[2,3] polymers,[4-6] proteins[7,8] or particles.[9-11] Emulsions are thermodynamically unstable and subject to destabilisation with time, even when dilute in their continuous phase. Common o/w emulsions have surfactant molecules adsorbed at the interfacial boundaries of the system, dictating a number of properties including stability[3,12] and elasticity.[13,14] The interfacial adsorption energy of these molecules can determine the long-term stability of emulsions.[10]

Previously, Weaver *et al.* have reported 'Engineered Emulsions' (EE), stabilised using a responsive, amphiphilic branched copolymer adsorbed at the o/w interface.[15] The polymer's strong interface adsorption arises from the addition of multiple hydrophobic groups per molecule via chain transfer reactions.[12,16] This branched copolymer allows reversible kinetic trapping of the emulsion droplets using a simple pH switch *via* inter-droplet hydrogen bonding to give the EE.

In Chapter 3, the role of the branched copolymer's composition and its effect on inter-droplet aggregation was investigated. As P5 yielded the most strain-resistant EE, this polymer was chosen for further study. This high stability meant that the resulting EEs were most suitable for a study of the long-term stability of these materials. It was hypothesised that the droplets might be stable enough to allow the selective removal of at least some of the water phase by dehydration, leading to an increased oil concentration, or larger Φ_{oil}.

In this Chapter, the production of dodecane o/w emulsion droplets stable enough to allow reversible formation of a new class of highly structured liquid is investigated. Judicious design of the polymer-surfactant architecture and composition allows non-covalent interactions to be used to stabilise droplets in both the free-flowing and "engineered" forms. These EE may then be utilised as templates in the formation of a 3D polymer-structured oil (PSO) comprising a single, low-viscosity oil phase in the form of droplets *via* the removal of water.

4.2. Results and Discussion

4.2.1. Reversible Transitions in Polymer Stabilised Emulsions

A P5 stabilised dodecane o/w emulsion (E5) was prepared using the method outlined in Chapter 2 (2.1.2). This process produced polydisperse, stable o/w emulsions ($D_{(4,3)}$ = 10.1 µm, span 1.08) due to the strong, interfacial attachment of P5.[16,17] It is worth noting that P5 is the main branched copolymer surfactant used throughout the rest of the thesis, as inter-droplet interactions appeared to be fastest in this system, yielding the most strain-resistant EE, as discussed in Chapter 3. In order to show the the polymer synthesis was reproducible, three identical co-polymerisations were conducted and analysed each time using ^{1}H NMR spectroscopy and THF GPC. The ^{1}H NMR spectra show good reproducibility between samples (Figure 4.1), with theoretical copolymer compositions in good agreement with compositions calculated by NMR (Table 4.1).

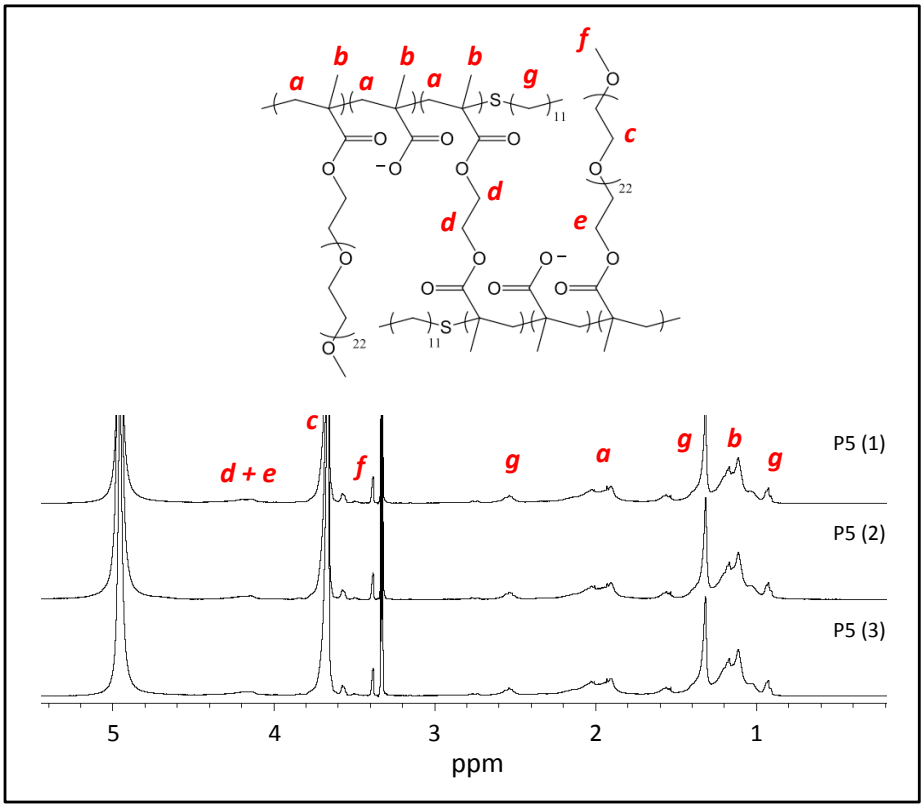

Figure 4.1. ^{1}H NMR spectra recorded in d_4-methanol for the three repeat syntheses of P5.

Table 4.1. Actual polymer compositions as calculated by ^{1}H NMR

ID	Polymer compositions as calculated by ^{1}H NMR
P5 (1)	$PEGMA_{4.5}/MAA_{95.5} - EGDMA_{9.2} - DDT_{10.1}$
P5 (2)	$PEGMA_{4.4}/MAA_{95.6} - EGDMA_{9.5} - DDT_{9.8}$
P5 (3)	$PEGMA_{4}/MAA_{96} - EGDMA_{9.4} - DDT_{10}$

GPC curves overlay well, suggesting similar molecular weight distributions were obtained in all cases (Figure 4.2(a)). M_w, M_n and Mark-Houwink α-values are shown in the table in Figure 4.2(b). M_w and M_n for each sample are in good agreement and are consistent with similar branched copolymers previously reported.[12,15,16,18] All samples showed PDIs between 3.15 and 3.74, suggesting a polydisperse system as expected of branched copolymers. α-values are all below 0.24, indicative of relatively compact structures, again suggesting branched architectures as found elsewhere.[15,18,19]

(a)

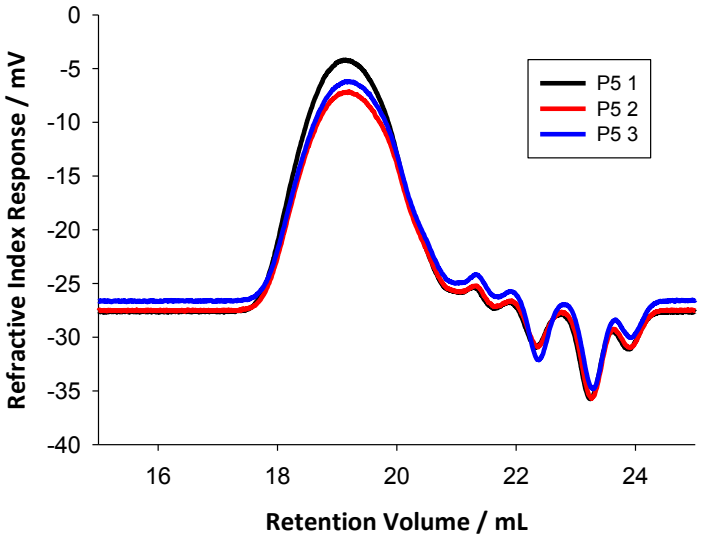

(b)

ID	M_w / g.mol^{-1}	M_n / g.mol^{-1}	PDI	α
P5 (1)	15,000	4,000	3.74	0.21
P5 (2)	14,400	4,100	3.47	0.19
P5 (3)	13,600	4,300	3.15	0.21

Figure 4.2. (a) GPC curves obtained for three repeat P5 samples. (b) Table of results comparing M_w, M_n, PDI and α-values of P5 repeats.

E5 formed EEs upon acidification to pH 2, by kinetically trapping the droplets in a mould or template. An EE monolith (Φ_{oil} = 0.70) comprising only water, n-dodecane and P5 was formed (Figure 4.3(a)), which became increasingly transparent, appearing to decrease in volume with time when left open to air at room temperature (Figure 4.3(b)). This change in monolith appearance was thought to be due to preferential evaporation of the aqueous phase. This process was reversible, as suggested by the rehydrated sample, shown in Figure 4.3(c), becoming opaque after exposure to HCl (1 M, 1 mL). This rehydrated structure could be disassembled by the addition of NaOH (1 M, 1 mL), to give a free-flowing emulsion (Figure 4.3(d)).

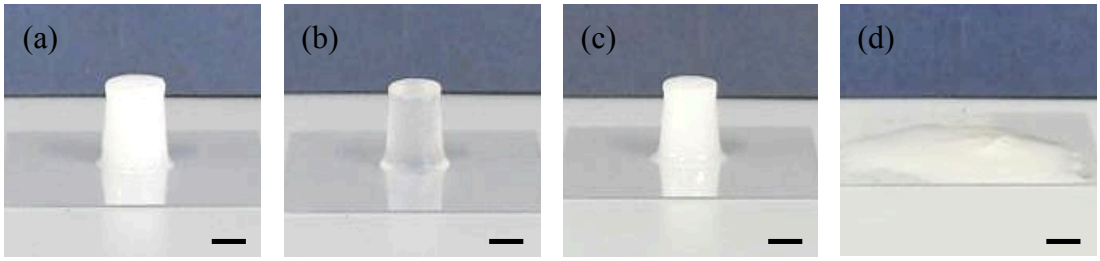

Figure 4.3. EE (Φ_{oil} = 0.70) formed from E5 (a) immediately after removal from a template, (b) monolith becomes a more transparent structure after 2 hours under ambient conditions, (c) shows (b) after exposure to HCl and (d) shows (c) after the addition of base (NaOH) to trigger disassembly. Scale bars represent 2.5 mm.

To provide evidence that increasing transparency in EE structures was due to dehydration, Karl Fischer titrations were employed in order to quantify the water content in the dodecane emulsion system's three different states (free-flowing, EE and 'dehydrated' EE). A volumetric Karl Fischer titration allows for detection of both large and trace amounts of water by measuring the consumption of iodine (I_2) in the reaction shown in Scheme 4.1. As a 1:1 reaction occurs between I_2 and H_2O, on determination of the amount of iodine consumed, the amount of water in a sample is calculated. This makes the Karl Fischer method ideal for the quantification of water content between these samples.

$$I_2 + 2H_2O + SO_2 \longrightarrow 2HI + H_2SO_4$$

Scheme 4.1. Consumption of iodine in a Karl Fischer titration used to determine water content.

The results of these titrations are shown in Table 4.2, quantified as percent water in each sample.

Table 4.2. Karl Fischer titration results showing water content of dodecane EEs, dehydrated EEs, rehydrated EEs and free-flowing emulsion.

EE Dehydration Time / hours	Water Content / %		
	Test 1	Test 2	Average
0	31.4	33.9	32.6
0.5	24.7	24.0	24.3
1	12.6	12.2	12.4
2	3.2	3.2	3.2
6	0.7	0.6	0.6
Rehydrated EE	30.6	29.9	30.3
Free-flowing emulsion	37.4	35.4	36.4

An EE monolith (150 μL) that had not been allowed to dehydrate contains 32.6 % water. When an EE is left open to air for 2 hours (21-22 ^{o}C), only 9.7 % of the initial water remains, i.e. the monolith comprises 3.2 % water. If an EE is allowed to dehydrate for 6 hours (21-22 ^{o}C), this number falls further, with only 1.9 % of the initial water content remaining. In this case, the monolith contains only 0.6 % water. Upon rehydration of an EE, dehydrated for 6 hours, by HCl (1 M, 0.5 mL) to form a hydrated EE, the water content increases to 30.3 %, almost as high as the water content in the original EE before dehydration (32.6 %). This provides good evidence not only of the dehydration process, but also the reversibility of dehydration by the simple addition of acid to the structure. After 2 hours of dehydration, EE monoliths are made up of 3.2 % water, 2 % P5 and 94.8 % dodecane. As these monoliths are held structurally by polymer-polymer interactions, upon loss of water a 3D PSO is formed.

In order to see how stable individual droplets were with respect to the dehydration, rehydration, redispersion process outlined in Figure 4.3, droplet sizes were measured by laser diffraction. The size of free-flowing E5 at pH 10 was compared to that of the free-flowing E5 obtained from rehydration and redispersion of a PSO, again at pH 10 (Figure 4.4).

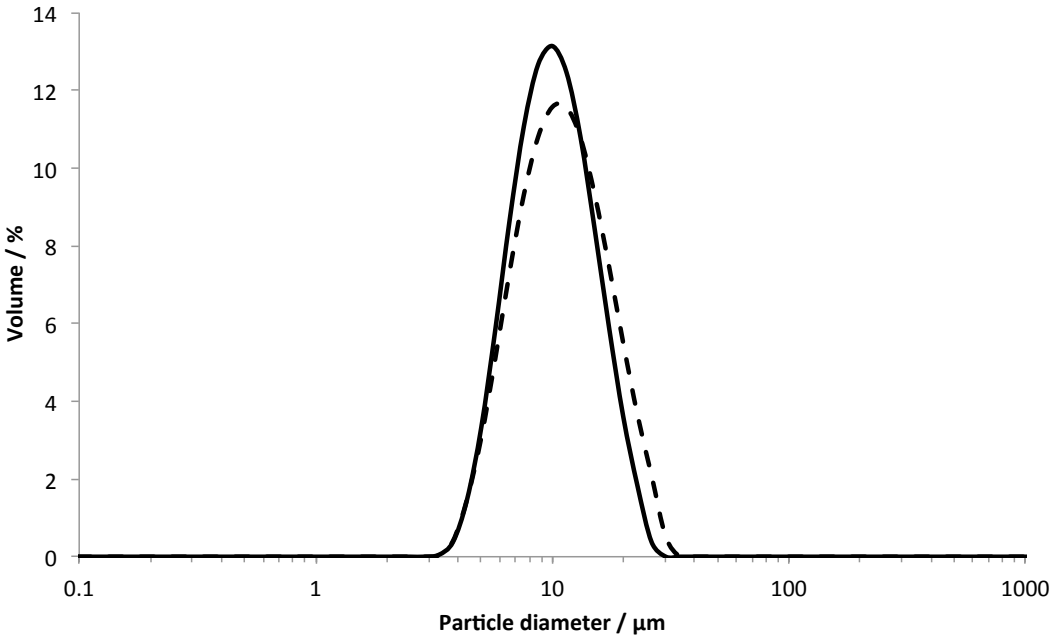

Figure 4.4. Overlayed laser diffraction size distributions of free-flowing E5 emulsion at pH 10 (solid line) and free-flowing rehydrated redispersed E5 EE (dashed line). The EE was left in air under ambient conditions for 2 hours before immersion in 1 M HCl for 10 minutes to rehydrate. Sample was then redispersed using 1 M NaOH and measured at pH 10.

The volume-average droplet diameter increased slightly throughout this process, from $D_{(4,3)}$ = 10.1 μm in the original free-flowing emulsion to $D_{(4,3)}$ = 11.1 μm in the redispersed sample. This may be indicative of incomplete redispersion, or slight droplet instability. The span also increased from 1.08 in the original sample to 1.22 in the redispersed sample, suggesting a slightly more polydisperse sample after redispersion. However, this result suggests that droplets are quite robust, remaining relatively stable through a range of different pH and droplet concentrations throughout the whole aggregation/dehydration/rehydration and redispersion process.

The loss of water from an EE structure leads to a gradual increase of Φ_{oil}, which resulted in a more transparent PSO. Transmittance was measured for both E5 hydrated EEs and dehydrated PSOs by ultraviolet-visible (UV-Vis) absorption spectroscopy (Figure 4.5) in order to compare the optical transparency of these materials to that of pure dodecane.

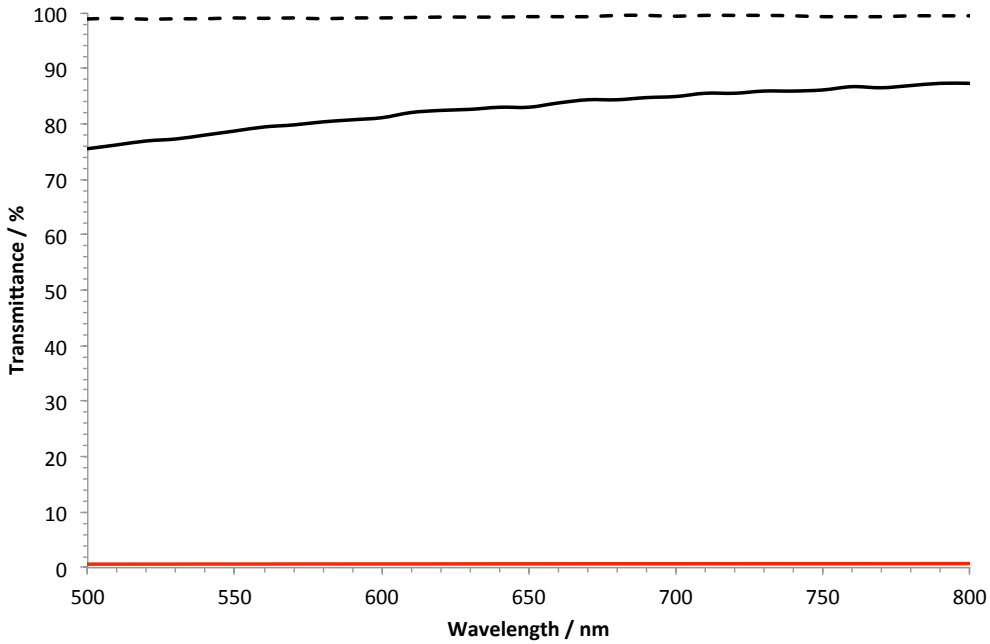

Figure 4.5. Transmittance spectra between wavelengths 500-800 nm for pure dodecane (dashed black line), an E5 EE (red line) and an E5 PSO dehydrated for 6 hours (solid black line).

The PSO measured in Figure 4.5 was formed *via* the 6 hour dehydration at 20 ^{o}C of an EE. The sample was allowed to dehydrate for 6 hours in order to achieve a high degree of dehydration (< 1 %), resulting in a highly transparent structure. The PSO sample displayed an average transparency of 82 % between wavelengths (λ) of 500-800 nm (in comparison with 98.98 % for pure dodecane). When comparing this to the EEs, which displayed 0.7 % transmittance, a large increase in transparency due to dehydration was measured. The increase in transparency measured is most likely due to a change in refractive index due to the loss of water from the structure.

As 91 % of the water in an EE is lost in the first 2 hours of dehydration, aggregates should undergo weight loss correlating to this process. Thermogravimetric analysis (TGA) was used to measure weight loss of a P5 stabilised dodecane EE (100 μL) at constant temperature (25 ^{o}C) over 4 hours; the results are shown in Figure 4.6.

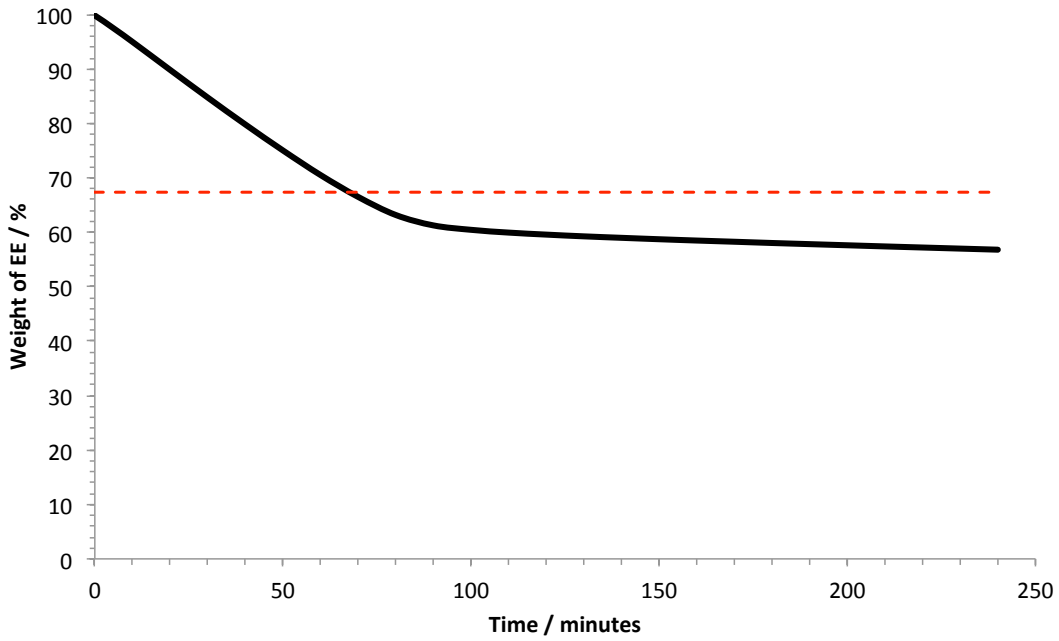

Figure 4.6. Weight of an EE (solid black line) over 4 hours, determined by TGA at 25 ^{o}C. The red dashed line represents the theoretical maximum dehydration as determined by Karl Fischer titration.

Looking at Figure 4.6, the initial weight loss of an E5 EE slows at around 90 minutes. However, weight loss appears to slowly continue for the duration of the measurement. The theoretical maximum weight loss due to dehydration is shown as a red dashed line, this corresponds to loss of all water content measured by Karl Fischer titration (32.6 %). The difference in predicted weight loss and actual weight loss may be due to the inherent volatility of dodecane, resulting in both dehydration and the slow loss of dodecane. At 120 minutes the structure is 59.6 % its original weight. Therefore, if we assume 3.2 % of the structure is water (as the results of the Karl Fischer titration suggest), then 84 % of the dodecane remains, which means 15.6 % of the dodecane is also lost during this initial 2 hours of dehydration. This loss in dodecane should lead to some droplet instability, potentially resulting in differences in the rehydrated, redispersed PSO emulsion in comparison to the original emulsion, as seen in laser diffraction (Figure 4.4). In order to check if weight loss continues after these initial 4 hours, an EE was prepared under identical conditions and was weighed using thermogravimetric analysis at a constant temperature (25 ^{o}C), this time for 72 hours (Figure 4.7).

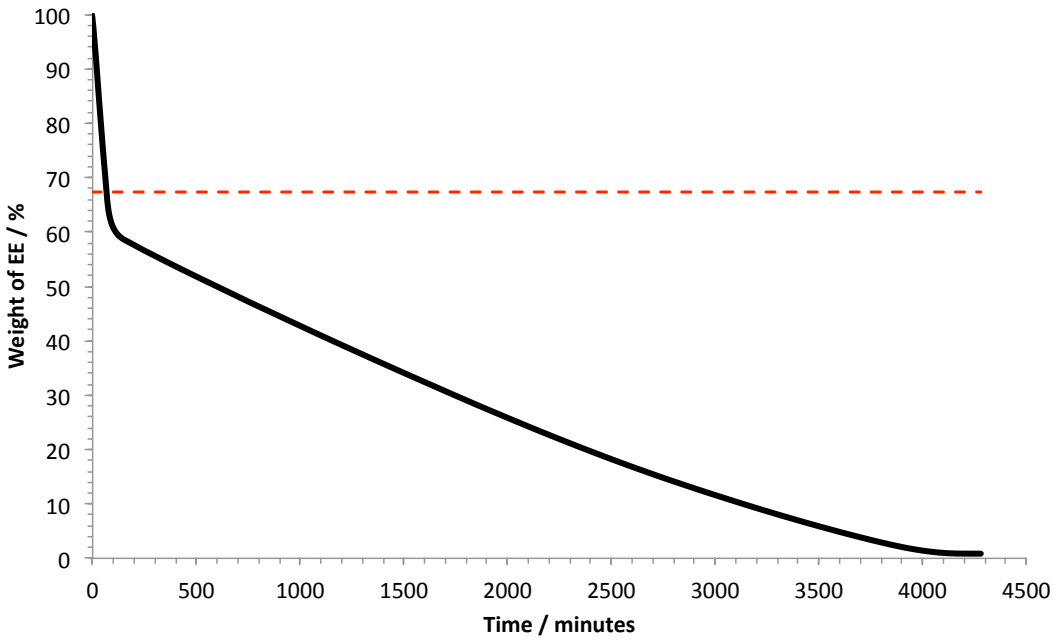

Figure 4.7. Weight of an EE (solid black line) over 72 hours, determined by TGA at 25 °C. The red dashed line represents the theoretical maximum dehydration as determined by Karl Fischer titration.

It can be seen in Figure 4.7 that after 4 hours, the EE's weight continues to decrease. Weight loss again appears to slow at around 90 minutes, in good agreement with the initial 4 hour measurement in Figure 4.6. After the initial 4 hours, the rate of dodecane loss is reduced to roughly 1.6 % per hour. Although dodecane has a boiling point of 216 °C, it has a vapour pressure of 0.21 mmHg at 25 °C. Therefore, at this temperature, dodecane is slightly volatile in air, so after 70 hours all of the dodecane is removed from the system.

4.2.2. Imaging Emulsion's Reversible Transitions

Microfluidic preparation of monodisperse dodecane droplets stabilised by P5 was used in order to image the dehydration process at the droplet level, *in situ*. Microfluidic preparation should allow monitoring of EE formation, PSO formation, rehydration and redispersion. Shearing instability at the interface between a water and oil stream at a microfluidic "T" junction was used to generate an E5 o/w emulsion (Figure 4.8). The chip has two inlets (*a* and *b*, in Figure 4.8) where copolymer solution (4 wt. %) and dodecane were introduced, respectively. Both liquids were loaded into 1 mL syringes and mounted on a syringe pump (PHD 2000, Harvard Apparatus). To obtain 25 μm diameter dodecane droplets, the flow rate of *a*

was set to 4 µL/minute, and the flow rate of *b* set to 1 µL/minute. A more detailed description of the microfluidic apparatus is given in Chapter 2.4.4.

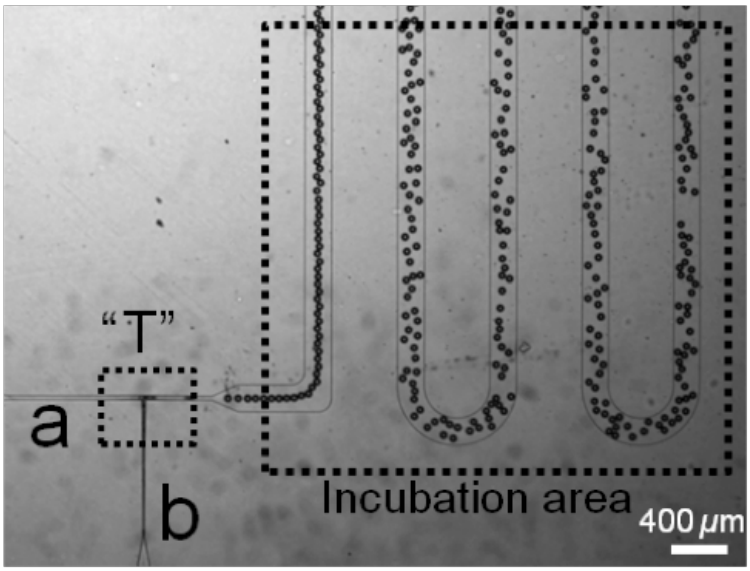

Figure 4.8. Microfluidic device used to generate oil-in-water droplets. "T" denotes the T junction where the copolymer solution shears the dodecane into droplets. a and b are inlets for the copolymer solution and dodecane respectively. The incubation area provides space for oil droplets to fully emerge into copolymer solution.

A 2D array of close-packed spherical droplets was prepared within microfluidic devices and kinetically trapped *via* acidification to form EEs (Figure 4.9(a) i-ii). Dehydration of the EEs revealed a progressive change in droplet morphology as the water from the interstitial sites between droplets was removed (Figure 4.9(a) iii-ix). Dehydration and subsequent PSO formation, was complete after 5 minutes in the microfluidic device, as evidenced by formation of analogous polyhedral droplets and the loss of water from droplets interstitial sites (Figure 4.9(a) ix). Reformation of EE *via* rehydration of the close-packed monodisperse PSO was achieved by slow addition of acidic water, reproducing highly spherical droplets (Figure 4.9(b)). Droplets rehydrated within 1-2 minutes after the addition of acid. All microfluidic experiments were carried out by the deMello group at Imperial College London.

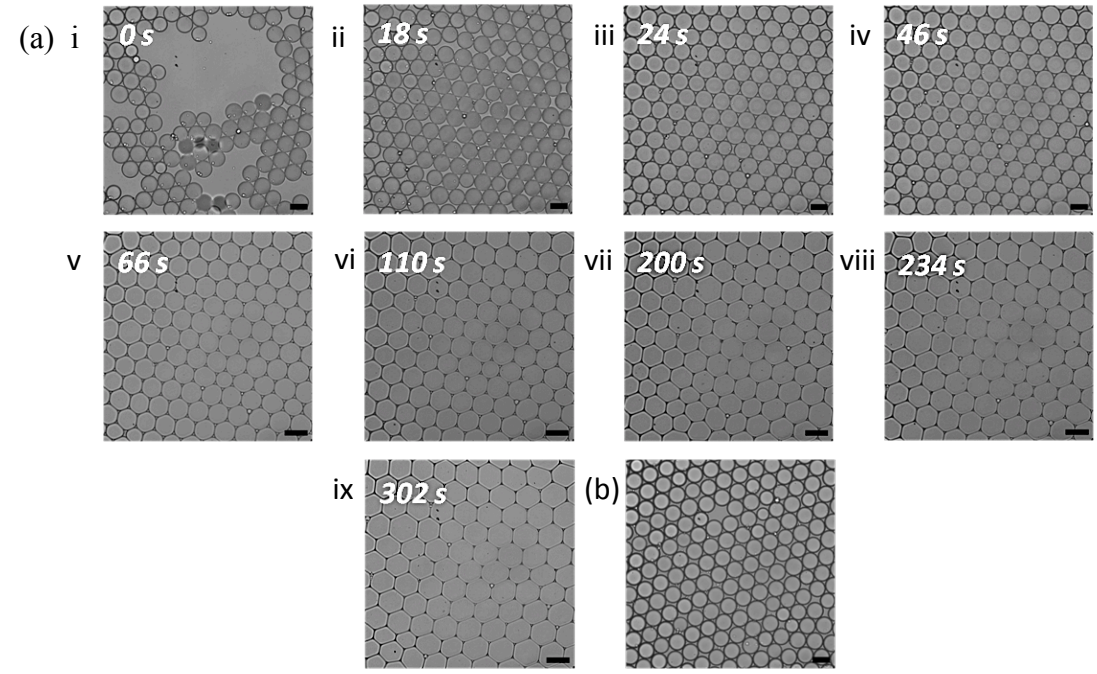

Figure 4.9. Monodisperse droplet transitions. (a) i, Dodecane droplets at pH 10. ii, Droplets assembling into 2D packed arrays 18 seconds after acid addition. iii-ix, Shape transition of 2D array of droplets during dehydration (over 5 minutes). (b) Rehydration of droplets following the addition of more acid. Scale bars represent 25 µm.

An E5 emulsion (Φ_{oil} = 0.70) was produced via homogenisation with the hydrophobic fluorescent dye 3,3'-dioctadecyloxacarbocyanine perchlorate (DiO) (0.05 wt. %) dissolved in the dodecane oil phase. The laser diffraction size distribution curve of this emulsion at pH 10 is shown in Figure 4.10.

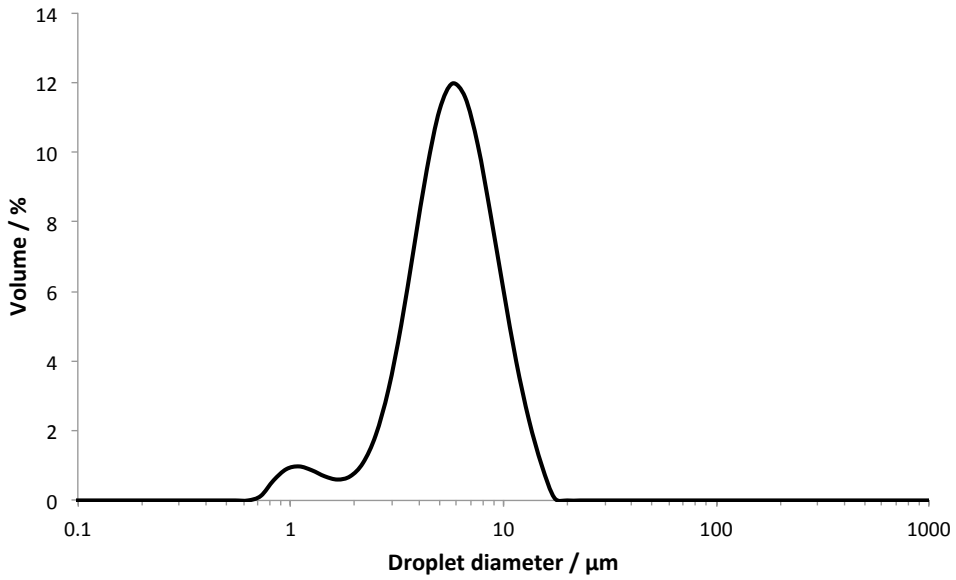

Figure 4.10. Laser diffraction of an E5 emulsion at pH 10 containing DiO in the oil phase.

From the laser diffraction studies it was found that droplets had a $D_{(4,3)}$ = 5.72 µm and a span of 1.25. The encapsulation of DiO allowed droplets to be imaged *via* fluorescent microscopy using a confocal microscope. Fluorescent microscopy confirmed that the dehydration-rehydration process also resulted in droplet morphology changes, in this case within a 3D structure (Figure 4.11 (a)-(d)).

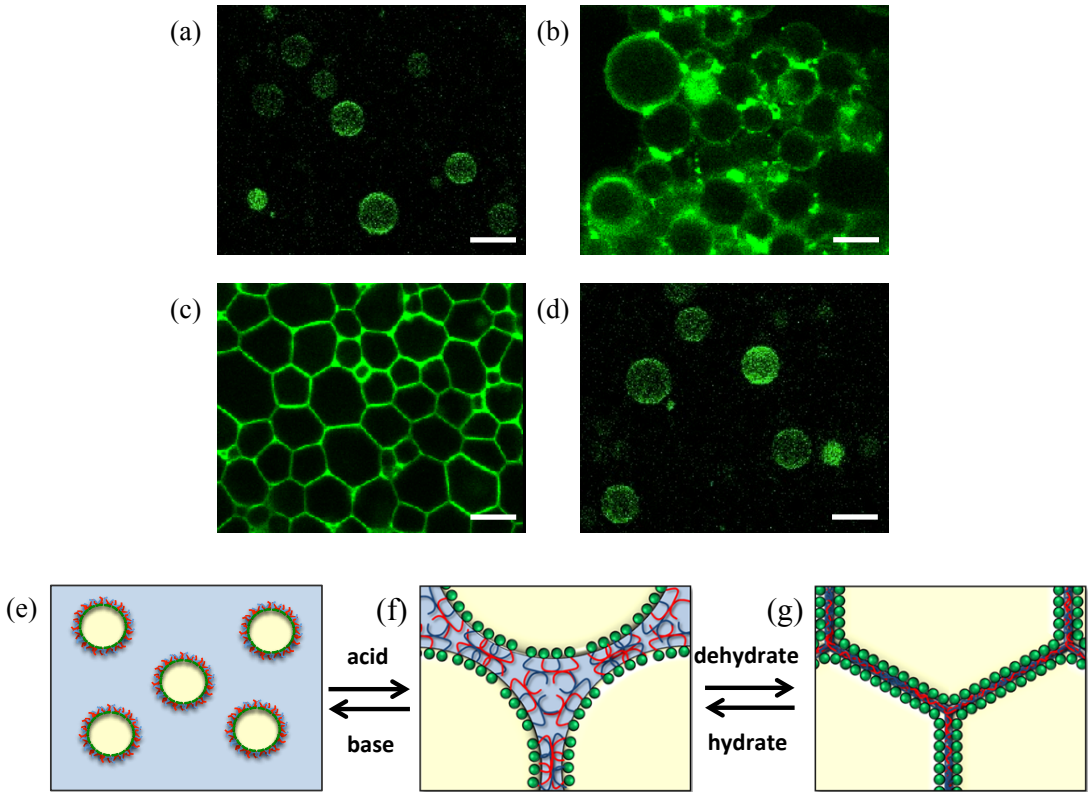

Figure 4.11. Confocal microscopy images of (a) the free flowing emulsion at pH 10, (b) an EE at pH 2, (c) a PSO after allowing an EE to dehydrate for 20 minutes and (d) a PSO after rehydration and redispersion. Scale bars represent 20 µm. Schematics of (e) free-flowing emulsion (f) an EE and (g) a PSO, assuming monodispersity.

Spherical droplets are observed in the free-flowing emulsion, EE and the rehydrated, redispersed PSO, (Figure 4.11 (a), (b) and (d)), whereas a random connected network of droplets can be seen in the PSO (Figure 4.11 (c)) due to the lack of water at interstitial sites. When comparing the packing of droplets within the 3D structure upon dehydration to that of the 2D structure in Figure 4.9(a)ix, packing becomes a lot more disordered. This is likely due to the fact that the droplets are different sizes in the emulsion forming the 3D structure, whereas droplets in microfluidics are monodisperse. An attempt to illustrate the change in droplet morphology in a 2D

PSO structure is shown in Figure 4.11(e)-(g), showing a schematic of the droplets in their different states. When comparing these with the real images, similar droplet distortions were observed in the confocal images due to removal of water from the interstitial sites. The packing of droplets imaged in confocal microscopy of the PSOs are a better representation of the droplets within a 3D PSO structure, such as a monolith, than the images of droplets produced *via* the microfluidic set up.

The microfluidic production and the confocal microscopy both appear to show that the polymer-polymer barrier between oil droplets is sufficient to prevent significant coalescence of droplets. It has been shown that aggregation/redispersion is possible for both larger samples, such as the production of an EE templated on the macro-scale (Figure 4.3), and small samples, for example those seen in microscopy.

4.2.3. Elasticity of Emulsions Between Switchable States

The effect that the degree of hydration within emulsion structures has on the strength of the material was investigated. As reversible dehydration had been demonstrated for an EE (3.2.1), its effect on the bulk strength of rehydrated aggregates and redispersed free-flowing emulsions was investigated. If a change in strength is brought about by dehydration of an EE to a PSO, then in principle changing the degree of hydration could control the elasticities of these materials. This change in elasticity, however, may also be reversible upon rehydration, resulting in materials with switchable mechanical strength. The bulk viscoelastic properties of an E5 dodecane emulsion in its different states were quantified using amplitude sweeps, in which G′ and G″ are plotted against strain amplitude (Figure 4.12). The procedure was similar to that outlined in Chapter 3.2.4, with any dehydration or rehydration occurring *in situ,* prior to measurement. Rheological properties were measured for the free-flowing droplets at pH 10, EEs at pH 2, PSOs, re-hydrated EEs and redispersed droplets, with the pH returned to pH 10 (Figure 4.12). The results of these measurements allow us to assess the reversibility of these multiple phase changes and their affect on the strength of the bulk system. G′ at 0.5 % strain, chosen as it lies in the LVE region of all these materials, is increased upon the formation of an EE (Figure 4.12(c)) from a free-flowing emulsion (Figure 4.12(a)). This is consistent with results shown in Chapter 3.2.4 when comparing an inter-droplet hydrogen bonding system (E4-E5) to a system that showed no aggregation (E6-E9).

The dispersed droplets display a low storage modulus of 5 Pa, but following acidification the EE displays a G′ of 1070 Pa. When an EE is dehydrated for 6 hours to form a single-phase PSO (Figure 4.12(e)), the G′ increases by an order of magnitude (approximately 2 x 10^4 Pa) to 19,600 Pa, suggestive of an increase in droplet structuring as suggested earlier in the Chapter when imaging the transition from an EE to a PSO (3.2.1).

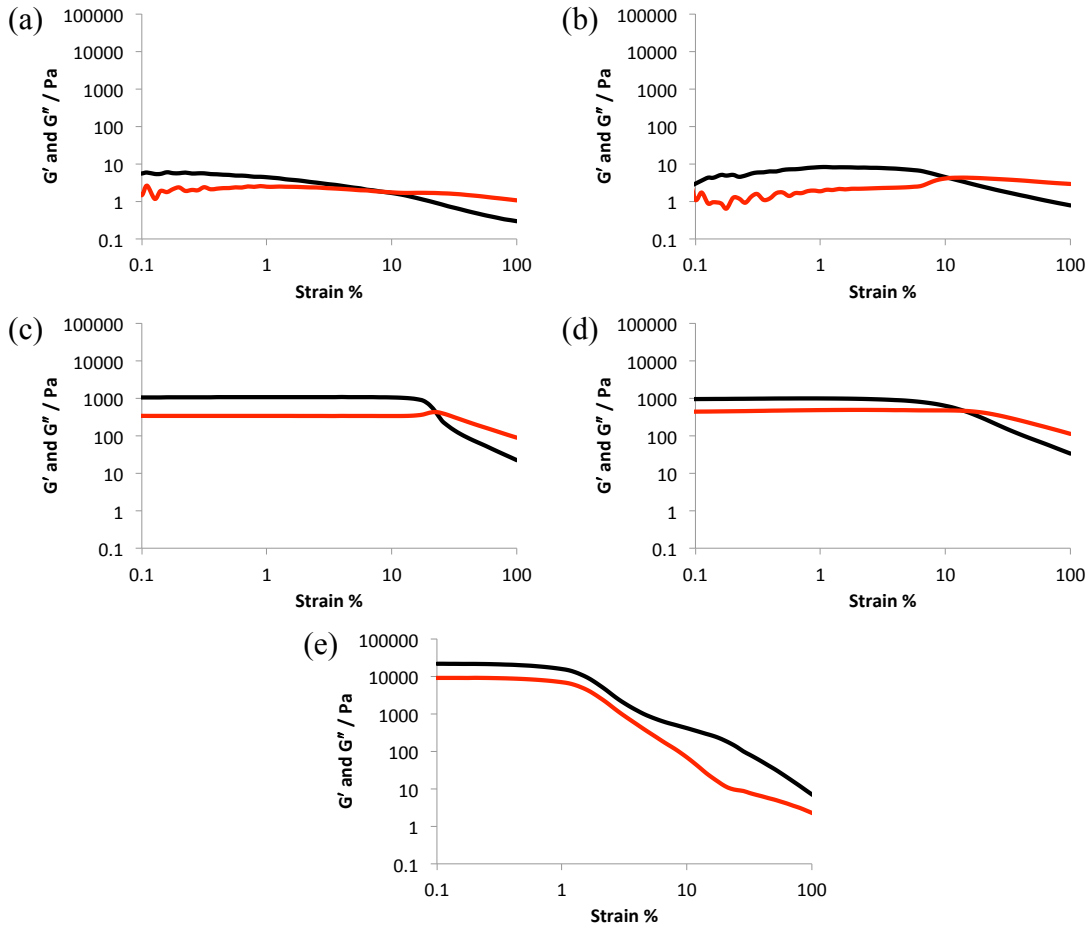

Figure 4.12. Amplitude sweeps of E5 emulsion samples showing both G' (black) and G" (red) for (a) a free-flowing emulsion, (b) a free-flowing emulsion from a rehydrated, redispersed PSO, (c) an EE aggregated for 2 hours, (d) an EE formed from a rehydrated PSO that was dehydrated for 6 hours and (e) a PSO dehydrated for 6 hours.

In the LVE region, G′ is greater than G″ in all samples, suggesting that all materials show a more elastic than viscous response to low strains. In free-flowing emulsions, this is likely due to droplet deformation contributing toward the elastic (G′) portion of the sample, providing these materials with some degree of measurable strength.

However, all samples, with the exception of the PSO (Figure 4.12(e)), start to become more liquid-like with increased strain (so G″ > G′). This is an indication of the structure breaking down and the sample exhibiting more viscous behaviour as the emulsion is destroyed, or demulsified. The point at which G″ > G′ was not observed for the PSO, most likely because a greater strain is required to completely destroy the structure. It is worth noting that in Figure 4.12(e), the PSO's G′ appears to go through a two-stage breakdown, the first at around 2 % strain, the second at around 10 % strain. As interstitial water has been removed from the system, this may cause some destabilisation upon increased strain. As droplets become close-packed upon dehydration, separated only by polymer-polymer networks, this reduced 'barrier' between droplets may make the PSO more susceptible to some coalescence, which may explain the slight increase in droplet size after rehydration and redispersion measured by laser diffraction in Figure 4.4. It is important to note that the second stage of the breakdown shows a similar shape to the G′ of an EE. This suggests that a similar process is undergone by both systems between strains of 10-20 %. As both systems contain inter-droplet polymer-polymer hydrogen bonding, the decrease in G′ could be due to the breaking of these interactions.

Figure 4.12 also shows rheological measurements of a rehydrated PSO (forming an EE) in (d) and a rehydrated and redispersed PSO (forming free-flowing E5) in (b). These measurements were made to test the reversibility of PSO formation and also to see what effect that had on the viscoelastic properties of both the reformed EE and free-flowing emulsion. The G′ values of all the measurements in Figure 4.12 were overlayed to illustrate reversibility in Figure 4.13. Upon rehydration of a PSO or redispersion of an EE, the G′ returns to a similar plateau (985 Pa and 7 Pa respectively), owing to the robustness of the constituent droplets throughout both processes. This is evidence of switchable gel strength in EE systems, with G′ values dictated by the degree of dehydration in the structure.

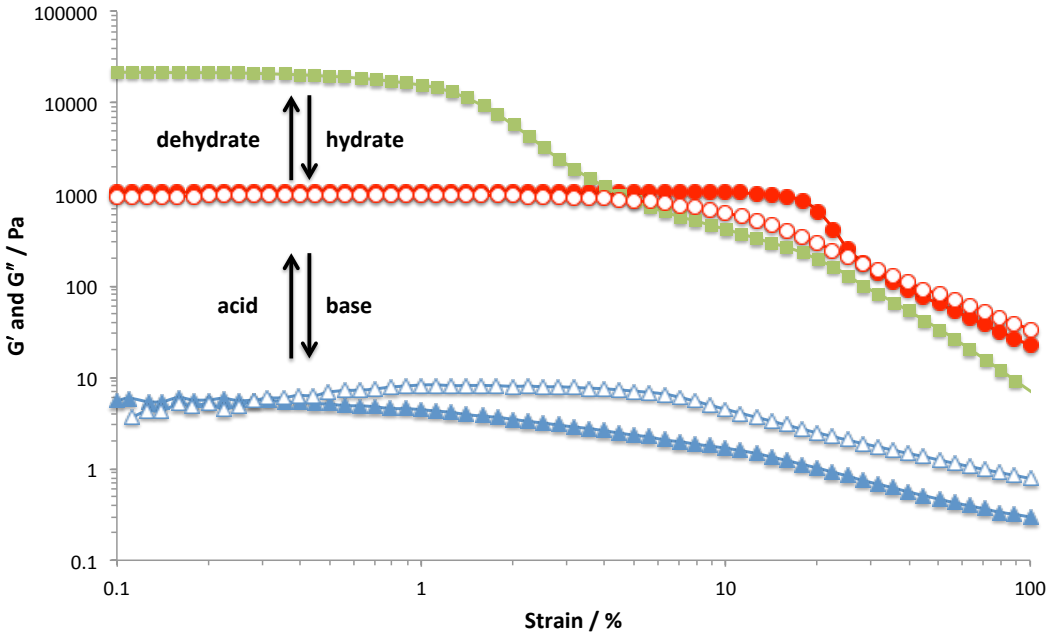

Figure 4.13. Reversible rheology showing resulting G' from strain sweeps for the dispersed droplets at pH 10 (blue closed triangles), EE droplets at pH 2 (red closed circles), dehydrated PSO (green closed squares), rehydrated EE at pH 2 (red open circles) and redispersed droplets at pH 10 (blue open triangles).

G′ values of free-flowing, dehydrated, rehydrated and redispersed samples are compared in Table 4.3.

Table 4.3. Table of G′, G″ and crossover point for each of the emulsion phases.

	Free-flowing	EE	PSO	Rehydrated EE	Redispersed free-flowing
G′ (LVE) / Pa	5	1070	19600	985	7
G″ (LVE) / Pa	2	338	8480	470	2
Crossover point / % Strain	9	23	N/A	14	11

When investigating each measurement alone, the crossover point (strain above which G″ > G′) can provide more information about individual samples (Table 4.3). This crossover point tells us the stage at which the sample has started to behave like more of a liquid than a solid, suggesting that the initial biphasic emulsion system has been broken down. For these systems, the crossover point increases upon aggregation of free-flowing emulsions to form an EE (from 9 to 23 %). However, upon rehydration of a PSO to an EE, the crossover point occurs at a strain of around 14 %. This

decrease is likely due to excess HCl not being fully removed when rehydrating the EE, contributing to the viscous properties of the structure and leading to a lower crossover point. When the sample is redispersed and allowed to cream the crossover point occurs at 11 %, showing good reversibility when reforming the free-flowing emulsion.

4.2.4. Engineered Emulsions and Polymer Structured Oils Containing Guest Molecules

Although engineered emulsions containing guest molecules, such as hydrophobic dyes, have been previously shown in the literature,[15] their role in the stability of PSO formation and the rehydration-redispersion process was not investigated. It is hypothesised that these processes should be unaffected by the encapsulation of hydrophobes, as the surface chemistry that dictates these transitions should remain unchanged. To investigate this, a complex EE structure made up of three different emulsion systems was produced (Figure 4.14). All systems were P5 stabilised dodecane o/w emulsions, one with no guest molecules encapsulated which appeared milky white, one containing Oil Red and another containing Oil Blue (both added at 0.1 wt. % with respect to the oil phase). The Oil Red and Oil Blue containing emulsions had volume-average droplet diameters of 9.6 μm and 8.3 μm and spans = 1.18 and 1.21, respectively. Encapsulation involves dissolving the guest molecule in the oil phase of the o/w system before homogenisation. The molecules should then be encapsulated within each oil droplet and dispersed throughout the water phase. The union flag in Figure 4.14 was created in a multi-step process. The red cross was prepared first by "painting" the free-flowing red emulsion (pH 10) roughly into the shape of a cross and then adding HCl (1 M) to form an EE. Excess EE was removed using a scalpel. The white and blue portions of the flag were added in a second and third step, using an identical paint-gel-sculpt procedure. Once produced, the EE was allowed to dehydrate for 2 hours to form the corresponding transparent PSO (Figure 4.14(b)). The PSO was then submerged in acid (HCl, 0.5 M) in order to rehydrate the structure. Opaque EEs reformed over 20 minutes (Figure 4.14(c)) after which addition of base and slight mixing caused rapid droplet disassembly and the reformation of a free-flowing emulsion due to returning steric and electrostatic stabilisation (Figure 4.14(d)).

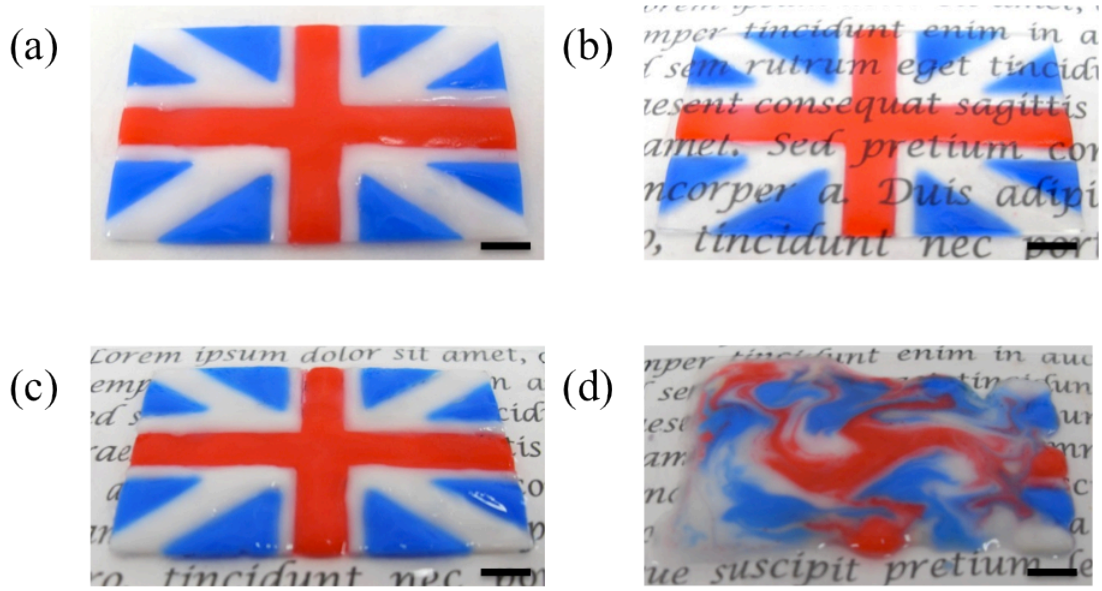

Figure 4.14. Digital images of reversible transitions of emulsion-based structures containing dyes. (a) An EE union flag. (b) The PSO formed from dehydration of (a) and placed on text to show its translucency. (c) The rehydrated PSO, returning to an opaque structure. (d) Redispersed EE at pH 10, forming free-flowing emulsion. Scale bars represent 5 mm.

It is worth noting that large, well-defined EEs are difficult to fabricate due to the slow diffusion of HCl throughout the concentrated emulsion. When a P5 emulsion comes into contact with the acid solution, aggregation is rapid. This can form blemishes on the surface of the emulsion, where it has initially aggregated quickly upon contact with HCl. This is why a scalpel was needed to remove excess EE, and to help shape the structure once acidified.

4.2.5. Triggerable Release from Polymer Structured Oils

A P5 dodecane o/w emulsion (Φ_{oil} = 0.70) containing the hydrophobic dye Lumogen® Rosa 285 (0.1 wt. %) in the oil phase was produced, the laser diffraction analysis of which is shown in Figure 4.15. The data were in good agreement with previously produced emulsions ($D_{(4,3)}$ = 8.13 μm, span = 1.22) and was used in the formation of a multi-layer EE (Figure 4.16).

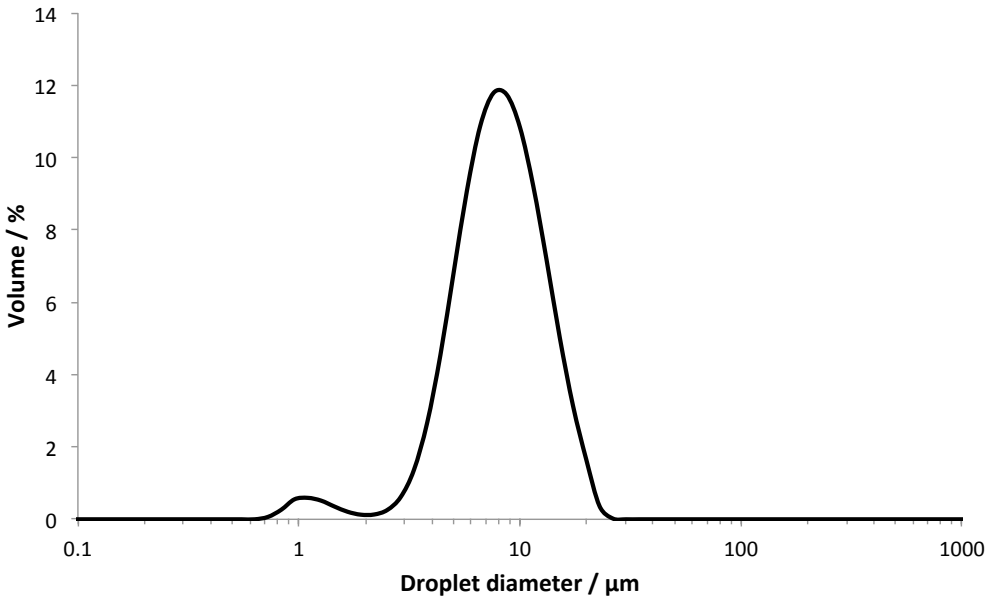

Figure 4.15. Laser diffraction size distribution curve result of a P5 stabilised dodecane o/w emulsion containing Lumogen® Rosa 285 (0.1 wt. %) in the oil phase.

When creating PSOs comprising two layers of EE, it was noticed that, if left overnight, guest molecules could diffuse between layers, suggesting that PSOs could potentially provide a controllable release mechanism for guest molecules. It is thought that dehydration in an EE system containing hydrophobes may result in triggered release due to the removal of the interstitial water layers. In order assess hydrophobe diffusion, a layered PSO was allowed to dehydrate for 24 hours (Figure 4.16). The top layer was a P5 dodecane o/w emulsion containing hydrophobic dye (Lumagen® Rosa 285, 0.1 wt. %) and the bottom layer was the same emulsion containing no guest molecules. After 24 hours, the bottom layer had become orange (Figure 4.16(b)), indicating some dye diffusion between layers had occurred.

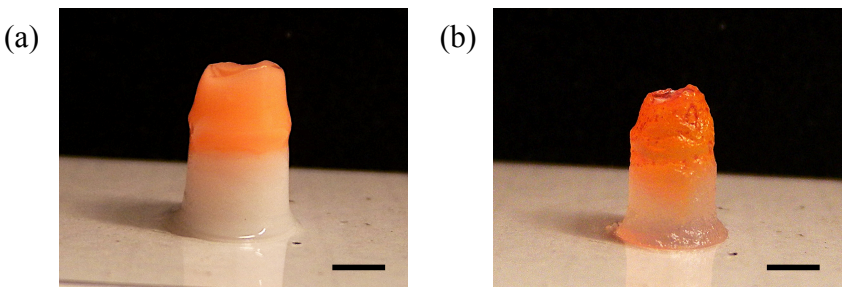

Figure 4.16. Multi-layered monolith made up of a hydrophobic dye containing layer (top) and a standard EE (bottom) (a) after production at t = 0 and (b) a PSO after 24 hours dehydration. The bottom layer appears to contain Lumogen® Rosa 285. Scale bars represent 2.5 mm.

In contrast to Figure 4.16, if a layered monolith was kept hydrated for long periods of time, for example by submersion in an acidic solution, no diffusion was observed. (Figure 4.17).

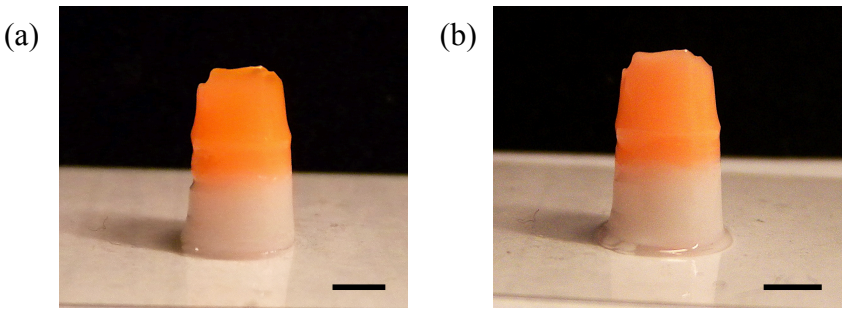

Figure 4.17. Multi-layered monolith made up of a hydrophobic dye containing layer (top) and a standard EE (bottom) (a) after production at t = 0 and (b) the same structure at t = 24 hours. Sample was kept hydrated by submersion in acid solution. Scale bars represent 2.5 mm.

When water was removed from interstitial sites upon dehydration, it may become possible for the hydrophobic dyes to diffuse though the polymer-polymer barrier into another oil droplet, shown schematically in Figure 4.18.

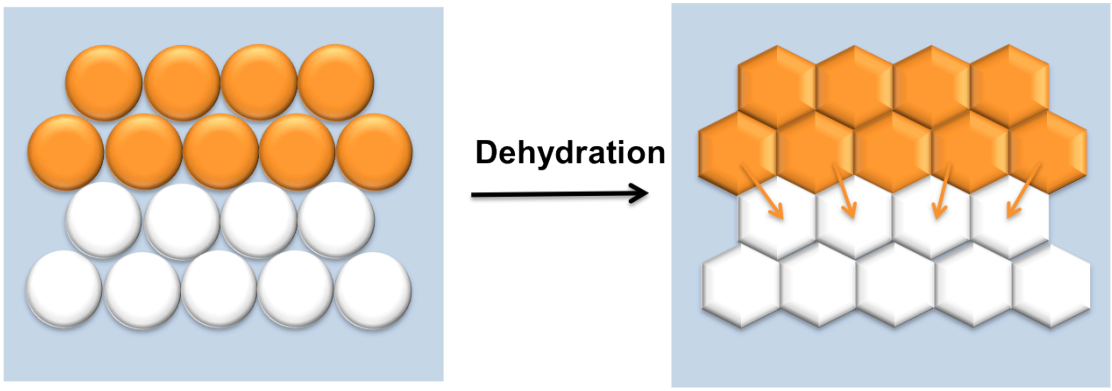

Figure 4.18. Schematic of dehydration-triggered diffusion in a monodisperse o/w emulsion system. Removal of water from interstitial sites allows diffusion of hydrophobes.

Before dehydration, the dye would also have to move through the continuous water phase, meaning diffusion from the oil droplet was much more unfavourable. The removal of most of this interstitial water means that not only will a larger surface area of droplets be in contact with other droplets, but also that most of the space between droplets will only consist of a polymer-polymer barrier. The loss of these water barriers means that hydrophobes should now diffuse between droplets more

easily. This hypothesis was measured quantitatively by monitoring the dye release kinetics of Oil Blue from a P5 dodecane EE into a surrounding dodecane reservoir and comparing it to release from an analogous PSO using UV-Vis spectroscopy (Figure 4.20). The laser diffraction size distribution curve for this Oil Blue containing emulsion (Φ_{oil} = 0.71) is shown in Figure 4.19, and is in good agreement with previously produced emulsions ($D_{(4,3)}$ = 8.25 μm and span = 1.21).

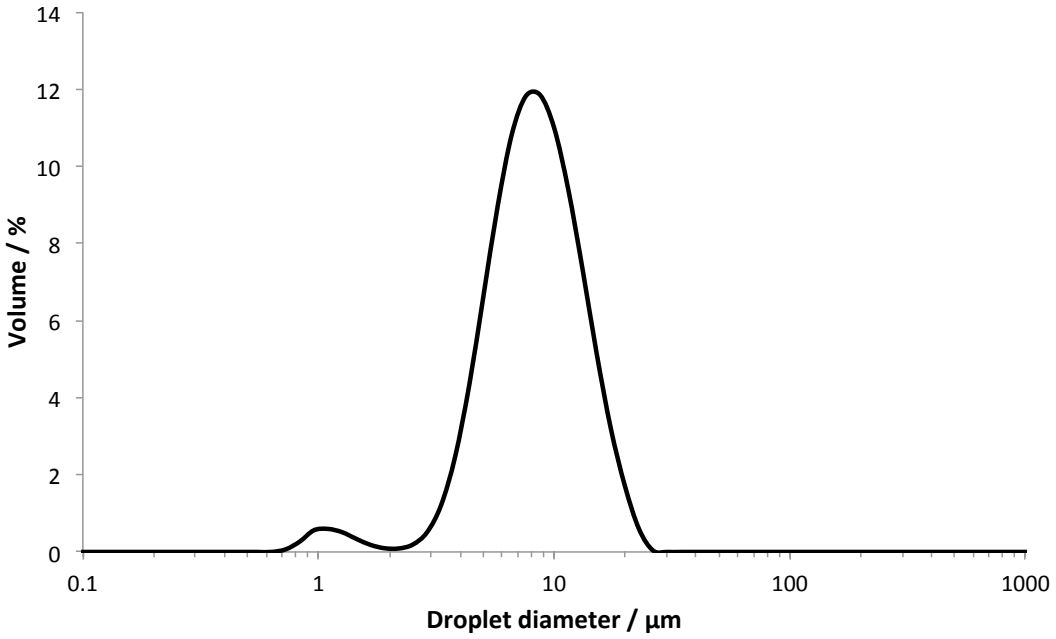

Figure 4.19. Laser diffraction size distribution curve obtained for a P5 dodecane o/w emulsion containing Oil Blue (0.1 wt. %) in the dispersed phase.

In contrast to biphasic EEs, which displayed no dye release over 3 hours, significant release was observed from the single-phase PSOs. The interstitial water barrier clearly inhibits hydrophobe inter-droplet diffusion throughout the structure, but no interstitial sites are present at the surface of the structure to prevent dehydration from the outer layer of droplets. Since no Oil Blue released into the surrounding dodecane oil phase was measured, some water must be present on the surface of the monolith, perhaps bound to the hydrophilic components of the polymeric surfactant. This water layer appears to be sufficient to prevent the release of Oil Blue into a continuous dodecane phase. Error bars in Figure 4.20 were calculated using the standard deviation of three repeats of each measurement.

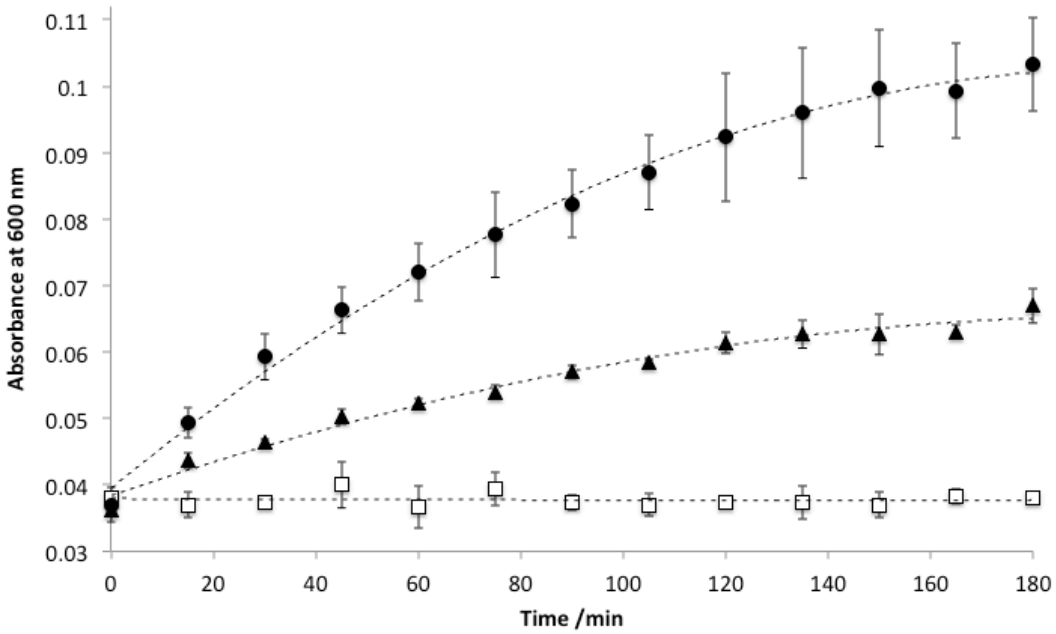

Figure 4.20. Release curves of Oil Blue dye from a pre-loaded dodecane EE (open squares) and a dodecane PSO prepared with P5 at a concentration of 2 w/v % (closed triangles) and 1 w/v % (closed circles).

As can be seen in Figure 4.20, the release of Oil Blue from the dodecane PSO could be accelerated by reducing the concentration of P5 used to stabilise the initial emulsion droplets. This result confirms that the diffusion process is dependent on the 'thickness' of the polymer network at the oil-oil interface. Any excess polymer in the water phase would also be deposited at the oil-oil interface upon dehydration. Therefore, with increased amount of P5, these droplet boundaries may become slightly thicker if more excess polymer is present in the water phase, potentially leading to lower rate of diffusion of hydrophobes from droplets. Therefore, release from these emulsion-based polymer-structured oils can be tuned by controlling the degree of hydration, with further refinement permitted by simply altering the concentration of polymer at the droplet interface.

Digital images of both P5 dodecane EEs and PSOs containing dye were captured before and after they were placed into a dodecane continuous phase (Figure 4.21). The EE did not appear to have released any dye into the surrounding dodecane reservoir after 2 hours (Figure 4.21(b)), in good agreement with dye release measured by UV-Vis spectroscopy in Figure 4.20. In contrast, the PSO had clearly released dye into the continuous oil phase after 2 hours (Figure 4.21(d)), again in good agreement with the previous work. A PSO containing dye could also be

rehydrated to form an EE before addition to the dodecane reservoir and, dependent on full rehydration, would also keep the hydrophobe encapsulated due to the return of water to the EEs interstitial sites.

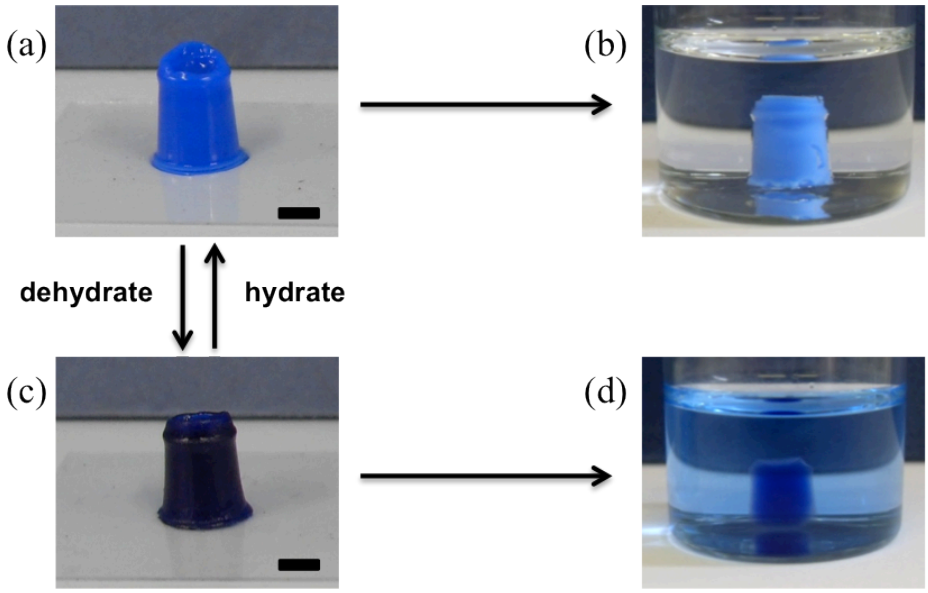

Figure 4.21. Digital images of (a) a dodecane EE containing oil blue, (b) the EE in dodecane with no dye release visible after 2 hours. (c) A dodecane PSO containing Oil Blue, (d) The PSO in dodecane after 2 hours. The surrounding dodecane appears to contain Oil Blue that has diffused from the PSO. Scale bars represent 2.5 mm.

4.2.6. Uptake of Hydrophobic Dye by Polymer Structured Oils

In order to investigate the sequestration of hydrophobes by PSOs, the uptake of Oil Blue was measured with varying degrees of EE dehydration and with increasing Oil Blue concentration in the surrounding dodecane reservoir. Small aliquots (10 µL) of the creamed layer of a P5 dodecane o/w emulsion was dripped into an acid reservoir (1 M HCl, 5 mL) and, upon contact with the acid, formed small spherical droplets immediately. These spheroids were then either kept hydrated in the acid reservoir or removed to initiate dehydration. Both EEs and PSOs at various dehydration levels were added to dodecane reservoirs containing various levels of Oil Blue for 60 minutes. Upon removal, the spheroids were washed twice with fresh dodecane in order to remove any excess Oil Blue on the spheroid surface. All spheroids were then dissolved in ethanol (100 µL) for measurement using UV-Vis spectroscopy (Figure 4.22), as dodecane, water, P5 and Oil Blue are soluble in this solvent. Error bars were calculated using the standard deviation from two repeats of each measurement.

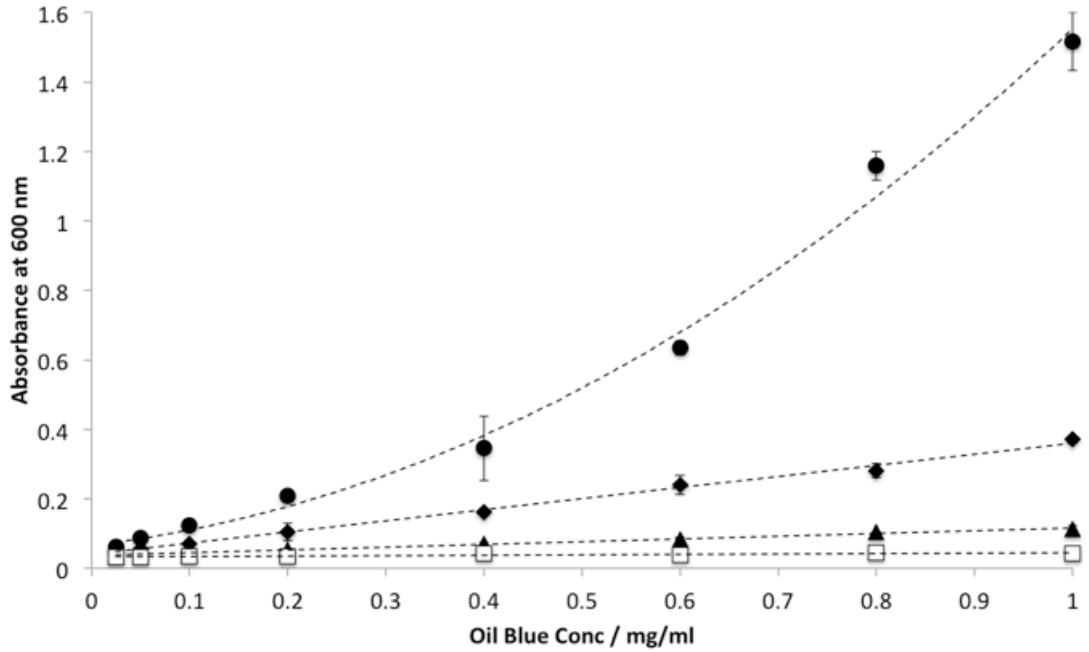

Figure 4.22. Oil Blue uptake in dodecane spheroids measured by absorbance at 600 nm. Spheroids were dehydrated at ambient temperatures for 0 minutes (open squares), 10 minutes (closed triangles), 20 minutes (closed diamonds) and 45 minutes (closed circles), all of which had been exposed to various concentrations of Oil Blue in dodecane.

From Figure 4.22, it can be seen that as the EE becomes a PSO, the spheroids sequestered more Oil Blue (closed diamonds and closed circles represent 20 and 45 minute dehydration respectively). When the EE was not allowed to dehydrate (open squares), regardless of the external Oil Blue concentration gradient, no Oil Blue peak appeared in the spectra (a background absorbance of around 0.035 is standard for the 96-well plate used). However, when the spheroids were allowed to dehydrate for 45 minutes, even when the Oil Blue was only present at 0.025 mg/mL in the surrounding dodecane reservoir, the absorbance increased to 0.062. Uptake therefore became easier due to dehydration. This again suggests that the trapped water at the droplet surfaces is enough to inhibit diffusion of encapsulated hydrophobes. No dye absorption into EEs was observed for up to three days, irrespective of dye concentration. This shows that the EE-to-PSO transition could allow these materials to be used as dehydration-triggered sequestration devices. Uptake was also captured using digital imaging on a larger scale (Figure 4.23).

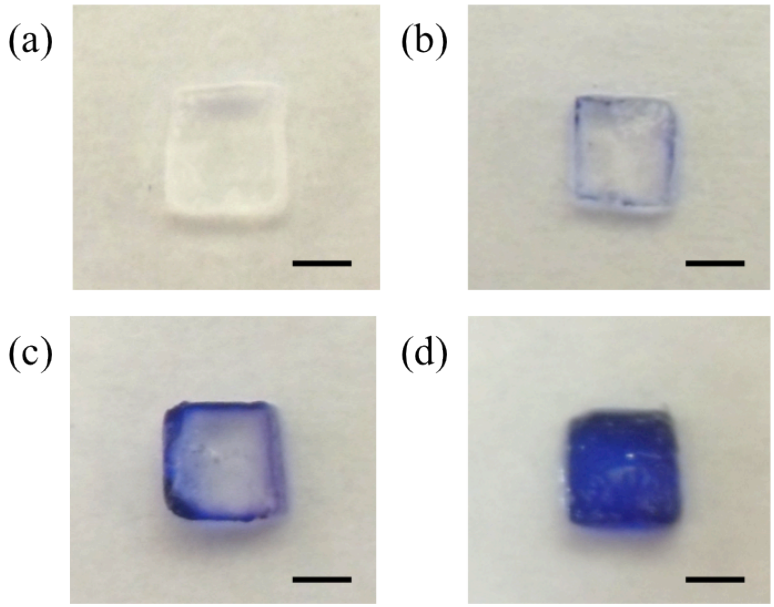

Figure 4.23. Uptake of Oil Blue (1 mg/mL) in dodecane to dodecane PSOs with time. (a) No exposure to Oil Blue, (b) 0.5 hours in reservoir (c) 1 hour and (d) 24 hours. Scale bars represent 2.5 mm.

Figure 4.23 shows the gradual uptake of Oil Blue in a larger PSO. Four 150 µL monoliths were cut into cuboids and allowed to dehydrate for 3 hours. The resulting monoliths were then placed in an Oil Blue (0.1 wt. %) in dodecane reservoir (10 mL) for varied lengths of time. Upon removal, the cuboids were sliced horizontally in order to observe the degree of Oil Blue sequestration in each sample. After 30 minutes in solution (Figure 4.23(b)), the Oil Blue had diffused into the structure's surface. After 60 minutes (Figure 4.23(c)), the Oil Blue had diffused slightly further into the monolith. When the sample was left in solution for 24 hours (Figure 4.23(d)), the structure appeared saturated with Oil Blue, becoming equilibrated with the surrounding reservoir.

4.3. Conclusion

Allowing an EE to dehydrate results in substantial changes in its physical properties at both the macro- and micron-scale. These include optical changes, reduction in volume, rheological transitions and, when looking at constituent droplets, morphology changes. All of these property changes are in fact reversible, and rehydration returns the PSO to the original engineered emulsion biphasic system.

This provides materials with switchable gel strengths as measured by the increase and decrease in G′ on dehydration and rehydration, respectively. This high stability towards coalescence during dehydration and shear, coupled with the responsiveness at the droplet surface provides the emulsions with extended shelf-lives, broader applications and allow them the potential to be used as versatile and functional synthetic building blocks. The copolymer surfactant provides inter-droplet interactions between individual building blocks and acts as a crude mimic of cell-cell interactions in biological systems.[20-22] Moreover, the applicability of these materials as novel encapsulation and release devices is demonstrated, with triggerable release upon dehydration controlled further simply by altering the concentration of copolymer used to stabilise dodecane o/w emulsions. Varied rates of hydrophobe sequestration are also demonstrated in EE and PSOs, dependent on the degree of dehydration the structure has undergone. Complete hydration appears to prevent both sequestration and release of hydrophones completely, demonstrating good control over the movement of hydrophobes both into and out of PSOs.

4.4. References

(1) Bibette, J.; Calderon, F. L.; Poulin, P. *Rep. Prog. Phys.* **1999**, *62*, 969.
(2) Cochin, D.; Laschewsky, A.; Nallet, F. *Macromolecules* **1997**, *30*, 2278.
(3) Pichot, R.; Spyropoulos, F.; Norton, I. T. *J. Colloid Interface Sci.* **2010**, *352*, 128.
(4) Mathur, A. M.; Drescher, B.; Scranton, A. B.; Klier, J. *Nature* **1998**, *392*, 367.
(5) Fujii, S.; Cai, Y. L.; Weaver, J. V. M.; Armes, S. P. *J. Am. Chem. Soc.* **2005**, *127*, 7304.
(6) Fujii, S.; Read, E. S.; Binks, B. P.; Armes, S. P. *Adv. Mater.* **2005**, *17*, 1014.
(7) Halling, P. J. *CRC Cr. Rev. Food Sci.* **1981**, *15*, 155.
(8) Dickinson, E. *Colloid. Surface. B* **1999**, *15*, 161.
(9) Pickering, S. U. *J. Chem. Soc.* **1907**, *91*, 2001.
(10) Binks, B. P. *Curr. Opin. Colloid Interface Sci.* **2002**, *7*, 21.
(11) Aveyard, R.; Binks, B. P.; Clint, J. H. *Adv. Colloid Interface Sci.* **2003**, *100-102*, 503.
(12) Woodward, R. T.; Slater, R. A.; Higgins, S.; Rannard, S. P.; Cooper, A. I.; Royles, B. J.; Findlay, P. H.; Weaver, J. V. *Chem. Commun.* **2009**, 3554.
(13) Niraula, B.; King, T. C.; Chun, T. K.; Misran, M. *Colloid. Surface. A* **2004**, *251*, 117.
(14) Wulff-Perez, M.; Torcello-Gomez, A.; Martin-Rodriguez, A.; Galvez-Ruiz, M. J.; de Vicente, J. *Food Hydrocolloids* **2011**, *25*, 677.
(15) Weaver, J. V. M.; Rannard, S. P.; Cooper, A. I. *Angew. Chem. Int. Ed.* **2009**, *48*, 2131.

(16) Weaver, J. V. M.; Williams, R. T.; Royles, B. J. L.; Findlay, P. H.; Cooper, A. I.; Rannard, S. P. *Soft Matter* **2008**, *4*, 985.
(17) Weaver, J. V. M.; Adams, D. J. *Soft Matter* **2010**, *6*, 2575.
(18) Chambon, P.; Chen, L.; Furzeland, S.; Atkins, D.; Weaver, J. V. M.; Adams, D. J. *Polym. Chem.* **2011**, *2*, 941.
(19) O'Brien, N.; McKee, A.; Sherrington, D. C.; Slark, A. T.; Titterton, A. *Polymer* **2000**, *41*, 6027.
(20) Tsai, C. J.; Ma, B. Y.; Kumar, S.; Wolfson, H.; Nussinov, R. *Crit. Rev. Biochem. Mol.* **2001**, *36*, 399.
(21) Klug, A. *Nature* **1983**, *303*, 378.
(22) Klug, A. *Angew. Chem. Int. Ed.* **1983**, *22*, 565.

CHAPTER 5

Large Volume, Macroscopically Defined, Responsive Engineered Emulsions Using a Homogenous pH Trigger

(Publication arising from this Chapter: **"Fabrication of large volume, macroscopically defined and responsive engineered emulsions using a homogeneous pH-trigger"**, R. T. Woodward, L. Chen, D. J. Adams, J. V. M. Weaver, *J. Mater. Chem.*, 2010, *25*, 5228-5234.)

List of Figures

List of Schemes

5.1. Introduction

In Chapter 3 it was shown that a simple one-pot copolymerisation allows the production of branched, pH-responsive copolymeric surfactants with varying molar ratios of EG:MAA. The ability of these copolymers to form stable, pH-responsive dodecane o/w emulsions was then investigated. Chapter 3 demonstrated that P5-stabilised emulsions exhibited the fastest rate of aggregation, yielding the most strain-resistant engineered emulsion. For these reasons it was decided that P5 was the best copolymer for study.

In Chapter 4, dodecane o/w EEs, stabilised using copolymer P5 were utilised for the production of PSOs. A PSO is formed by the removal of water from an EE, forming an aggregate comprising only one liquid phase. Chapter 4 also demonstrated encapsulation within oil droplets and triggered release upon the formation of a PSO from a dye-loaded EE.

In previous Chapters, only monoliths and complex structures of low volume were produced as the volume of the EE that is readily achievable within a reasonable time scale is limited by inefficiencies in the diffusion of HCl through the emulsion structure. Furthermore, the addition of acid solution to the surface of a templated emulsion can form localised blemishes and not result in a homogeneous surface structure (i.e. as templated). However, larger volumes of P5-stabilised emulsion could be produced if a more homogeneous pH change could be generated. Hydrolysis of glucono-δ-lactone (GδL) lowers the pH homogeneously throughout an aqueous solution.[1] GδL is a naturally occurring molecule found in grapes[2] and is commonly used as an acidulant, i.e. an acid used in food production to lower pH. For this reason GδL has been used in a number of processes including the acidification of milk,[3-5] the curing of meats[6] and as a flavouring agent in a range of foods.[7] In addition to food production, GδL has previously been utilised as a homogeneous pH trigger in the formation of hydrogels.[8-11] As well as being a homogeneous pH trigger, GδL can result in stronger gels and better reproducibility, but so far this method does not appear to have been used for the homogeneous pH change of an emulsion system. In this Chapter, the use of GδL as a homogeneous pH trigger in a pH-responsive P5 dodecane o/w emulsion to form larger, well-defined EEs is investigated. In contrast to conventional acidification strategies, such as the addition

of concentrated acid solutions, a homogeneous pH trigger also allows the formation of EEs to be monitored *in situ* via rheometry, thus allowing investigation of the evolution of an emulsion system's strength during acidification.

5.2. Results and Discussion

5.2.1. Hydrolysis of glucono-δ-lactone

GδL is a cyclic ester (a lactone), which undergoes hydrolysis in aqueous solution to give gluconic acid in equilibrium (Scheme 5.1).[1] GδL is highly water-soluble (59 g/100 mL at 20 ^{o}C),[12] and hydrolysis only begins once the solid has been dissolved in water. This allows homogeneous pH change to occur throughout the o/w emulsion system, without the need for diffusion when using HCl to lower pH. This may allow the formation of much larger, more well-defined EEs which are not possible when acidifying *via* the addition of HCl solution.

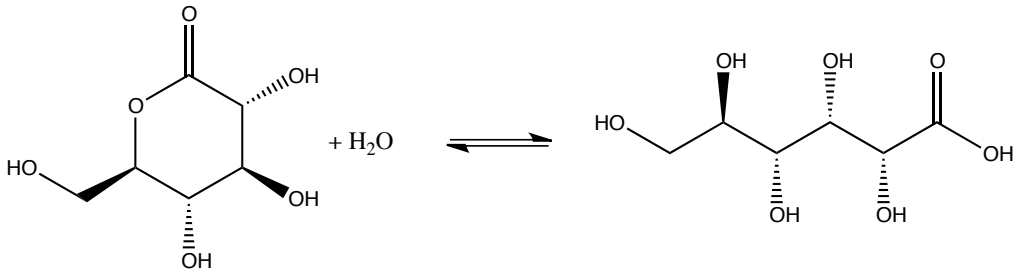

Scheme 5.1. Schematic representation of the hydrolysis of GδL, resulting in a chemical equilibrium between the lactone and the acid form.

As hydrolysis is dependent on both temperature and concentration,[1] initially the pH change of solutions containing different amounts of GδL was measured. All solutions were made using distilled water with an initial pH of 6.8. The GδL solutions were then left at room temperature (20.5 ^{o}C) for 4 hours, after which the pH was measured again. Increasing the initial concentration of GδL shifts the equilibrium to the right, resulting in a higher concentration of gluconic acid and a lower final solution pH (Figure 5.1).

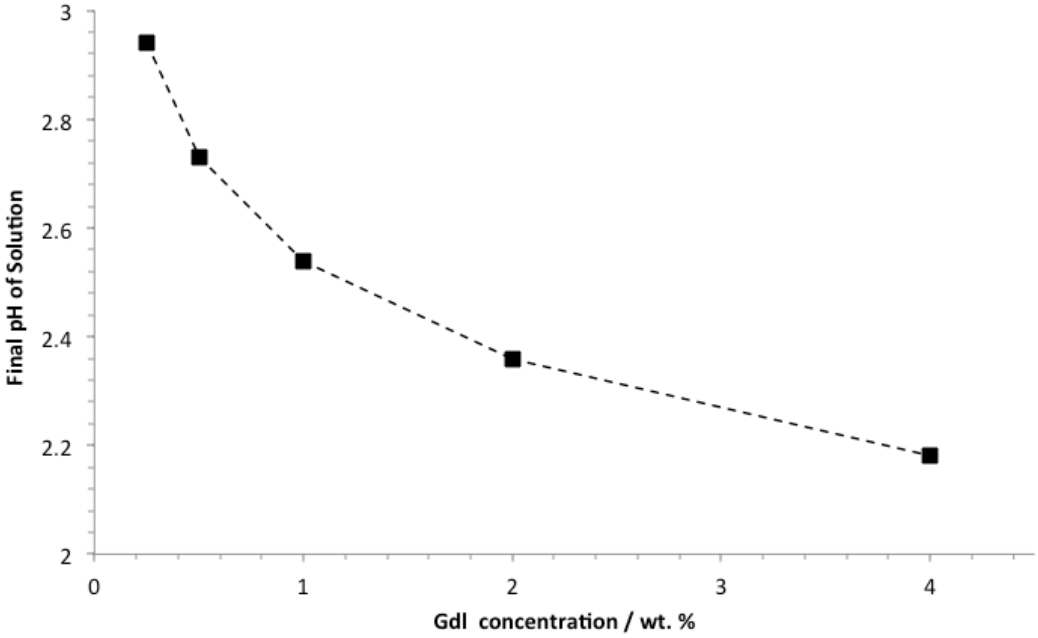

Figure 5.1. Final pH of GδL solutions after 4 hours at 20.5 ^{o}C against initial concentration of GδL.

Dodecane o/w emulsions (Φ_{oil} = 0.70) were prepared as described previously in Chapter 3.2.2, using P5 (2 wt. %) as a polymeric surfactant. The pH measurements of GδL solutions in Figure 5.1 are not directly applicable to dodecane o/w systems. The difference between GδL hydrolysis in water and a P5 emulsion system arises due to the protonation of MAA groups during acidification in the emulsion system. This results in a higher final solution pH in the emulsions than in the GδL solutions alone (Figure 5.2). A general reduction in pH upon the production of gluconic acid is still observed, so these measurements were performed in order to ensure that the pH of the system was below the apparent pK_a of MAA in P5 (p$K_a \approx 5$).[13] Varied pK_a values of MAA are reported in the literature, possibly due to PMAA exhibiting different values to the monomer, believed to be due to hydrophobic interactions within the copolymer chains.[14-16] Therefore, if a final pH of pH 4 or below is achieved in the emulsion system and an EE was formed, maximum protonation of MAA residues was assumed, meaning all copolymerised MAA groups should become available for hydrogen bonding with the EG repeat units present. GδL solution was added directly to the emulsion systems (1 mL of creamed layer) and gently mixed until dissolved. The samples were then placed in the fridge (4 ^{o}C) for 1 hour and again allowed to cream before pH monitoring began in order to allow direct

comparison with the rheology data. The sample was slowly stirred and the pH change was monitored *in situ* using a pH meter (Figure 5.2).

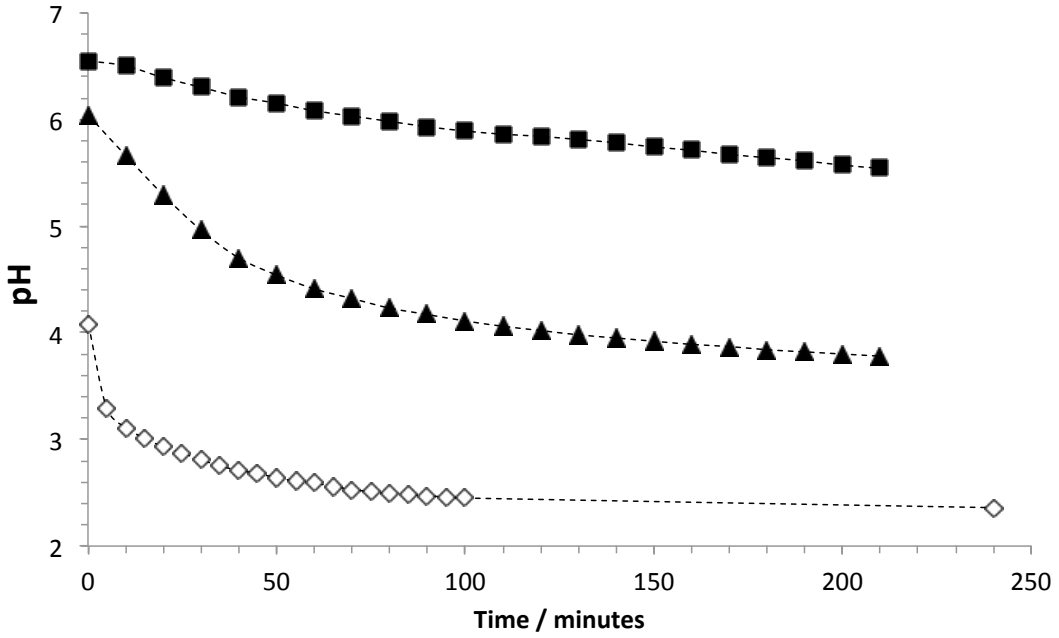

Figure 5.2. pH change with time at 18.5 °C for: 1 % GδL solution and dodecane emulsion (squares); 2 % GδL solution and dodecane emulsion (triangles); 2 % GδL solution alone (diamonds).

The effectiveness of this homogeneous pH trigger in the P5-stabilised pH-responsive dodecane emulsion system was investigated by aggregating around 150 μL of the creamed layer (Φ_{oil} = 0.70) in a mould using a similar method to that reported in Chapter 4, and also previously in the literature (Figure 5.3).[13] GδL (2 wt. %) was dissolved into the aqueous phase of the emulsion and the resulting mixture was immediately added to a mould. The sample was then left at ambient temperature for 2 hours to allow sufficient GδL hydrolysis to attain pH 4 or below. An engineered emulsion was produced (Figure 5.3(b)), which was redispersed after 30 minutes by raising the solution to pH 10 using NaOH (1 M, 0.5 mL) (Figure 5.3(c)). Optical microscopy was performed on small samples of the emulsion (20 μL) in each of its states (Figure 5.3(d)-(f)) (before aggregation, the EE and the redispersed EE) to see if GδL hydrolysis and redispersion brought about any droplet instability. Samples were aggregated for optical microscopy by the addition of GδL solution (4 wt. %, 10 μL) *in situ* and redispersed by the addition of NaOH solution (1 M, 20 μL).

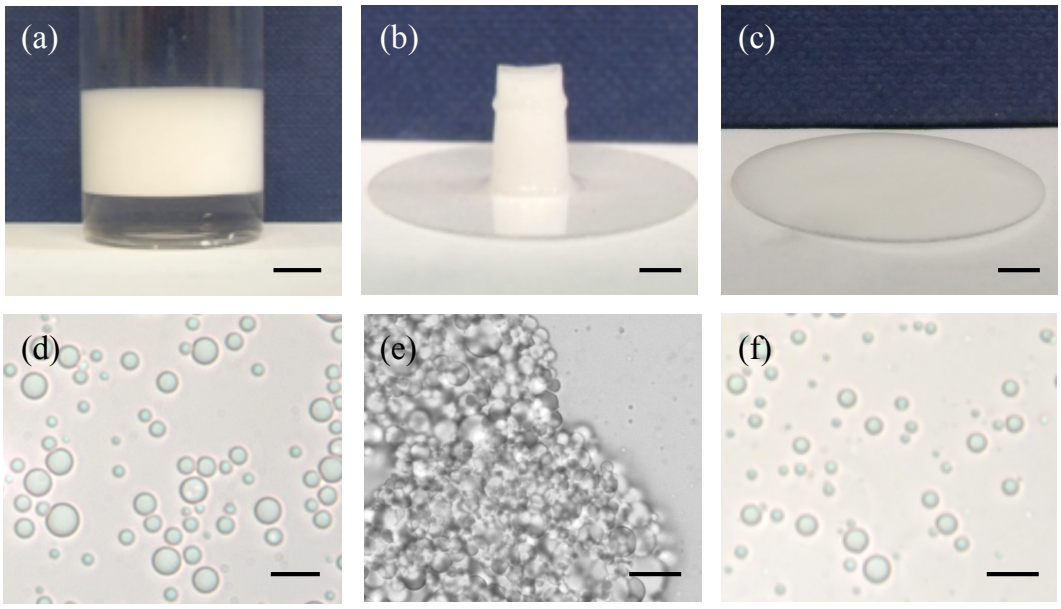

Figure 5.3. Digital and light micrograph images of dodecane emulsion (a) + (d) stabilised using P5 at pH 10, (b) + (e) aggregated using GδL, < pH 4 and (c) + (f) redispersed engineered emulsion at pH 10, showing the process is reversible. Scale bar in (a) represents 5 mm, in (b) & (c) 2.5 mm and in (d) – (f) 20 µm.

The light micrographs shown in Figure 5.3 suggest that droplets remain stable throughout the aggregation and redispersion process, with no visible evidence of coalescence occurring. It can be seen in Figure 5.3(e) that the engineered emulsion is made up of a network of individual droplets interacting at their surface, similar to previous findings.[13] Laser diffraction was also performed on the free-flowing emulsion creamed layer (40 µL in 80 mL of pH 10 solution) and compared to free-flowing emulsion formed from an EE (150 µL), aggregated using GδL (2 wt. %) and redispersed using NaOH (1 M, 0.5 mL) (Figure 5.4). Average volume droplet diameter and span increased slightly in the redispersed sample ($D_{(4,3)}$ = 10.93 µm, span = 1.24) in comparison to the free-flowing emulsion ($D_{(4,3)}$ = 10.48 µm, span = 1.16), which is in agreement with results found in Chapter 4.2.1 for HCl aggregated monoliths. This increase is less than that seen previously, most likely as the EE was not allowed time to dehydrate to a PSO so loss of oil was minimised.

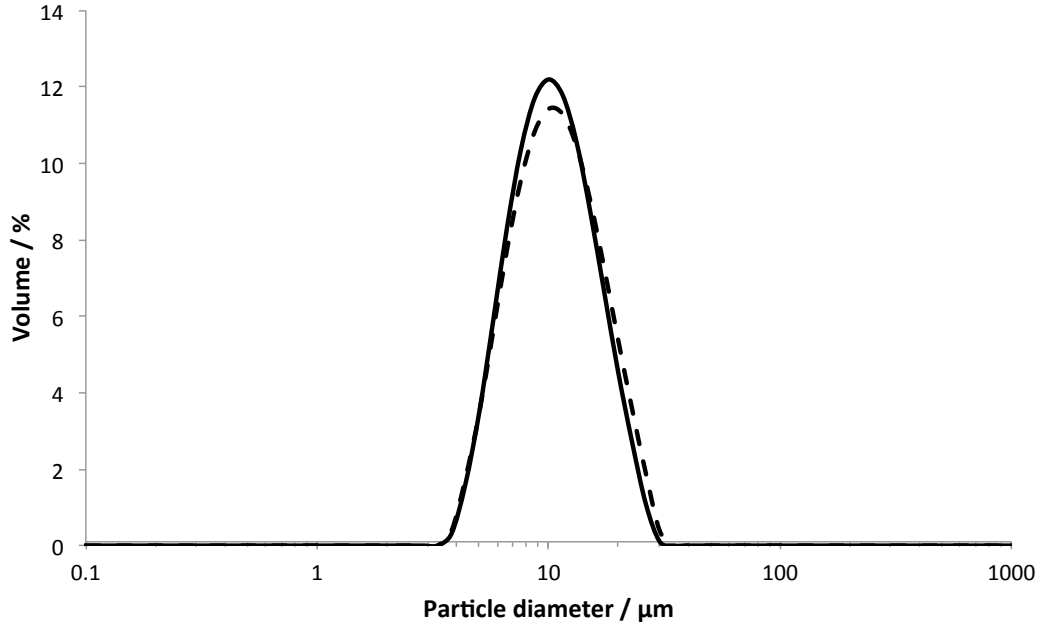

Figure 5.4. Overlayed laser diffraction size distribution for the dodecane emulsion droplets before (solid black line) and after (dashed black line) EE formation by GδL and redispersion by NaOH.

The stability of a GδL dodecane-engineered emulsion was observed over time (Figure 5.5) to see if any demulsification occurred when in the aggregated state. After 4 hours, although no demulsification was evident, the size of the monolith had reduced, suggesting that the aggregate had lost some volume *via* dehydration and some oil loss, similar to the same emulsions aggregated using HCl in Chapter 4.2.1 (Figure 4.3). However, these dehydrated monoliths do not appear as opaque upon dehydration, possibly due to the presence of precipitated GδL upon the removal of water from the monolith.

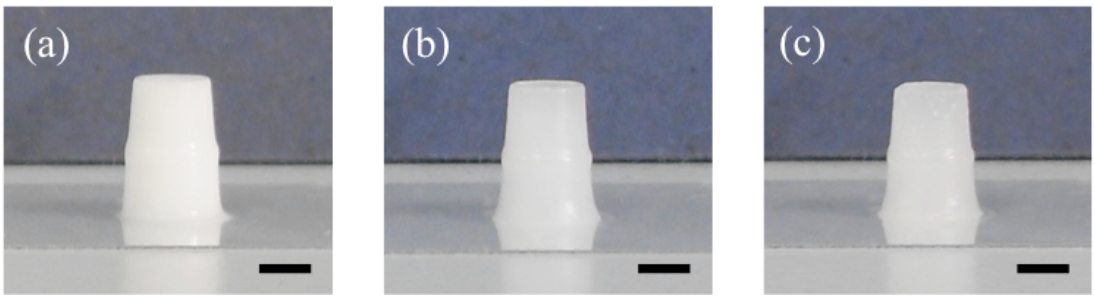

Figure 5.5. Stability of GδL-aggregated dodecane-engineered emulsion with time, showing a slight decrease in volume. However, aggregate does not become opaque as seen in a HCl aggregated EE. (a) t = 0, (b) t = 2 hours and (c) t = 4 hours. Scale bars represent 2.5 mm.

Although a change in volume was observed for an engineered emulsion, no demulsification occurred visually, illustrating the stability of not only the GδL engineered emulsion as a whole, but also the branched copolymeric surfactant at the interface during dehydration with GδL present.

5.2.2. Rheology of GδL systems

As it was now decided that 2 wt. % GδL was sufficient to take the system to below the pK_a of the MAA groups, the homogeneous pH change that triggers the dispersed-to-aggregated phase transition allows measurement of the change in strength of the system *in situ* using rheology. When a P5 dodecane emulsion (Φ_{oil} = 0.70) is acidified homogeneously, the effect that this method of aggregation had on the strength and stiffness of the resulting EE was investigated. Initially, the transition from free-flowing emulsion to EE was monitored by measuring the magnitude of the storage modulus (G') and loss modulus (G") against time (Figure 5.6). Samples for time sweep measurements were prepared by gently mixing 2.5 mL of creamed emulsion with a GδL solution (2 wt. %, 2 mL). The resulting sample was stored in a fridge (4 ^{o}C) for 1 hour to limit hydrolysis while the excess water phase could be removed by additional creaming. The GδL-loaded emulsion (2.5 mL) was then transferred to the rheometer.

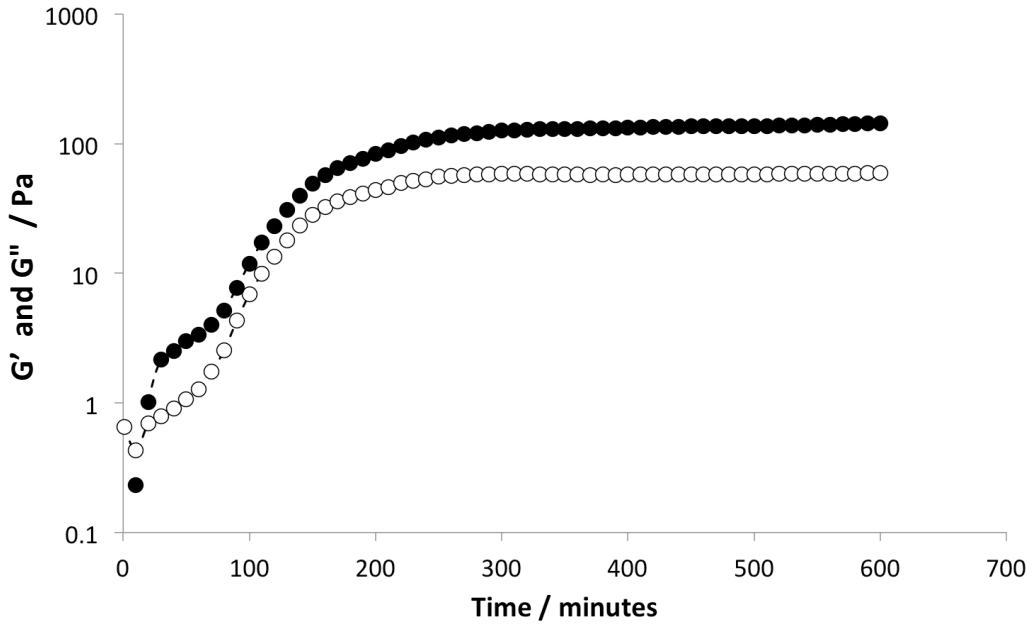

Figure 5.6. Variation of G' (filled circles) and G" (empty circles) with time after the addition of a 2 wt. % GδL solution to a P5 dodecane emulsion at 19 ^{o}C.

Figure 5.6 initially shows a larger G", suggesting a more liquid-like structure, possibly due to incomplete creaming, resulting in a lower Φ_{oil}. However, G' becomes greater than G" after around 20 minutes. It is thought that this initial rise in G' is due to further creaming, meaning that the sample became more concentrated where it is in contact with the rheometer. This is also supported by the pH monitoring of emulsion systems during GδL hydrolysis (Figure 5.2). This result shows that after 20 minutes the pH of the system is 5.3, which is above the apparent pK_a of MAA (p$K_a \approx$ 5), suggesting that inter-droplet hydrogen bonding has not caused this increase in G'. However, the rate of G' increases again at around 90 minutes. If we look at the pH of the emulsion system at this time, this value (pH 4.2) is low enough to trigger droplet aggregation. This experiment allowed measurement of the initiation of aggregation *via* changes in gel strength, which had not been possible using the diffusion of 1 M HCL as an assembly trigger. The initial 90 minutes in Figure 5.6 show a slow increase in the storage modulus of roughly only 0.1 Pa/minute, representing a creaming process. The G' then increases from around 10 Pa to 130 Pa over the next 200 minutes, reaching a constant G' value. This suggests that initial production of gluconic acid slowly lowers the pH to below the pK_a of copolymerised MAA, triggering aggregation once the MAA groups have been protonated.

Rheological measurements also allowed comparison of gel strength resulting from both GδL and HCl kinetically-trapped dodecane EEs. Samples of the emulsions cream layer (2.5 mL) were acidified *in situ*, by either the addition of HCl (0.5 mL) or GδL (2 wt. %) directly to the emulsion. Both samples were left to aggregate for 2 hours, after which any excess acid was removed and a strain sweep was carried out on both samples, giving a measurement of the magnitude of G' and G" under increasing strain and constant pH. G' at 0.5 % strain (in the LVE region of both samples) was 1,130 Pa and 1,380 Pa for the HCl- and GδL-aggregated samples, respectively. Homogeneous pH change may result in a slightly more uniform structure, resulting in a rise in G'. Both samples showed G' > G" in the LVE region as expected. The point at which the G' of the GδL sample (Figure 5.7) reached 90 % of its LVE region value was at around 16 % strain, suggesting that at this point the engineered emulsions begin to break down. This number was similar in the HCl system, where G' reached 90 % of its LVE region value at 14 % strain. The crossover

point (G" > G') occurred at ~25 % strain in both samples which, as mentioned previously, is the point when the structure becomes more liquid-like than solid-like.

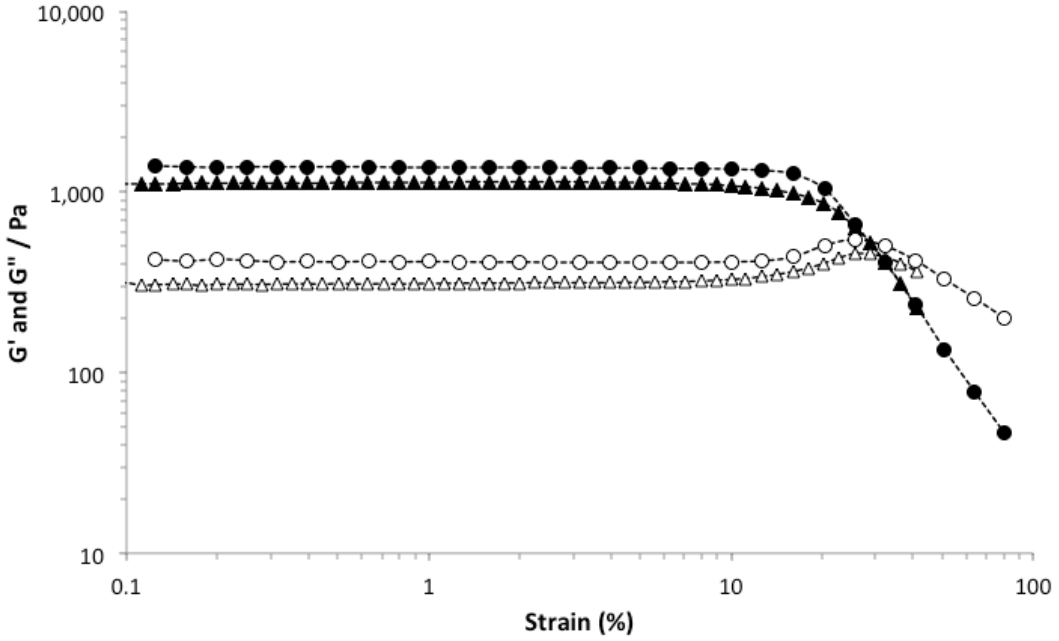

Figure 5.7. Overlay of strain sweep for both HCl aggregated (triangles) and GδL aggregated (circles) P5 dodecane emulsions. G' are represented by closed shapes and G" by open shapes.

When both results are overlayed (Figure 5.7), it can be seen that the shape of both the storage and loss moduli, and the point at which G' starts to decrease in the two samples are very similar, indicating that the strength of the EE is independent of the method of acidification. This suggests that, although the model of aggregation may vary between the two methods, the resulting gel strength is comparable, which implies that a similar ordered structure is obtained in both cases. This is in contrast to the peptide systems reported by Adams *et al.*, in which the kinetics of aggregation are important in determining the final G'.[17,18] Figure 5.7 suggests that an EE's G' is probably controlled by the number of potential interactions available *via* droplet packing, rather than by the method of aggregation. We can see that both aggregates start to break down at similar strains, reinforcing the similarities between the two EEs and suggesting that similar interactions are involved in both cases.

Variations in the moduli between the time sweep and strain sweep are likely due to differences in preparation. Variations in water content between samples may bring about different G' values. As seen in Chapter 4.2.3, upon dehydration of EE structures a larger G' is measured. Therefore it is plausible that increased water content in the time sweep sample could result in a lower G' and G". Evidence of

creaming is present in the first 20 minutes of the measurement, which is already indicative of excess water present in the system.

5.2.3. Fabrication of large volume engineered emulsions

Having studied the benefits of GδL-triggered dodecane EE formation, the formation of shape-controlled, large volume-templated structures was investigated. These structures would not be feasible within a reasonable time frame using a conventional pH trigger method, due to the slow diffusion of acidic solutions throughout the system. Therefore, to create a large volume EE, GδL (2 wt. %) was added directly to the cream layer of a standard P5 (2 wt. %) dodecane emulsion (5 mL) (Φ_{oil} = 0.70) and slowly stirred for 30 seconds. The resulting mixture was then transferred to a mould. Due to the large amount of GδL added, the system was allowed to hydrolyse and kinetically trap the droplets for roughly 4 hours to ensure complete acidification. Upon removal of the mould, a 5 mL macroscopically-defined EE was produced (Figure 5.8(a)) which had remained in the form of the mould. After 30 minutes, NaOH (1M, 1 mL) was added and continually re-pipetted over the structure to investigate the reversibility of droplet assembly in the resulting aggregate. After 5 minutes, redispersion had visibly started to occur (Figure 5.8(b)) and after around 20 minutes complete disassembly was observed (Figure 5.8(c)), although this was aided by gentle agitation.

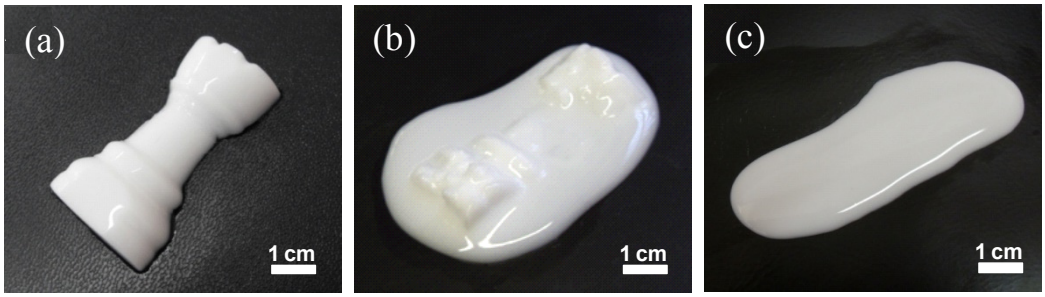

Figure 5.8. Digital images of large scale, template-designed P5-stabilised dodecane EE (a) at pH 2, after removal from template, (b) 5 minutes after addition of 1 M NaOH to (a) and (c) 20 minutes after addition of base, complete disassembly was observed.

Both the kinetically trapped and the free-flowing emulsion droplets are stable when using a conventional 1 M HCl acidifier.[13] In Chapter 4.2.1 it was shown that upon redispersion of HCl EEs, the average droplet size increased slightly, indicating a

small amount of droplet instability. A similar investigation was performed when using GδL to create a larger EE. Droplet size and span also increased slightly in this system, indicating a similar level of stability, at least during this process, to the formation of small volume EE by HCl and GδL (Figure 5.9). The free-flowing emulsion had a $D_{(4,3)}$ = 6.31 and a span of 1.23, whereas the redispersed rook sample had a $D_{(4,3)}$ = 6.76 and a span of 1.56.

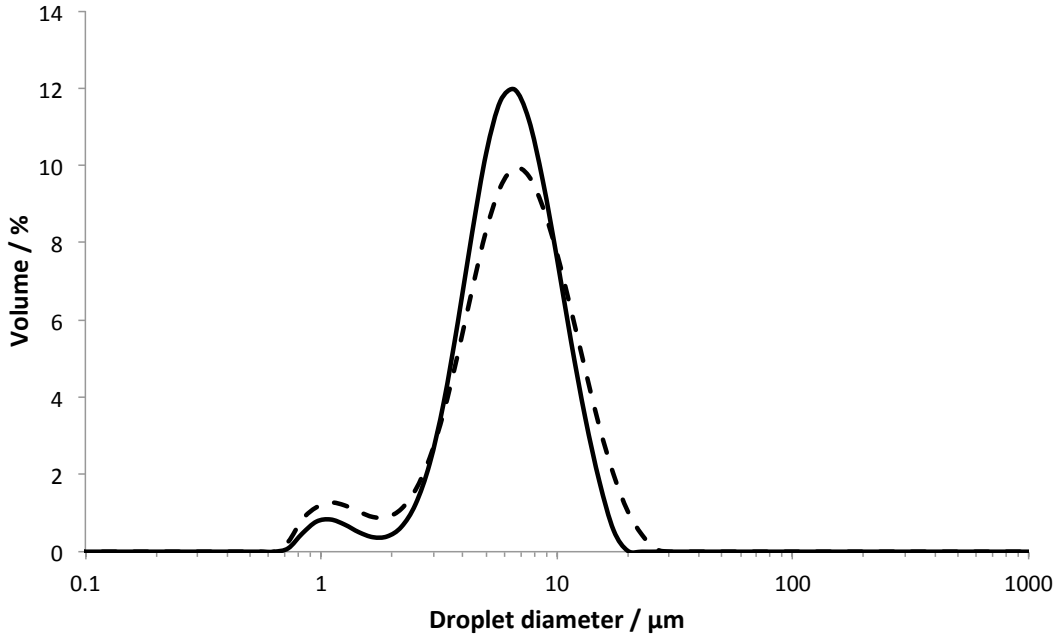

Figure 5.9. Overlayed laser diffraction size distributions of the dodecane emulsion droplets before (solid line) and after (dashed line) GδL-triggered emulsion engineering at pH 10.

To demonstrate further scalability of this process, a larger volume EE (Figure 5.11) was prepared by trapping 180 mL of the emulsion's creamed layer within a plastic beaker using the addition of GδL. Large volumes of emulsion were produced by adding dodecane (50 mL) to a pH 10 P5 aqueous solution (2 wt. %, 50 mL) and mixing the two using a more powerful homogeniser (Polytron PT2100, 28,000 rpm for 4 minutes, using a 20 mm diameter crown dispersion head rotor stator). This resulted in P5-stabilised dodecane o/w emulsions as previously described. This was repeated six times to give a combined emulsion volume of 600 mL. Each homogenisation run produced reproducible droplet size distributions ($D_{(4,3)}$ = 2.78–2.94 µm and span = 1.55–1.66), all shown in Figure 5.10. The relatively low average droplet diameters are due to the higher homogenisation speeds used.

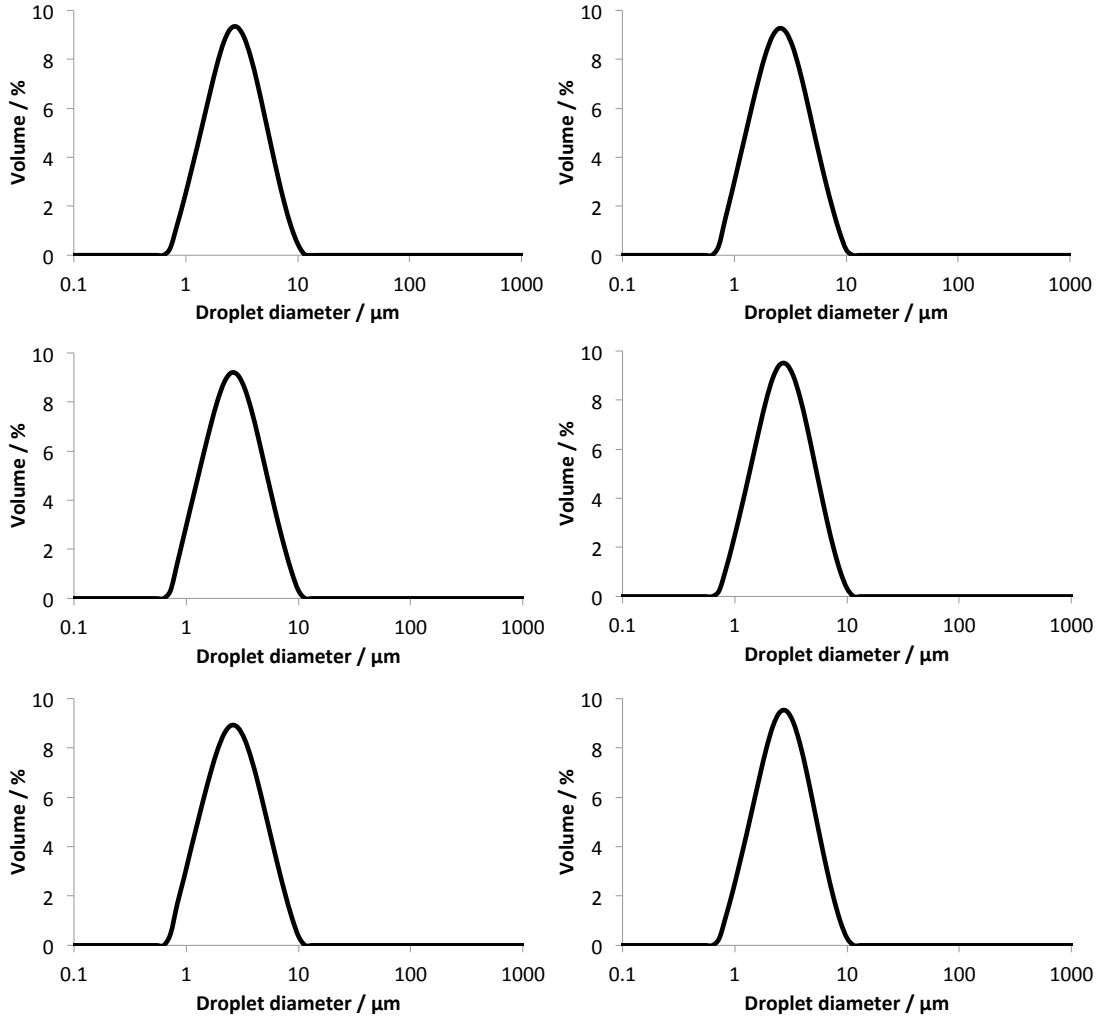

Figure 5.10. Laser diffraction size distribution of P5 dodecane o/w emulsions (all $\Phi_{oil} \approx 0.70$) at pH 10, all samples prepared on a large scale (100 mL volume in total for each sample)

The emulsions were equilibrated for 24 hours, after which time 180 mL of the creamed layers was transferred to a large mould (plastic beaker), and mixed gently with GδL (3.6 g, 2 wt. % based on the total emulsion volume). This monolith was left overnight before the mould was removed. This volume represents an increase of three orders of magnitude over previous engineered emulsions using a 1 M HCl trigger. Complete emulsion trapping occurred and the dimensions conformed well to those of the mould.

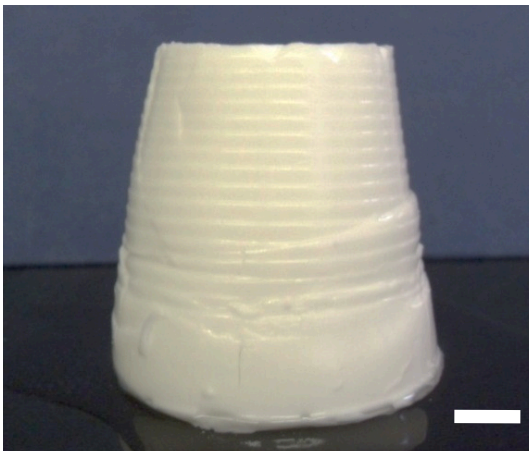

Figure 5.11. Large volume (180 mL) GδL-triggered dodecane engineered emulsion. Scale bar represents 1 cm.

GδL allows another advantage over conventional HCl acidification. Using GδL enabled the creation of much more complex multi-layered monoliths using a simple method. Emulsion droplets which contained blue and red hydrophobic dyes (0.1 wt. %) were produced and sequential layers of each emulsion (30 μL) were added to a small mould immediately after GδL (2 wt. %) addition and allowed to aggregate. Removal of the mould revealed an engineered emulsion comprising a number of layers with well-defined interfaces (Figure 5.12(a)), with some containing encapsulated dyes and others containing no guest molecules (white layers). Although complex structures are possible using HCl aggregation, as shown in Chapter 4.2.4, their production is difficult and time consuming, involving the careful addition of HCl solution, and the sculpting of structures with a scalpel. If a multi-layered monolith is prepared *via* the addition of HCl without any sculpting, a poorly defined monolith is produced (Figure 5.12(b)).

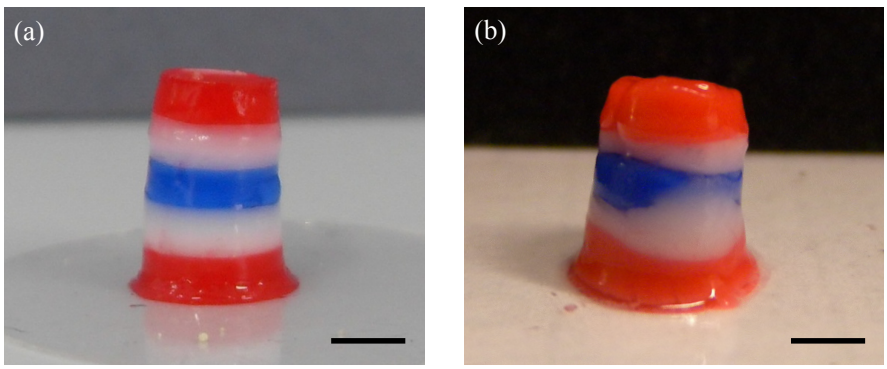

Figure 5.12. (a) GδL aggregated multi-layered monolith with well-defined interfaces, (b) HCl aggregated multi-layered monolith with poorly defined interfaces Scale bar represents 2.5 mm.

When using conventional methods, HCl is deposited on top of the free-flowing emulsion in the mould; immediate kinetic trapping of emulsion droplets on the surface upon contact with HCl results in distorted surfaces. Unless the top of the EE is removed using a scalpel, this results in non-homogenous surfaces between samples. In contrast, a homogeneous pH change *via* the hydrolysis of GδL resulted in undisturbed surfaces in aggregates. This uniform acidification allows the simple formation of much more complex structures, as in Figure 5.12, due to the lack of distortion on each surface layer from the deposition of HCl.

5.3. Conclusion

In this Chapter, the scalability of engineered emulsion formation was demonstrated *via* the use of a homogeneous pH trigger. The engineered emulsion volume was increased by 1000x and a relatively slow, homogeneous pH change allowed the investigation of the formation of engineered emulsions by rheometry. In theory, the volume of engineered emulsion that can be prepared using GδL as an acidifier is limited only by the volume of emulsion that can be prepared and template size. This is in stark contrast to acidification by the diffusion of HCl solution, as structures only a few hundred microliters in volume are possible within a reasonable time frame. It was shown that the reversibility of the system is maintained when using GδL, and the emulsion droplets retain their structural integrity during the assembly/disassembly process, as with conventional acid addition. This method provides a simple strategy to produce large, complex engineered emulsions, which could potentially widen their range of applications. GδL is cheap and readily available, making it a good replacement for HCl as an acidifier in the formation of EEs. This approach also eliminates the need to handle strong acids.

5.4. References

(1) Pocker, Y.; Green, E. *J. Am. Chem. Soc.* **1973**, *95*, 113.
(2) Wright, T. *Food Allergies: Enjoying Life with a Severe Food Allergy*; Class Publishing Ltd, London, **2001**.
(3) Lucey, J. A.; Tamehana, M.; Singh, H.; Munro, P. A. *Food Res. Int.* **1998**, *31*, 147.
(4) Lucey, J. A.; Singh, H. *Food Res. Int.* **1997**, *30*, 529.

(5) Dickinson, E.; Merino, L. M. *Food Hydrocolloids* **2002**, *16*, 321.
(6) Tarte, R. *Ingredients in Meat Products: Properties, Functionality and Applications*; Springer, New York, **2008**.
(7) Ash, M. *Handbook of Preservatives*; Synapse Info. Resources, New York, **2004**.
(8) Adams, D. J.; Butler, M. F.; Frith, W. J.; Kirkland, M.; Mullen, L.; Sanderson, P. *Soft Matter* **2009**, *5*, 1856.
(9) Raeburn, J.; Pont, G.; Chen, L.; Cesbron, Y.; Levy, R.; Adams, D. J. *Soft Matter* **2012**, *8*, 1168.
(10) Sutton, S.; Campbell, N. L.; Cooper, A. I.; Kirkland, M.; Frith, W. J.; Adams, D. J. *Langmuir* **2009**, *25*, 10285.
(11) Chen, L.; Revel, S.; Morris, K.; Serpell, L. C.; Adams, D. J. *Langmuir* **2010**, *26*, 13466.
(12) Igoe, R. S. *Dictionary of Food Ingredients*; Springer, New York, **2011**.
(13) Weaver, J. V. M.; Rannard, S. P.; Cooper, A. I. *Angew. Chem. Int. Ed.* **2009**, *48*, 2131.
(14) Ruiz-Perez, L.; Pryke, A.; Sommer, M.; Battaglia, G.; Soutar, I.; Swanson, L.; Geoghegan, M. *Macromolecules* **2008**, *41*, 2203.
(15) Olea, A. F.; Thomas, J. K. *Macromolecules* **1989**, *22*, 1165.
(16) Dong, H. T.; Du, H. B.; Qian, X. H. *J. Phys. Chem. A* **2008**, *112*, 12687.
(17) Adams, D. J.; Butler, M. F.; Frith, W. J.; Kirkland, M.; Mullen, L.; Sanderson, P. *Soft Matter* **2009**, *5*, 1856.
(18) Adams, D. J.; Mullen, L. M.; Berta, M.; Chen, L.; Frith, W. J. *Soft Matter* **2010**, *6*, 1971.

CHAPTER 6

Reversible aggregation of responsive polymer-stabilised colloids and the pH-dependent formation of porous scaffolds

(Publication arising from this Chapter: **"Reversible aggregation of responsive polymer-stabilized colloids and the pH dependent formation of porous scaffolds"**, R. T. Woodward, C. Hight, U. Yildiz, N. Schaeffer, E. M. Valliant, J. R. Jones, M. M. Stevens, J. V. M. Weaver, *Soft Matter*, 2011, *7*, 7560-7566.)

List of Figures

6.1. Introduction

The ability to fine-tune interactions between colloids is a key challenge in the generation of new controlled-structure functional nanomaterials.[1] Colloids capable of switching their properties while in solution from non-interacting dispersions to interacting assembled materials *via* a response to external stimuli have previously been reported.[2-4] The ability to fabricate large-scale, functional objects from the assembly of smaller molecules, such as nanoparticles, allows a significant degree of control in the design of functional materials. More importantly, simple triggering of a property change at the surface of these constituent particles allows for on demand disassembly or release of actives from these larger, more complex structures.[5]

Polymeric particles can be considered particularly useful colloidal building blocks as they can be prepared with controllable sizes over a reasonably large range[6] and their properties can be varied simply by monomer selection and/or post-functionalisation.[7] More complex properties can also be readily incorporated *via* design of polymeric materials, such as the ability to encapsulate and release materials, or responsiveness to more than one external stimuli.[8] A number of synthetic routes to polymeric particles are commonly used, including self-assembly and the cross-linking of copolymers.[9-12] Another strategy is to form polymeric particles using a template. One form of template particularly relevant to this work is an emulsion droplet. If oil droplets containing an active are dispersed in a continuous water phase and are made up of a volatile oil that is easily removed, the content of the droplet upon removal of the oil can form colloidal particles.[13] This is referred to as an emulsion-solvent-evaporation (ESE) process.[14] ESE enables reproducible particle formation of well-characterised polymers without the need for particle synthesis.[15] Due to the simplicity of this process, colloids comprising two or more polymeric materials are possible, yielding particles that may be significantly more difficult to produce otherwise. The ESE process has been used to aid drug solubilisation and delivery,[16,17] and also in the fabrication of highly-ordered structures of colloid particles.[18-20]

As an initial emulsion template is necessary for ESE, surfactant molecules obviously play a significant role.[21,22] Amphiphilic copolymers can be viewed as more convenient, alternative surfactants due to the advantages they offer over small molecule surfactants,[23,24] such as greater interfacial adsorption, similar to particulate

surfactants,[25-27] and the ability to encapsulate materials *via* self-assembly or rearrangement.[28,29] Amphiphilic copolymers often produce more stable emulsions than small molecule surfactants, making them similar to particle-stabilised emulsions in this sense. Dellacherie's group have used amphiphilic copolymers to create stable colloids using the ESE process along with stabilising emulsions using dextran derivatives containing various grafted hydrophobic units.[30-32]

In Chapter 3 it was determined that P5 stabilised dodecane emulsions exhibited the fastest rate of inter-droplet aggregation to form engineered emulsions.[33] In this Chapter, the translation of this pH-responsiveness from the surface of an oil droplet to the surface of poly(methyl methacrylate) (PMMA) nanoparticles by the ESE process is investigated. We hypothesise that, upon the successful removal of a volatile oil phase containing PMMA, the surface functionality may be translated to the PMMA particle's surfaces, resulting in polymer nanoparticles capable of inter-particle interactions at low pH. At high pH, when the MAA groups on P5 are deprotonated, this should provide similar electrostatic and steric stabilisation for the colloid particles as it confers on the emulsion droplets. Thus emulsion droplets stabilised with the P5 copolymer may act as transient templates from which polymer colloids are fabricated.

6.2. Results and Discussion

6.2.1. pH Responsive Nanoparticles and Triggered Aggregation

A $PEGMA_5/MAA_{95}$ – $EGDMA_{10}$ – DDT_{10} (P5) stabilised, ethyl acetate (EtOAc) o/w emulsion was produced by homogenisation (24,000 rpm) of a pH 10 P5 (2 wt. %) aqueous phase (3 mL) with an equal volume of EtOAc for 2 minutes. PMMA (8 wt. %, M_w = 15,000 $g.mol^{-1}$) was dissolved in EtOAc by stirring and gentle heating (40 ^oC) for 30 minutes prior to homogenisation. After homogenisation, the resulting emulsion was immediately diluted in a pH 10 aqueous solution (120 mL) to minimise any aggregation when EtOAc begins to evaporate. The removal of EtOAc was aided by gently purging the emulsion with air overnight. This dilution results in a solution containing 0.48 mg/mL of P5 and 1.9 mg/mL of PMMA, or 2.4 mg/mL of total polymer. As the ratio of polymeric surfactant to PMMA does not change throughout this study, concentrations shall be quoted as total polymer in mg/mL. The

removal of the EtOAc volatile oil phase was utilised to try to produce surface functionalised PMMA polymer nanoparticles by the ESE technique. A schematic representation of the process yielding pH-responsive nanoparticles is outlined in Figure 6.1.

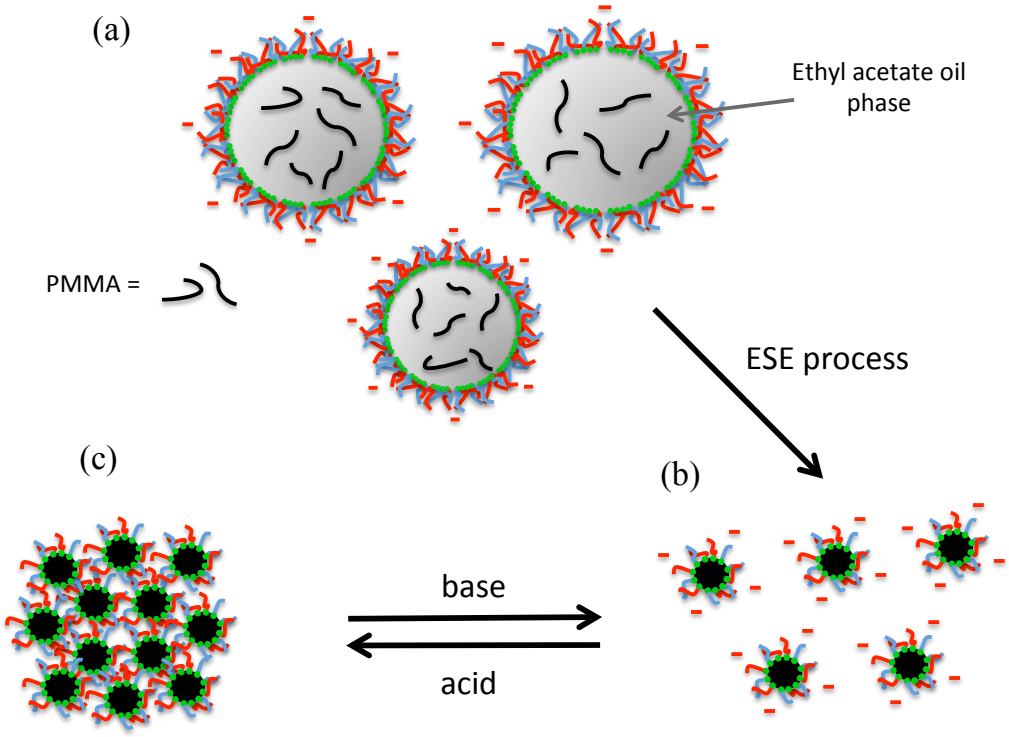

Figure 6.1. A schematic representation of (a) EtOAc/PMMA droplets, stabilised using pH-responsive branched copolymer surfactant P5, (b) pH-responsive PMMA colloids after emulsion-solvent-evaporation process and (c) aggregated colloids at low pH.

P5 was selected to stabilise this emulsion due to the rate of aggregation exhibited in inter-droplet aggregation in Chapter 3 and for its strong surface adhesion afforded by its hydrophobic chain ends. It was hoped that this pH-responsiveness would be translated from the surface of the EtOAc oil droplets to the surface of PMMA nanoparticles. PMMA was selected for its inherent hydrophobicity, allowing good solubility in the volatile EtOAc oil phase. PMMA with a number-average molecular weight of 15,000 g.mol^{-1} was chosen as it gave the most reproducible particles upon the removal of EtOAc. The initial emulsion prior to removal of the oil phase cannot be characterised using conventional methods such as laser diffraction. This is because the substantial dilution of the emulsion may result in the accelerated evaporation of EtOAc. As EtOAc is slightly water-soluble, dissolution may also play

a part in the rapid production of colloidal particles. Therefore, to try to prove the existence of these transient EtOAc droplets, light micrographs of the concentrated emulsion before dilution were taken immediately after homogenisation. By not diluting these droplets before imaging, they could be imaged before the EtOAc was able to evaporate, enabling us to see that the initial droplet size is in the range of 2-8 μm (Figure 6.2). This in good agreement with droplets stabilised using the same branched copolymer that contained a non-volatile oil phase,[33-35] as shown in previous Chapters.

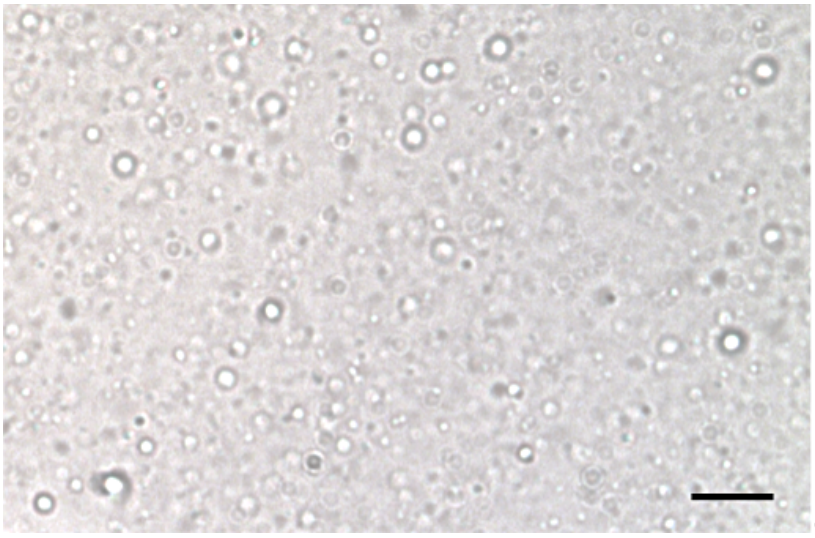

Figure 6.2. Ethyl acetate/PMMA droplets immediately after homogenisation in pH 10 water. Scale bar represents 20 μm.

Following the dilution of the EtOAc/PMMA droplets shown in Figure 6.2, the resulting solution was gently purged with air for 24 hours to aid the removal of any remaining volatile oil phase. After this time, it was assumed that EtOAc had been removed from the system as laser diffraction measurements gave repeatable size distributions and particles did not appear to further decrease in size (Figure 6.3). A sample of the dilute pH 10 nanoparticles (2.4 mg/mL, 3 mL) was added to the Mastersizer dispersion unit containing pH 10 aqueous solution (80 mL) at a stirring rate of 1,100 rpm. This measurement allowed for the rough comparison of the size of the resulting nanoparticles with the initial emulsion droplets. The significant difference between the two is a good indication of the removal of EtOAc.

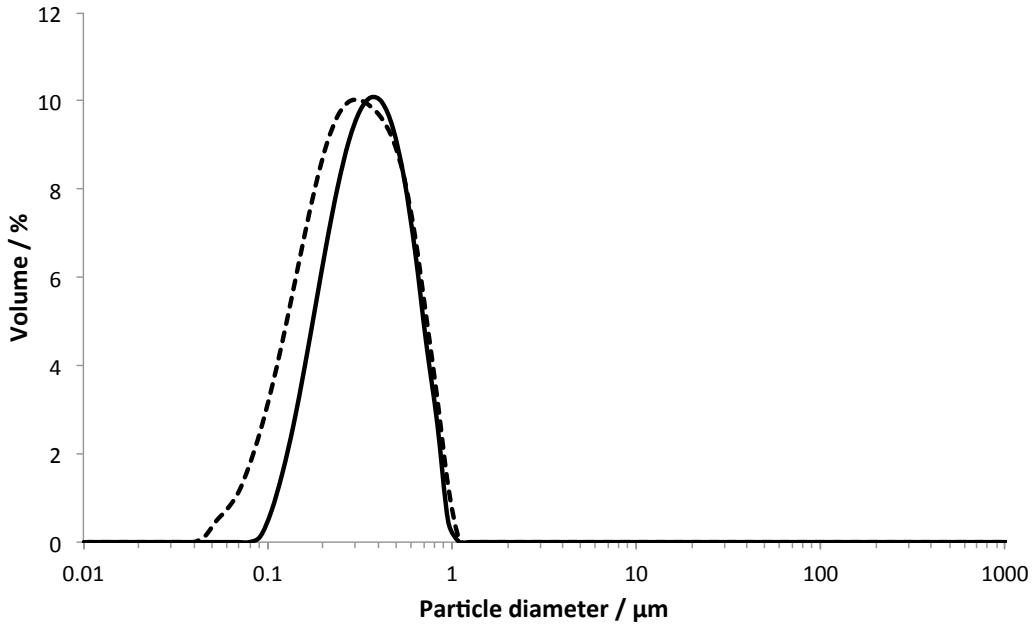

Figure 6.3. Laser diffraction size distributions of dilute P5 stabilised PMMA particles (3 mL, 2.4 mg/mL) 24 hours after production in pH 10 water (solid line) and the same sample measured under the same conditions after 2 years (dashed line). These results have been normalised with respect to the y axis for ease of comparison.

From the measurement in Figure 6.3, the sample obtained 24 hours after homogenisation (solid line) has a $D_{(4,3)}$ = 356 nm and a span of 1.34. This may be indicative of a broad distribution within the initial emulsion droplets, which has already been observed in the optical micrographs shown in Figure 6.2. A broad distribution could also suggest some coalescence of droplets before removal of the oil phase, resulting in larger particles. However, the resulting colloids are stable over long periods of time, with the laser diffraction measurements showing only a small change in particle size over 2 years (dashed line in Figure 6.3). After 2 years the same sample, measured under the same conditions, has a $D_{(4,3)}$ = 318 nm and a span of 1.7, suggesting the particles are kept well dispersed by the polymeric surfactant at their surface due to subsequent steric and electrostatic stabilisation. This slight decrease in size is probably due to sedimentation of larger particles over 2 years, resulting in a slightly lower average particle diameter. It could also be due to a small amount of EtOAc removal after the initial 24 hours which could also explain the increase in span.

A polymeric surfactant with an EG:MAA ratio of 2:1 (P6 from Chapter 3) was also used instead of P5 in the formation of a similar EtOAc/PMMA emulsion. 3

mL of a pH 10 P6 (2 wt. %) solution was homogenised with an equal amount of EtOAc containing PMMA (8 wt. %, M_w = 15,000 g.mol^{-1}) and immediately diluted in pH 10 water (120 mL). As with the P5 EtOAc emulsion, the removal of the volatile oil phase was aided by gentle purging of the emulsion with air overnight. The resulting material was measured using laser diffraction, under the same conditions as the P5 particles (Figure 6.4).

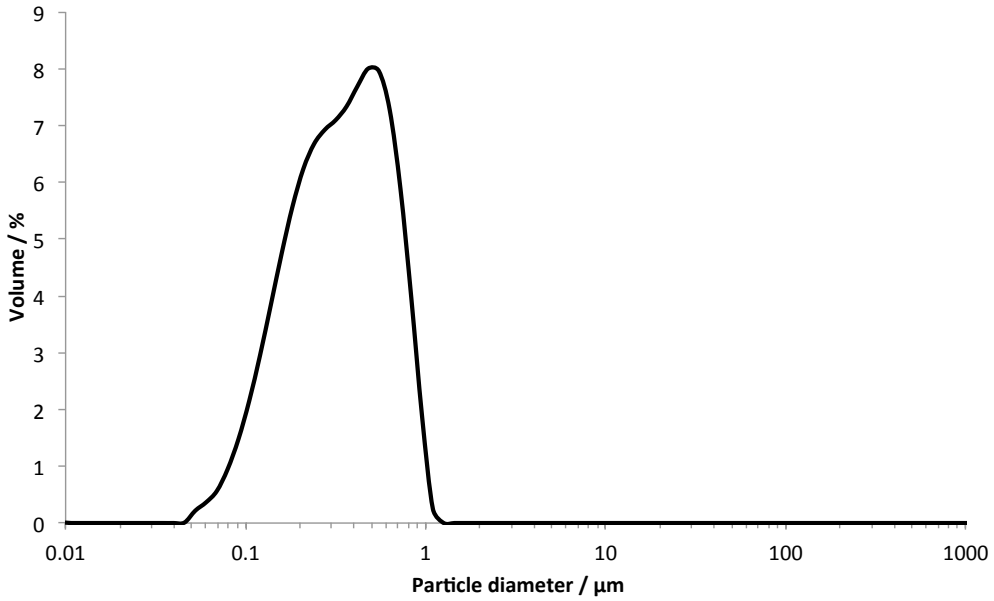

Figure 6.4. Laser diffraction size distribution of dilute P6 stabilised PMMA particles (3 mL) 24 hours after production in pH 10 water.

P6 particles are a similar size to the colloids formed from a P5 EtOAc o/w emulsion (358 nm compared to 320 nm, as measured using laser diffraction at pH 10). The span of P6 colloids is slightly larger than that of the initial P5 colloids (1.67 compared to 1.34), indicating a more polydisperse distribution of particles. This may be due to slight variations in the time taken to dilute the particles after homogenisation. As EtOAc is volatile and has some degree of solubility in water particles may start to form quickly post-homogenisation. Therefore, if the emulsion is not diluted immediately, this may lead to some coalescence and consequently a more polydisperse sample.

The pH-dependant colloidal stability of both samples was investigated using laser diffraction. Samples were initially sized under the same conditions as the pH 10 measurements earlier. However, the change in particle size with subsequent additions

of acid and base was measured *in situ* (Figure 6.5). Since both EG and MAA residues are present on the surface of the P6 particles, these residues will undoubtedly hydrogen bond to some extent under acidic conditions. However, the presence of excess EG may provide a steric stabilisation mechanism, limiting the hydrogen bonding to only intra-colloid bonding.[33]

It can be seen in Figure 6.5 that the same steric hindrance and electrostatic stabilisation at pH 10, which prevents inter-droplet aggregation or coalescence in Chapter 3, is translated to the surface of these colloidal particles. When the solution was switched to pH 2 using HCl (1 M, 0.5 mL) after 3 minutes, P5 colloids showed an increase in particle size indicative of aggregation. This enabled multiple pH switches, allowing measurement of the reversibility of the particle aggregation process. This reversibility was also seen in P5 stabilised dodecane o/w droplets in Chapter 4, indicating a good translation of functionality from droplet surfaces to PMMA nanoparticles. The assembly and disassembly process could be repeated multiple times without significant deterioration in the assembly/disassembly rate, presumably due to the stability of the nanoparticles in solution.

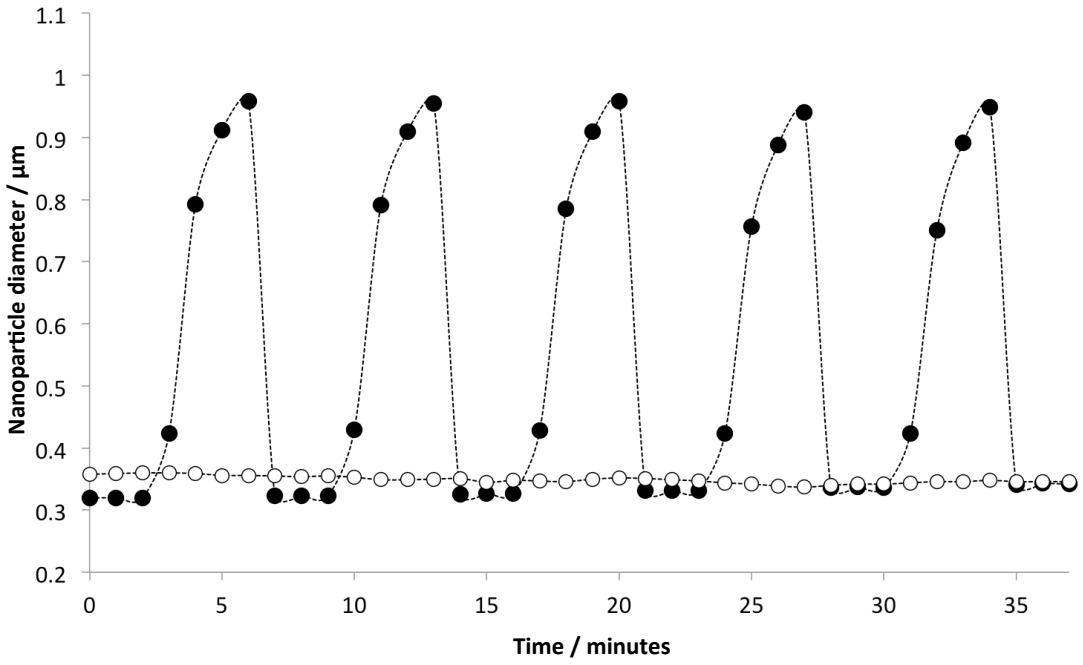

Figure 6.5. Laser diffraction measurements showing effect of pH change on average particle diameters. Filled circles represent P5 functionalised colloids; open circles represent P6 polymer functionalised colloids. pH is lowered (~pH 2) and raised (~pH 10) by the addition of HCl and NaOH every 3 and 4 minutes respectively.

P6 particles did not exhibit any change in size upon the lowering of solution to pH 2 *via* addition of HCl (1 M). This was expected and is in good agreement with P6 stabilised dodecane emulsions measured in Chapter 3, which showed no inter-droplet aggregation upon lowering the solution pH. This suggests that the steric hindrance provided by excess PEGMA in Chapter 3 is also translated to the PMMA particles.

In order to obtain digital images of aggregation, a solution of P5 stabilised PMMA nanoparticles (2.4 mg/mL, 20 mL) was acidified *via* the addition of HCl (1 M, 0.5 mL), as shown in Figure 6.6. Accumulation of the particles was rapid and large aggregates were visible within one minute (Figure 6.6(b)), indicating that the pH-responsive polymer that stabilised the initial emulsion had, at least to some extent, stabilised the nanoparticles at the surface following the ESE process. After 24 hours, the pH was raised again to approximately pH 10 using NaOH (1 M, 1 mL) and, after slight agitation, redispersion was observed almost immediately (Figure 6.6(d)). This further confirms efficient branched copolymer adsorption during the ESE process, and also shows that we have the ability to tune surface functionality of both emulsion droplets (Chapter 3) and polymer nanoparticles.

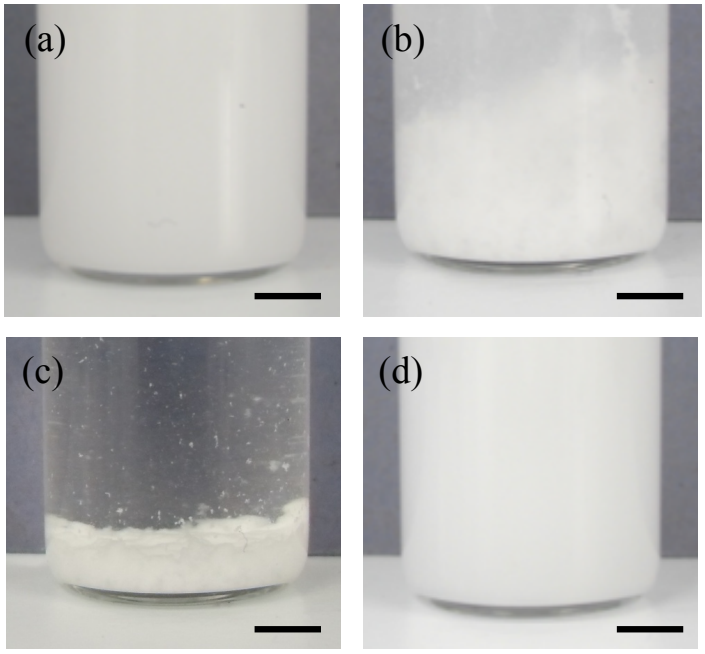

Figure 6.6. Digital photographs illustrating the physical appearance of aqueous dispersions of pH responsive nanoparticles at (a) pH 10, (b) pH 2, 2 minutes after acidification, (c) pH 2, 24 hours after acidification and (d) immediate redispersion at pH 10 with slight agitation. Scale bars represent 5 mm.

As the transition from an emulsion droplet to a PMMA particle involves a large change in surface area, the role of any free, un-adsorbed copolymer in the aggregation of these colloid particles was considered.

6.2.2. Measuring Free-Polymer in Solution and Its Effect On Aggregation

After ESE the polymeric surfactant appears to transfer to the surface of the resulting colloidal particles. With such a large loss in volume when changing from emulsion droplet to colloid particle, some copolymer may desorb from the oil droplet surface during ESE or multiple particles may be formed from one droplet to minimise the reduction in surface area. If desorption of copolymer does occur, it may influence aggregation of colloidal particles upon lowering the pH due to free, un-adsorbed copolymer remaining in solution. A schematic representation of this process is shown in Figure 6.7.

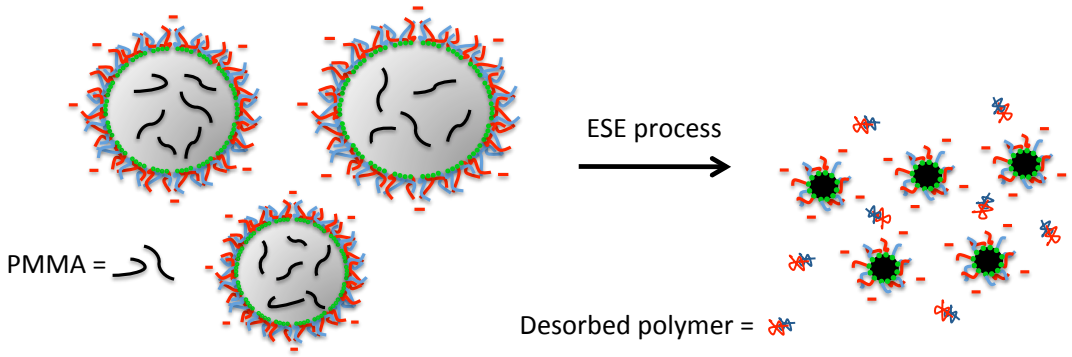

Figure 6.7. Schematic of potential copolymer desorption during the ESE process resulting in free copolymer in solution.

The amount of free copolymer in the nanoparticle solution was calculated using both tensiometry and inductively-coupled plasma mass spectrometry (ICP). In both cases, solutions containing known amounts of free polymer P5 were measured in order to create a calibration curve, both shown in Figure 6.8. ICP was used to measure the sulfur content of samples and tensiometry determined the surface tension of the aqueous solutions. The sulfur content and surface tension of samples containing unknown amounts of P5 were then measured and the amount of free copolymer was calculated.

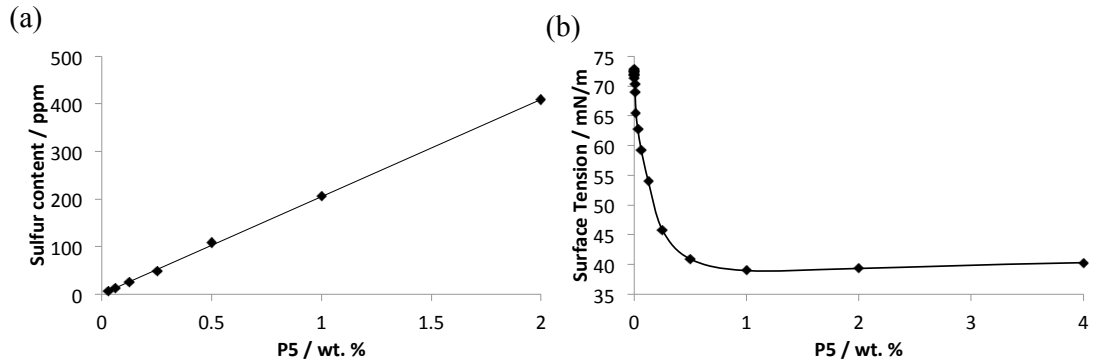

Figure 6.8. Calibration curves of solutions of copolymer with known concentrations (0-2 wt. %) (a) by determining sulphur content using ICP and (b) by surface tension of copolymer solutions.

After dilution, the colloid solution contains 0.048 wt. % of the pH-responsive branched copolymer. In order to measure the free copolymer in solution, particles were sedimented *via* centrifugation (14,000 rpm, 20 minutes), after which a sample of the supernatant was removed for analysis. The amount of free copolymer in the supernatant solution was determined to be 0.028 wt. % using ICP and 0.029 wt. % using tensiometry or 59 % of the total copolymer present. This shows that after the ESE process, roughly 59 % of the P5 in the colloid sample is present in the water phase. This is in contrast to the P5 dodecane o/w emulsion system discussed in Chapter 3, which had only 5 % non-adsorbed P5. We can therefore assume that around 54 % of the P5 becomes desorbed from droplet surfaces during the ESE process. During ESE, a large change in surface area is observed. If we assume that each particle can only be formed using one oil droplet template, the number of particles produced is limited to the amount of initial droplets formed. Droplet sizes between 2-8 μm were observed after homogenisation in optical microscopy (Figure 6.2), so we shall assume that the average droplet size is around 5 μm. The resulting colloids have a diameter of roughly 0.35 μm, therefore the surface areas can be estimated and compared. The surface area of a sphere is $4\pi r^2$, resulting in a surface area of 78.54 μm^2 for the oil droplets and 0.38 μm^2 for the colloid particles. Therefore after ESE, the surface area available at the particle/water interface is only 0.48 % of what it was before removal of the oil phase. This dramatic reduction in surface area presumably accounts for the large amount of copolymer desorption observed during the ESE process.

As such a large amount of free copolymer is present, the influence this has on the rate of aggregation was investigated. Excess P5 was removed *via* washing of the particles by centrifugation (14,000 rpm, 20 minutes) and the resulting supernatant was removed. The sedimented particles were redispersed in distilled water, the pH of which had been adjusted to pH 10 by the addition of NaOH (1 M). After one wash, the amount of free copolymer in solution was 0.002 wt. %, or 6.9 % of the initial free copolymer after ESE. The colloids were then washed once more, at which point the amount of free copolymer was negligible. The laser diffraction size distributions of washed particles and the particles as produced are overlayed in Figure 6.9. Washed particles exhibit a $D_{(4,3)}$ of 350 nm and a span of 1.77, in good agreement with unwashed particles measured for comparison ($D_{(4,3)}$ = 320 nm, span = 1.81).

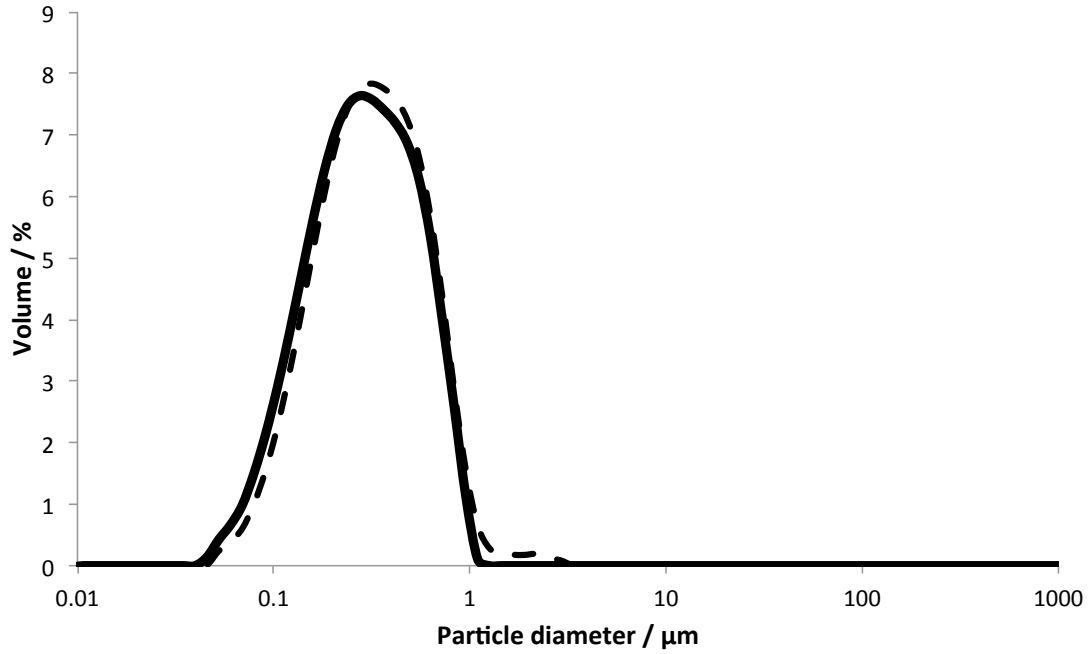

Figure 6.9. Laser diffractions size distributions of dilute, washed P5 stabilised PMMA particles (3 mL) in pH 10 water (dashed line) and a sample of dilute, standard P5 stabilised PMMA (3 mL, 2.4 mg/mL) in pH 10 water.

Washed particles were then aggregated and compared to samples containing free copolymer and the effect of the addition of excess amounts of P5 to the washed colloid solutions was investigated (Figure 6.10).

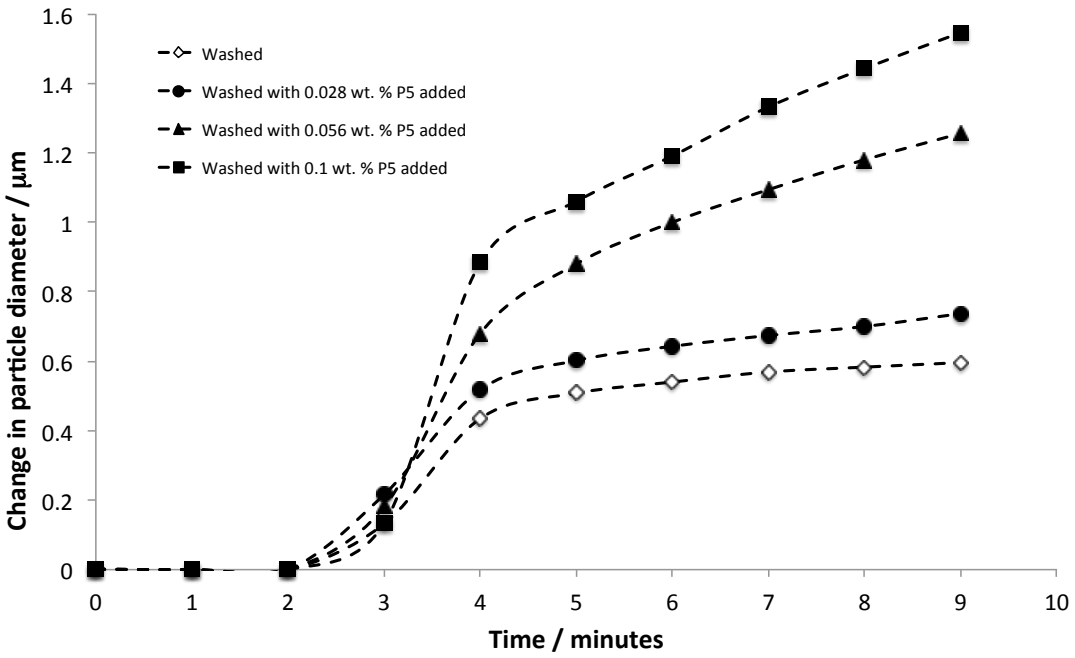

Figure 6.10. Rate of change in volume-average particle diameter as a function of time with increasing amounts of added free P5. P5 was added to samples (3 mL) before addition to the Mastersizer dispersion unit, which contained pH 10 solution (80 mL). The pH of all solutions was lowered to pH 2 after 2 minutes.

When comparing the aggregation of unwashed particles (Figure 6.5) to that of washed particles with 0.028 wt. % P5 added in Figure 6.10, the initial increase in particle size is in good agreement. Therefore upon the addition of the equivalent amount of free P5 found in the unwashed particles to washed particles, aggregation returns to the original rate. With the addition of increasing non-adsorbed P5, aggregation becomes quicker, implying that any free copolymer present may bridge particles, promoting inter-colloid attraction.

To further show that functional branched copolymers are present in the washed PMMA nanoparticles, an experiment using a cationic dye was devised. Using this method, adsorption of the cationic dye (Toluidine Blue O) by anionic particles may be possible. Colloids were produced from a number of EtOAc emulsions stabilised using polymeric surfactant (2 wt. %) containing different ratios of EG:MAA as synthesised in Chapter 3, including 1:0 (P9), 1:1 (P5) and 1:2 (P4). Emulsion preparation and subsequent EtOAc removal were performed under the same conditions as described earlier in the Chapter. Each of the particle solutions were washed twice, again as described previously, to remove excess copolymer in solution

and the resulting particles were mixed with a solution of Toluidine Blue O (0.5 mM) at pH 10 for 1 hour. The resulting suspensions were then centrifuged (14,000 rpm, 20 min) to isolate the colloidal particles along with any dye that had been adsorbed onto them. The water phase was replaced with fresh water (pH 10) and the particles redispersed *via* stirring overnight (~16 hours). The resulting dispersions were then centrifuged once more to separate any remaining unadsorbed dye. Particles were left to dry overnight at 35 ^{o}C and digital images were recorded to show the levels of dye adsorbed on the colloid surfaces (Figure 6.11). These images show no adsorption when MAA groups are not present in the polymer (P9) (a), with the most adsorption seen when the MAA comprises 66% of the EG:MA ratio (P4) (c). As the EG groups are neutral at both low and high pH, no electrostatic adsorption occurred at the particle surface when MAA groups were not present. When anionic MAA groups are present, the cationic dye molecules will bind to these groups, resulting in the particles acquiring a purple colour. This result showed that the anionic MAA groups in the polymeric surfactant are able to bind with Toluidine Blue O at high pH, indicating the polymer's presence in the particles. It can also be seen in Figure 6.11 that with increasing concentration of MAA groups, the particles appeared darker, indicating that more binding had occurred.

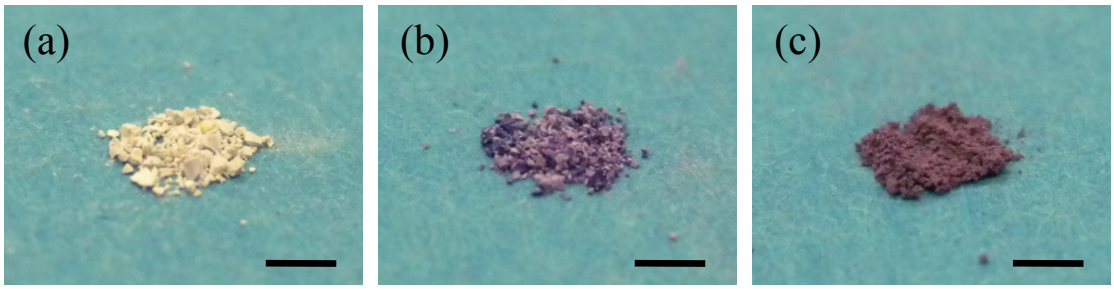

Figure 6.11. Washed PMMA particles stabilised with copolymers containing different EG:MAA ratios from Chapter 3 after exposure to Toluidine Blue O solutions, followed by the removal of excess Toluidine Blue O and drying. (a) P9 stabilised particles (0 % MAA), (b) P5 stabilised particles (50 % MAA), (c) P4 stabilised particles (66 % MAA). The purple colour of the cationic dye can be seen in samples containing MAA residues. Scale bars represent 4 mm.

6.2.3. Nanoparticle Aggregates

Having demonstrated the ease of triggered aggregation in pH-responsive copolymer nanoparticles, a higher-order assembly process of nanoparticles was investigated.

The aggregation of the PMMA nanoparticles could be exploited to prepare pH-responsive, macroscopic materials. An aqueous P5 stabilised PMMA colloid (14 mL, 2.4 mg/mL) was prepared in its dispersed state (pH 10) as described earlier, in the presence of free P5 branched copolymer (0.028 wt. %) (Figure 6.12(a)). The solution was then acidified to pH 2 using HCl (1 M, 1 mL), causing the particles to aggregate and leading to visible sedimentation due to EG-MAA hydrogen bonding between adjacent surfaces (Figure 6.12(b)). The resulting solution, with sedimented aggregates, was then centrifuged (4,500 rpm, 20 minutes) in order to pack them together, resulting in a monolithic pellet, which was removed from the centrifuge tube (Figure 6.12(c)). Based on the results from the emulsion systems, if the particle has pH-responsive copolymer adsorbed onto its surface, then the PMMA colloidal particles should undergo intra- and inter-colloid hydrogen-bonding between surfaces. The removal of water from interstitial sites of the pellets by dehydration (a process seen in engineered emulsions in Chapter 4) is investigated later in the Chapter, section 5.2.4.

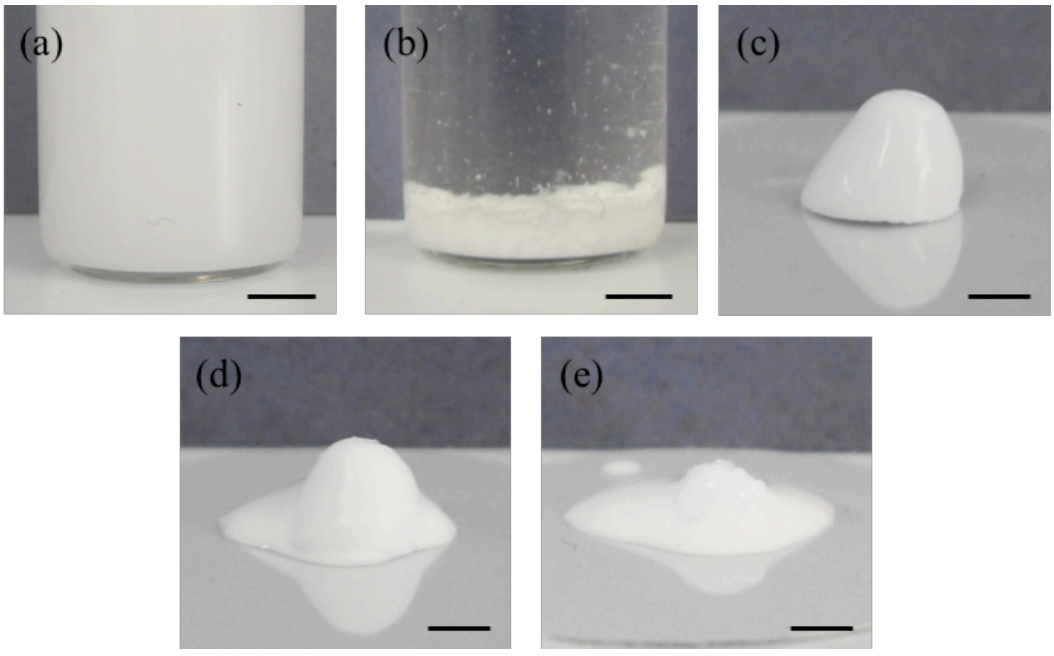

Figure 6.12. Digital images of the reversible colloid aggregation and monolith preparation (a) P5 stabilised PMMA colloids dispersed at pH 10, (b) acidified particles after HCl addition, (c) pellet formation following centrifugation of acidified colloids, (d) pellet after NaOH was added, t = 1 minute, (e) pellet at t = 5 minutes, after addition of NaOH. Scale bars in (a) and (b) represent 5 mm, scale bars in (c), (d) and (e) represent 2 mm.

The pellets produced can be redispersed when exposed to base, just as emulsion droplets and particles in solution can be, as shown in previous work[33] and in Chapter 4. This is shown in Figure 6.12(d) and (e), in which NaOH (1 M, 0.5 mL) was dropped onto the pellet and slightly agitated, enabling swift redispersion.

The aggregation of the particles into monolithic structures allows simple production of layered pellets *via* the successive additions of varying colloid samples. To create these varied samples, P5 solutions (2 wt. %, 3 mL, pH 10) were homogenised with an EtOAc phase (3 mL) containing PMMA (M_w = 15,000 g.mol^{-1}, 8 wt. %) and a hydrophobic dye (0.1 wt. %). The hydrophobic dye was either Oil Red or Oil Blue. The resulting emulsion was quickly diluted into pH 10 water (120 mL) and gently purged with air overnight to remove the EtOAc. The resulting particles displayed near-identical sizes irrespective of dye loading. An example of this is shown in Figure 6.13, which shows the laser diffraction size distributions of Oil Blue containing P5-stabilised PMMA nanoparticles and standard P5 PMMA particles.

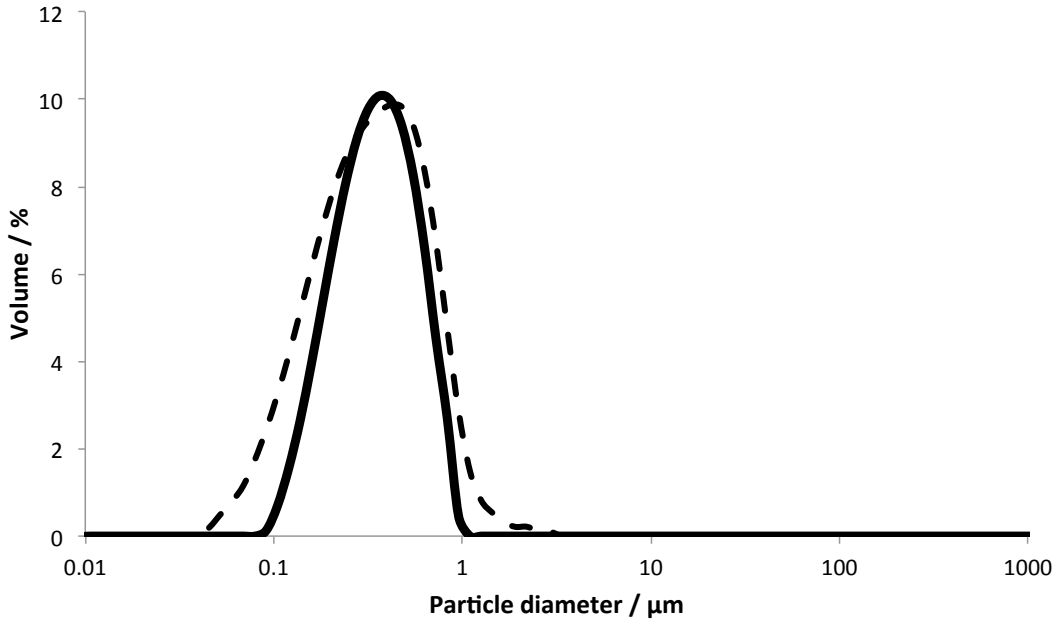

Figure 6.13. Overlaid laser diffraction size distributions of dilute P5 stabilised PMMA particles (3 mL, 2.4 mg/mL) 24 hours after production, in pH 10 water (80 mL) (solid line) and P5 stabilised PMMA particles containing Oil Blue (0.1 wt. %) measured under the same conditions (dashed line). These results have been normalised with respect to the y axis for ease of comparison.

The Oil Blue-containing particles (dashed line) exhibited a $D_{(4,3)}$ of 374 nm and a span of 1.86. From Figure 6.13, it is clear that the Oil Blue particles are slightly more polydisperse than the standard P5 PMMA nanoparticles, most likely due to the presence of the Oil Blue. Particles containing different hydrophobic dyes could be layered on top of one another due to surface-surface interactions of inter-layer particles to form a layered monolithic structure (Figure 6.15). Layering of particles was done by acidification of samples (15 mL, 2.4 mg/mL) to pH 2 using HCl (1 M, 0.5 mL), followed by centrifugation (4,500 rpm, 20 minutes). The resulting supernatant was then removed, and the same centrifuge tube was then filled with another colloid sample at pH 10 and the process was repeated. This method is outlined schematically in Figure 6.14.

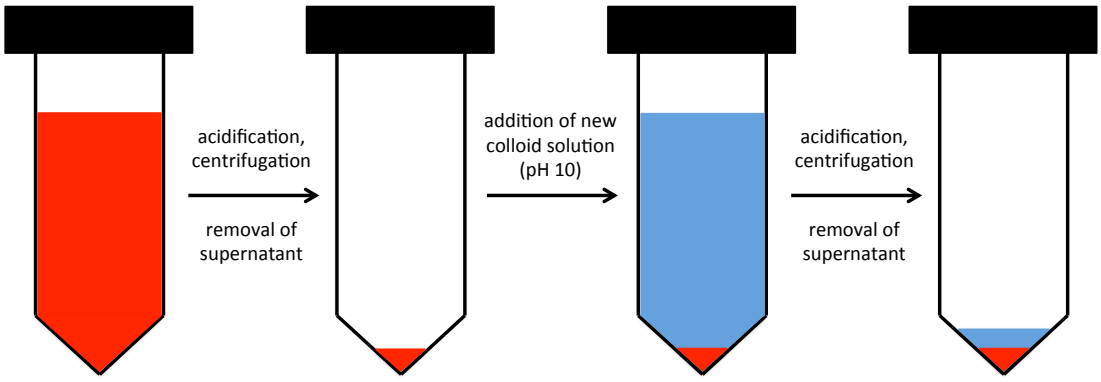

Figure 6.14. Schematic representation showing the formation of a layered pellet by successive acidification and centrifugation of particle solutions. After the formation of the red pellet, the supernatant is removed and replaced by an Oil Blue encapsulated particle solution at pH 10. This is then acidified to pH 2 and centrifuged, yielding a layered pellet.

The size of the deposited layer could be determined by simply controlling the volume and concentration of the colloidal solution acidified and centrifuged. The size of the resulting monoliths is in principle restricted only by the efficiency of colloidal sedimentation, and the volumes of particles that can be produced.

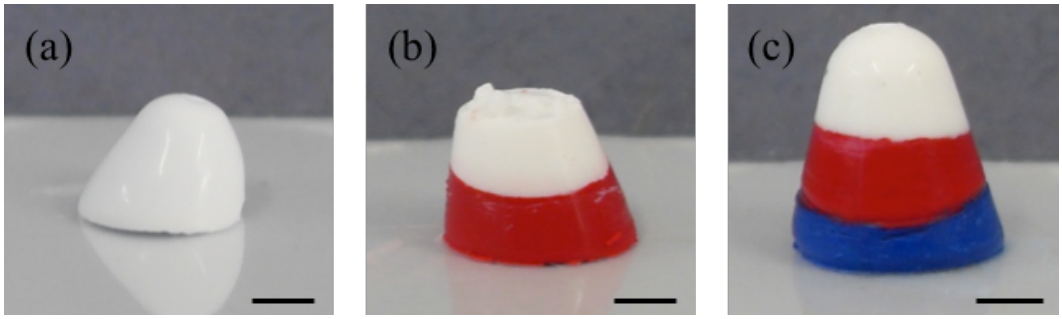

Figure 6.15. Colloidal aggregates, each layer formed from the acidification of P5 stabilised PMMA particles (15 mL, 2.4 mg/mL of total copolymer). (a) One layer with no dye encapsulated, (b) pellet consisting of two layers, the lower containing a Oil Red (c) A complex three-layered colloid pellet with layers containing both Oil Red and Oil Blue dyes. Scale bars represent 2 mm.

Layered engineered colloids could also undergo redispersion easily in the presence of base (Figure 6.16). If redispersion of a three-layered monolith takes place, particles with different guest molecules encapsulated no longer exist in discrete layers, but will be homogeneously dispersed throughout the solution (Figure 6.16(b)). Upon re-acidification and colloid aggregation the monolith is reformed with the three colloid populations randomly distributed throughout the resulting pellet (Figure 6.16(c)). This process outlines the ease of encapsulating hydrophobic materials within a pH-responsive 'capsule'. Although the materials discussed are limited to hydrophobic dye/polymer combinations, other relevant hydrophobic molecules such as drugs or catalysts could potentially be dispersed easily throughout solution.

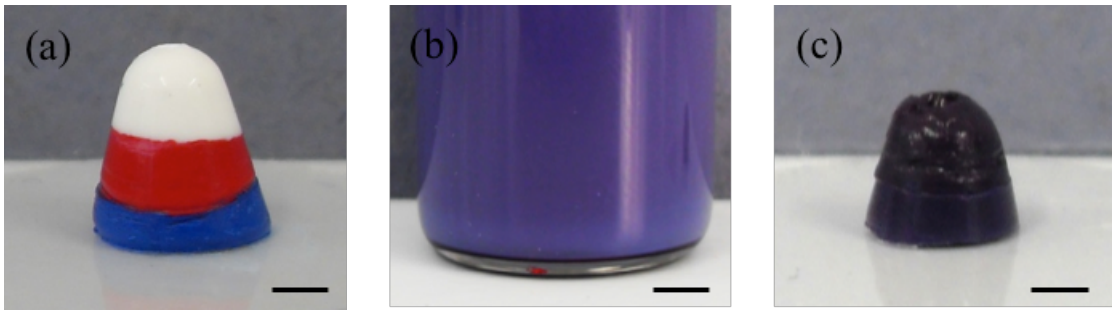

Figure 6.16. A complex three-layered pellet comprising standard P5 PMMA particles (white), particles containing Oil Red (red) and particles containing Oil Blue (blue) (a) initially at pH 2, (b) redispersed in pH 10 water (10 mL), (c) after re-acidification and centrifugation of dispersion (b). Scale bars in (a) and (c) represent 2 mm, 5 mm in (b).

6.2.4. Dehydration of Colloid Monolith for Formation of Porous Scaffolds

After the formation of these colloidal aggregates, it was noticed that, if left to stand in air, the structures undergo a slight decrease in volume. It was initially assumed that this was a result of the monolith undergoing dehydration. Further analysis of the hydrated and dehydrated colloid monoliths was performed in order to quantify the volume change or water loss, initially using thermogravimetric analysis (TGA) to quantify the level of colloid monolith dehydration with time, as with the engineered emulsions in Chapter 4, Figure 4.6. The weight of a freshly-made pellet, composed of standard P5 PMMA particles (from 15 mL of dilute colloid solution, 2.4 mg/mL), was measured at constant temperature (25 ^{o}C) until a constant weight was obtained (Figure 6.17(a)). From this measurement, the water content was calculated to be 55 wt. %, assuming that no water is left in the structure. Weight loss starts to slow at roughly 70 minutes, and ceases almost completely after around 300 minutes, suggesting that dehydration ceases after 5 hours.

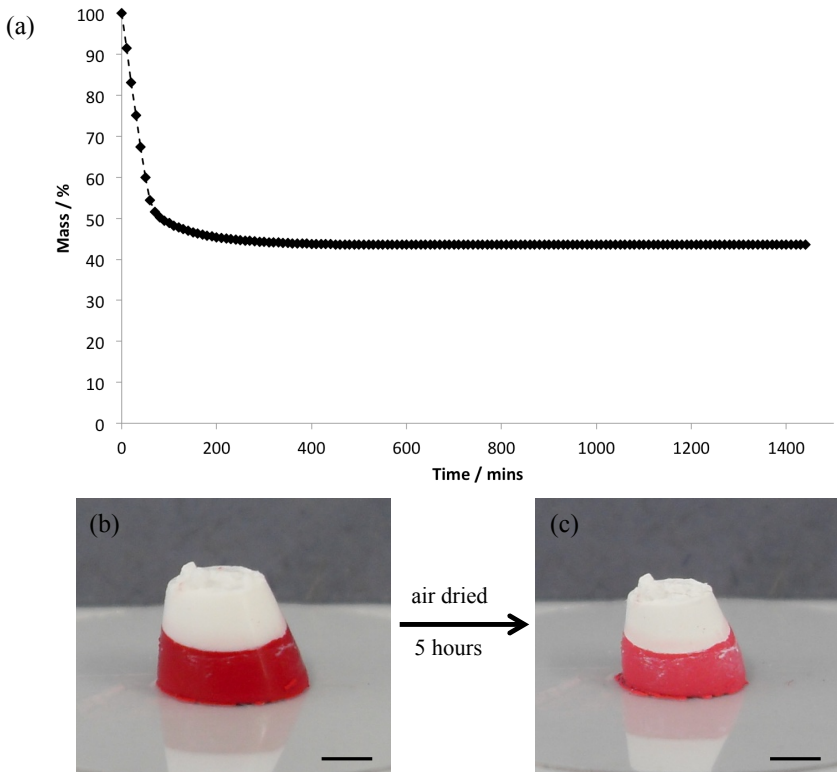

Figure 6.17. (a) Gravimetric weight loss curve for monolith as a function of time (298 K) (b) Pellet at 0 minutes (c) Dehydrated pellet at 300 minutes, 57.5 % of volume of hydrated pellet. Scale bars represent 2 mm.

A visible change in volume was observed for a monolith left for 300 minutes to dehydrate as shown in Figure 6.17(b) and (c), with (b) showing a monolith initially after aggregation and (c) showing the same monolith after 5 hours. The volume change can be approximately calculated by treating the sample shape as a frustum both before and after aggregation. The equation for this calculation is shown in (1).

$$V = \frac{\pi h}{3}(R_2^2 + R_1R_2 + R_1^2) \quad (1)$$

In this equation h represents the height of a frustum, R_1 and R_2 are the radii of the two bases.

From the images in Figure 6.17(b) and (c), it can be calculated that the dehydrated monolith is 57.5 % of the volume of its hydrated form, meaning that a reduction in volume of approximately 42.5 % occurs upon dehydration. This roughly correlates with the weight loss observed in the TGA, suggesting that around half the volume of the aggregates is made up of water. Upon dehydration, the interstitial sites where there was water should become pores within the colloid scaffold, but a change in volume suggests that some of these inter-colloid regions collapse, resulting into a more compact internal structure. If these aqueous voids could be retained in the dehydrated state, then a much more porous structure would remain. In order to investigate this possibility, a colloidal monolith was created and immediately frozen for freeze-drying. The volume reduction upon the removal of the water in the structure was only roughly 11.4 %, in contrast to the air-dried monolith created as a control, which showed a 48.3 % reduction in volume (Figure 6.18). It was expected that the resulting monoliths produced *via* both methods of dehydration should show degrees of measurable porosity, but the degree of porosity might vary.

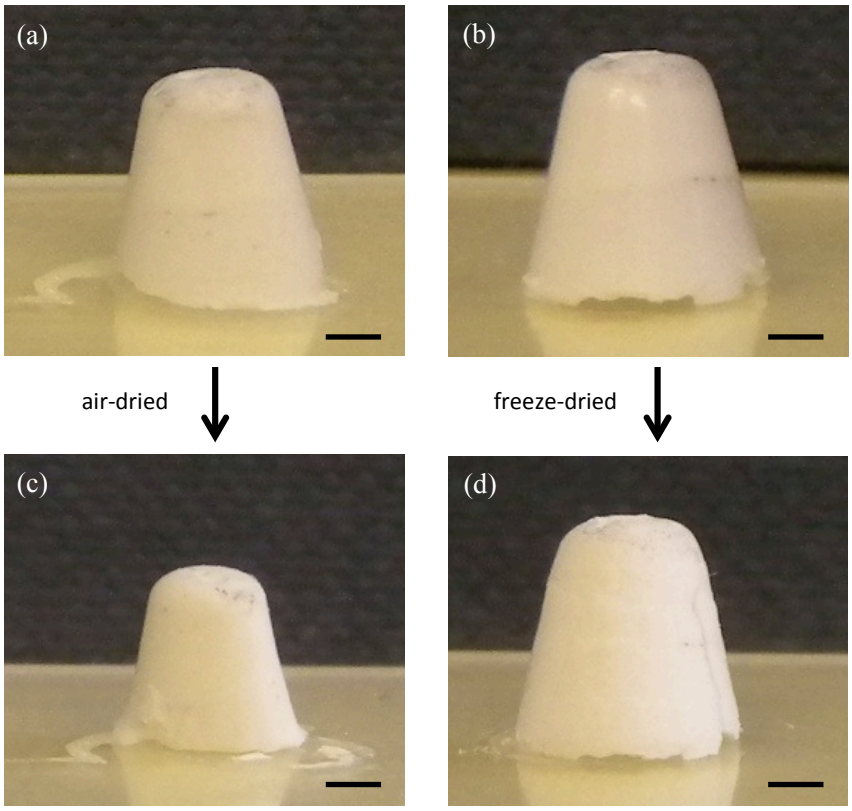

Figure 6.18. (a) Pellet to be air-dried, (b) pellet to be freeze-dried, (c) air-dried pellet, t = 24 hours and (d) freeze-dried, t = 24 hours. Scale bars represent 2 mm.

A number of techniques were used to probe the differences in pore volume and bulk porosity of these two systems. The first was scanning electron microscopy (SEM) in order to observe any qualitative differences between the two samples at high magnification. The SEM images showed some fused particles, with large gaps between aggregates, possibly leading to a more open structure for the freeze-dried monolith (Figure 6.19(b)) in comparison to the air-dried monolith (Figure 6.19(a)). The latter had a much more intricate structure, possibly leading to limited porosity on the surface of the aggregate. This difference between structures was expected as larger pores should arise in the freeze-dried structure due to the freeze concentration effect. Impurities have very low solubility in ice crystals,[36] therefore upon freezing of the water in an aggregated structure, the concentration of polymer particles at the edge of the ice crystals starts to increase, pushing some particles closer together, resulting in what looks like some fused particles. On removal of this water by freeze-drying, large pores remain where the ice crystals once where, leading to a material containing much larger pores throughout the structure.[37]

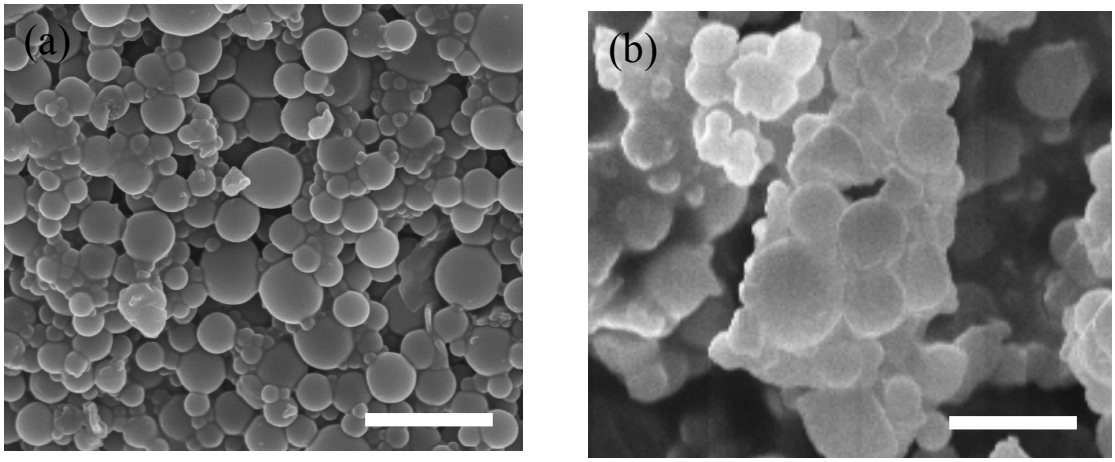

Figure 6.19. SEM images for internal microstructure of colloids assembled via the acidification and centrifugation (4,500 rpm, 20 minutes) of 15 mL of colloid solution for (a) air-dried and (b) freeze-dried monoliths. Scale bars represent 1 μm.

Porosimetry involves the intrusion of a non-wetting liquid at high pressure in order to assess the pore size distribution. In the case of mercury intrusion porosimetry the liquid is mercury, and the pore size is calculated based on the external pressure needed to force the mercury into pores. The porosity was measured for approximately 20 mg of each sample. Diameters of the larger pores visible by SEM for the freeze-dried sample was in good agreement with the monomodal pore size distribution measured *via* mercury intrusion porosimetry (Figure 6.20). This finding suggests that porosity, and perhaps more importantly pore size, may be controlled by the level of colloid compaction and method of dehydration of the monoliths.

A distinct, reproducible macropore size of 176 nm was measured for the freeze-dried monolith (Figure 6.20). In comparison, measurements performed on air-dried samples showed no significant intrusion and results showed small amounts of non-reproducible intrusion into multimodal pore volumes.

It is worth noting that the freeze-dried monolith had 1.03 mL g^{-1} of mercury intrusion, but an equal mass of the air-dried sample had only 0.37 mL g^{-1}. This confirms that the total porosity of a dehydrated, aggregated sample is influenced by the method of drying.

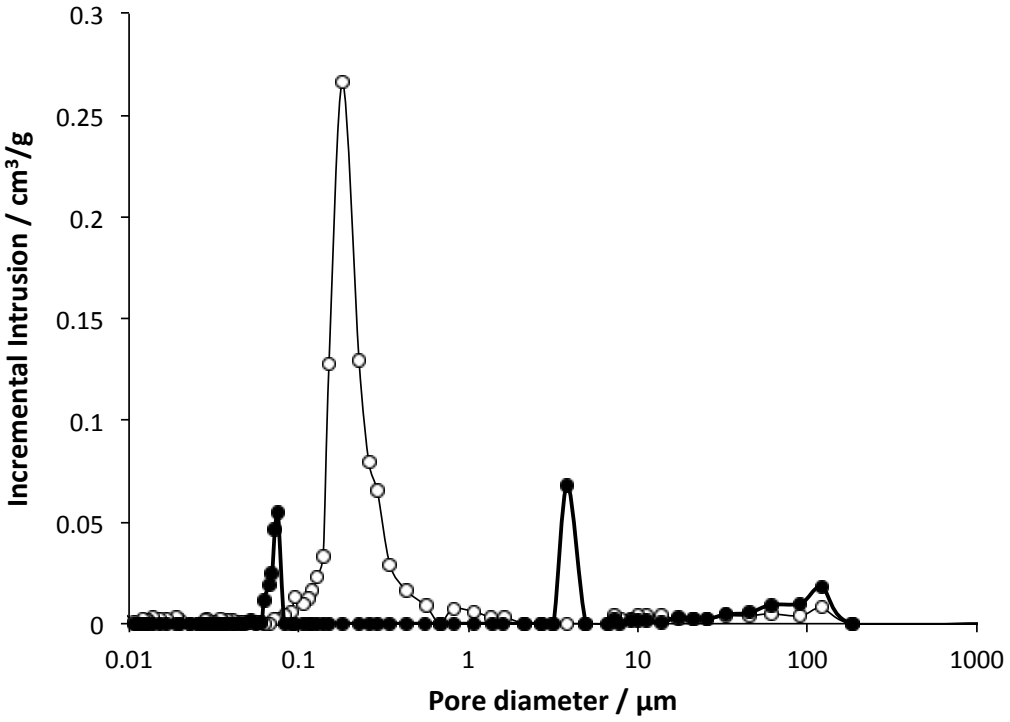

Figure 6.20. Pore size distribution measured *via* mercury intrusion porosimetry for the air-dried (closed circles) and freeze-dried (open circles) monoliths, both dehydrated overnight.

6.3. Conclusions

A convenient emulsion-templated solvent-evaporation technique was used to generate PMMA colloids with volume-average diameters of 300-350 nm and surface functionality that is dictated by the branched copolymer surfactant composition. The colloids were stable in basic solution due to simultaneous steric and electrostatic stabilisation provided by PEG and MAA residues. Reduction of the solution pH induced a transition from a dispersed state to aggregation when the EG:MAA molar ratio on the colloid surfaces is equal. The aggregation process is reversible on addition of base, as seen in emulsion droplet interactions in Chapter 4. Analogous colloids prepared with EG-rich surfaces were unresponsive to pH changes, which demonstrates that inter- versus intra-colloid interactions can be effectively controlled by subtle variation of the stabiliser composition, again similar to emulsion systems shown in Chapter 3.

The role of free copolymer in particle solutions was investigated, and it was demonstrated that a more rapid rate of particle aggregation occurred with increasing

amounts of free copolymer added. This free copolymer may 'bridge' between particles, aiding the faster formation of colloidal aggregates.

Furthermore, we demonstrate successful encapsulation of different hydrophobic dyes within the colloids and the production of monolithic structures composed of PMMA nanoparticles with controllable porosities. The persistence of the surface function during assembly allows triggered disassembly of the stable monoliths, suggesting that these hierarchical materials may serve as the basis for the development of responsive scaffold materials.

6.4. References

(1) Min, Y. J.; Akbulut, M.; Kristiansen, K.; Golan, Y.; Israelachvili, J. *Nature Mater.* **2008**, *7*, 527.

(2) Grzelczak, M.; Vermant, J.; Furst, E. M.; Liz-Marzan, L. M. *ACS Nano* **2010**, *4*, 3591.

(3) Boal, A. K.; Ilhan, F.; DeRouchey, J. E.; Thurn-Albrecht, T.; Russell, T. P.; Rotello, V. M. *Nature* **2000**, *404*, 746.

(4) Baalousha, M. *Sci. Total Environ.* **2009**, *407*, 2093.

(5) Berger, S.; Zhang, H. P.; Pich, A. *Adv. Funct. Mater.* **2009**, *19*, 554.

(6) Zhang, L. Y.; Hu, Y.; Jiang, X. Q.; Yang, C. Z.; Lu, W.; Yang, Y. H. *J. Control. Release* **2004**, *96*, 135.

(7) Woodward, R. T.; Slater, R. A.; Higgins, S.; Rannard, S. P.; Cooper, A. I.; Royles, B. J.; Findlay, P. H.; Weaver, J. V. *Chem. Commun.* **2009**, 3554.

(8) Woodward, R. T.; Olariu, C. I.; Hasan, E. A.; Yiu, H. H. P.; Rosseinsky, M. J.; Weaver, J. V. M. *Soft Matter* **2011**, *7*, 4335.

(9) O'Reilly, R. K.; Hawker, C. J.; Wooley, K. L. *Chem. Soc. Rev.* **2006**, *35*, 1068.

(10) Fujii, S.; Cai, Y. L.; Weaver, J. V. M.; Armes, S. P. *J. Am. Chem. Soc.* **2005**, *127*, 7304.

(11) Liu, S. Y.; Weaver, J. V. M.; Tang, Y. Q.; Billingham, N. C.; Armes, S. P.; Tribe, K. *Macromolecules* **2002**, *35*, 6121.

(12) Read, E. S.; Armes, S. P. *Chem. Commun.* **2007**, 3021.

(13) Jeffery, H.; Davis, S. S.; Ohagan, D. T. *Pharm. Res.* **1993**, *10*, 362.

(14) Lai, M. K.; Tsiang, R. C. C. *J. Microencapsul.* **2005**, *22*, 261.

(15) Chognot, D.; Leonard, M.; Six, J. L.; Dellacherie, E. *Colloid. Surface. B* **2006**, *51*, 86.

(16) Lassalle, V.; Ferreira, M. L. *Macromol. Biosci.* **2007**, *7*, 767.

(17) Song, C. X.; Labhasetwar, V.; Murphy, H.; Qu, X.; Humphrey, W. R.; Shebuski, R. J.; Levy, R. J. *J. Control. Release* **1997**, *43*, 197.

(18) Velev, O. D. *Science* **2000**, *287*, 2240.

(19) Kim, S. H.; Lee, S. Y.; Yi, G. R.; Pine, D. J.; Yang, S. M. *J. Am. Chem. Soc.* **2006**, *128*, 10897.

(20) Manoharan, V. N.; Elsesser, M. T.; Pine, D. J. *Science* **2003**, *301*, 483.

(21) Graves, R. A.; Moiseyev, R.; Freeman, T.; Mandal, T. K. *J. Biomater. Sci.-Polym. Ed.* **2005**, *16*, 585.

(22) Khoee, S.; Yaghoobian, M. *Eur. J. Med. Chem.* **2009**, *44*, 2392.

(23) Chevalier, Y. *Curr. Opin. Colloid Interface Sci.* **2002**, *7*, 3.

(24) Garnier, S.; Laschewsky, A.; Storsberg, J. *Tenside Surfact. Det.* **2006**, *43*, 88.

(25) Bibette, J.; Calderon, F. L.; Poulin, P. *Rep. Prog. Phys.* **1999**, *62*, 969.

(26) Binks, B. P. *Curr. Opin. Colloid Interface Sci.* **2002**, *7*, 21.

(27) Pickering, S. U. *J. Chem. Soc.* **1907**, *91*, 2001.

(28) Kataoka, K.; Harada, A.; Nagasaki, Y. *Adv. Drug Deliv. Rev.* **2001**, *47*, 113.

(29) Torchilin, V. P. *Adv. Drug Deliv. Rev.* **2006**, *58*, 1532.

(30) Chognot, D.; Leonard, M.; Six, J. L.; Dellacherie, E. *Colloid. Surface. B* **2006**, *51*, 86.

(31) Chognot, D.; Six, J. L.; Leonard, M.; Bonneaux, F.; Vigneron, C.; Dellacherie, E. *J. Colloid Interface Sci.* **2003**, *268*, 441.

(32) Rouzes, C.; Leonard, M.; Durand, A.; Dellacherie, E. *Colloid. Surface. B* **2003**, *32*, 125.

(33) Weaver, J. V. M.; Rannard, S. P.; Cooper, A. I. *Angew. Chem. Int. Ed.* **2009**, *48*, 2131.

(34) Woodward, R. T.; Chen, L.; Adams, D. J.; Weaver, J. V. M. *J. Mater. Chem.* **2010**, *20*, 5228.

(35) Woodward, R. T.; Weaver, J. V. M. *Polym. Chem.* **2011**, *2*, 403.

(36) Deville, S.; Saiz, E.; Tomsia, A. P. *Acta Mater.* **2007**, *55*, 1965.

(37) Qian, L.; Zhang, H. F. *J. Chem. Tech. Biotechn.* **2011**, *86*, 172.

CHAPTER 7

Multi-Responsive Polymer-Stabilised Magnetic Emulsions in the Formation of Magnetic Engineered Emulsions

(Publication arising from this Chapter: **"Multi-responsive polymer-stabilized magnetic engineered emulsions as liquid-based switchable magneto-responsive actuators"**, R. T. Woodward, C. I. Olariu, E. A. Hasan, H. H. P. Yiu, M. J. Rosseinsky, J. V. M. Weaver, *Soft Matter*, 2011, *7*, 4335-4340.)

List of Figures

7.1. Introduction

Magnetic nanoparticles (mNPs) are growing increasingly important in the field of materials research. They have many potential applications including nanomedicine,[1] hyperthermic probes,[2,3] and targeted delivery.[4] The ability to control mNP location and movement *in vivo* is of particular interest when designing or synthesising new functional biomaterials. When looking at controlled mNP movement, a distinction can be made between dispersed, or 'free' mNPs and mNPs immobilised within a larger, more hierarchical, structure. Although these materials both show responsiveness to an external magnetic field, their properties differ significantly. Dispersed mNPs display relatively unrestricted movement in an external magnetic field, whereas structures containing immobilised mNPs can behave as magneto-actuators.[5-7]

Controlling the movement of disperse mNPs using external magnetic fields is a useful concept exploited in a number of research areas such as cell separation,[8] accumulation at specific target sites,[9] and towards controlling cell behaviour.[10] However, at this scale Brownian motion can interfere with magnetisation. A simple solution to this problem is either to aggregate mNPs[11] or to isolate mNPs within confined domains; thus the overall magnetisation of the assembled mNPs becomes the sum of the particles present. A lot of work has been published on aggregation and isolation methods, including encapsulation within polymer latexes,[12] microgels,[13] inorganic colloids,[14,15] polymer networks[16] and emulsion droplets.[17,18] Immobilising mNPs onto or within a matrix results in the forces acting on the mNPs being transferred to that matrix.[9,19]

Emulsions have long been used as an important formulation tool by industry but have more recently emerged as useful responsive materials in their own right.[20-22] Emulsions allow a number of distinct phases (i.e., oil and water) to co-exist as a free-flowing fluid dispersion and are able to encapsulate diverse material. The introduction of magnetic nanoparticles into responsive emulsions is a route to biphasic multifunctional materials. O/w emulsions have previously been prepared with magnetic dispersed phases such as organic ferrofluids.[17,23] W/o emulsions can also be prepared with a continuous ferrofluid phase and the internal, non-magnetic, phases of these materials can be deformed on application of a magnetic field.[24]

Emulsions stabilised using magnetic microgels have also been prepared, meaning the mNPs are located at the oil–water interface.[25] In another example Fe_3O_4 particles have been used to stabilise a liquid-air interface, resulting in 'liquid marbles'.[26] Combining emulsion technology with magnetic nanoparticles can currently be achieved in a number of ways, resulting in confined mNPs.

It was shown in Chapter 3 that the emulsion droplet surface composition could be controlled to a high level by simple manipulation of the branched copolymer functionality. Inter-droplet interaction is possible by MAA/EG hydrogen bonding, forming engineered emulsions (EEs).[27] EE formation is reversible as demonstrated in Chapter 4, so EEs can be disassembled by addition of base, to reform free-flowing emulsions.

This Chapter investigates the encapsulation of oleophilic mNPs in the formation of an o/w surface functionalised emulsion where the internal oil phase is a ferrofluid and the droplet surface functionality allows the formation of EEs by changing the solution pH. Both the dispersed and aggregated states are investigated for magnetic properties to find out if, in the aggregated state (acidic pH), the droplet magnetic responses are combined, and result in the engineered emulsion acting as a magneto-actuator.

7.2. Results and Discussion

7.2.1. Synthesis and Characterisation of Multi-Responsive Emulsions

In order to create oleophilic mNPs, poly(2-(diethylamino)ethyl methacrylate) (PDEAEMA) was grown from the surface of post-functionalised hydrophilic superparamagnetic iron oxide (Fe_3O_4). This was performed via bromosilanisation of the nanoparticle surface (Figure 7.1(a)) followed by atom transfer radical polymerisation (ATRP) of DEAEMA (Figure 7.1(b)). The details of both these reactions are given in Chapter 2.7.3.

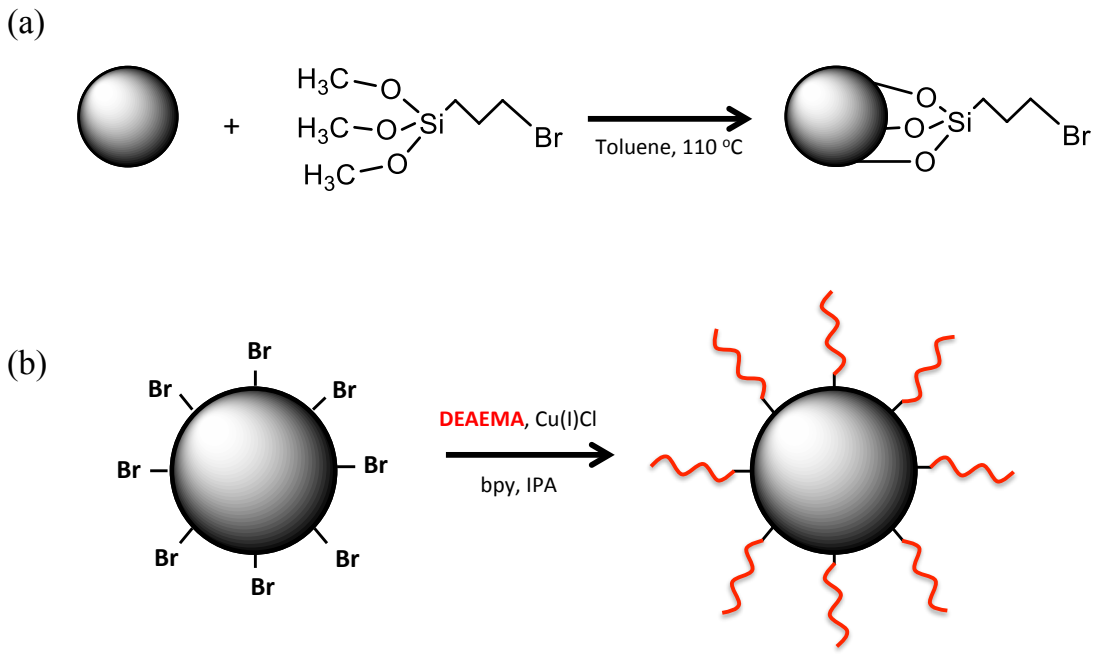

Figure 7.1. Schematic of the synthetic route to PDEAEMA-mNPs. (a) Reaction between 25 nm Fe_3O_4 and 3-bromopropyl trimethoxysilane yielding bromo-functionalised Fe_3O_4, (b) ATRP of DEAEMA from bromine atoms on the particle surface.

Fourier transform infrared (FTIR) spectroscopy can be used to determine functional groups present within a sample as molecules absorb specific frequencies which are characteristic of their structure. This technique was employed in order to investigate if polymerisation of DEAEMA from the surface of the mNPs was successful (Figure 7.2). The nanoparticles, after the attempted polymerisation of DEAEMA, displayed peaks for the organic groups CH_3, CH_2 at 2900-2800 cm^{-1} and C=O at 1729 cm^{-1}, both of which are present in PDEAEMA. This is indicative of a successful polymerisation from the nanoparticle surface. If we compare this to the bromosilanated particles, no C=O peak is present, and a small peak is present at around 2900 cm^{-1}, arising from the addition of the bromine functionality (step (a) in Figure 7.1).

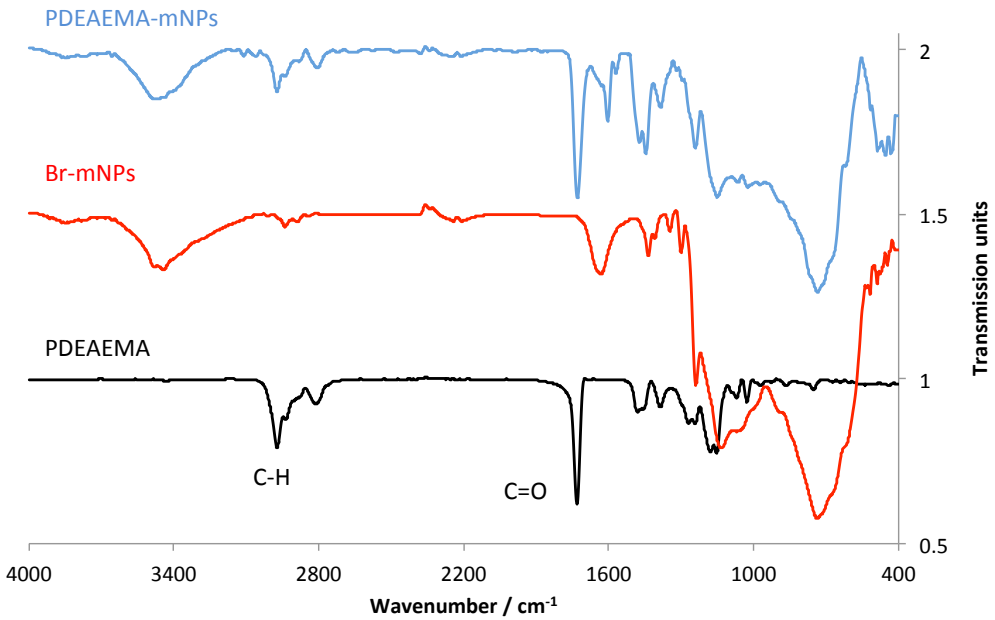

Figure 7.2. FTIR spectra of PDEAEMA homopolymer (black), bromine functionalised mNPs (red), and oleophilic PDEAEMA-mNPs (blue).

Elemental analysis was also used to confirm the composition of the organic content of the PDEAEMA-mNPs. Br-mNPs had C: 0.94 %, H: 0.39 % and no nitrogen. As expected, PDEAEMA-mNPs showed higher organic content, C: 3.61 %, H: 0.66 %, and N: 0.54 %. Transmission electron microscopy (TEM) was also employed in order to observe any change in size or morphology due to the polymerisation of DEAEMA, the results of which are shown in Figure 7.3.

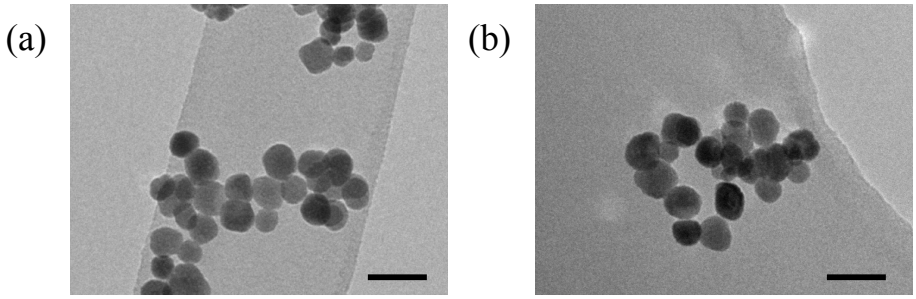

Figure 7.3. TEM images of (a) standard Fe_3O_4 as purchased and (b) PDEAEMA-functionalised magnetic nanoparticles. Scale bars represent 50 nm.

TEM images confirmed that the PDEAEMA-mNPs remained discrete, and showed that particles did not exhibit any significant changes in size or morphology during post-functionalisation.

DEAEMA was used due to its inherent oleophilicity at neutral to high pH, although it is also pH-responsive and can become more hydrophilic at low pH (Figure 7.4(a) and (b) respectively). With a large enough layer of PDEAEMA on the surface of the particles, the particles should inherit the hydrophobicity of this polymer at neutral to high pH (Figure 7.4(a)).

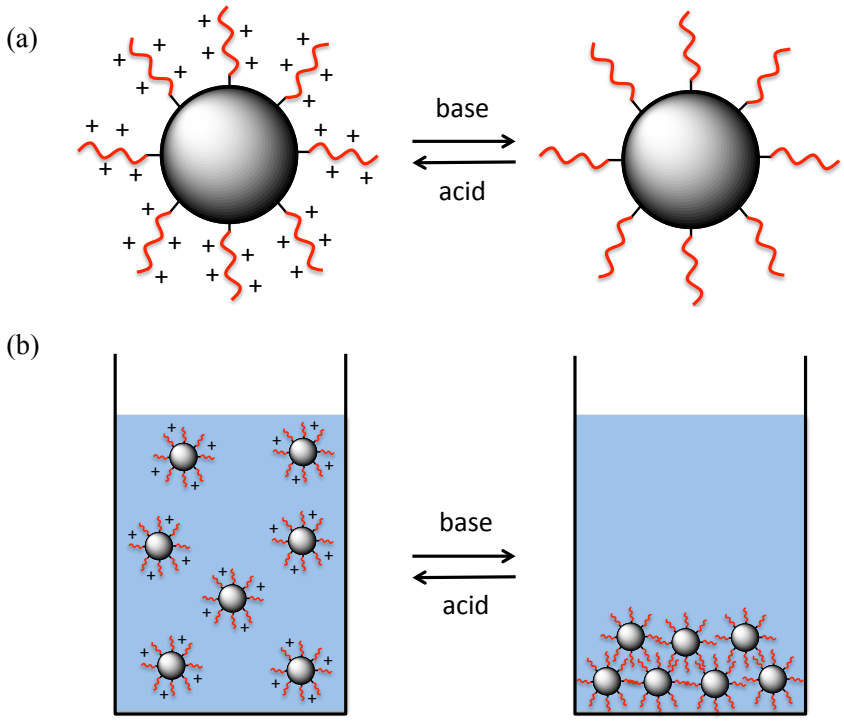

Figure 7.4. Schematic representation of the pH-responsiveness of PDEAEMA-mNPs: (a) cationic at low pH allowing particle dispersion and neutral at high pH, which renders the particles hydrophobic (b) demonstration of particle behaviour in water, hydrophilic at low pH, so particles disperse, and hydrophobic at high pH, so PDEAEMA mNPs become insoluble in water.

This switchable hydrophobicity is demonstrated in Figure 7.5 by adding PDEAEMA-mNPs (0.1 wt. %) to both acidic and basic solutions (pH adjusted with 0.2 mL of 1 M HCl and 0.2 mL of 1 M NaOH respectively). It can be seen that, upon raising the solution pH, PDEAEMA-mNPs crash out of the aqueous solution and sediment due to their hydrophobicity. It is worth noting that particles could be removed from both solutions via the application of a magnetic field.

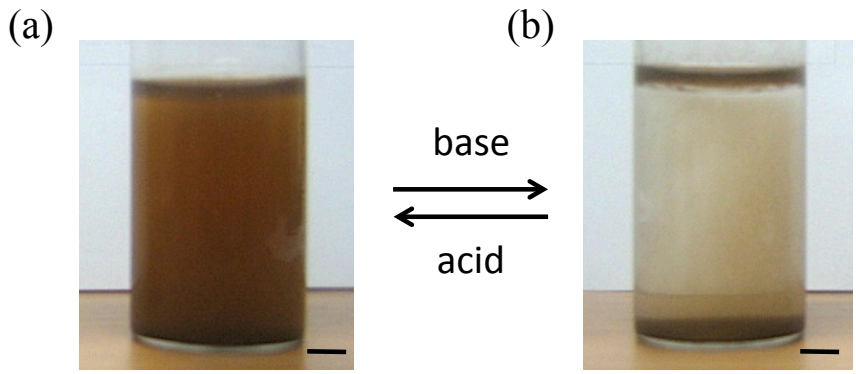

Figure 7.5. Digital images of PDEAEMA-mnPs (0.1 wt. %) in (a) pH 2 solution and (b) pH 10 solution. Scale bars represent 5 mm.

With this increased oleophilicity, PDEAEMA-mNPs (0.17 wt. %) were dissolved in n-dodecane (3 mL) and homogenised (24,000 rpm, 2 minutes) with a pH 10, P5 solution (2 wt. %, 3 mL). This enabled encapsulation of the PDEAEMA-mNPs within the oil phase of a P5-stabilised dodecane o/w emulsion. After creaming, the emulsion's Φ_{oil} was 0.70, which is similar to previous systems. This process is shown schematically in Figure 7.6. It was hypothesised that this would result in magnetic oil droplets with a functionalised, pH-responsive surface, or a multi-responsive emulsion.

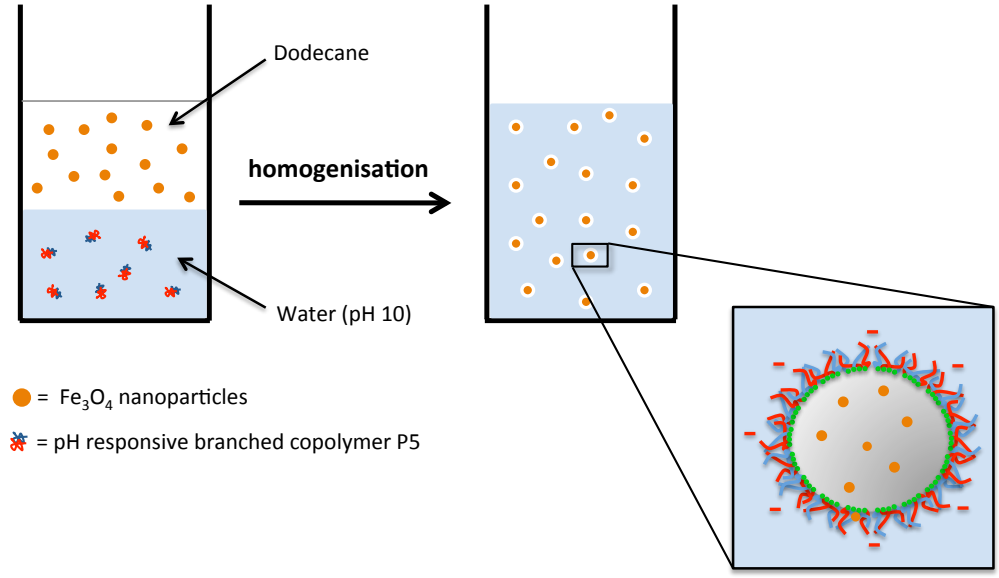

Figure 7.6. Schematic showing the production of oil-in-water emulsions with mNPs encapsulated in the resulting oil droplets.

These emulsion droplets were of a similar size to that of the P5-surface responsive emulsions made in Chapter 3 and Chapter 4 ($D_{(4,3)}$ = 6.9 μm, span = 1.06). The presence of the mNPs appeared to show no adverse effects on the size or dispersity of the resulting pH-responsive emulsions. A laser diffraction measurement of this emulsion is overlayed with that of a standard P5 dodecane o/w emulsion in Figure 7.7(a). Although the standard emulsion has a bimodal distribution, it is clear that this size distribution is similar to that of the PDEAEMA-mNP containing emulsion.

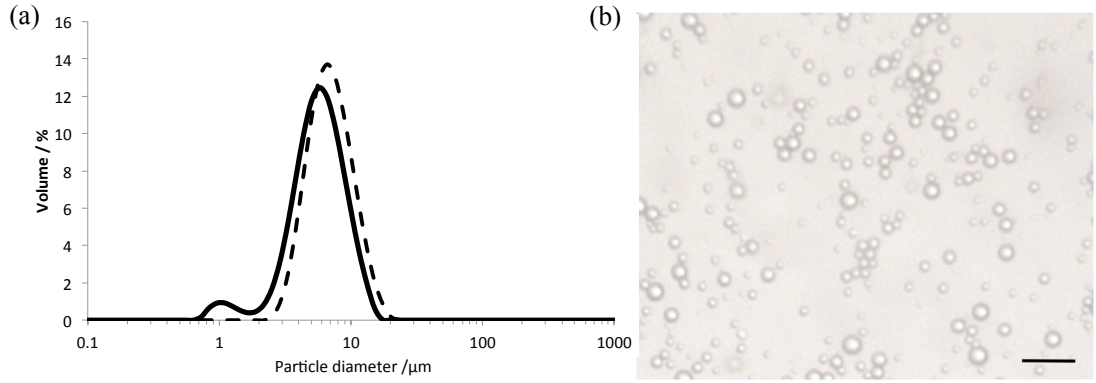

Figure 7.7. (a) Laser diffraction measurement of a P5 dodecane emulsion containing PDEAEMA-mNPs (0.17 %) at pH 10 (dashed line) and a standard P5 dodecane emulsion at pH 10 (solid line). (b) Light micrograph of the same PDEAEMA-mNP containing emulsion at pH 10. Scale bar represents 20 μm.

Light microscopy was used to provide further evidence for the mNPs having no effect on the resulting droplet sizes and morphologies (Figure 7.7(b)). The light micrographs also show dispersed droplets with no sign of coalescence.

7.2.2. Comparison of Magnetic and Non-Magnetic, Free-Flowing Emulsions

By dissolving mNPs into the oil phase and creating an emulsion, we aim to create oil droplets capable of responding to a magnetic field. A simple way of investigating the magnetic response of droplets is to compare an emulsion with no encapsulated material (a standard P5 dodecane o/w emulsion), to that which contains mNPs in the presence of a magnetic field. Both samples were allowed to disperse across the surface of a pH 10 water reservoir and a magnet was submerged in the centre of the solution. The response of each emulsion was then photographed over time (Figure

7.8). The non-magnetic emulsion remains dispersed across the air-water interface with time, whereas the magnetic emulsion accumulates above the magnet over the same period of time. This demonstrates that the emulsion containing mNPs responds to the magnetic field, whereas the non-magnetic emulsion does not.

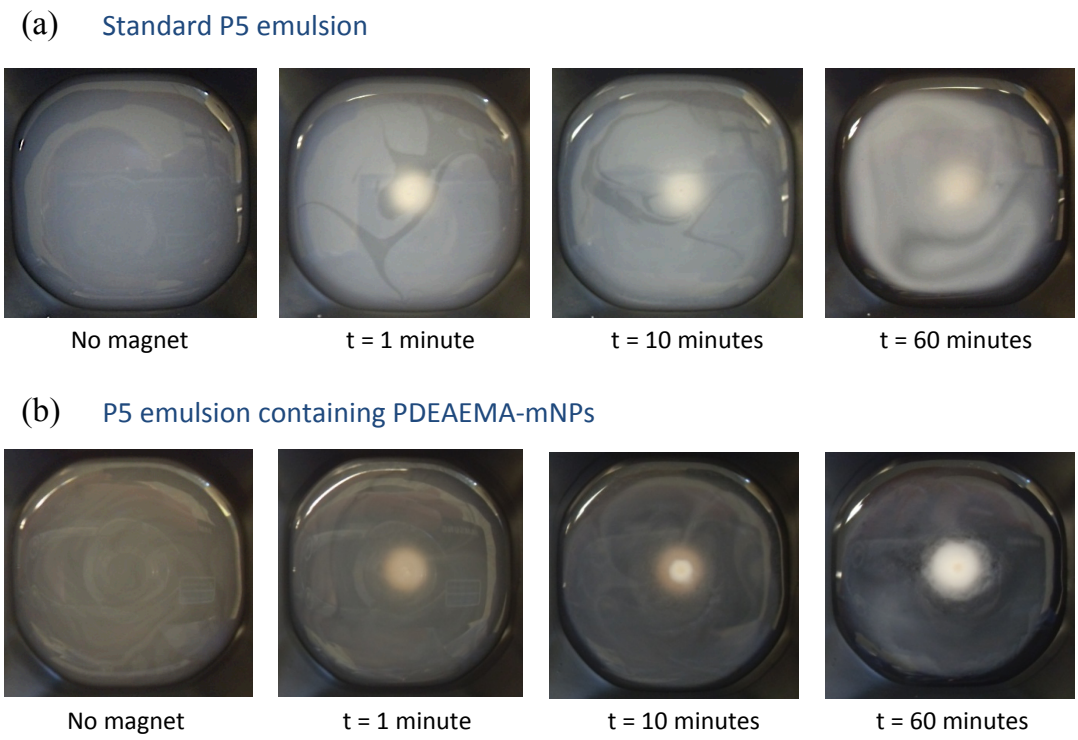

Figure 7.8. Digital images of emulsion droplets stabilised with P5 at basic pH in the presence of a magnet. (a) Non-magnetic droplets remain dispersed at the air-face interface and (b) magnetic droplets accumulate above the magnet over time.

7.2.3. Engineered Emulsions Containing PDMAEMA-mNPs

A sample (150 μL) from the creamed surface-functionalised magnetic emulsion at pH 10 (Figure 7.9), described earlier in 7.2.1, was taken and transferred to a mould. HCl (100 μL, 1 M) was the dropped onto the surface of the sample and allowed 2 hours to diffuse throughout the emulsion. This acidification triggers inter-droplet hydrogen bonding and, upon removal of the mould, the magnetic emulsion droplets are kinetically trapped and conform to the dimensions of the template, resulting in an 'engineered emulsion' (Figure 7.9(b)).[27]

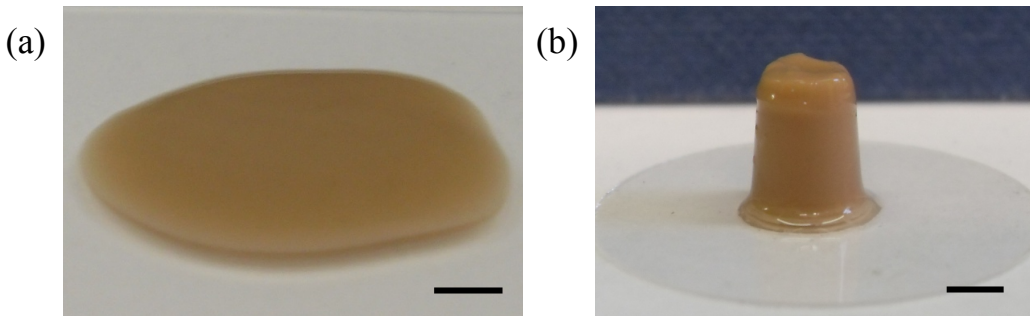

Figure 7.9. P5-stabilised, PDEAEMA-mNP-containing dodecane emulsion, (a) free-flowing at pH 10 and (b) 2 hours after acidification in a mould by 1 M HCl, following the template removal. Scale bars represent 5 mm in (a), 2.5 mm in (b).

The rate at which aggregation proceeded in the magnetic emulsion was then measured using laser diffraction, allowing comparison with that of the native emulsion (Figure 7.10). The samples were initially measured three times at pH 10 at one measurement per minute. The pH in the dispersion unit was then lowered to around pH 2 *via* the addition of HCl (0.5 mL, 1 M) and the resulting increase in particle size was measured. From this result, shown in Figure 7.10, the rate of aggregation of the PDEAEMA-mNP containing emulsion is similar to that of the native emulsion, so it can be inferred that the mNPs have no effect on the rate of inter-droplet aggregation.

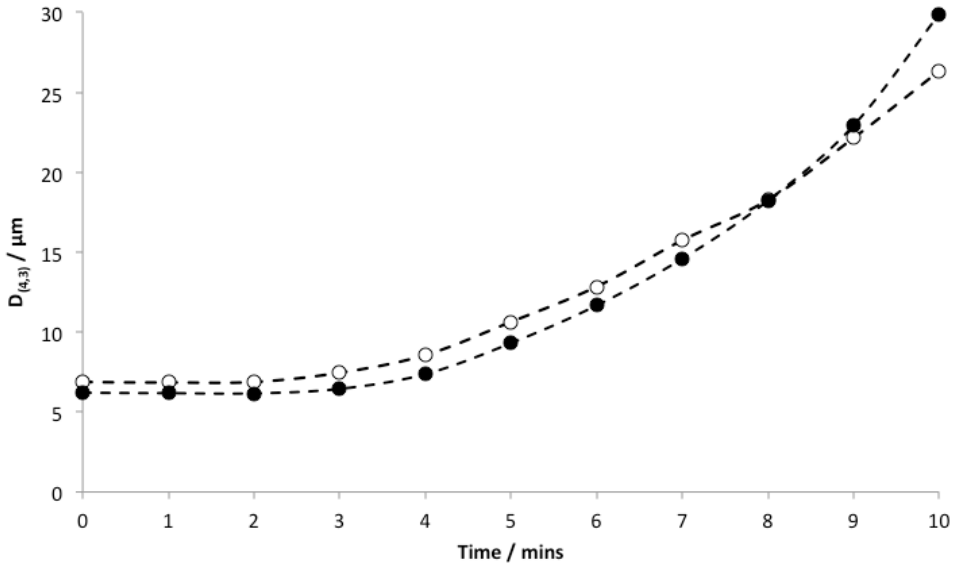

Figure 7.10. Rate of droplet aggregation against time for the P5 stabilised, dodecane, PDEAEMA-mNP containing emulsion (closed circles) and a standard P5 stabilised dodecane emulsion (open squares). Acidification occurs after 2 minutes.

As the rate of aggregation between samples was very similar, the engineered emulsion's gel strength and resistance to strain of both a standard P5 emulsion and a magnetic P5 emulsion was investigated using rheometry. A sample of each emulsion's creamed layer (2.5 mL) was acidified for 2 hours *in situ*, *via* the addition of 1 M HCl (0.5 mL). After this time, any excess HCl was removed, and amplitude sweeps were performed on the resulting engineered emulsions, in order to see if the presence of mNPs had any effect on the samples G' and G" (Figure 7.11). The magnetic engineered emulsion was in good agreement with the standard engineered emulsion, suggesting that there is little difference in gel strength between these two aggregates. G' for the magnetic emulsion at 0.5 % strain (1,070 Pa) is the same as that for the non-magnetic emulsion, while the G" measurements are 338 Pa and 283 Pa respectively. This small difference in G" is likely due to some excess HCl remaining in the magnetic emulsion during measurement, leading to a slightly higher viscous response in comparison to the standard.

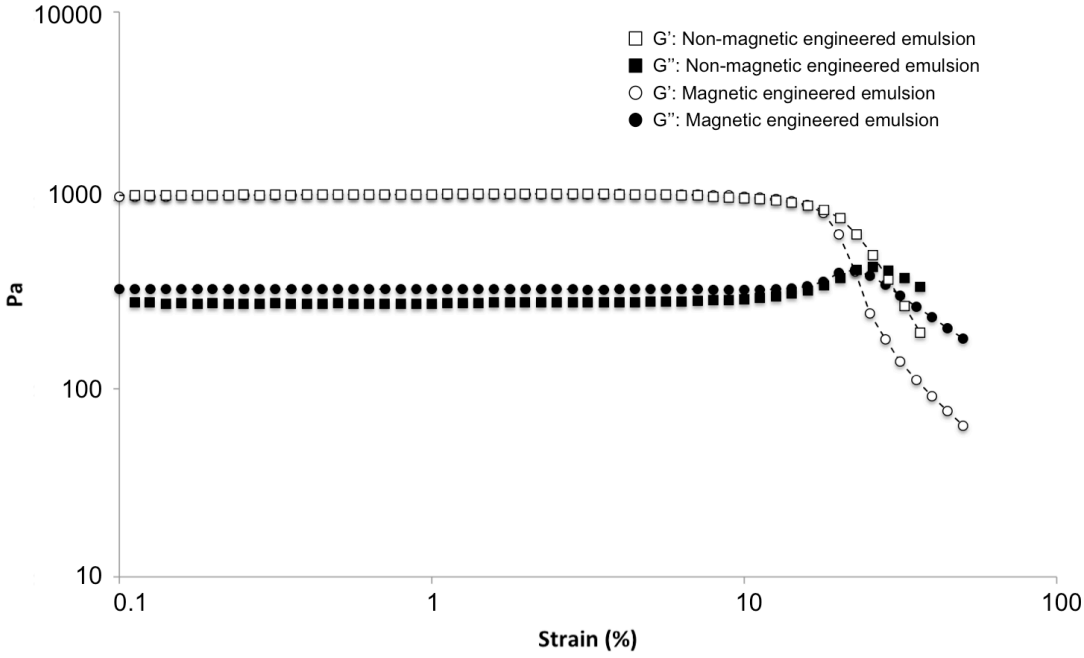

Figure 7.11. Amplitude sweeps for the native EEs and the magnetic engineered emulsion.

Thus the rheology data shows that encapsulation of the mNPs has no effect on the resulting EE strength. The strain at which both samples break down (the crossover point, at which G">G') is larger in the standard EE (36 % strain in comparison to 29

% strain in the magnetic emulsion). This suggests that the presence of PDEAEMA-mNPs has some effect on the EE's resistance to increased strain, but this difference is only small and may be due to slight differences in preparation methods.

7.2.4. Magnetic Engineered Emulsions in the Presence of a Magnetic Field

It has already been shown that the free-flowing emulsion responds to an external magnetic field, therefore the responsiveness of a magnetic engineered emulsion was also investigated. An engineered emulsion was produced by transferring a sample of the P5 stabilised magnetic emulsion's creamed layer (150 µL) to a mould, and acidifying *via* the addition of HCl (1 M, 100 µL). This templated emulsion was then left to aggregate for 90 minutes before any excess HCl and the mould were removed. The engineered emulsion was then exposed to a magnet (Figure 7.12).

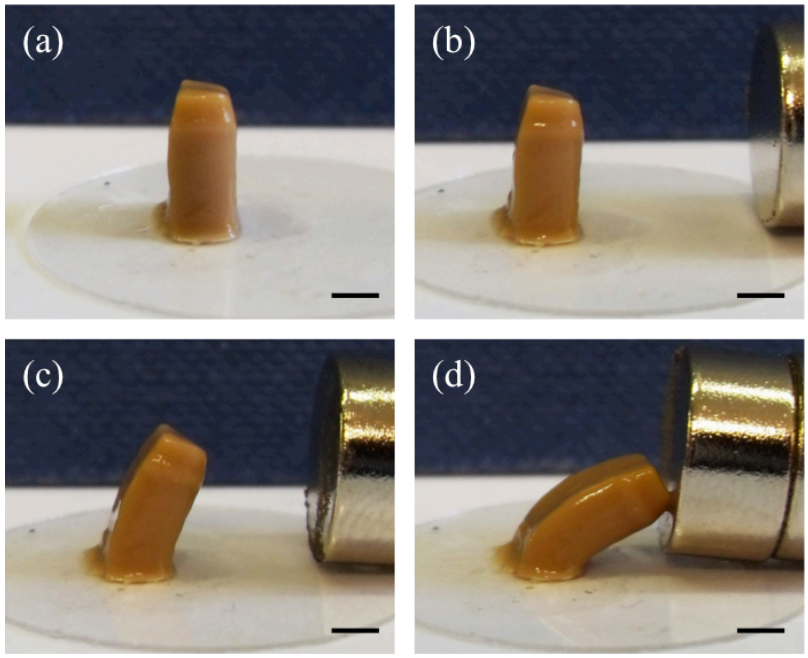

Figure 7.12. P5 stabilised magnetic engineered emulsion (a) in the absence of a magnetic field and (b-d) at increasing magnetic field strength (reduced magnet distance). Scale bar represents 2.5 mm.

With no magnet present, as in Figure 7.12(a), the monolith stands straight. When a magnet is moved closer to the engineered emulsion, the aggregate starts to lean toward the source of the magnetic field (Figure 7.12(b-d)). The engineered emulsion

may have some affinity for the glass slide, as upon application of the magnetic field, the bottom of the structure does not respond to the magnet as much as the top. However, these images provide good evidence of the EEs responsiveness to an external magnetic field.

One potentially useful property of engineered emulsions is their ability to disassemble back to form free-flowing emulsions. Therefore, having assessed the structure's response to a magnet, the PDEAEMA-mNP containing engineered emulsion was redispersed via the addition of base (NaOH 1 M, 0.5 mL). Complete dispersion into a liquid was observed around 5-10 minutes after the addition of base, with slight agitation. Upon visual inspection of the now free-flowing emulsion, no phase-separated oil was seen, suggesting that no demulsification had occurred. However, in contrast to the non-magnetic pH responsive emulsion, the average droplet diameter ($D_{(4,3)}$) measured by laser diffraction showed a large increase from 6.9 μm to 12.6 μm suggesting that some droplet coalescence had occurred (both measurements are overlayed in Figure 7.13).

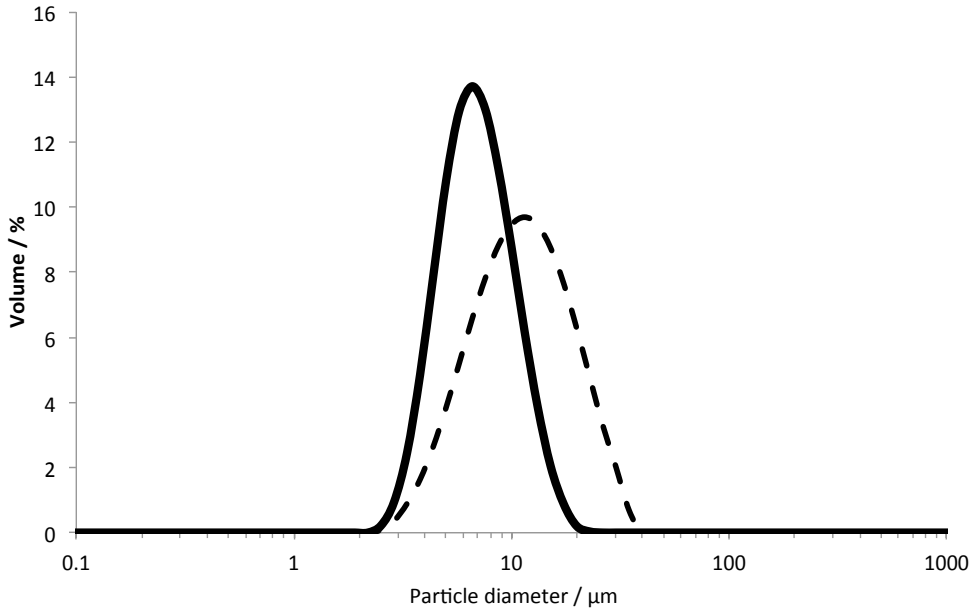

Figure 7.13. Laser diffraction measurements at pH 10 of the free-flowing, magnetic P5 dodecane emulsion (solid line) and a redispersed magnetic P5 dodecane EE (dotted line) after exposure to a magnetic field.

This indicates that these magnetic nanoparticle-containing droplets are either not as stable to the aggregation and redispersion process, or that some coalescence occurs

during the response to an external magnetic field. As droplets in an engineered emulsion are relatively immobile in comparison to a free-flowing emulsion, the pull of a magnetic field may cause some mNPs to leave the emulsion droplet they are encapsulated in, allowing the movement of oil or coalescence.

Magnetic hysteresis measurements (MvH) were performed on the assembled magnetic engineered emulsions and the PDEAEMA-mNPs using a superconducting quantum interference device (SQUID). When magnetic particles are very small (<35 nm), they display superparamagnetic behaviour.[28] This means that the particles consist of a single magnetic domain, rather than a number of domains with individual spins as in ferromagnetic materials. These samples show little or no hysteresis in varying magnetic fields due to the rapid response of particles to the fluctuating magnetic field. Both the polymer-functionalised mNPs and the magnetic-engineered emulsion samples were superparamagnetic at 300 K (Figure 7.14), meaning the mNPs superparamagnetism was successfully transferred to the engineered emulsion structure. Negligible hysteresis is detected, which is typical for superparamagnetic nanoparticles of this size.[29]

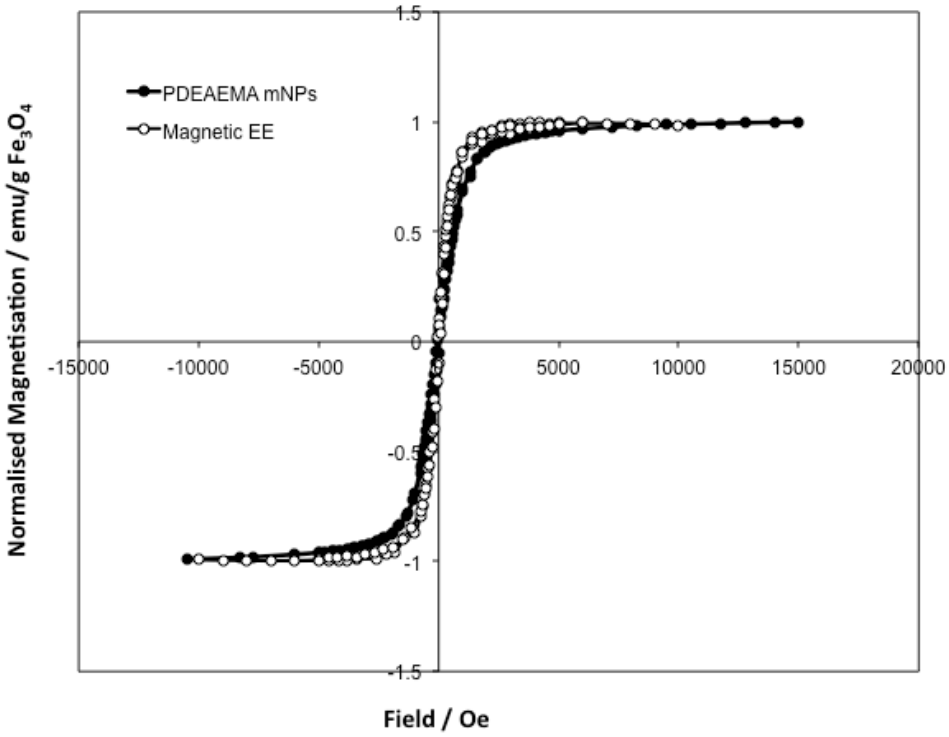

Figure 7.14. SQUID magnetisation plot for the oleophilic, PDEAEMA Fe_3O_4 mNPs and the magnetic-engineered emulsion at 300 K.

Magnetic and non-magnetic engineered emulsion spheroids were produced by dropping 10 μL of either the magnetic or the non-magnetic pH-responsive emulsion droplets into acidic water (0.2 M HCl, 10 mL). Upon contact with the acid these drops of free-flowing emulsion rapidly form spherical engineered emulsions. Using an external magnetic field, these spheroids could be moved around the acidic solution easily, even being held at the bottom of the water phase regardless of the dodecane in the spheroids having a lower bulk density (0.75 $g.cm^{-3}$) than the surrounding water phase (1.00 $g.cm^{-3}$), simply by placing the vial on top of a magnet (Figure 7.15).

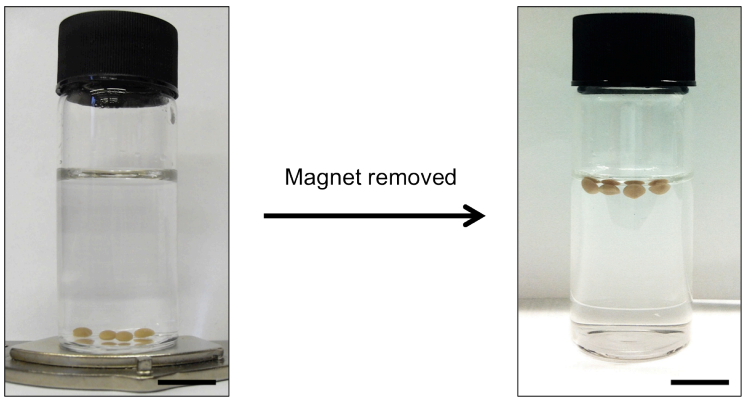

Figure 7.15. Spheroids (10 μL each) containing PDEAEMA-mNPs can be held at the bottom of a vial filled with acidic water using a magnet. Removal causes spheroids to return to the upper water surface. Scale bars represent 1 cm.

The spheroids allow a simple observation of the responsiveness of magnetic engineered emulsions, easily comparable to non-magnetic engineered emulsion samples. Spheroids, both magnetic and non-magnetic, were placed in a reservoir of acidic water (0.2 M, 25 mL) with a tapered opening at one end (Figure 7.16(a)). A magnet was then placed roughly 1 cm below the reservoir in order to selectively isolate the mNP-containing engineered emulsion spheroids from the random mixture of magnetic and non-magnetic aggregates. Slow movement of the magnet across the area of the reservoir isolated and grouped the brown magnetic spheroids (Figure 7.16(b)). The magnetic spheroids could then easily be removed from the reservoir by dragging the magnet through the tapered opening (Figure 7.16(c and d)), demonstrating not only selective movement of the spheroids, but the non-responsiveness of standard non-magnetic engineered emulsions.

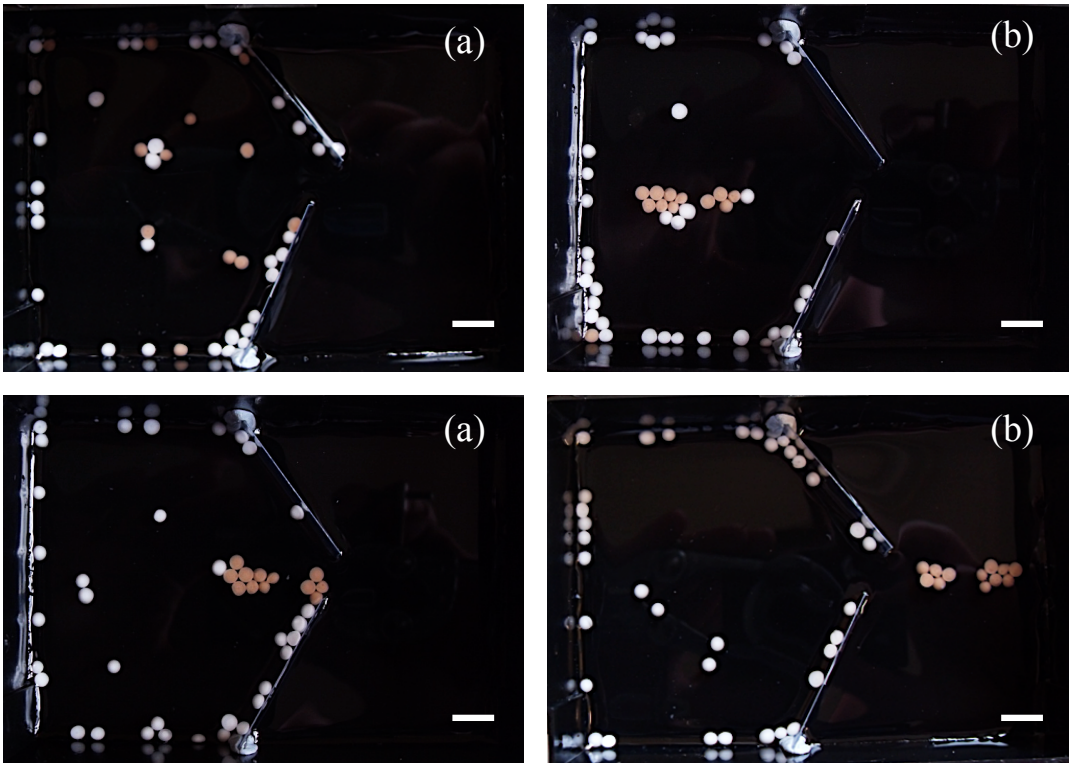

Figure 7.16. (a) Random mixture of magnetic (brown) and non-magnetic (white) engineered emulsion spheroids in water (pH 2). (b) Selective trapping of magnetic emulsion spheroids in the presence of non-magnetic engineered emulsion spheroids using a magnetic field. (c – d) Removal of isolated magnetic spheroids. Scale bars represent 1 cm.

Having demonstrated a response to an external magnetic field, the magnetic-engineered emulsion's ability to respond to a constantly moving magnetic field was investigated. The emulsion assembly strategy was exploited by co-assembling predetermined ratios of magnetic engineered emulsion with non-magnetic engineered emulsion. The design was chosen such that a non-spherical magnetic rod-shaped EE was kinetically trapped within a spherical non-magnetic, conventional EE. The resulting magnetic engineered emulsion stirrer bar comprised a magnetic droplet volume fraction of 0.19 (relative to the total emulsion volume present,). This site-isolated assembled emulsion structure floated on the surface of water (acid pH) and rotated when a revolving magnetic field was applied (Figure 7.17). The speed of rotation attained for this assembled structure was 6 rpm, but in principle this could be increased by encapsulating higher concentrations of mNPs or by increasing the magnetic field strength. The rotation could be turned on and off by stopping and starting the rotating magnetic field. Thus localised domains of magnetic particles

trapped within a conventional engineered emulsion can induce a mechanical (rotational) response. It is worth noting that the trapped magnetic EE does not need to be rod-shaped to enable rotation, but this shape was simple to create and allowed easier imaging of the rotation. This confirms that relatively small quantities of encapsulated magnetic material can readily direct the motion of larger non-magnetic engineered emulsions that, in principle, could be encapsulating various additional cocktails of actives including drugs and biomolecules.

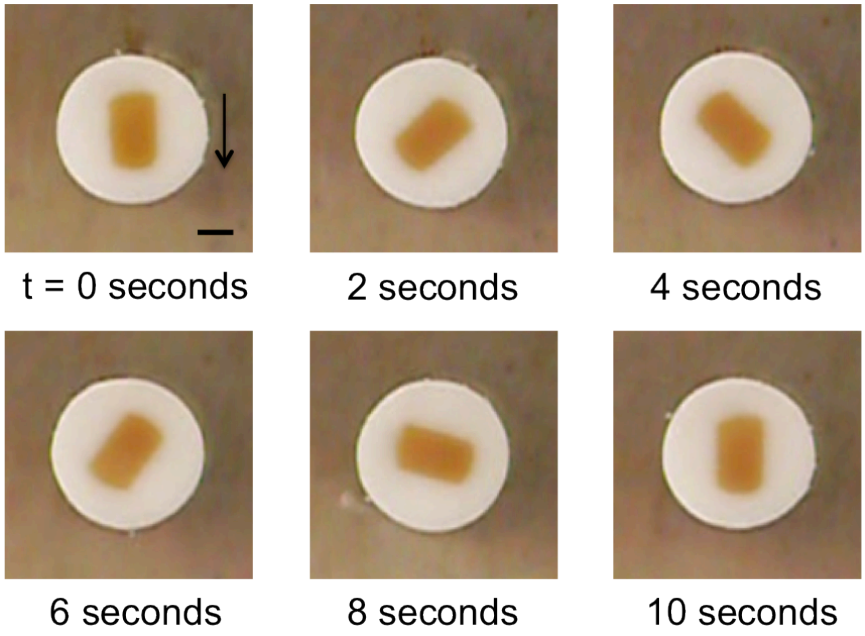

Figure 7.17. Sequenced images recorded every 2 seconds of site isolated magnetic emulsion stirrer bar floating on water in a revolving magnetic field. Scale bar represents 2.5 mm.

7.3. Conclusion

It has been demonstrated that mNPs with PDEAEMA surfaces can be encapsulated within stable, surface-functionalised o/w emulsion droplets. The emulsions produced display both responsiveness to a magnet and also to a pH change due to droplet surface functionality. This surface functionality can be used to trigger a reversible transition of these emulsions from free-flowing fluid dispersions to engineered emulsion structures. The resulting EEs exhibit similar rates of aggregation and gel strengths to standard, non-magnetic EEs, suggesting that the presence of PDEAEMA-mNPs has no effect on the surface functionality of emulsion droplets.

A simple pH switch can not only kinetically trap droplets; it can also change their response to a magnetic field. Free-flowing droplets appear to respond similarly to a ferrofluid, displaying relatively unrestricted movement in a magnetic field, whereas engineered emulsions display magneto-actuation behaviour, responding as one object that has adopted the magnetic responsiveness of the constituent mNPs. Lastly, it was demonstrated that a small quantities of magnetic EE could directly influence the motion of non-magnetic EEs when both systems were incorporated into one structure.

7.4. References

(1) Boyer, C.; Whittaker, M. R.; Bulmus, V.; Liu, J. Q.; Davis, T. P. *NPG Asia Mater.* **2010**, *2*, 23.
(2) Gneveckow, U.; Jordan, A.; Scholz, R.; Bruss, V.; Waldofner, N.; Ricke, J.; Feussner, A.; Hildebrandt, B.; Rau, B.; Wust, P. *Med. Phys.* **2004**, *31*, 1444.
(3) Lao, L. L.; Ramanujan, R. V. *J. Mater. Sci.-Mater. M.* **2004**, *15*, 1061.
(4) Alexiou, C.; Jurgons, R.; Schmid, R. J.; Bergemann, C.; Henke, J.; Erhardt, W.; Huenges, E.; Parak, F. *J. Drug Target.* **2003**, *11*, 139.
(5) Messing, R.; Schmidt, A. M. *Polym. Chem.* **2011**, *2*, 18.
(6) Qin, J.; Asempah, I.; Laurent, S.; Fornara, A.; Muller, R. N.; Muhammed, M. *Adv. Mater.* **2009**, *21*, 1354.
(7) An, H. N.; Picken, S. J.; Mendes, E. *Soft Matter* **2010**, *6*, 4497.
(8) Safarik, I.; Safarikova, M. *J. Chromatogr. B* **1999**, *722*, 33.
(9) Kubo, T.; Sugita, T.; Shimose, S.; Nitta, Y.; Ikuta, Y.; Murakami, T. *Int. J. Oncol.* **2000**, *17*, 309.
(10) Dobson, J. *Nature Nanotechnol.* **2008**, *3*, 139.
(11) Lai, J. J.; Hoffman, J. M.; Ebara, M.; Hoffman, A. S.; Estournes, C.; Wattiaux, A.; Stayton, P. S. *Langmuir* **2007**, *23*, 7385.
(12) Caruso, F.; Susha, A. S.; Giersig, M.; Mohwald, H. *Adv. Mater.* **1999**, *11*, 950.
(13) Deka, S. R.; Quarta, A.; Di Corato, R.; Falqui, A.; Manna, L.; Cingolani, R.; Pellegrino, T. *Langmuir* **2010**, *26*, 10315.
(14) Yiu, H. H. P.; Niu, H. J.; Biermans, E.; van Tendeloo, G.; Rosseinsky, M. J. *Adv. Func. Mater.* **2010**, *20*, 1599.
(15) Gong, X. Q.; Peng, S. L.; Wen, W. J.; Sheng, P.; Li, W. H. *Adv. Func. Mater.* **2009**, *19*, 292.
(16) Szabo, D.; Szeghy, G.; Zrinyi, M. *Macromolecules* **1998**, *31*, 6541.
(17) Bibette, J. *J. Magn. Magn. Mater.* **1993**, *122*, 37.
(18) Brown, P.; Butts, C. P.; Cheng, J.; Eastoe, J.; Russell, C. A.; Smith, G. N. *Soft Matter* **2012**, *8*, 3545.
(19) Reinicke, S.; Dohler, S.; Tea, S.; Krekhova, M.; Messing, R.; Schmidt, A. M.; Schmalz, H. *Soft Matter* **2010**, *6*, 2760.
(20) Amalvy, J. I.; Unali, G. F.; Li, Y.; Granger-Bevan, S.; Armes, S. P.; Binks, B. P.; Rodrigues, J. A.; Whitby, C. P. *Langmuir* **2004**, *20*, 4345.

(21) Fujii, S.; Cai, Y. L.; Weaver, J. V. M.; Armes, S. P. *J. Am. Chem. Soc.* **2005**, *127*, 7304.
(22) Dinsmore, A. D.; Hsu, M. F.; Nikolaides, M. G.; Marquez, M.; Bausch, A. R.; Weitz, D. A. *Science* **2002**, *298*, 1006.
(23) Montagne, F.; Mondain-Monval, O.; Pichot, C.; Mozzanega, H.; Elaissari, A. *J. Magn. Magn. Mater.* **2002**, *250*, 302.
(24) Dikanskii, Y. I.; Nechaeva, O. A.; Zakinyan, A. R. *Colloid J.* **2006**, *68*, 137.
(25) Brugger, B.; Richtering, W. *Adv. Mater.* **2007**, *19*, 2973.
(26) Zhao, Y.; Fang, J.; Wang, H.; Wang, X.; Lin, T. *Adv. Mater.* **2010**, *22*, 707.
(27) Weaver, J. V. M.; Rannard, S. P.; Cooper, A. I. *Angew. Chem. Int. Ed.* **2009**, *48*, 2131.
(28) Aharoni, A.; Jakubovics, J. P. *IEEE Trans. Magn.* **1988**, *24*, 1892.
(29) Zheng, Y. H.; Cheng, Y.; Bao, F.; Wang, Y. S. *Mater. Res. Bull.* **2006**, *41*, 525.

CHAPTER 8

Conclusions and Future Work

List of Tables

8.1. Chapter 3

The role of pH-responsive branched copolymer surfactant composition in controlling inter-droplet aggregation to form engineered emulsions (EE) was investigated. A one-pot vinyl polymerisation was used to synthesise copolymers containing different ratios of monofunctional monomers EG and MAA, while branching monomer (EGDMA) and chain transfer agent (DDT) were always added in feed molar equivalences of 10 % relative to the total MFM. The effect that changing this molar ratio had on the kinetics of droplet aggregation and the mechanical strength of resulting EEs was demonstrated. Aggregation kinetics of dilute droplets shows that equimolar ratios of EG:MAA promote the fastest aggregation, as well as yielding the strongest gel in terms of resistance to strain.

Table 8.1. Summary of results of varying EG:MAA ratios in both degree of aggregation after 10 minutes at pH 2, and the resulting gel strengths

ID	EG:MAA	Increase in $D_{(4,3)}$ at pH 2 / µm[a]	G' of acidified emulsion / Pa[b]	Strain at which G' reaches 90 % its LVE region value / %[b]
E1	0:1	0.56	17,900	1.4
E2	1:6	3.7	22,800	1.4
E3	1:4	3.11	34,600	1.6
E4	1:2	23.71	2,320	4.5
E5	1:1	39.06	932	14.2
E6	2:1	0	10	3.5
E7	4:1	0	28	1.4
E8	6:1	0	69	1.4
E9	1:0	0	21	2.2

[a] Measured by laser diffraction 10 minutes after reducing pH to pH 2. [b] Measured using amplitude sweeps on acidified emulsions in rheology.

These design rules were then utilised to create a selective droplet assembly process by localising each group to different droplet surfaces, creating both MAA surfaces and EG surfaces individually. The kinetics of aggregation of a binary mixture of both these droplet systems was then compared to a system in which EG and MAA were present in equimolar amounts on each droplet surface in order to show that the binary mixture could aggregate in a selective manner.

Engineered emulsions may have potential in applications in which encapsulation and triggered accumulation are desired. This Chapter demonstrates that emulsion droplets stabilised by structurally similar branched copolymers (and with functionality that varies only very subtly) can be used to control pH triggered inter-droplet interactions. The high degree of control achieved here demonstrates that judicious design of the copolymer composition may result in further optimisation of controlled interactions.

8.2. Chapter 4

Chapter 4 demonstrated the use of dodecane o/w EEs as templates for the formation of polymer-structured oils (PSOs). By selective removal of water from the interstitial sites of EE droplets *via* dehydration, a single-phase structure was created comprising discrete droplets held structurally by polymer-polymer interactions at the droplet surfaces. The formation of a PSO was reversible: reforming the EE was achieved simply by the addition of acidic solution to the single-phase structure. This reversibility was investigated using rheology, demonstrating that the emulsion systems had switchable gel strengths, depending on their states of dehydration or rehydration.

EEs were also used as encapsulation devices for hydrophobic dyes. The formation of PSOs from these EEs provided a triggered diffusion/release mechanism. Removal of water from the EE structure allowed the diffusion of hydrophobes between droplets, or from droplets into a surrounding hydrophobic environment. PSOs were also capable of sequestration of hydrophobes from a surrounding environment, while EEs were not. This suggests potential applications for EEs in the controlled delivery of large payloads. This Chapter is also a good demonstration of the inherent stability of these droplets, forming a single-phase PSO reversibly with

only very small amounts of droplet destabilisation being measured. The investigation of encapsulation and release of other, more commercially important, hydrophobes such as drugs, may provide these materials with a wider range of applications. Triggered release from EEs formed using polymeric surfactants with small changes in composition may allow further control over the rate of diffusion to and from droplets.

8.3. Chapter 5

Homogeneous acidification was investigated by the hydrolysis of glucono-δ-lactone (GδL) in the continuous aqueous phase of an emulsion, and was utilised in the formation of EEs. Engineered emulsions with volumes three orders of magnitude larger than previously reported were produced and, in principle, the volume of EE that may be produced by homogeneous acidification is limited only by the volume of emulsion that can be prepared and templated. The reversibility of the system is maintained, so even large EEs can still be redispersed to produce free-flowing emulsions when acidified using GδL, maintaining the structural integrity of individual droplets, as in HCl-aggregated systems.

Slow hydrolysis of GδL allowed *in situ* rheological measurements, providing valuble insight into the aggregation process. Rheology measurements also demonstrated that the gel strength of the resulting EE is independent of the method of acidification.

This method of acidification provides a simple strategy to large, complex engineered emulsions. This may widen the range of applications, as the volume of EEs is no longer limited by the method of acidification.

8.4. Chapter 6

An emulsion-solvent-evaporation technique was employed on a P5 stabilised ethyl acetate o/w emulsion to generate PMMA colloids with surface functionality. Similar to an EE system, a reduction in solution pH to pH 2 induced aggregation of PMMA colloids when EG and MA were present in a 1:1 ratio. Aggregation was reversible on the addition of base. PMMA particles with EG-rich surfaces were also produced, which were unresponsive to pH changes, as seen for emulsion systems in Chapter 3.

Aggregated colloids could be fabricated into 3D structures and varied methods of drying can be used to control the macroporosity within these structures. Further optimisation of the particle surface may render these aggregates useful as biological scaffolds capable of triggered disassembly. More control over the dehydration process may yield aggregated structures with varied porosity, providing a system in which pH-responsive scaffolds with controlled pore size and/or volume are easily produced.

8.5. Chapter 7

The encapsulation of oleophilic, PDEAEMA-functionalised mNPs within robust, P5 stabilised, dodecane o/w emulsion droplets was demonstrated. The resulting emulsions display magnetic responsivity and the pH-responsiveness at droplet surfaces can be used to trigger a reversible transition of these emulsions from free-flowing fluid dispersions to form EEs. The magnetic response of these two distinct states is entirely different, with free-flowing emulsions displaying relatively unrestricted movement in an external magnetic and the EEs displaying magneto-actuation behaviour. This triggerable transition may find applicability in biomedical situations whereby remote-control of free-flowing droplets may be used to non-invasively accumulate emulsions at predetermined sites within the body. Localised pH variations could then trigger droplet assembly and the onset of magneto-actuation behaviour. While such applications will inevitably require optimisation of surface chemistries, an example of which was demonstrated in Chapter 3, these results provide a useful platform from which such studies may be launched.

Finally, due to the strength of EE emulsions and their ability to encapsulate relatively large payloads, their advantages in terms of incorporating mixtures of encapsulated materials for delivery applications presents a new model for the design of responsive vehicles for targeted and specific *in vivo* applications.